NEW π-CONJUGATED MATERIALS FOR MOLECULAR ELECTRONIC AND LIGHT-EMITTING DEVICES

RUKKIAT JITCHATI

USTINOV COLLEGE

DEPARTMENT OF CHEMISTRY

DURHAM UNIVERSITY

A thesis submitted for the degree of Doctor of Philosophy at the Durham University.

August 2009

STATEMENT OF COPYRIGHT

DECLARATION

The work described in this thesis was carried out in the Department of Chemistry at the Durham University between October 2005 and July 2009. All the work was carried out by the author unless otherwise stated and has not been previously submitted for a degree at this or any other university.

TABLE OF CONTENTS

Acknowledgements

I would like to thank my supervisor Professor Martin R. Bryce for his help and guidance with the project, and his help in proof-reading this thesis. I especially thank Dr Changsheng Wang for practical suggestions and advice in the laboratory when needed. X-ray crystal structures were solved by Dr Andrei S. Batsanov. Molecular wire characterisations using STM were performed in the laboratories of Professor Geoffrey J. Ashwell, (Bangor University) and Professor R. J. Nichols (Liverpool University). Data from MCBJ was provided by Professor C. Schönenberger (University of Basel, Switzerland). The LEC device studies were performed in Professor Monkman's group in the Department of Physics, Durham University. I also give a credit to service staff of the chemistry department for NMR, mass and elemental analysis. I would like to thank my lab members (Cy 104), particularly Jamie and Kate who helped to make my life in UK a lot easier and also Kiran, Katy, Shachi and ex-members. Special thanks to Thai friends Nim, Bank, P' Fai, P' Mauy, Bass and Thai staff in Numjai restaurant (P' Por, P' Eed and P' Vee) where we had a good time in Durham. More importantly, thanks to Teaw (Kitty) for sharing a happy time with me since the past until now, and more in the future. My family, ex-supervisor, teachers and lecturers also are credited with helping me along the way.

Finally, I thank the Thai Government who have awarded me a scholarship for Bachelor, Master and Ph.D degrees.

Publications

Huber, R.; Gonzalez, M. T.; Wu, S.; Langer, M.; Grunder, S.; Horhoiu, V.; Mayor, M.; Bryce, M. R.; Wang, C.; **Jitchati, R.**; Schonenberger, C.; Calame, M. *J. Am. Chem. Soc.* **2008**, *130*, 1080-1084.

Haiss, W.; Wang, C.; **Jitchati, R.**; Grace, I.; Martin, S.; Batsanov, A. S.; Higgins, S. J.; Bryce, M. R.; Lambert, C. J.; Jensen, P. S.; Nichols, R. J. *J. Phys.: Condens. Matter* **2008**, *20*, 374119.

Rothe, C.; Chiang, C.-J.; Jankus, V.; Abdullah, K.; Xianshun, Z.; **Jitchati, R.**; Batsanov, A. S.; Bryce, M. R.; Monkman, A. P. *Adv. Funct. Mater.* **2009**, *19*, 2038-2044.

Jitchati, R.; Batsanov, A. S.; Bryce, M. R. *Tetrahedron* **2009**, *65*, 855-861.

Abbreviations

A	Amperes
abs	Absorbance
Ac	Acetyl
acac	Acetonylacetate
AFM	Atomic force microscope
Alq_3	Tris(8-hydroxyquinoline)aluminium
BJ	Break junction
CIE	Commission Internationale d'Eclairage
CV	Cyclic voltammetry
DCM	Dichloromethane
DFT	Density functional theory
DMF	*N*,*N*-Dimethylformamide
DMSO	Dimethyl sulfoxide
EBL	Electron-blocking layer
EL	Electroluminescence
EML	Emission layer
EQE	External quantum efficiency
ET	Electron transport
fac	Facial
FIrpic	Iridium bis[(4,6-difluorophenyl)-pyridinato-N,C^2]picolinate
HOMO	Highest occupied molecular orbital
HT	Hole transporter
I	Current
$Irppy_3$	Tris(2-phenylpyridine)iridium
ITO	Indium tin oxide
LEC	Light-emitting cell
LUMO	Lowest unoccupied molecular orbital
M	Molar
Me	Methyl

MEH-PPV	Poly[2-(2-ethylhexyloxy)-5-methoxy-*p*-phenylenevinylene]
mer	Meridional
MC	Metal-centred
MCBJ	Mechanically controllable break junction
mp	Melting point
NMR	Nuclear magnetic resonance
OAE	Oligo(aryleneethynylene)
OPE	Oligo(phenyleneethynylene)
OPV	Oligo(phenylenevinylene)
OFET	Organic field-effect transistor
OLED	Organic light-emitting device
OMCT	Organic molecular charge transporter
OPVD	Organic photovoltaic device
OTE	Oligo(thienylethynylene)
OXD	1,3,4-Oxadiazole
PBD	5-(4-Biphenyl)-2-(4-*tert*-butylphenyl)-1,3,4-oxadiazole
PEDOT	Poly(3,4-ethylenedioxythiophene)
PLQY	Photoluminescence quantum yield
PMMA	Poly(methylmethacrylate)
PPV	Poly(*p*-phenylene vinylene)
PSS	Poly(styrene sulphonate)
SPM	Scanning probe microscopy
STM	Scanning tunelling microscopy
TEA	Triethylamine
THF	Tetrahydrofuran
TIPB	Triisopropyl borate
TMS	Trimethylsilyl
TMSA	Trimethylsilylacetylene
TPD	*N,N'*-Diphenyl-*N,N'*-bis(3-methylphenyl)(1,1'-biphenyl)-4,4'-diamine
UV-Vis	Ultraviolet- visible

Overview

For the past forty years "*inorganic*" silicon and gallium arsenide semiconductors have been the backbone of the semiconductor industry. However, there has been a growing research effort in "*organic* electronics". The attraction of this field has been the ability to modify chemical structures of organic molecules in ways that could directly impact the properties of the materials when deposited in thin film form. While there was always a hope that organic materials would ultimately have uses in applications occupied by "*inorganic*" materials. Recently, *organic* and *organometallic* compounds are of interest as organic semiconductors in applications such as organic light-emitting diodes (OLEDs),[1-10] organic molecular charge transporters (OMCTs) or molecular wires,[11-44] organic photovoltaic devices (OPVDs) or solar cells,[45-51] and organic field-effect transistors (OFETs).[52-56]

This thesis reports the synthesis and characterisation of new π-conjugated organic and organometallic compounds for *organic* electronics applications. The thesis is divided into three chapters:

Chapter 1

The synthesis of Oligo(Aryleneethynylene)s (OAEs) for molecular wire applications.

Chapter 2

The synthesis of charged iridium(III) phenanthroline and bipyridine complexes for organic light emitting diode applications.

Chapter 3

N-Arylation of nitrogen heterocycles with 2,4-difluoroiodobenzene

Chapter 1

The synthesis of oligo(aryleneethynylene)s (OAEs) for molecular wire applications.

Abstract

The synthesis and characterisation of a range of oligo(aryleneethynylene) derivatives end-capped with cyanoethylthio and acetylthio groups are described. Sonogashira cross-coupling reactions have been key steps. These molecules are designed as molecular wires for conductance studies, including single-molecule conductance using Scanning Tunelling Microscopy (STM) and break junction techniques. Solution UV-Vis absorption and fluorescence spectroscopy have been used to assess conjugation in the backbones, e.g. a sequential red shift is observed for molecules with 1, 2 and 3 fluorene units in the backbone (**41** (**RJ 11**), **45** (**RJ 13**) and **47** (**RJ 14**); λ_{max} (abs.) 364, 371, 378 nm, respectively) and a blue shift for molecules **35** (**RJ 8**) and **49** (**RJ 17**) is observed. The results of STM studies in Professor Ashwell's group (Bangor University) show symmetrical *I–V* characteristics for **35** (**RJ 8**), **41** (**RJ 11**), **43** (**RJ 12**) and **47** (**RJ 14**) assembled on gold. Preliminary STM results show length-independent current jumps for the molecules, which is inconsistent with theory: longer molecules should show lower conductance. The length independence suggests that the assembled molecules are being contacted by the STM tip along the backbone, not at the terminal sulfur. Most of the STM experiments show a single current jump, consistent with one molecule being contacted. However, some experiments with **43** (**RJ 12**) show double or even triple current jumps, suggesting simultaneous contact to two and three molecules. The conductance study of compound **RJ 32** with *I(t)*, *I(s)* and *BJ* techniques in Professor R. Nichols' group (Liverpool University) shows that the different techniques favour differing current peaks, with the *BJ* technique giving a higher propensity to higher current peaks, while the *I(t)* and *I(s)* method favour the lower current. A study using MCBJ experiments in Professor C. Schonenberger's group (University of Basel) show that oligo(phenyleneethynylene) (OPE) derivatives have lower conductance than oligo(phenylenevinylene) (OPV) analogues and alkoxy side chains on OPEs do not affect the single-molecule conductance.

Introduction

Molecular-scale electronics

A major force behind the science of molecular electronics is the fact that the microelectronics industry is approaching a limit for the miniaturisation of conventional, solid-state, semiconductor components.[57] In the mid-1960s, Moore observed that the minimum device size on a semiconductor chip was halving approximately every 18-24 months. This process has continued and is now known as Moore's Law. Lithographic techniques which produce the circuitry on silicon wafers are limited by the wavelengths at which they operate. Molecular-scale electronics involves very different concepts from traditional inorganic electronics.[58] Nanometer-sized organic molecules are chemically synthesised with tailored optoelectronic properties. These molecules are functionalised for interconnecting into electronic circuits using self-assembly techniques at metal or semiconductor surfaces. The aim is to explore fundamentally new science and to provide very dense, low-power, low-cost circuits. The idea that a few organic molecules, or even a single molecule, when aligned between electrodes would behave as a diode with the organic bridge acting like a wire, was first proposed by Aviram and Ratner in 1974.[59-61]

Individual molecules (not crystalline assemblies or films) have the advantage of being ca. 10^6 times smaller in area than modern silicon devices. This size scale offers great advantages for components in future computational devices. Synthetic chemistry gives unprecedented functional group diversity with control over molecular structure and properties such as rectifiers,[62-65] transistors,[66,67] amplifiers,[68] switches[69,70] or logic gates.[71] If working devices are to be developed, new fabrication methods and probes must be found which enable the molecules to be connected in a controlled manner into hybrid organic/semiconductor device architectures.[72,73]

Molecular Junctions [74,75]

Molecular conductance junctions are structures in which single molecules or small groups of molecules conduct electrical current between two electrodes. In such junctions, the connection between the molecule and the electrodes greatly affects the current-voltage (*I-V*) characteristics. The basic requirement is that a molecule is attached (wired) to two electrodes to form metal-molecule-metal junctions. It may then be possible to measure the electrical properties. Despite several experimental and theoretical advances, including increased understanding of simple systems (e.g. alkanedithiols), there is still limited agreement between experimental and theoretical studies of many systems. In experimental approaches a range of techniques have aided understanding.[76]

Scanning tunnelling microscopy (STM) or scanning probe microscopy (SPM)

This technique can provide electrical measurements on single molecules. The junction conductance is measured from a molecule anchored to a surface and then the chemical bonding is achieved between the molecule and the STM tip (Figure 1A). Lindsey et al.[77] showed that molecules of 1,8-octanedithiol contact gold clusters at both ends of the molecule to provide measurable current-voltage characteristics. Dithiol molecules which adsorbed conventionally on a Au surface have pendant SH groups which can react with Au nanoparticles. The particle/molecule/substrate assembly is a nearly symmetric molecular junction which may be addressed with an STM or AFM probe. A schematic diagram and representative results are shown in Figure 1A. The particle/molecule/substrate structure with covalent Au-S bonds at both ends yielded two important conclusions. First, the conductance was much higher when a covalent bond existed at both ends of the molecule, indicating faster electron transfer for the covalent contact compared to the physisorbed contact (i.e. no thiolate end group). Second, a series of current/voltage curves was observed for different probe positions, as shown in Figure 1B. At all points along these curves, the current was an integral multiple of a "fundamental curve" with the smallest current. A histogram of these integer multipliers for >1000 junctions is shown in Figure 1C. The authors argue that the apparent quantisation of conductivity could be caused by the probe tip contacting multiple

particles or by a given particle being bonded to multiple molecules in parallel. In either case, the "fundamental" curve must be that of a single molecule suspended between the Au substrate and the Au nanoparticle, with covalent Au-S bonds at both ends.

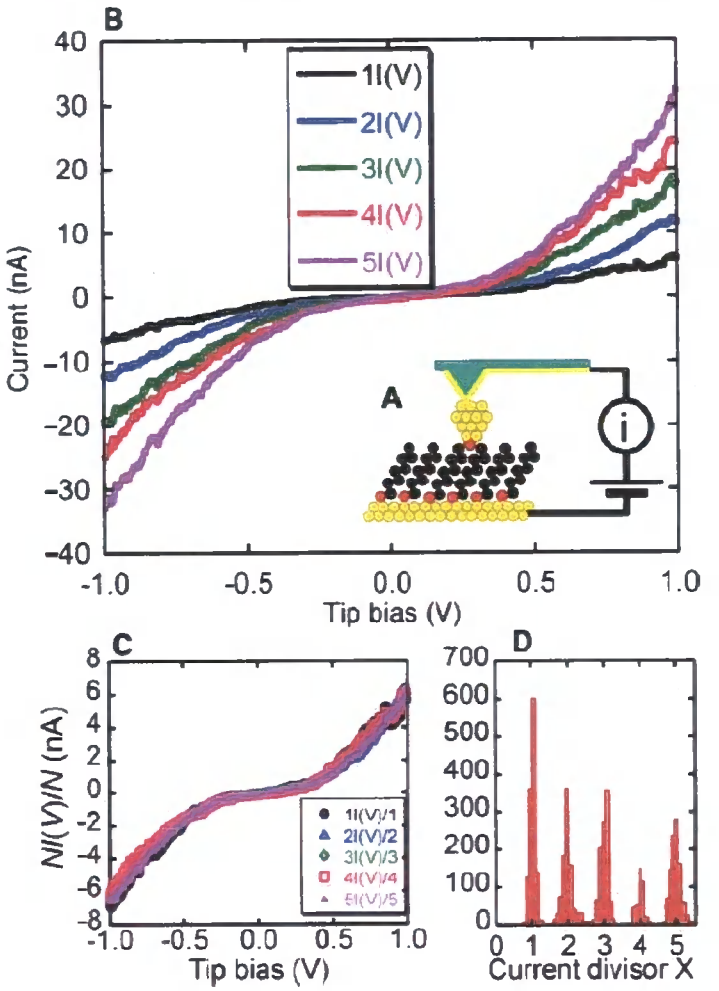

Figure 1. (**A**) Schematic of an octanedithiol monolayer with a Au nanoparticle top contact, probed with AFM. (**B**) $I(V)$ curves measured with the apparatus diagrammed in (**A**). The five curves shown are representative of distinct families, $N\,I(V)$, that are integer multiples of a fundamental curve, $I(V)$ (N = 1, 2, 3, 4 and 5) (**C**) Curves from (**B**) divided by $N\,I(V)$, i.e., 1, 2, 3, 4 and 5. (**D**) Histogram of the observed current as multiples of a fundamental value which is identified as the conductance of a single molecule (from reference 77).

STM experiments, namely the *I(s)* methods, were reported in 2003 by Haiss *et al.*[18] The starting point for these measurements is the adsorption of a low coverage of 6-[1'-(6-mercapto-hexyl)-[4,4']bipyridinium]-hexane-1-thiol iodide (**6V6**) on a Au(111) surface. The attachment of a low coverage dithiol phase was achieved by immersion of the gold films for 15 s in 0.05 mM methanolic solutions. After attachment, the samples were thoroughly washed in ethanol and blown dry with nitrogen. This procedure results in flat-lying molecules and enables the formation of single-molecule wires with high probability. To attach a molecule to the STM tip (Au), the tip is lowered onto the surface by fixing the tunnelling current I_0 at relatively high values and then the tip is lifted, whilst keeping a constant position in the x–y plane. The current decay shows distinctive current plateaux (of height I_w) when molecular wires bridge the gap between the tip and substrate, whereas in the absence of wire formation the current simply decreases nearly exponentially with tip–sample separation. As discussed previously, the current plateaux have been related to electron tunnelling through molecular wires bridging the STM tip and the substrate.

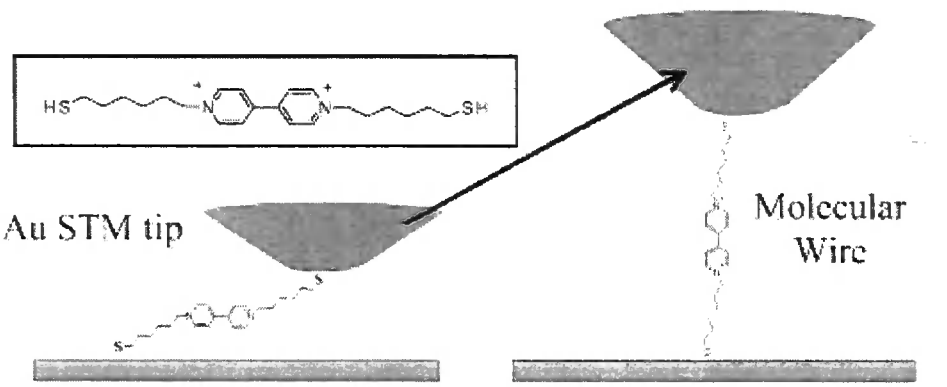

Figure 2. Schematic diagram of the *I(s)* experiment performed to study electrical properties of single molecules **6V6** (from reference 18).

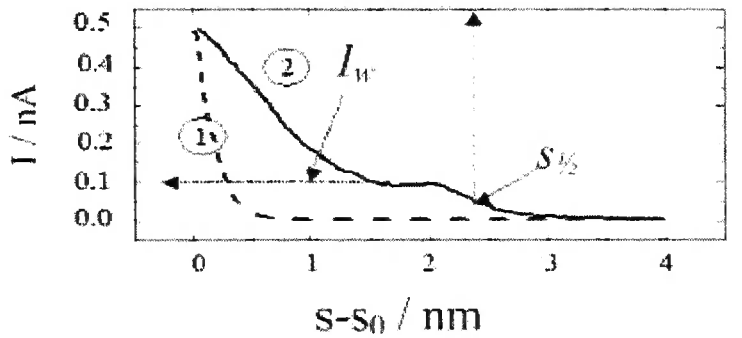

Figure 3. Current decay curves obtained by the *I(s)* technique for **6V6** on Au(111) in air (1) baseline for a clean Au surface and (2) in the presence of **6V6** molecular wires between the tip and the substrate (from reference 18).

The *I(t)* technique is given in detail here.[21] As stated above, dithiols adsorbed on gold for short times at low concentrations form a flat-lying phase from which it is possible to form a molecular bridge between tip–substrate contacts. The *I(t)* technique monitors these events in the time domain. When molecular bridges are formed, a sudden current jump is observed, the magnitude of which (I_w, $I_w = I - I_0$; I = current, I_0 = tunnelling current before the observation of the current jump) is proportional, in the low current limit, to the applied tip–substrate potential. Thus, the conductivity of the molecules in the gap can be calculated from the characteristic current jumps in the tunnelling current (I) as a function of time (t).

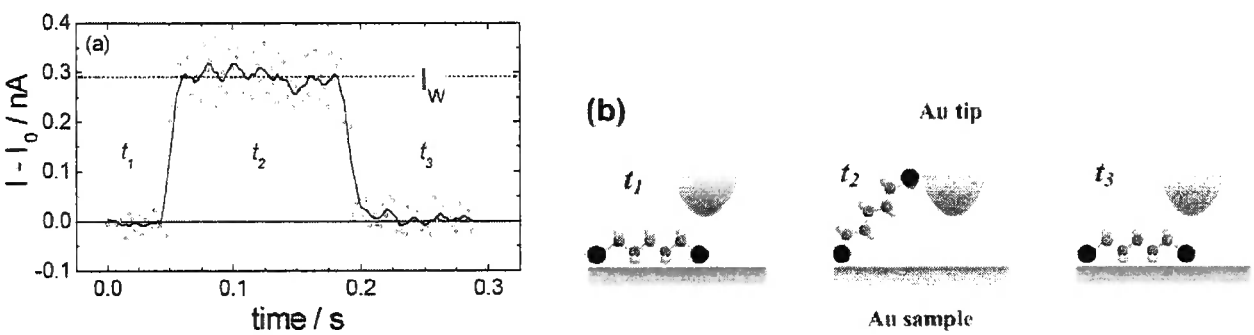

Figure 4. Typical current jumps recorded on Au(111) with the *I(t)* technique for 1,8-octanedithiol, (b) Schematic diagram of the experiment, showing the spontaneous formation of a molecular wire between the tip and the substrate. At t_1 and t_3 the molecule is detached from the tip. At t_2 the molecule is attached to both the tip and the sample, giving rise to an increased current (I_w) (from reference 21).

Data using the *I(t)* method for an OPE derivative (**CSW-558**) which was synthesised by Dr. C. Wang in our group are shown in Figure 5.[78]

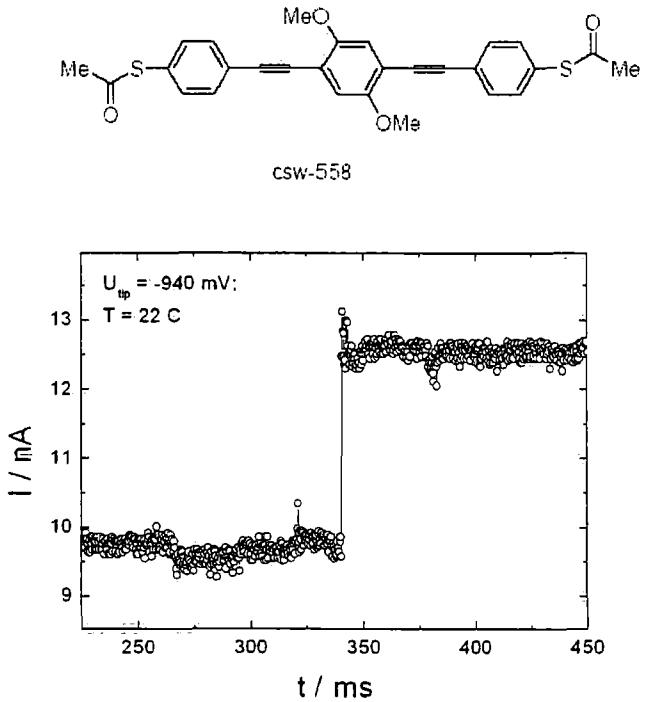

Figure 5. Typical current jump of ca. 3 nA recorded using the molecular wire of **CSW-558** to bridge the gap by the *I(t)* method (from reference 78).

Mechanically controllable break junctions (MCBJ).

The mechanism of this process is shown below. The gold tunnel is constructed by the bending of materials (Figure 6a). After the gap is formed, a solution of the molecule to be studied (in this case 1,4-benzenedithiol) forms a self-assembled monolayer (SAM) on the gold electrodes (Figure 6b). The solvent then evaporates and the molecules bridge the gap and the (single) molecular conductance can be measured.[79]

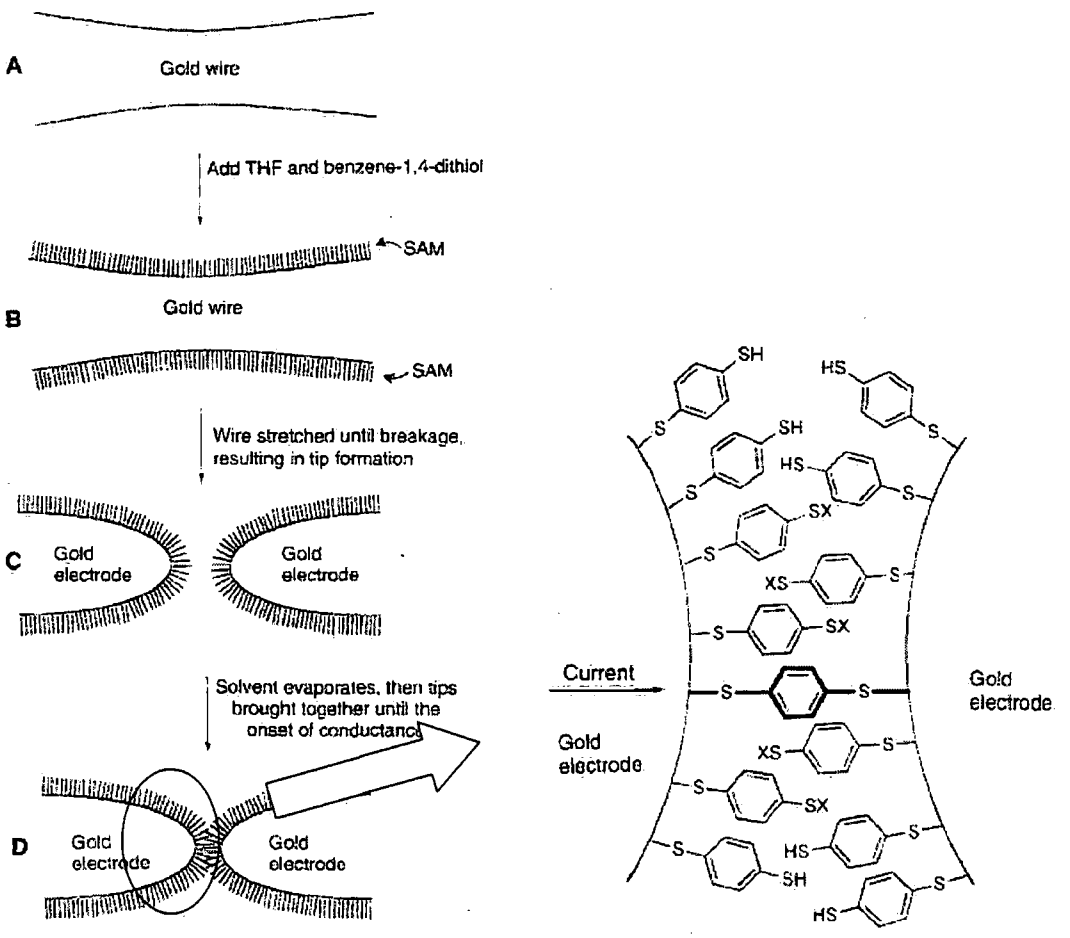

Figure 6. Measurement process of MCBJ with gold terminals (a) gold tunnel (b) 1,4-benzenedithiol self assembly (c) gold bending (d) molecular bridge junction (from reference 79).

Recently, Gonzalez and co-workers (University of Basel)[80] have developed new STM-based break junction methods and studied molecular junctions of octanedithiol molecules, as shown in Figure 7. Figure 7a shows the suspended 100 nm wide region in the centre of the gold leads. The principle of the formation of a metal-molecule-metal bridge during the breaking process can be described step by step. First, the Au-bridge gets thinner (Figure 7b), until a rather stable single-atom contact is established. A plateau in the $G(z)$ curve is then expected around G_0. When the atomic contact is finally lost, the conductance decreases strongly. This decrease may be interrupted if a metal-molecule bridge is formed (Figure 7c). In that case, another plateau in the $G(z)$ curve is anticipated.

Similar to atomic junctions, this metal-molecule-metal bridge holds the two sides together via its chemical bonds and postpones the breaking open of the Au electrodes (Figure 7d). Using conductance jumps and focusing on the plateau values, these methods effectively eliminate background conductance values. The MCBJ data for octanedithiol is shown in Figure 7e which shows that the conductance value obtained from this experiment is ca. $10^{-4}G_0$.

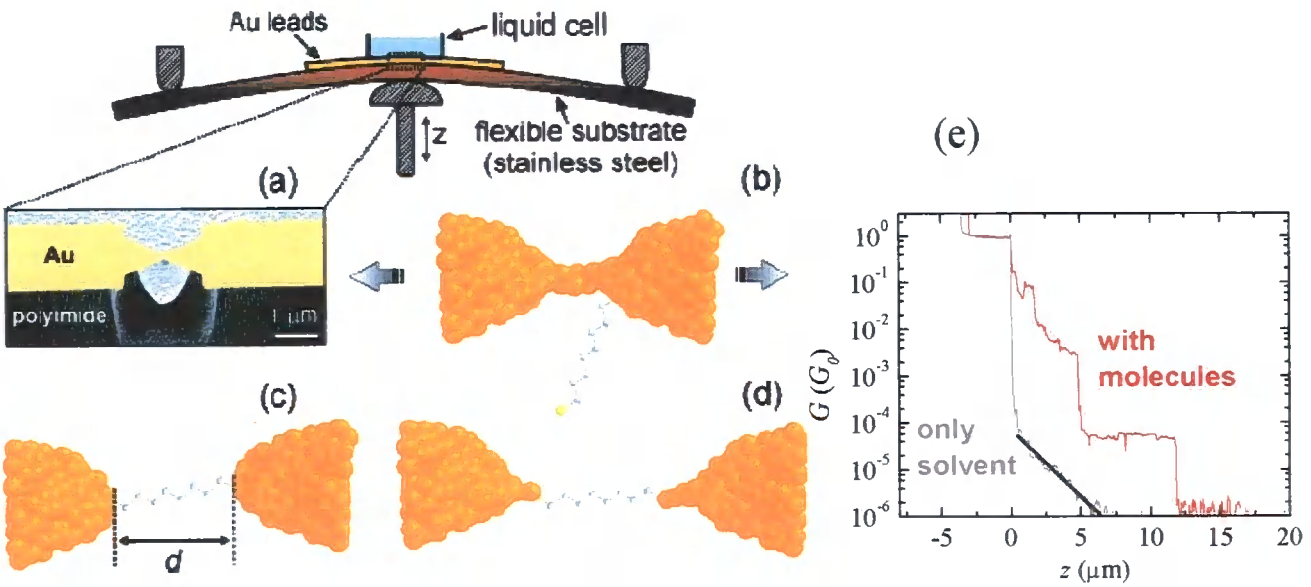

Figure 7. (**a**) Schematics of the MCBJ (**b**) starting from the fused Au (**c**) a molecule locks between gold junction (**d**) the Au-octanedithiol-Au junction (**e**) the MCBJ data of octanedithiol (from reference 80).

Electromigration Break Junction

Wenjie Liang and co-workers[81] introduced a different technique for measuring the conductance of molecular wires as shown below (Figure 8). An e-beam-patterned metal constriction is formed on an aluminium pad. The sample is placed under vacuum at cryogenic temperatures after immersion in solution or exposure to vapour of the desired molecules to cause molecular adsorption in the region where the gap will be created. When a high current is passed through the constriction, electromigration-induced junction breaking occurs.

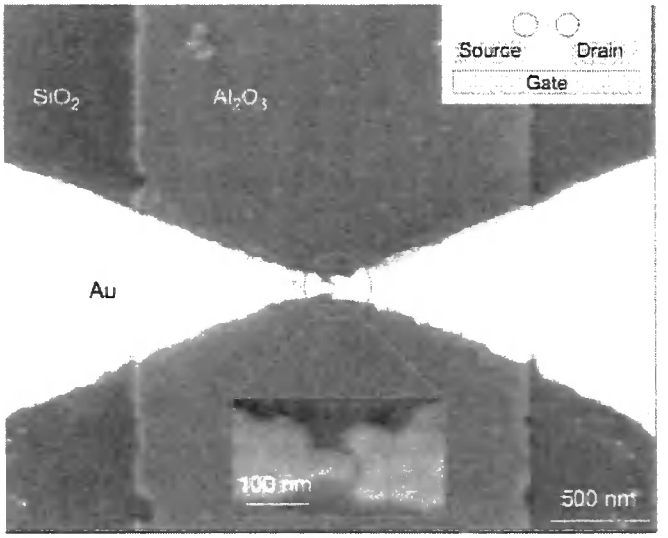

Figure 8. Electromigration break junction (from reference 81).

Organic molecular charge transporters (OMCTs) or "molecular wires"

Molecules which display wire-like behaviour are at the forefront of today's molecular electronics research.[82-84,12] The term "molecular wire" describes an organic or organometallic system which facilitates intramolecular electron- or charge-transport from one site to another, usually under the control of an external electrical, electrochemical or photonic stimulus.[20,85,86]

Functional, monodisperse, π-conjugated monomers and oligomers with rod-like backbones, which are available in lengths from *ca.* 1 to >10 nm, are of particular interest from experimental and theoretical viewpoints.[87,29,27,11] A wide range of molecules have been studied, including alkanedithiols,[88-90] oligo(aniline)s,[91] poly(ferrocenylalkyne) linkages,[26] azobenzene derivatives[92] and oligo(thiophene)s.[93-96] Especially, sp^2-carbon based oligo(arylenevinylene) and sp-carbon based oligo(aryleneethynylene) molecular wires have been intensely targeted due to their conducting properties. A specific example of oligo(arylenevinylene)s is oligo(phenylenevinylene)s (OPVs).[97,98]

Oligo(aryleneethynylene)s; (OAEs)

Aryleneethynylenes are attractive candidates for use in metal–(molecular wire)–metal structures because of the benefits of a length persistent π system and the lack of *Z/E* isomerism compared to OPVs. OAEs have a cylindrical structure for which coplanar molecular conformations can be readily obtained to maximise conjugation. However, the barrier to rotation about the aryl–ethynyl bond is low, estimated at <1 kcal mol^{-1}, so although coplanar conformations of the arylene rings are sometimes observed in the crystalline state, their structures in solution or in molecular junctions may be less well-ordered.[99,100] The general structure of OAEs is $(–aryl–C\equiv C–)_n$ where aryl groups are phenyl, thienyl, fluorenyl and pyridyl. Specific examples of OAEs are (i) oligo(thienylethynylene)s (OTEs)[14,31] when thiophene is the backbone aromatic unit, (ii) oligo(fluorenylethynylene)s (OFEs) containing the fluorene unit which is widely used in light-emitting materials with high photoluminescence quantum yields, and has good thermal and oxidative stability[101-103] and (iii) oligo(phenyleneethynylene)s (OPEs) which are widely studied for advanced materials applications.[104,16,15]

Figure 9 shows recent calculated structures at density functional theory (DFT) level and their relative energies of OPEs.[100] It can be seen that coplanar rings have lower energies. The energy of **3'e** is twice as large as **2'e**. This is because **3'e** has twice the number of orthogonal bonds. However, there is a difference of only 4.8 kcal mol^{-1} between the most conjugated (most stable) conformation **3'a** and the least stable (least conjugated; most twisted) **3'e**.

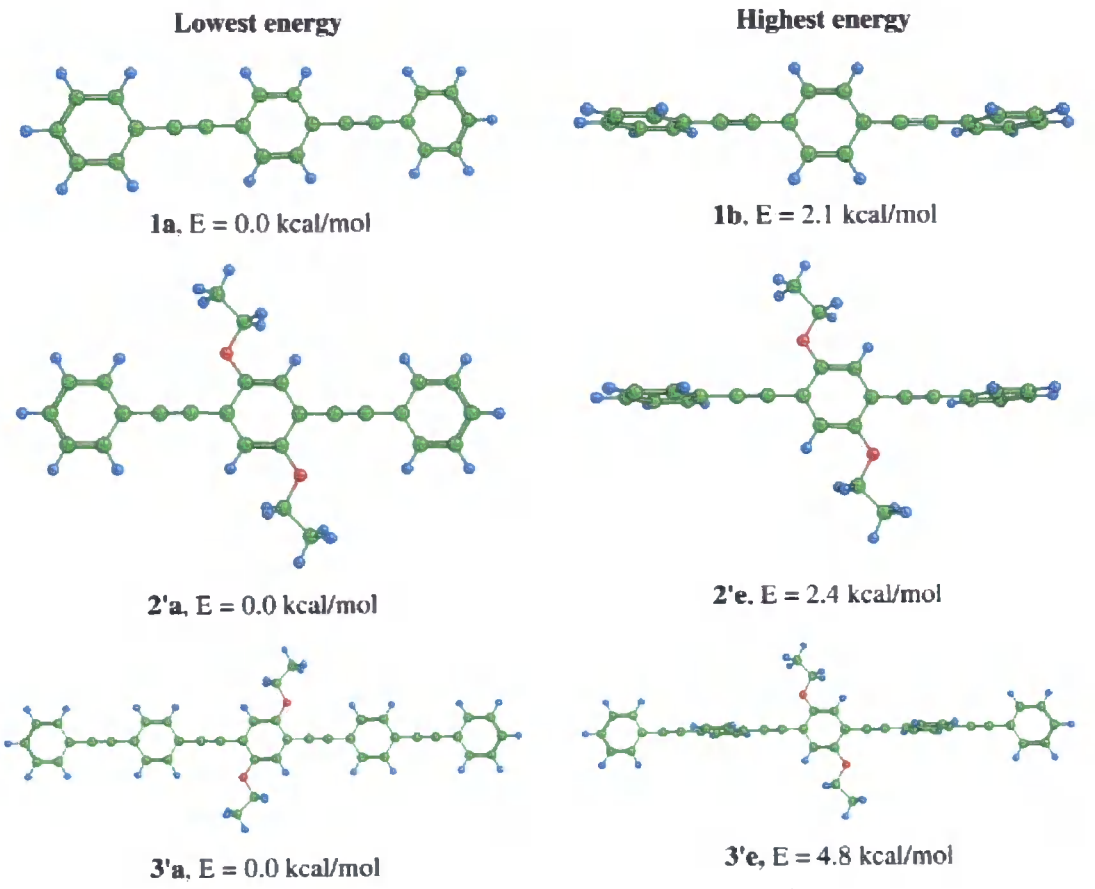

Figure 9. Most stable planar conformations and least stable twisted orthogonal conformations of phenyleneethynylenes by AM1 semiempirical calculations (from reference 100).

The planar conformations (Figure 10, left) have maximum conjugation of the phenyl electrons through one of the π–bonds of each acetylene unit. This conjugation is broken when a phenyl ring twists. However, this is partly compensated for by involvement of the second π–bond of the acetylene (Figure 10, right).

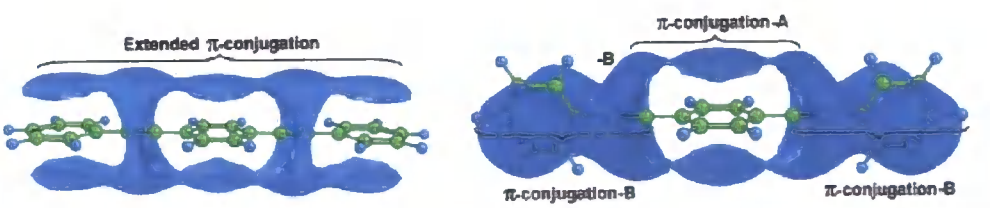

Figure 10. π–Conjugation features for OPE in different conformations (from reference 100).

The OPE family is versatile and can incorporate fluorene, fluorenone,[28] and bipyridine[105] in the backbone. Moreover, the side chains of OPEs can vary from akyl,[13] alkoxy,[106] nitro,[107] pyridine or dendrimer[108] for studies of optical and electronic conductivity properties.

Recent work by Wang in our laboratory has incorporated 9-fluorenone units into the backbone of aryleneethynylene oligomers.[23] A specific structure **CSW-11** is shown below. Fluorenone has good chemical stability to a range of synthetic transformations, combined with the reversible formation of radical anions under electrochemical conditions. This has led to novel redox-active molecular wires.

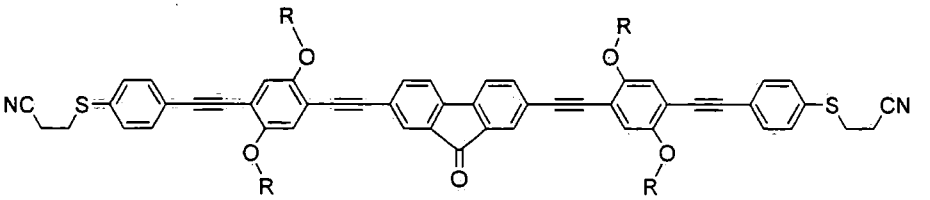

CSW-11

The single-crystal X-ray structure (Figure 11) shows an almost planar conformation for the molecular backbone, with the planes of all rings parallel to within 13°. As expected, the central 2,7-diethynylfluorenone unit is not linear, the two –C≡C–aryl–C≡C–aryl–S rods form an angle of *ca.* 160°. This is one of the longest OPEs to be characterised crystallographically.

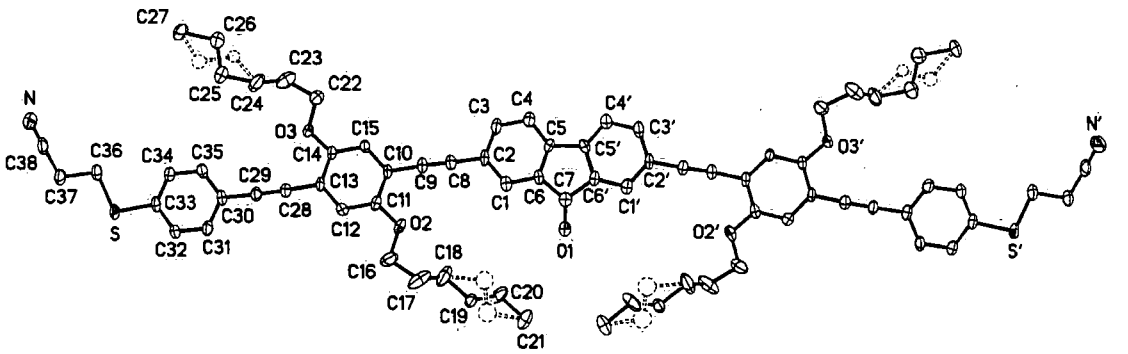

Figure 11. The X-ray crystal structure of the ca. 4 nm molecule **CSW-11** (calculated from intramolecular S---S distance) synthesised in our group (from reference 23).

For studies of conductance, the wire molecules need terminal thiols (or protected thiols) for bonding with metal surfaces. These are the most widely-used terminal groups,[109] although alternatives have received less attention, *e.g.* nitriles,[110] isocyanides[111] and pyridyl units.[89] Because free thiols can be difficult to synthesise and purify and they are smelly and easily form disulfides, they are usually avoided and synthesised as their thioacetate-protected derivatives,[112] which can be cleaved by base to yield the thiolate which self-assembles on the metal surface. However, this is not ideal as Tour et al. have reported that on some occasions undesirable side-reactions can occur during the deprotection, including sulfoxide formation.[113] Assembly of thioacetates can occur without added base, although the fate of the acetate group is not clearly established under these conditions. Not only the acetyl group has been used to protect thiols, but also silyl groups can be used.[92] In our laboratory we favour the cyanoethyl protecting group, i.e. S-CH_2-CH_2-CN, which is very cleanly removed with base, e.g. sodium methoxide, to form thiolate and volatile H_2C=CH_2-CN gas. Moreover, the increased stability of the 2-cyanoethylthio group (compared to thioacetate) is advantageous for some Sonogashira reactions, enabling the use of higher temperatures, longer reaction times, and an increased amount of amine base. In addition, the stability of the final products is increased compared to that of acetyl analogues. If required, the cyanoethylthio group can be converted into the thioacetate at the end of the synthesis.

In addition, it is not only monoyne-OPEs which are of interest, but also diyne-OPEs have been synthesised for studies of stability, structure, and optoelectronic properties in our group.[30,114]

General aims

It is important to establish how small changes in molecular structure will affect the molecular conductivity. Our first target systems were variants of **CSW 558** (studied previously in our group – Figure 5) with modified aromatic cores. The aromatic cores which were chosen are di(hexyloxy)phenylene, thiophene, pyridine, fluorene, 9,9-dihexylfluorene and 2,2'-dimethoxy-4,4'-biphenyl. We also sought to vary the length of the aromatic core from one, two and three fluorene units. Moreover, Ashwell, Bryce et al. have discussed the self-assembly and electronic properties of 9-[(4-pyridyl)methylene]fluorene with a pendant pyridine unit and established that the pyridine can be protonated. After protonation with HCl and combination with a sulfonated phthalocyanine counterion, *I-V* characteristics became unsymmetrical as shown in Figure 12.[115]

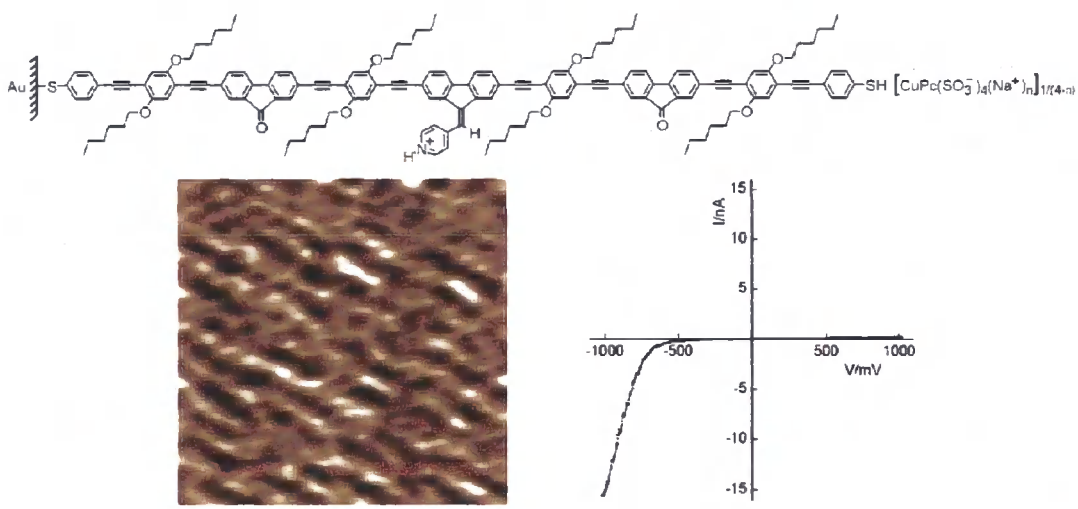

Figure 12. Protonated wire ionically coupled with a sulfonated phthalocyanine counterion, showing STM image and unsymmetrical *I-V* characteristics (from reference 115).

We decided to synthesise a molecule with a pyridine unit as a proton acceptor conjugated into the OPE backbone (not pendant as in Figure 12). The interest here is that the pyridine nitrogen will be basic and its protonation could be a means of changing the

electrical characteristics of the molecule. The pyridinium cation should make the wire a stronger electron acceptor.

We also targeted OPE derivatives with a thiol unit at only one end to study the possibilities of STM tip contact with a terminal phenyl ring and π–π stacking in the junction. Indeed, in 2008 during the course of our work, the Basel group concluded from MCBJ studies that an intermolecular π–π stacking interaction between monothiolated OPE molecules is strong enough to induce the formation of molecular junctions as depicted in Figure 13.[116]

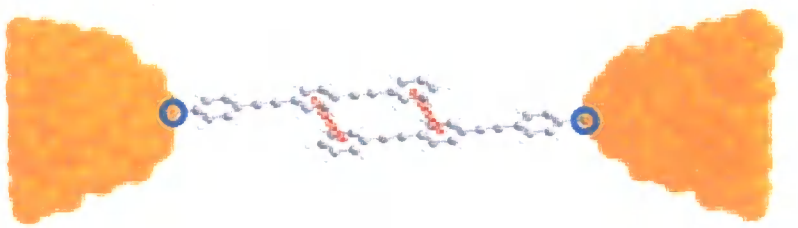

Figure 13. Schematic representation of the proposed staggered π–π stacking configuration of a pair of OPE–monothiol molecules in a gold-molecule-gold MCBJ (from reference 116).

Recently, our collaborators at Liverpool University found that by using the *I(s)* technique, **CSW 558** showed single-molecule conductance values at ~0.9 nA. Interestingly, the histograms also present the conductance values of ~0.3 nA (Figure 14) which we believe arises from the conductance of two π–π stacked molecules similar to that reported by the Basel group. To explore this further, we decided to synthesise new OPEs with a thiol substituent at only one end.

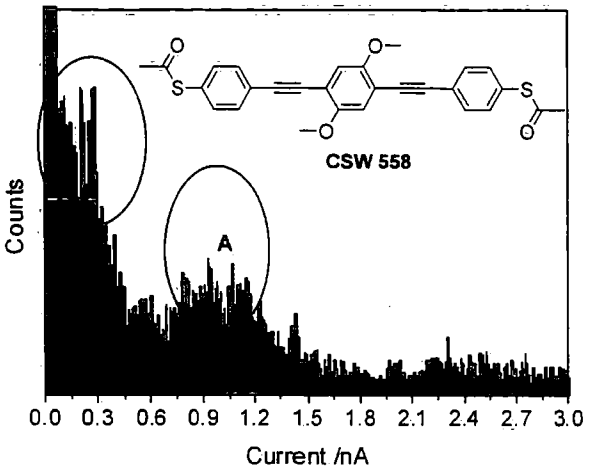

Figure 14. The *I(s)* histograms of **CSW 558** present peaks at ~0.3 nA assigned to π–π stacking of two molecules and at ~0.9 nA (**A** group) from the single molecule conductance.

Figure 15 shows all our target molecular wires with protected thiol end-groups (PG).

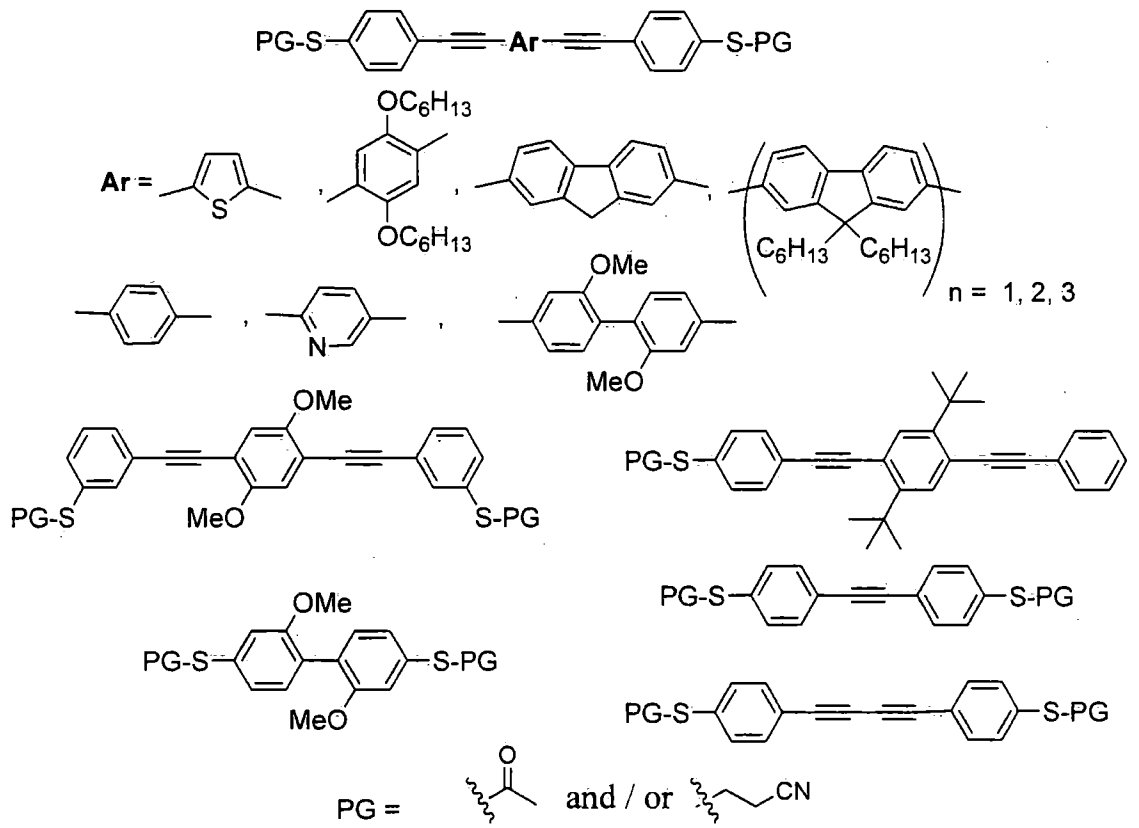

Figure 15. The structures of our targets.

The general synthesis of aryleneethynylenes

The synthesis of aryleneethynylenes starts from dihalo aromatics. For the Sonogashira reaction, we preferred to use the diiodoarene and 2 equivalents of the terminal alkyne building block with the thiol protected as the cyanoethyl derivative.

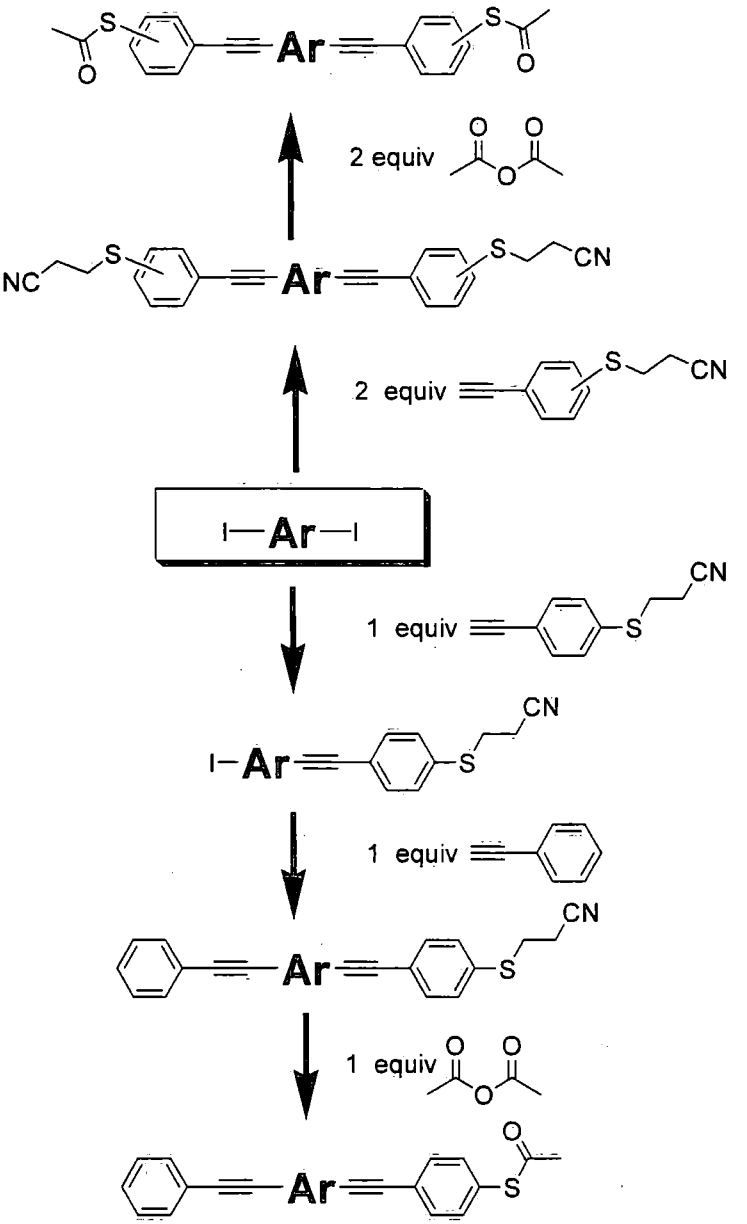

Figure 16. The general synthesis of oligo(1,4-aryleneethynylene)s terminated with either one or two thioacetate groups.

Results and Discussion

The synthesis of *para*-protected thiol terminal alkyne (8)

We identified the terminal alkyne **8** as the key building block for terminal groups in our new OAE wires. Dr Wang in our group has developed the 7-step synthesis of **8**.[23] With modification of some steps, compound **8** was synthesised in 6 steps with the overall yield of 54% shown in Scheme 1. The commercially available 4-bromothiophenol was protected by using *t*-butyl chloride to get product **2** in 87% yield. Then compound **2** was changed to the iodo analogue with *n*-BuLi and I_2 to give iodo product. Without purification, the *t*-butyl group was transformed into an acetyl group using boron tribromide and acetyl chloride. This procedure gave **4** in 79% yield for the two steps from **2**. In the next step the acetyl group was removed by reaction with KOH in methanol to get 4-iodothiophenol **5** in 96% yield. Compound **5** was then converted into its cyanoethyl-protected derivative **6** with 3-bromopropionitrile and base in 98% yield. Sonogashira reaction of iodobenzene derivative **6** with trimethyl silylacetylene (TMSA) gave **7** in 94% yield. Finally, removal of the TMS protecting group afforded product **8** as a pale yellow oil in 88% yield.

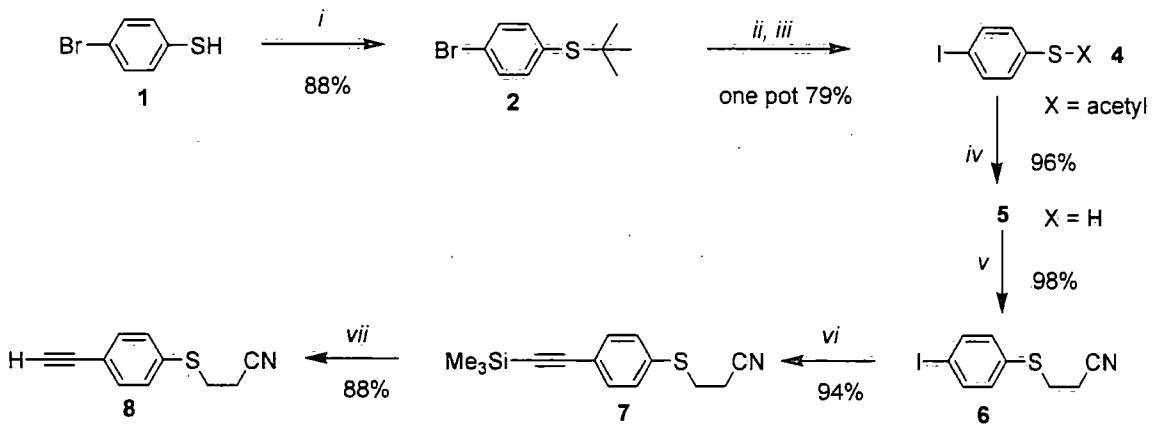

(i) *t*-BuCl/$AlCl_3$ (ii) a) *n*-BuLi/THF -78 °C b) I_2 -78 °C – RT (iii) a) BBr_3/DCM b) AcCl

(iv) KOH /MeOH (v) $Br(CH_2)_2CN$, K_2CO_3 / DMF (vi) TMSA, $Pd[PPh_3]_2Cl_2$, CuI, TEA / THF

(vii) K_2CO_3 / DCM:MeOH

Scheme 1. Synthetic protocols for the terminal alkyne building block **8**.

Moreover, we have now improved and considerably shortened the synthesis of **8** from **1** in 3 steps shown in Scheme 2. 4-Bromothiophenol was reacted with bromopropionitile and base to give cyanoethyl-protected product **9** in 94 % yield. Then, Sonogashira reaction of compound **9** with TMSA under standard conditions with triphenylphosphine as a co-ligand gave silyl-protected alkyne **7** in 87% yield. Finally, removal of TMS with the same method as used previously gave product **8**. This procedure was conveniently carried out to give ca. 7 g batches of **8** in an overall yield from **1** of 72%

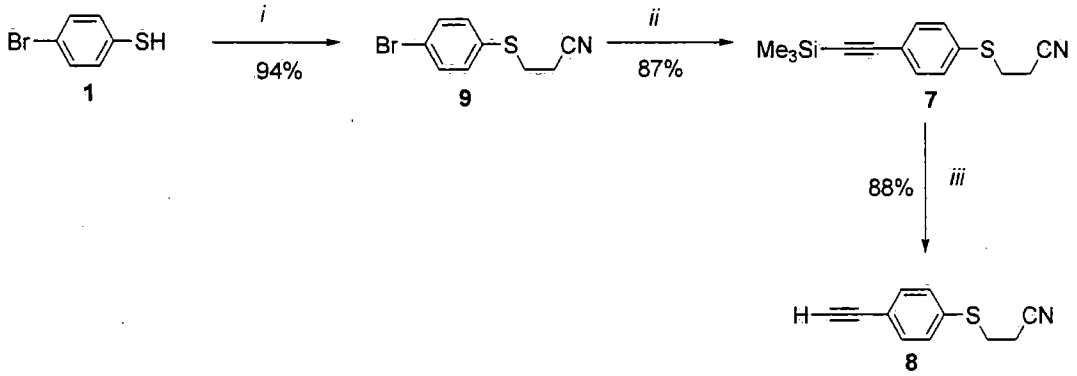

(i) $Br(CH_2)_2CN$, K_2CO_3 / DMF (ii) TMSA, $Pd[PPh_3]_2Cl_2$, PPh_3, CuI, TEA / THF

(iii) K_2CO_3 / DCM:MeOH

Scheme 2. New synthetic route to the building block **8**.

The synthesis of *meta*-protected thiol terminal alkyne (13)

Reagent **13** was needed for the synthesis of OPE derivatives with a *meta*-phenylthiol terminal substituent, e.g. compound **50** (**RJ 39**), rather than the usual *para*-isomer **8**. We have found that the palladium(0) reagent $Pd[PPh_3]_4$ increases the reactivity in the Sonogashira step compared to the palladium(II) reagent $Pd[PPh_3]_3Cl_2$. For this reason, the synthesis of **13** in Scheme 3 used $Pd[PPh_3]_4$ as the catalyst.

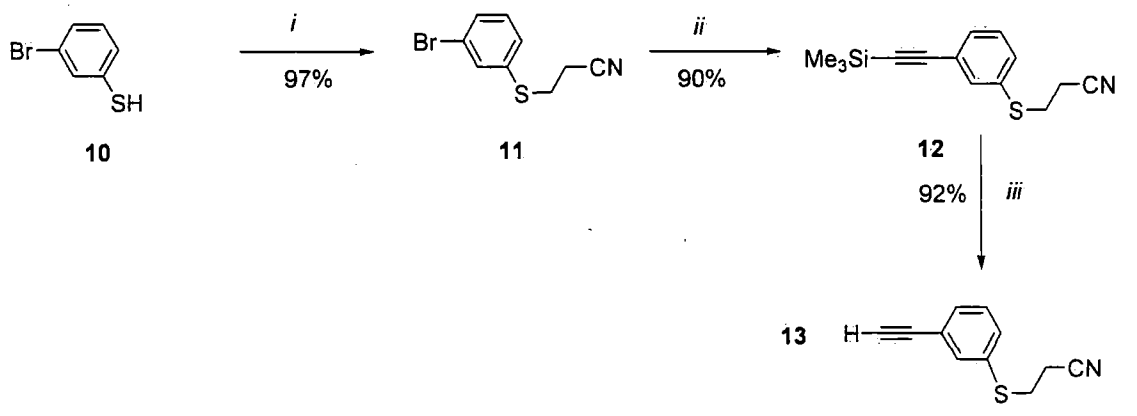

(i) $Br(CH_2)_2CN$, K_2CO_3 / DMF (ii) TMSA, $Pd[PPh_3]_4$, CuI, TEA / THF

(iii) K_2CO_3 / DCM:MeOH

Scheme 3. The synthesis of the *meta* terminal buiding block **13**.

The synthesis of 1,4–diiodoarene reagents

The diiodoarenes needed for our target OPEs are shown in Figure 17. Some of them are commercially available, specifically, the benzene, thiophene, fluorene and pyridine derivatives. Others are known in literature, e.g. **16**,[117] **37**,[78] **19**,[118] **33**[119] and **36**.[120] However, **20** and **21** are new compounds for which the synthetic methods are summarised below.

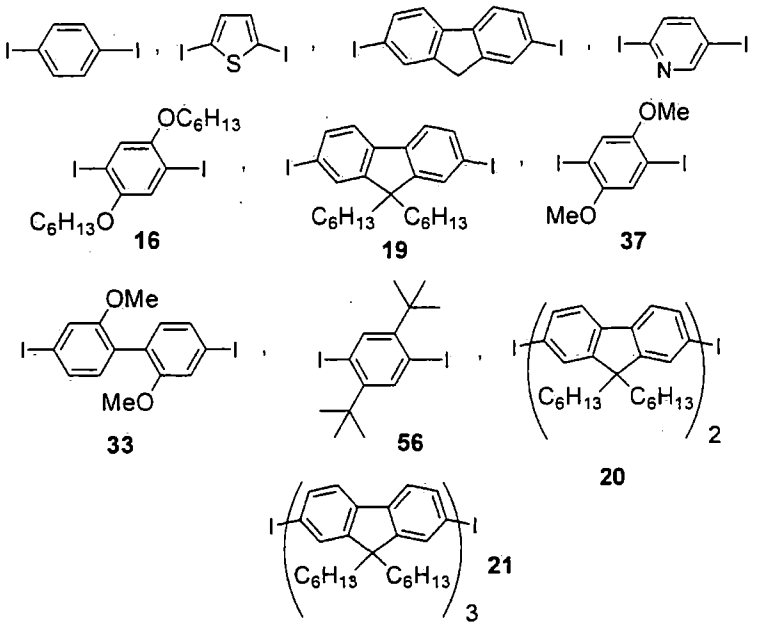

Figure 17. The structures of diiodoaryl compounds.

The synthesis of diiodo-bisfluorene (**20**)

Compound **20** was synthesised from known starting material **24** which was available in our laboratory.[121] The route started from dibromo-fluorene **22**. One bromine was changed to trimethylsilyl by trapping the mono-lithio derivative with trimethylsilyl chloride. Then the other bromine was changed to a boronic acid group **24** for Suzuki reaction in the next step. Bis(trimethylsilyl)fluorene **25** was obtained by reaction of **24** with **23** and **25** was then reacted with ICl in dichloromethane, as shown in Scheme 4, to get the desired product **20**.

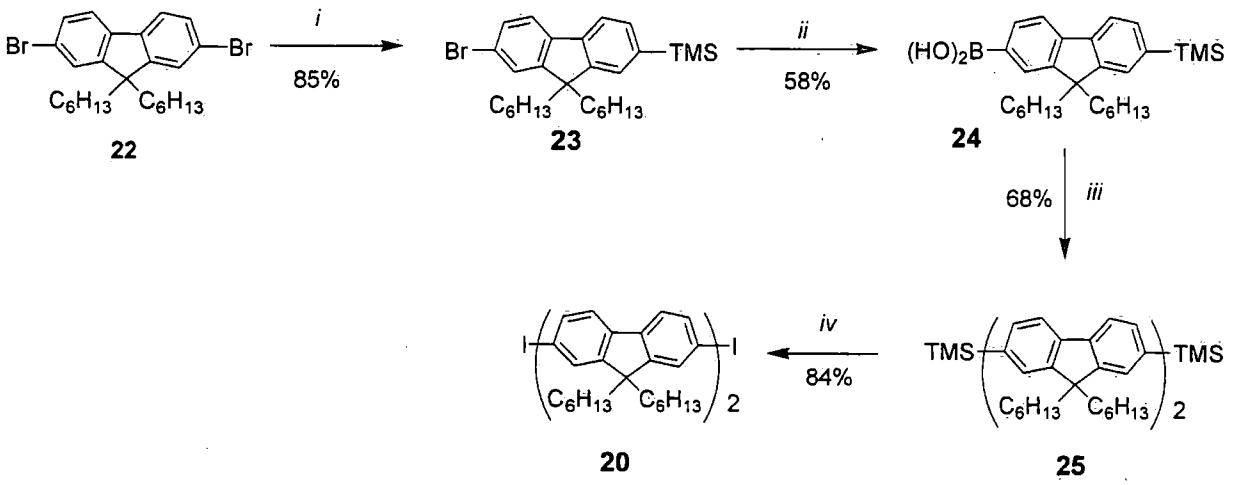

(i) a) n-BuLi/THF, b) TMSCl (ii) a) *n*-BuLi/THF, b) $B(iPrO)_3$ (iii) **23**, $Pd(PPh_3)_4$, 2 M $NaCO_3$, toluene (iv) ICl, DCM

Scheme 4. Synthesis of diiodo-bisfluorene (**20**).

The synthesis of diiodo-trisfluorene (**21**)

In the case of the trifluorene reagent **21**, we started with the same precursor **22**. The standard Suzuki coupling reaction between known diboronic acid **26**[122] and 2 equivalents of **23** gave a 3-fluorene chain molecule **27** with trimethylsilyl units at both ends. Finally, conversion of TMS to I with ICl formed the diiodo target product **21** in good yield (70 %).

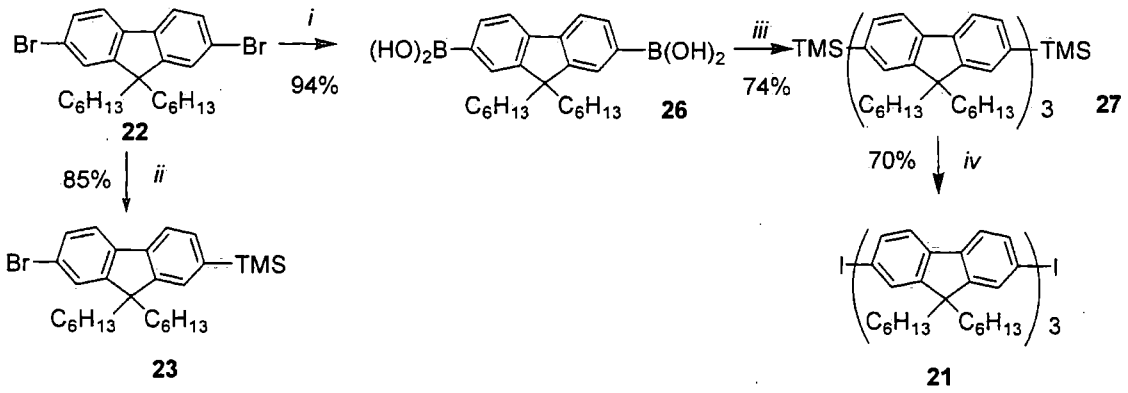

(i) a) n-BuLi/THF, b) $B(iPrO)_3$ (ii) a) n-BuLi/THF, b) TMSCl (iii) **23**, $Pd(PPh_3)_4$, 2 M $NaCO_3$/toluene (iv) ICl/DCM

Scheme 5. Synthesis of diiodo-trisfluorene (**21**).

The synthesis of twisted biphenyl **30**, **33** and **RJ 32**

The synthesis of twisted biphenyl derivatives (Scheme 6) started from commercial 3-methoxynitrobenzene **28**, which is reported in the literature for the synthesis of **33**.[119] With slight modification, the procedure involved reduction and dimerisation in one-pot to form diamine **29**. Next the iodo substituents were introduced into the molecule by a diazotisation reaction and then converted to the target product **33**. With the diamine **29** in hand, we also synthesized dibromo derivative **30** which was characterised by its single X-ray structure shown in Scheme 6. From **29**, the twisted molecule **RJ 32** (without an alkyne unit) was also created to study its conductance in comparison to its biphenyl and fluorene (i.e. planar) analogues. Compound **30** was synthesised as a possible alternative precursor to **RJ 32** but was not needed. Moreover, compound **33** was used to synthesise a twisted OAE derivative (see Table 1).

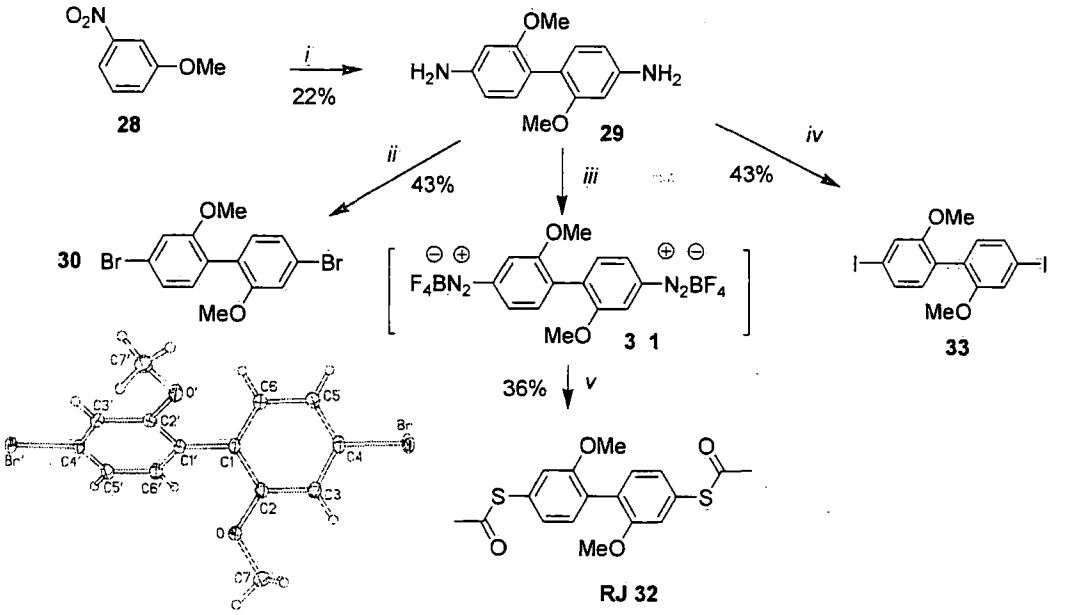

i) $NaBH_4$, DMSO, 110 °C then HCl (*ii*) $NaNO_2$, HBr then CuBr (*iii*) $NaNO_2$, HBr then $NaBF_4$ (*iv*) $NaNO_2$, HCl then KI (*v*) $KSCOCH_3$, DMSO

Scheme 6. The synthesis of dimethoxybiphenyl derivatives and X-ray molecular structure of **30** (biphenyl dihedral angle = 57°).

Synthesis of protected thiol terminated OAEs

The general Sonogashira reaction of building block **8** and various diiodo-arenes under standard Sonogashira conditions, namely $Pd[PPh_3]_2Cl_2$, CuI, and mixed TEA:THF as the solvent, is shown in Scheme 7. Moderate to good yields of OAE products are shown in Table 1. The mono-substituted product was usefully isolated in low yield.

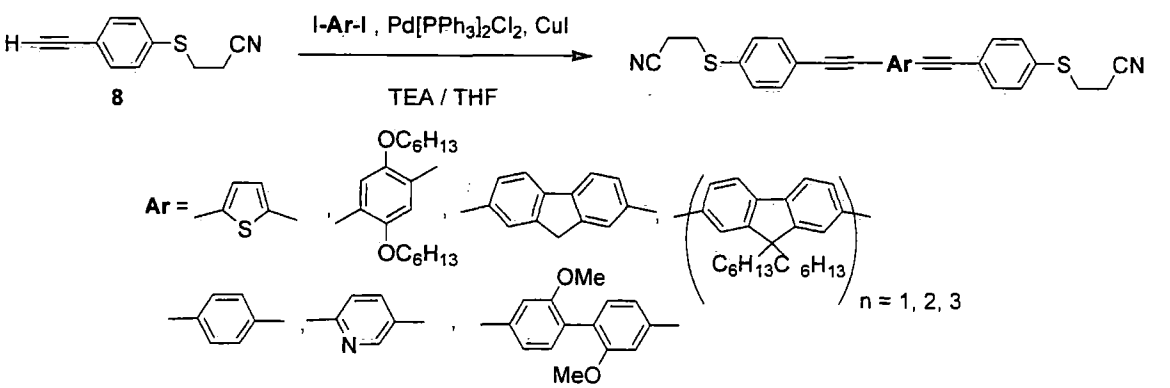

Scheme 7. The synthesis of thiol-protected OAE derivatives.

Table 1. Summary of the synthesis of new oligo(arylenethynylene)s

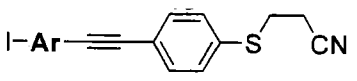

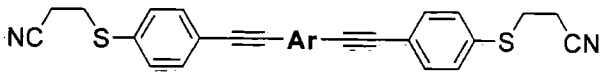

mono-substituent di-substituent

Ar	yield	
	mono-substituent	di-substituent
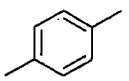	-	87 % **63 (RJ 16)**
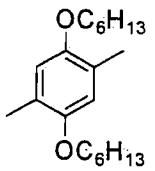	4 % **34**	88 % **35 (RJ 8)**
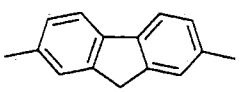	7 % **36**	90 % **37 (RJ 9)**
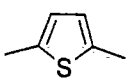	6 % **38**	90 % **39 (RJ 10)**
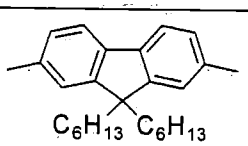	13 % **40**	63 % **41 (RJ 11)**
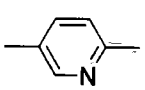	9 % **42**	88 % **43 (RJ 12)**
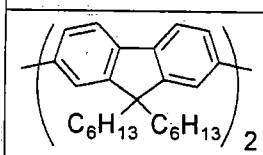	17 % **44**	62 % **45 (RJ 13)**
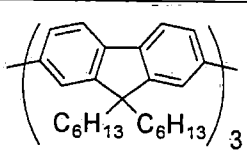	28 % **46**	59 % **47 (RJ 14)**
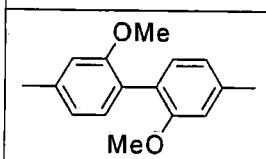	-	90 % **49 (RJ 17)**

The same method was applied to synthesise the *meta* linked OPE **50** (**RJ 39**) in good yield. The molecular structure of **50** (**RJ 39**) was confirmed by single crystal X-ray diffraction as depicted in Figure 18 and crystal packing shown in Figure 19.

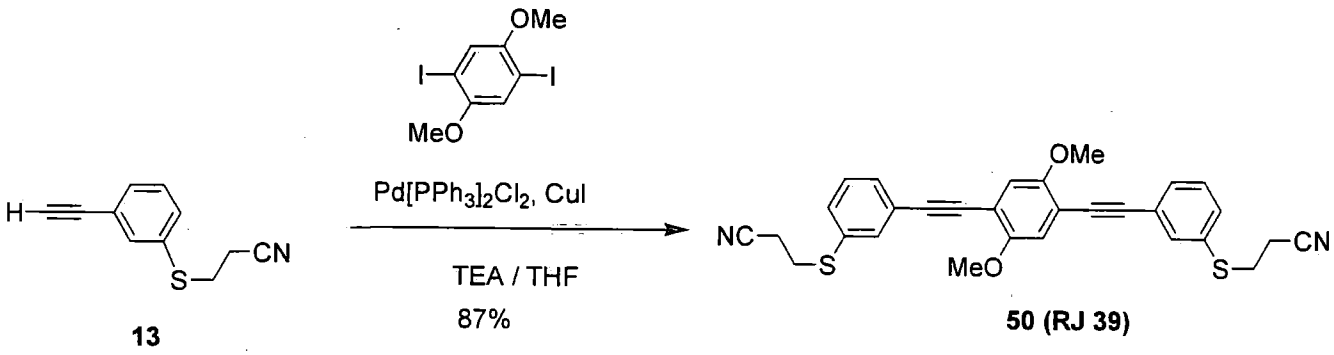

Scheme 8. The synthesis of *meta* linked OPE; **50** (**RJ 39**).

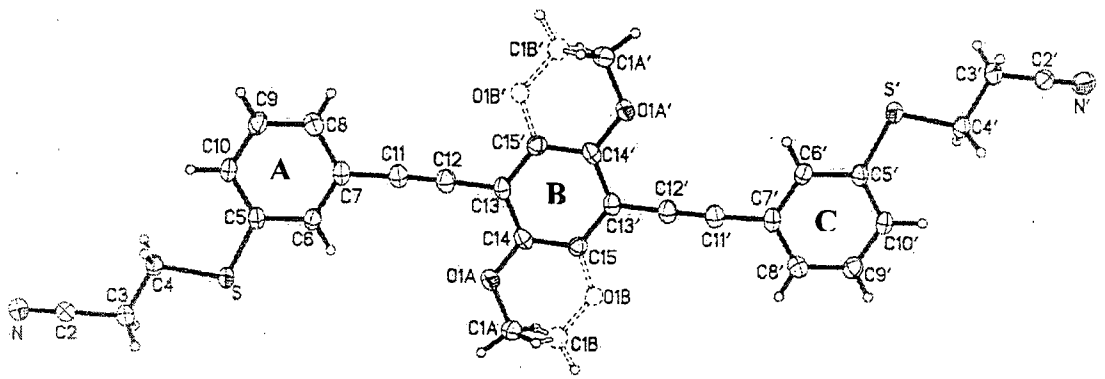

Figure 18. The molecu lar structure of **50** (**RJ 39**). Bond distances S...S′ =17.3 Å, dihedral angle of **A**, **B** rings and **B**, **C** rings = 1.5 °.

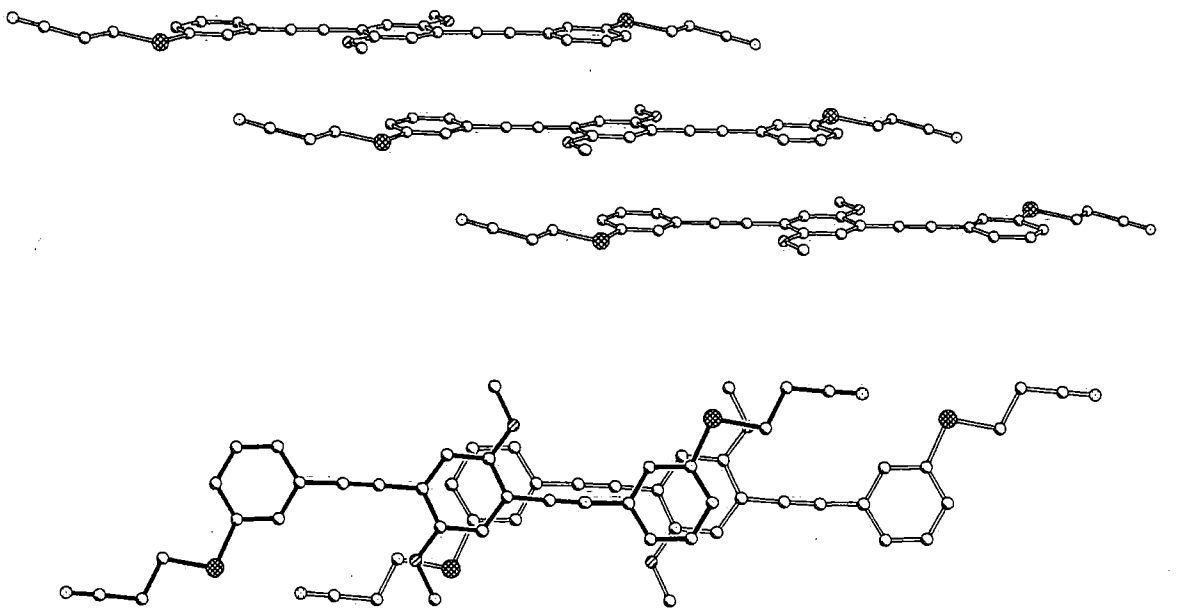

Figure 19. Crystal packing of **50** (**RJ 39**), plane-centroid distance 3.57 and 3.60 Å, centroid-centroid distance 3.74 Å.

Synthesis of bulky OPEs **53** (**RJ 40**) and **51** (**RJ 41**)

One equivalent of building block **8** in the Sonogashira reaction with diiodo reagent **56** gave **52** as the major product (35% yield), alongside the minor product **51** (**RJ 41**) (16% yield). Then compound **52** was coupled with phenylacetylene to get the target product **53** (**RJ 40**). The synthetic pathway is shown in Scheme 9. The single crystal X-ray structure of **51** (**RJ 41**) is shown in Figure 20.

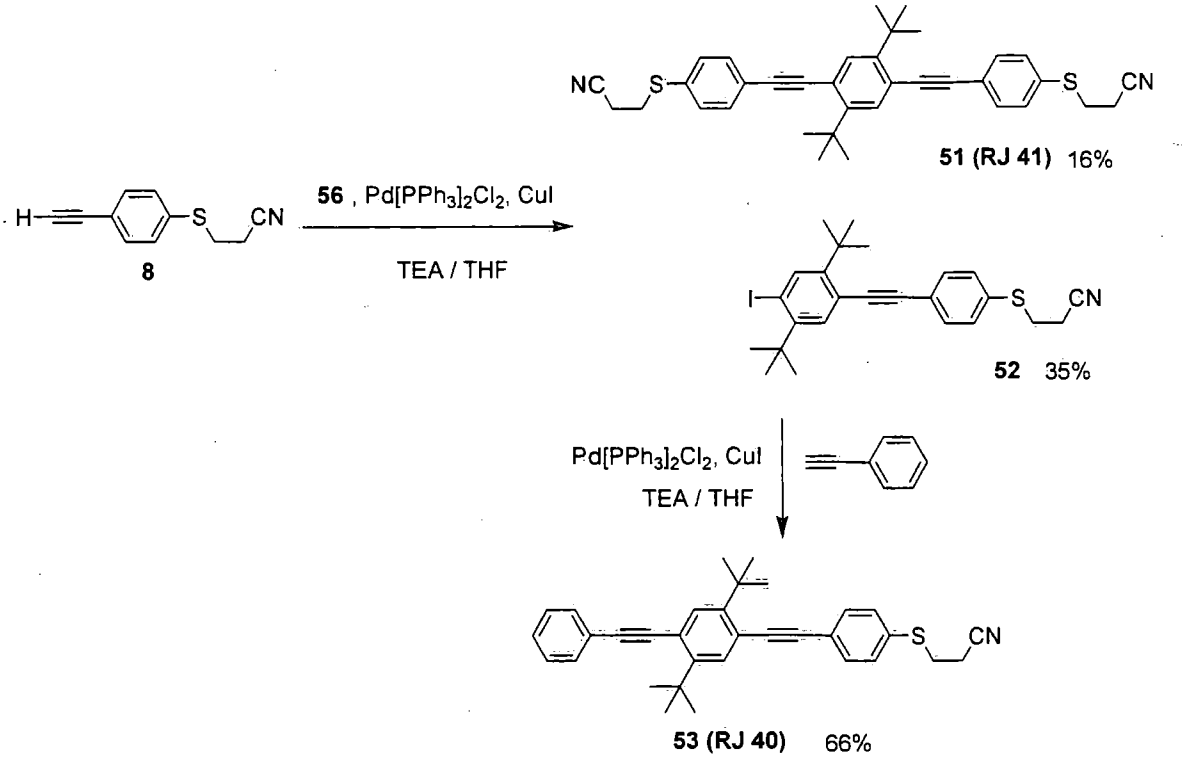

Scheme 9. The synthesis of mono and bis terminal protected thiol OPEs **53** (**RJ 40**) and **51** (**RJ 41**).

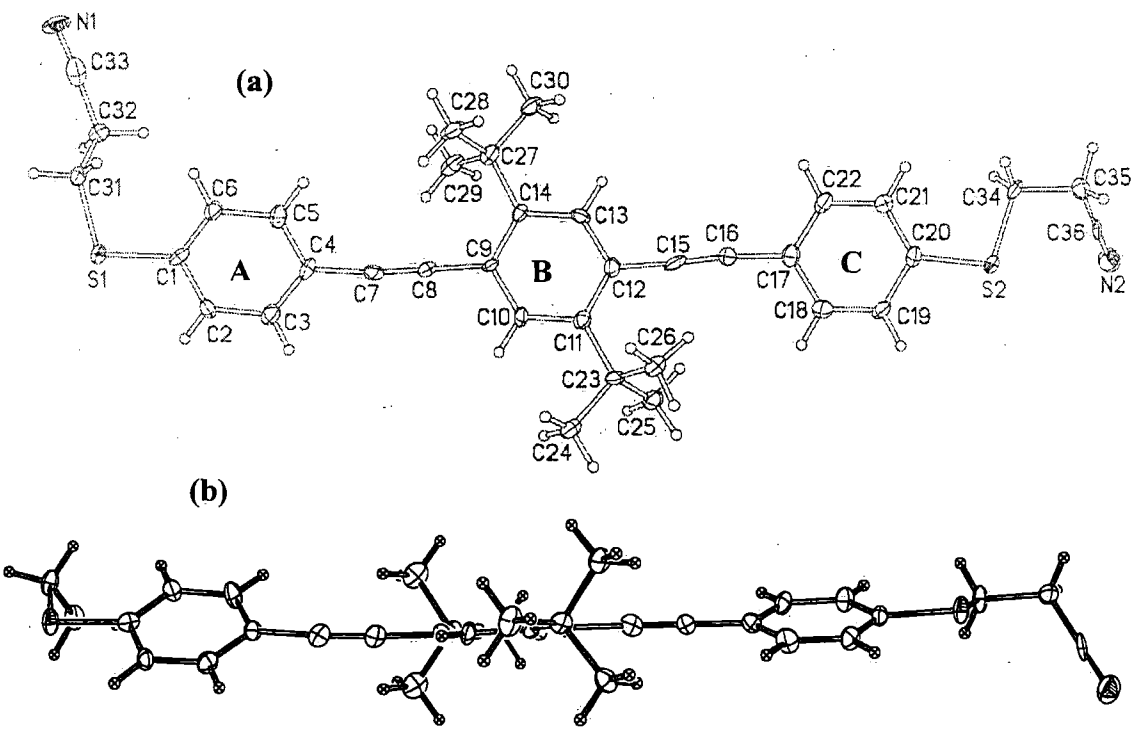

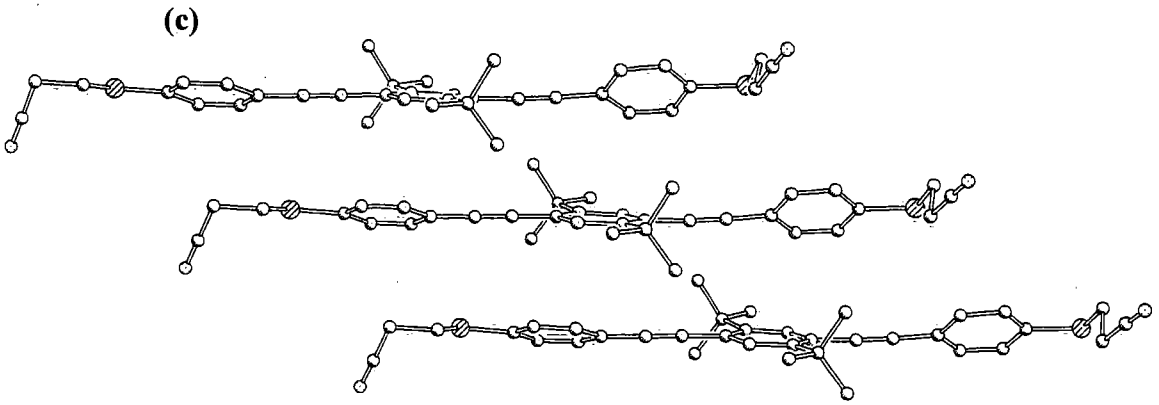

Figure 20. The molecular structure of **51** (**RJ 41**) (a) top view onto central ring **B** (b) side view (c) molecular packing. Bond distances S...S' = 20 Å, dihedral angle of **A**, **B** rings = 39 ° and **B**, **C** rings = 20 °, centroid-centroid distance 4.42 and 4.08, centroid-plane distance 4.20 and 3.86 Å.

The synthesis of diphenyl mono- and di-yne derivatives with protected thiols

A common side-product of Sonogashira reactions of **8** was the oxidative dimerisation of the terminal alkyne to give butadiyne derivative **54**.

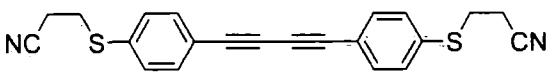

54

We decided to make an analogue of **54** with one triple bond to compare their electronic properties. Accordingly, cross-coupling building block **8** with iodobenzene **6** gave mono-akyne **55** with terminal cyanoethyl groups.

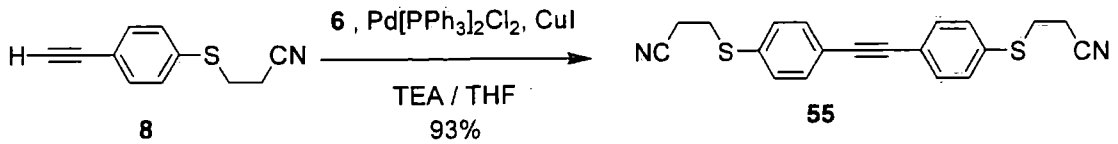

8 **55**

Scheme 10. The synthesis of mono-alkyne **55**.

A preliminary single crystal X-ray structure of compound **55** is shown in Figure 21.

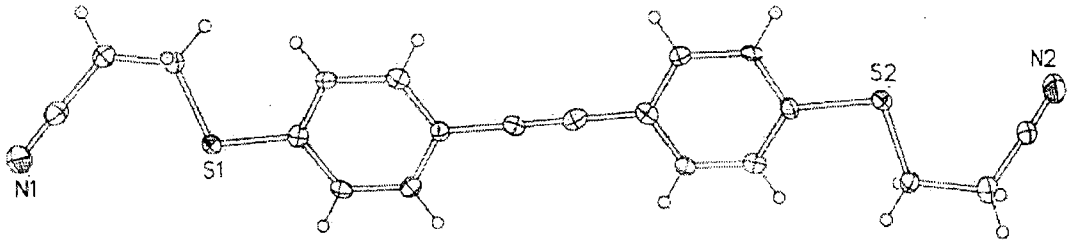

Figure 21. The molecular structure of **55**. Bond distances S…S′ = 13.2 Å, dihedral angle between the two phenyl rings = 3.58 °

The conversions of cyanoethyl to acetyl protecting groups

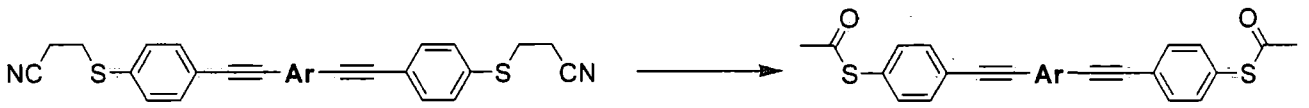

The cyanoethyl protecting group, which served as a stable protected thiol in the synthetic schemes, was readily converted into the acetyl group which is generally preferred by our collaborators for self-assembly prior to conductance studies.

The cyanoethyl protecting groups can be easily converted in a one-pot reaction to acetyl groups as shown in the conversion of **35** (**RJ 8**) to **57** (**RJ 8Ac**) in 70% yield. **57** (**RJ 8Ac**) gave single crystals suitable for X-ray analysis and the structure is shown in Figure 22 and crystal packing in Figure 23.

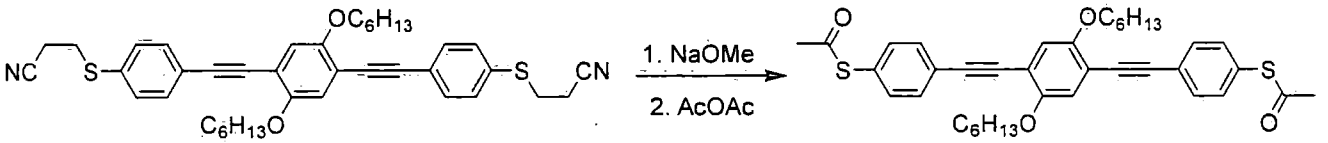

RJ 8 **57 (RJ 8Ac)** 70%

Scheme 11. The conversion of the cyanoethyl protecting groups of **35** (**RJ 8**) to yield **57** (**RJ 8Ac**).

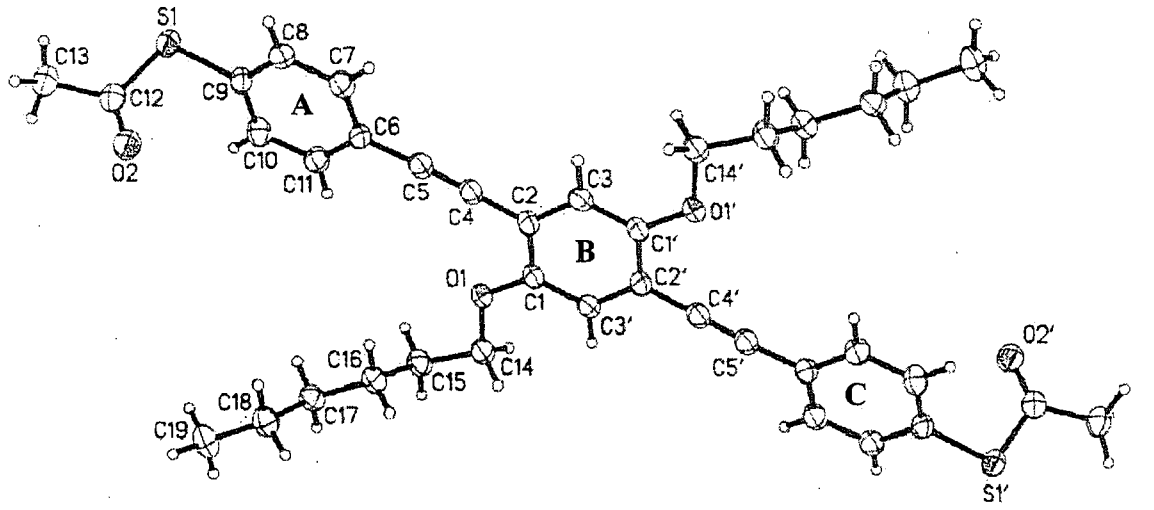

Figure 22. The molecular structure of **57** (**RJ 8Ac**). Bond distances S...S′ = 20 Å, dihedral angle of **A**, **B** rings and **B**, **C** rings = 11 °.

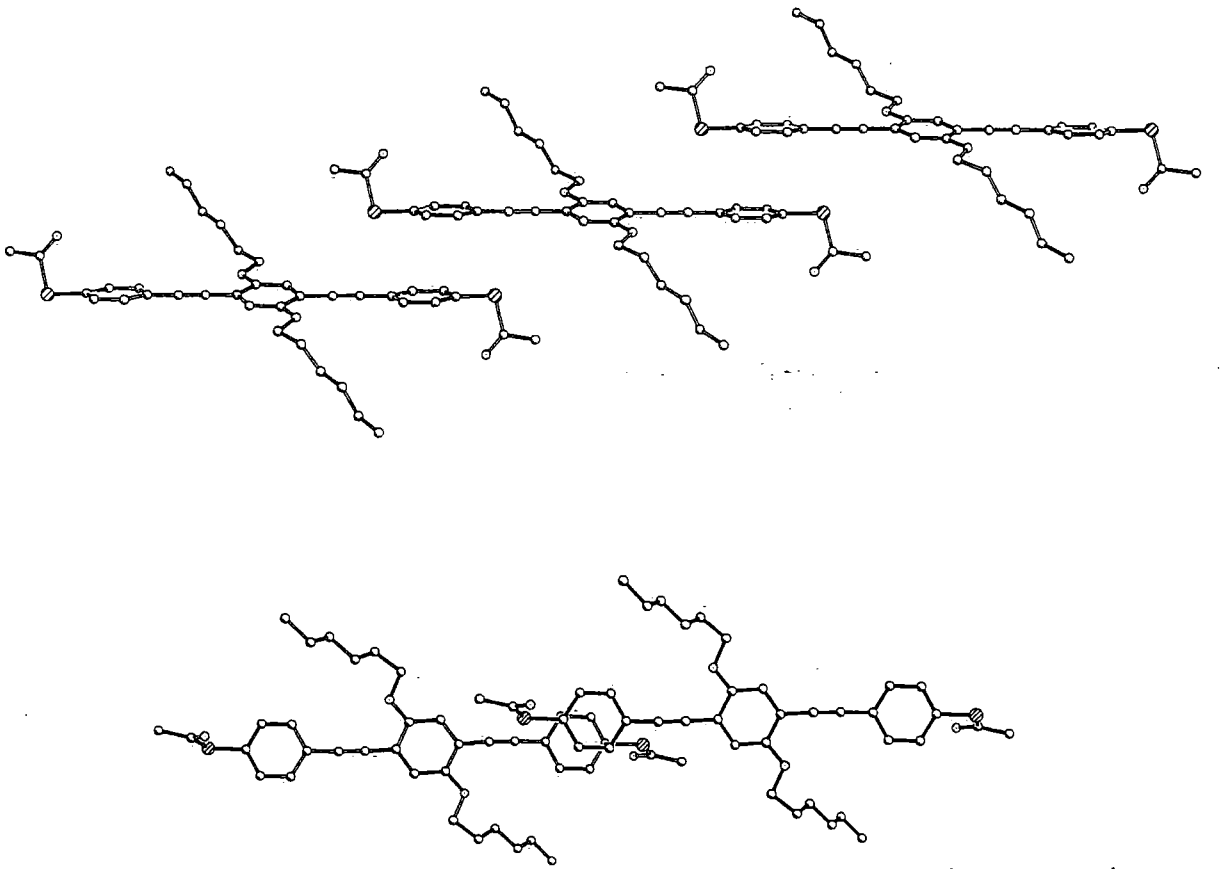

Figure 23. Crystal packing of **57** (**RJ 8Ac**) terminal rings parallel; interplanar separations 3.70 Å, centroid-centroid distance 3.86 Å.

Similarly, both **53** (**RJ 40**) and **51** (**RJ 41**) were converted to their acetyl analogues **59** (**RJ 40Ac**) and **58** (**RJ 41Ac**) in 90 and 97 % yields, respectively.

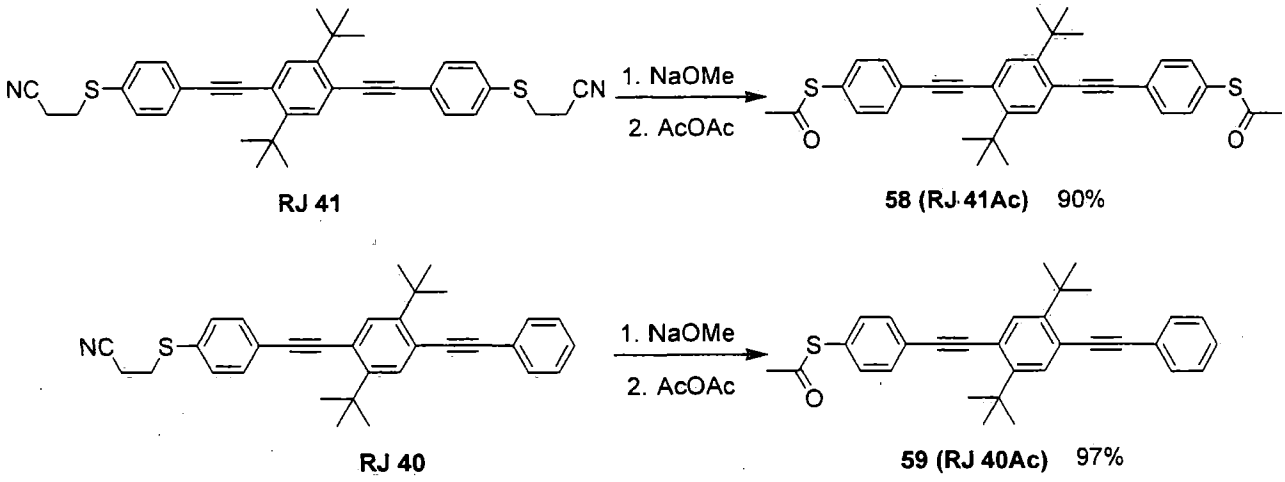

Scheme 12. The conversions of the protecting groups of **53** (**RJ 40**) and **51** (**RJ 41**) to **58** (**RJ 41Ac**) and **59** (**RJ 40Ac**).

Figure 24 shows the single-crystal structure of mono-thioacetyl derivative **59** (**RJ 40Ac**) which was obtained by X-ray analysis.

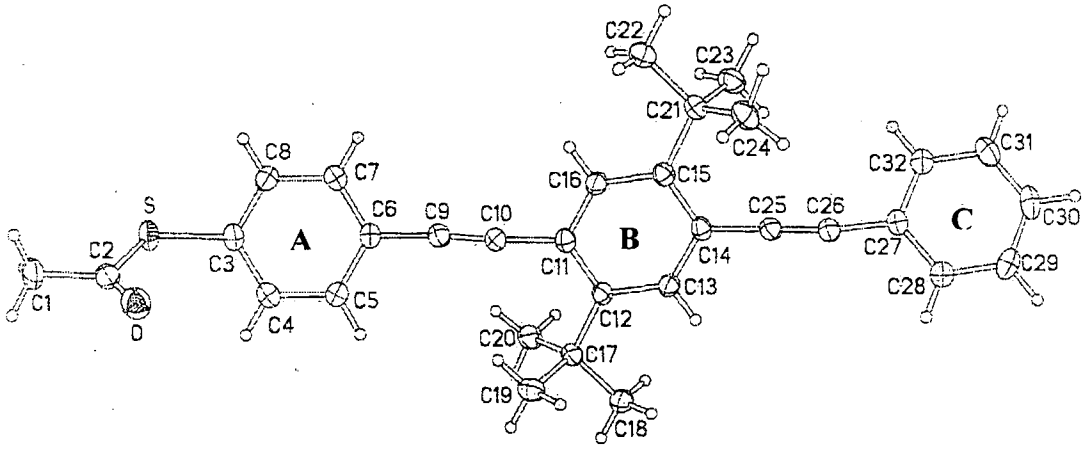

Figure 24. The molecular structure of **59** (**RJ 40Ac**). Dihedral angle of **A**, **B** rings = 20 ° and **B**, **C** rings = 32°.

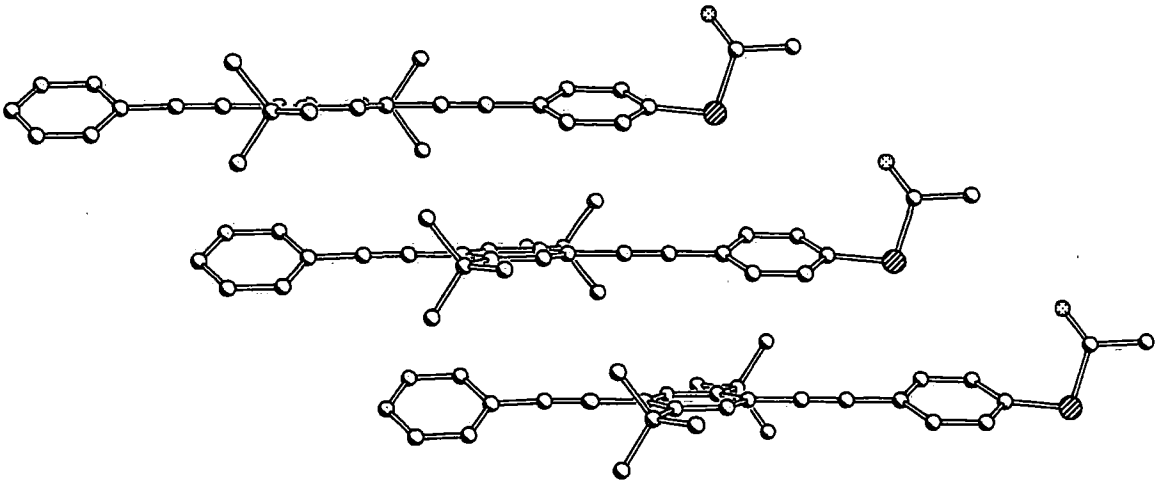

Figure 25. Crystal packing of **59** (**RJ 40Ac**), centroid-centroid distance 4.45 and 4.52, interplanar separation between parallel central rings 3.93 Å.

Not only strongly basic sodium methoxide but also the more weakly basic tetrabutylammonium hydroxide (TBAOH) can deprotect the cyanoethyl group, as shown in Scheme 13. TBAOH was chosen for **38** due to the possible sensitivity of the butadiyne unit. Then, acetylation by acetic anhydride afforded diacetyl protected product **60**.

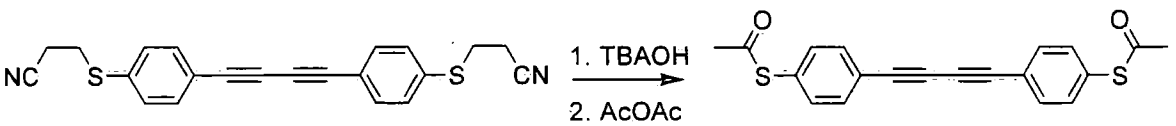

38 **60** 82%

Scheme 13. The conversions of the cyanoethyl protecting groups of **38**.

Similarly, mono-alkyne **39** was converted to **61** (Scheme 14).

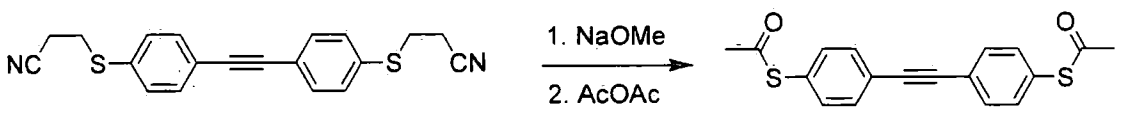

39 **61** 92%

Scheme 14. The conversions of the cyanoethyl protecting groups of **39**.

For **RJ12** the conversion of the cyanoethyl protecting groups to give **62** (**RJ 12Ac**) worked well when using CsOH as a base. Using NaOMe as base on several occasions unexpectedly resulted in unreacted starting material and no **62** (**RJ 12Ac**) was detected by NMR analysis of the reaction mixture.

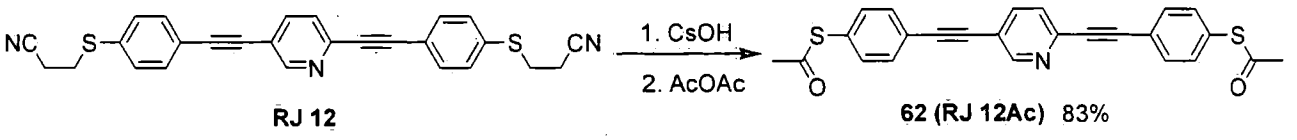

RJ 12 **62 (RJ 12Ac)** 83%

Scheme 15. The conversion of the cyanoethyl protecting groups of **43** (**RJ 12**).

Absorption and emission spectra of new oligo(1,4-aryleneethynylene)s

The absorption and emission spectra of the OAEs in DCM solution at room temperature are summarised in Table 2.

Table 2. Summary of absorption and emission of oligo(aryleneethynylene)s

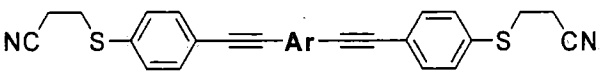

Code	Ar	λ_{max} (nm) in DCM	
		absorption	emission
35 (RJ 8)	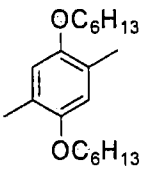	325, 380	413
37 (RJ 9)	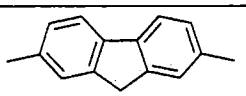	358	384
39 (RJ 10)	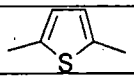	362	403
41 (RJ 11)	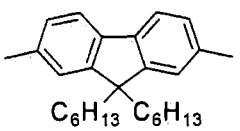	364	404
43 (RJ 12)	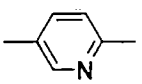	345	400

45 (RJ 13)	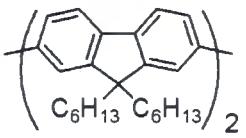	371	407
47 (RJ 14)	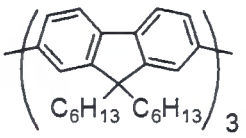	378	414
49 (RJ 17)	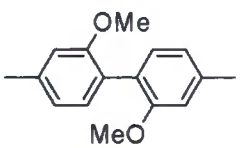	333	388

All the OAEs show an absorption band in the UV region between 333-380 nm. Interestingly, the λ_{max} absorption data of **35** (**RJ 8**) and **49** (**RJ 17**) are 380 and 333 nm, respectively. It can be explained that **49** (**RJ 17**) shows less π-conjugation than **35** (**RJ 8**) because of the twisted biphenyl ring core. The fluorene derivatives **37** (**RJ 9**) and **41** (**RJ 11**) with planarised biphenyl cores have λ_{max} 358 and 364, respectively, i.e. red shifted compared to **49** (**RJ 17**). The spectra of **35** (**RJ 8**) and **49** (**RJ 17**) are shown in Figure 26.

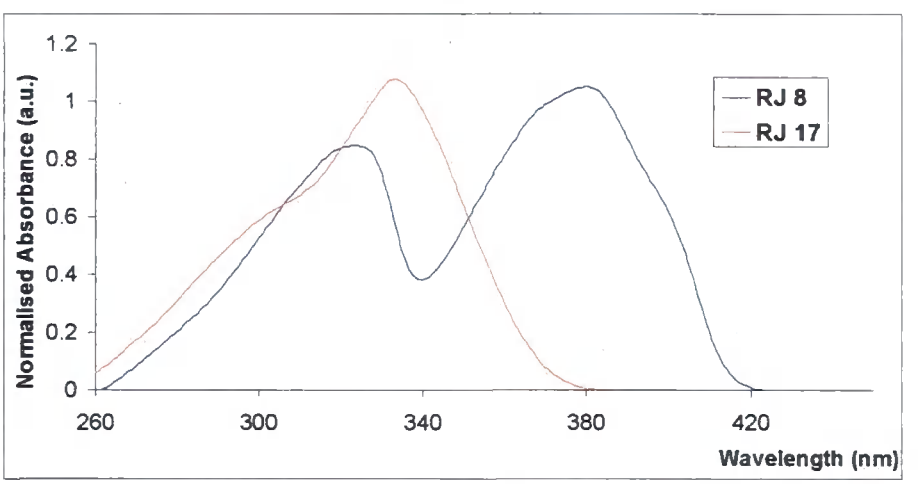

Figure 26. The UV-Vis absorption spectra of **35** (**RJ 8**) and **49** (**RJ 17**) in DCM solution.

A sequential red shift has been found with increasing the number of fluorene units from 1, 2 to 3 (**41** (**RJ 11**), **45** (**RJ 13**) and **47** (**RJ 14**)) with the λ_{max} absorptions at 364,

371 and 378 nm, respectively (Figure 27). This is consistent with extended conjugation through the longer molecules.

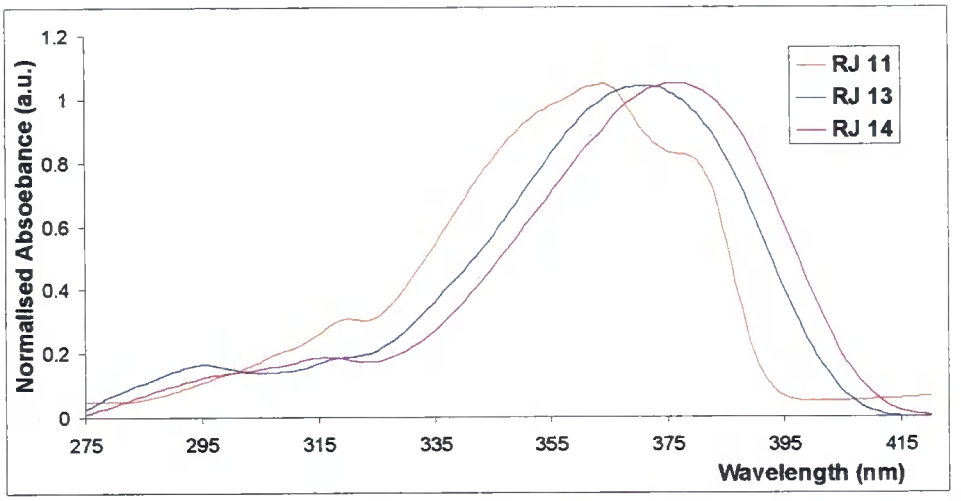

Figure 27. The UV-Vis absorption spectra of **41 (RJ 11)**, **45 (RJ 13)** and **47 (RJ 14)** in DCM solution.

The reason for synthesising the OAE derivatives reported in this thesis was to study their self-assembly and conductance properties. For this aspect of the work many of the compounds have been supplied to Professor G. J. Ashwell at Bangor University or to Professor R. J. Nichols at Liverpool University. Representative STM data obtained by workers in these laboratories are presented below. These data illustrate that our molecules are suitable for these characterisation studies.

The study of OAEs with scanning tunnelling microscopy (STM) techniques at Bangor University

The self assembled monolayers (SAMs) of OPE derivative **35 (RJ 8)** (Figure 28) were fabricated by immersing gold-coated substrates in a tetrahydrofuran solution of **35 (RJ 8)** (0.1 mg cm^{-3}) to which sodium methoxide was added to facilitate removal of the cyanoethyl group(s). Substrates were repeatedly immersed for 15 min intervals and washed each time with THF to remove physisorbed material from the surface. Throughout this process, self-assembly was monitored from the frequency change for deposition on gold-coated 10 MHz quartz crystals, which prior to use were washed with

chloroform, methanol and water and then plasma cleaned. The frequency saturated to a constant value after ca. 300 min and a Sauerbrey analysis of the data provided a mean area of ca. 0.58 nm^2 $molecule^{-1}$ for the chemisorbed wire (Figure 29a). Essentially identical data were obtained in the absence of deprotecting agent, showing that the cyanoethyl group deprotects readily in the presence of gold, as observed previously for thioacetates.[115] The SAMs on gold-coated highly oriented pyrolytic graphite (HOPG) were investigated by scanning tunnelling microscopy (STM) and scanning tunnelling spectroscopy (STS) using a gold tip. Significantly, SAMs for the most part exhibited symmetrical *I–V* characteristics (Figure 29b). Using the *I(t)* technique, the SAMs of **35** (**RJ 8**) showed a current jump of ca. 0.2-0.3 nA (Figure 29c) ascribed to a single molecule between the Au substrate and the Au tip. A histogram plot of the observed current jumps from ca. 100 experiments is shown in Figure 29d.

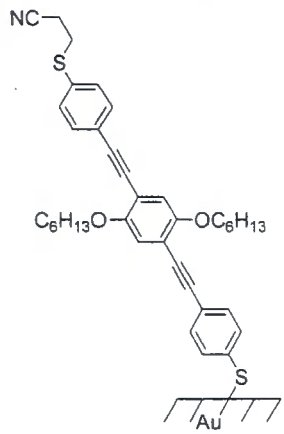

Figure 28. Molecular wire structure of **35** (**RJ 8**) with the terminal sulfur retaining the cyanoethyl group intact when assembled without the deprotecting agent.

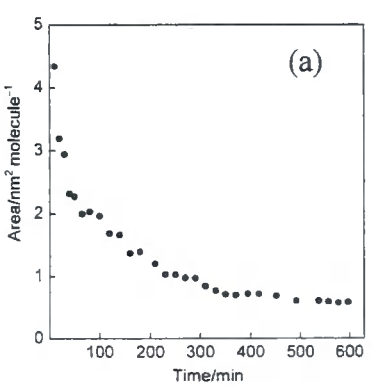

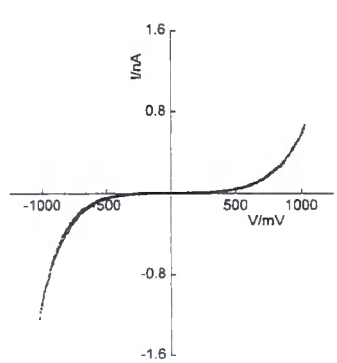

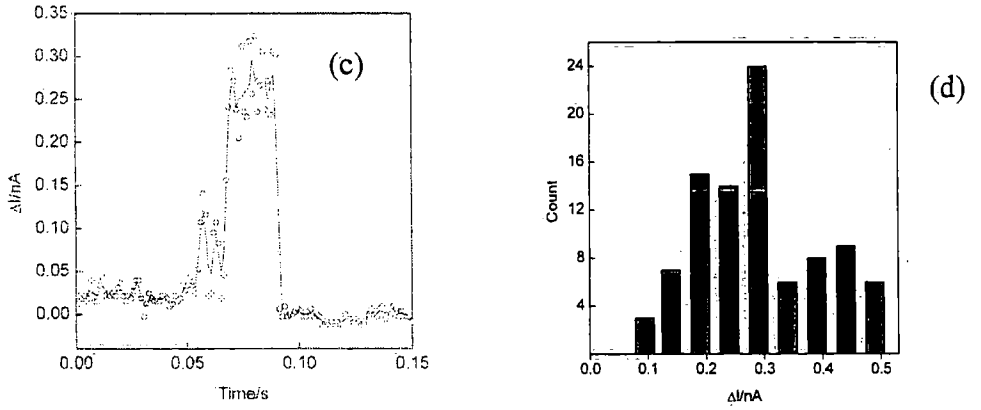

Figure 29. (a) Variation of the mean molecular area with the combined period of self-assembly of **35** (**RJ 8**). (b) Symmetical *I–V* characteristics of the Au–**35** (**RJ 8**) structure contacted by a Au probe. (c) The SAMs of **35** (**RJ 8**) show current jumps of ca. 0.2-0.3 nA. (d) Histogram of the observed current jumps with a notable grouping at 0.2-0.3 nA. Data obtained at a set point current of 300 mV.

Data for **41** (**RJ 11**), **43** (**RJ 12**) and **47** (**RJ 14**) obtained by analogous STM techniques are summarised in Table 3. The Sauerbrey analysis (density on the gold surface) show that **47** (**RJ 14**) is the biggest and **35** (**RJ 8**) is the smallest OPE in this series. Symmetrical *I-V* characteristics have been obtained from all OPEs; **41** (**RJ 11**), **43** (**RJ 12**) and **47** (**RJ 14**) as expected for symmetrical wire-like molecules located between gold contacts. SAMs were also investigated by the "current-jump" technique. Studies were performed with the gold probe located at a fixed height above the surface and as the current was monitored as a function of time. The results show that **41** (**RJ 11**) and **47** (**RJ 14**) have the same value current jump at 0.09 nA. This may be due to conformational effects of the molecule in the junction, or a different point of contact of the tip to the molecule, e.g. contacting the fluorene π-system rather than the terminal sulfur atom.

Table 3. Summary of the study of conducting OAEs by STM techniques

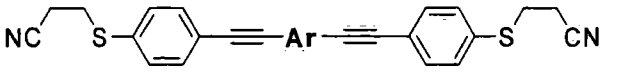

Code	Ar	density (nm^2 $molecule^{-1}$)	symmetrical *I/V*	current jump (nA)
35 (RJ 8)	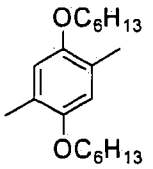	0.58	yes	0.3
41 (RJ 11)	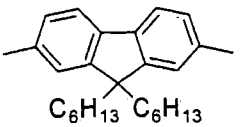	1.35	yes	0.09
43 (RJ 12)	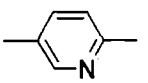	No data	yes	0.5, 1.0, 1.5
47 (RJ 14)	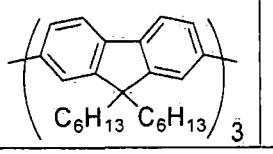	2.20	yes	0.09, 0.15

Pyridine derivative **43** (**RJ 12**) gave particularly interesting results. Most STM experiments show the single current jump at ca. 0.5 nA but about 5 % of experiments show a double current jump consistent with attachment of 1 and 2 molecules at ca. 0.5 and 1.0 nA. (Figure 30 a and b). Even a third molecule (triple jump: ca. 1.4-1.5 nA) is possibly seen in the gap in Figure 30c. This was observed on a few occasions – the cleanest data are shown. It is likely that this multiple bridging was due to a particular structure of the STM tip used on these occasions and not due to any intrinsic property of the molecule **43** (**RJ 12**). It was observed less frequently (and less cleanly) with other OAE derivatives. From these initial results it is not clear if all the data represent molecules really bridging the substrate and tip, or perhaps attached at only one site, with intermolecular π–π interactions between them. More experiments are in progress.

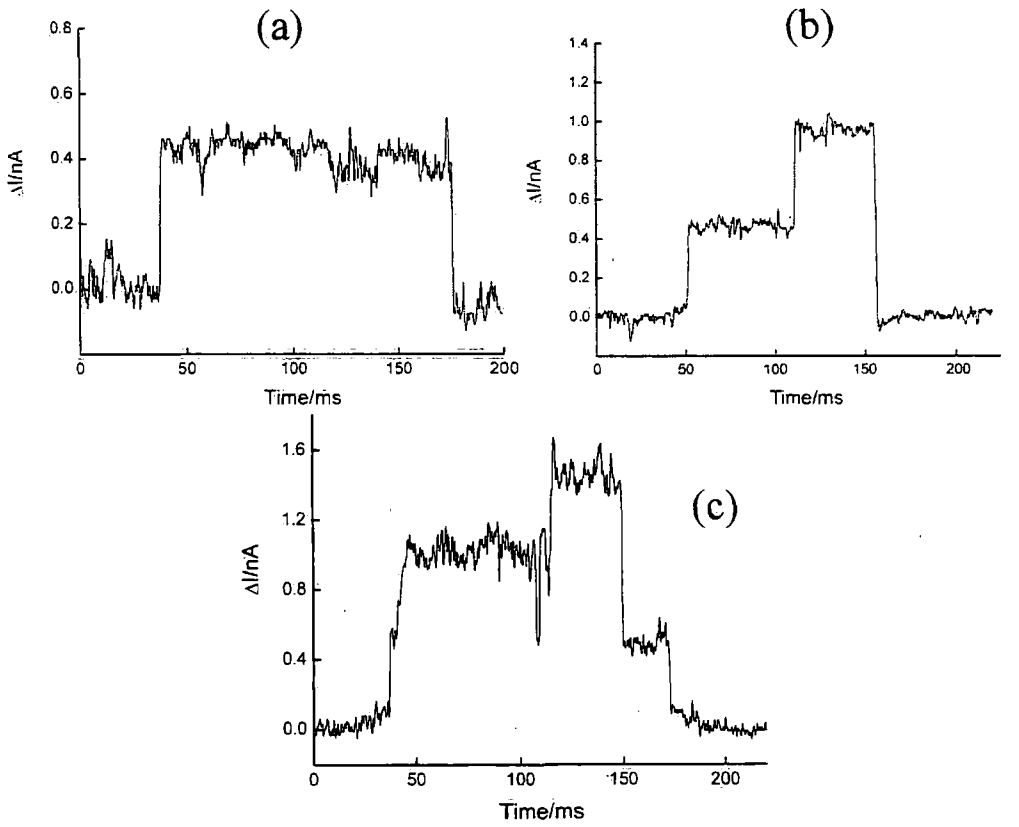

Figure 30. (a) the single current jump of ca. 0.5 nA (b) the double current jump showing ca. 0.5 and 1 nA from 1 and 2 molecules, respectively; (c) possibly a triple jump of **43** (**RJ 12**).

The study of conductivity with scanning tunnelling microscopy (STM) at Liverpool University.

RJ 32 was studied using *I*(*s*), *I*(*t*) and break junction (*BJ*) methods.

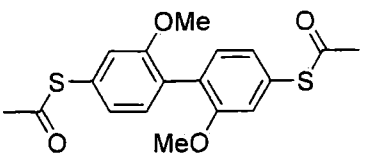

RJ 32

Firstly, Figure 31 shows the *BJ* result. Figure 31a shows the typical conductance scans recorded during the tip withdrawal. Figure 31b shows a linear representation of the current and Figure 31c a logarithmic representation of the conductance of the resulting histogram. These differing peaks have been assigned to different contact configurations

of the thiol head groups and the gold contacts. Three groups are defined as **A**, **B** and **C** which are not simple multiples of each other. On the other hand, $\mathbf{A_2}$ is double the current value of $\mathbf{A_1}$ and these sub-peaks ($\mathbf{A_1}/\mathbf{A_2}$, $\mathbf{B_1}/\mathbf{B_2}$ and $\mathbf{C_1}/\mathbf{C_2}$) have been attributed to one and two molecules in the junction, respectively.

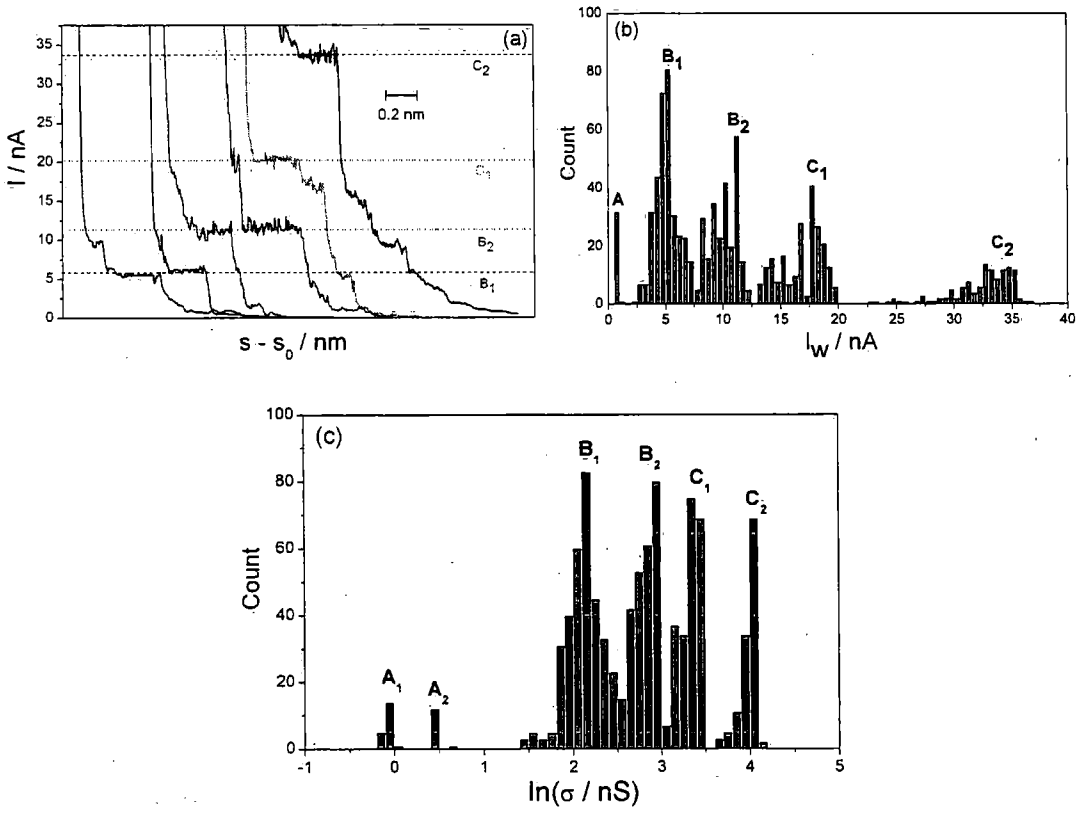

Figure 31. (a) Typical scans recorded during the tip withdrawal when compound **RJ 32** molecular junctions are formed and then broken at a bias voltage of 600 mV using the *BJ* method. (b) Histogram of current values constructed from 52 individual *BJ* scans for **RJ 32**. (c) A log scale conductance histogram using the data shown in b.

Secondly, Figure 32a shows example *I*(*s*) curves recorded for compound **RJ 32** where no contact between tip and surface was established prior to retraction (*I*(*s*) method). The resulting histograms (Figure 32b) differ from those of the *BJ* technique in that one group of peaks is favoured and is marked $\mathbf{A_1}$ (with a shoulder marked $\mathbf{A_2}$) in Figure 31b. Clearly the differing techniques (*BJ* and *I(s)* methods) favour differing current peaks, with the *BJ* technique giving a higher propensity to higher current peaks

(Groups **B** and **C** in Figure 31c), while the *I(s)* method favours the lower current **A** group of peaks. In the case of alkanedithiols these differences have been attributed to differing gold junction formations and Au-S contact configurations with the *BJ* technique likely to result in higher roughness following cleavage of the metallic junction. In the case of the *I(s)* technique it has been shown that upon increasing the step density of the gold substrate the **B** and **C** peaks increase in intensity relative to the **A** peaks. For rough substrates the **B/C** peaks predominate, consistent with the proposal that the *BJ* method favours contact to high defect density sites.

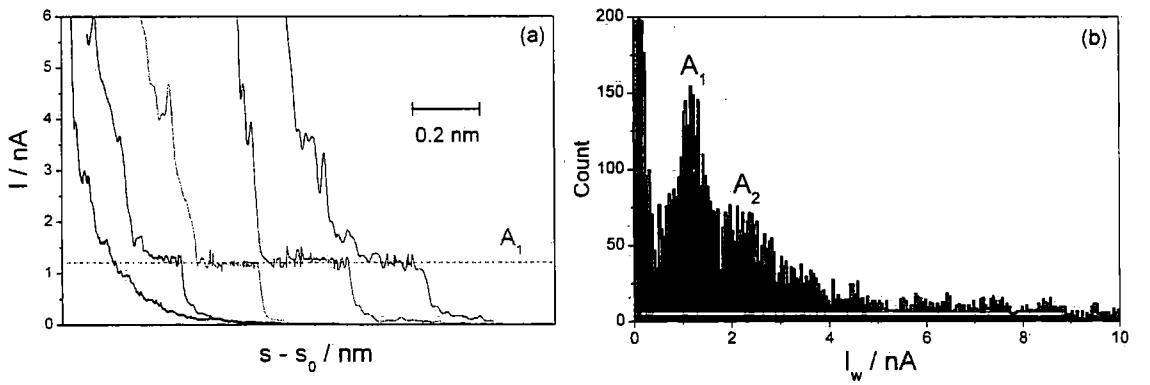

Figure 32. (a) Typical *I*(*s*) example scans performed for **RJ 32**. For clarity the coloured curves were stacked on the x-axis. (b) Corresponding histogram of current values constructed from 26 individual *I*(*s*) curves for **RJ 32**. I_0 = 10 nA, U_t = 600 mV.

Finally, Figure 33 shows results of the *I*(*t*) method for compound **RJ 32**. Clear up-and-down current jumps in Figure 33a are attributed to the attachment and detachment of thiol-linked molecular bridges between the gold tip and sample. Similar to the *I*(*s*) method, the low current jumps are favoured and classified as $\mathbf{A_1}$ and $\mathbf{A_2}$ in the histogram in Figure 33b.

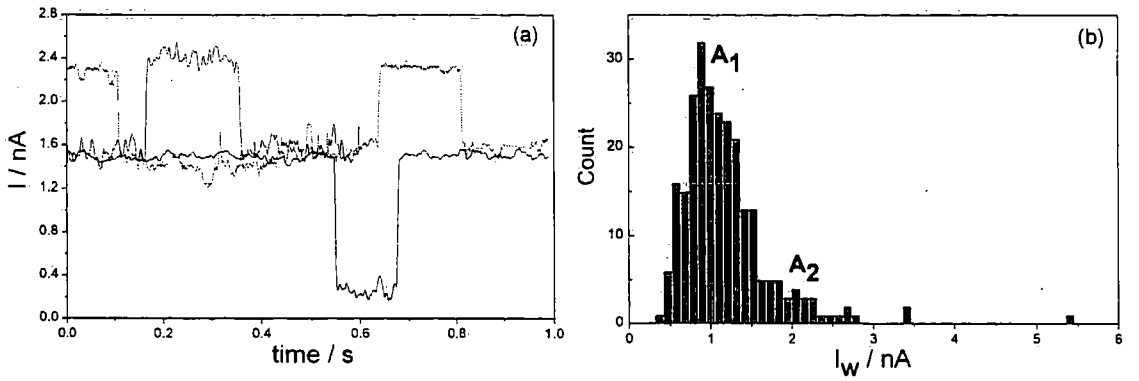

Figure 33. (a) *I(t)* method for compound **RJ 32** showing typical current jumps. The corresponding histogram constructed from 250 jumps with I_0 = 1.5 to 5 nA and U_t = 600 mV is shown in (b).

An interesting conclusion from the data obtained in Liverpool is that the added twist caused by the methoxy substituents does not have a significant effect on the single-molecule conductance values of **RJ 32** (1.60 nS) which is very similar to that of the biphenyl analogue without the methoxy groups (1.67 nS). However, the planarising biphenyl derivative, as the 9,9-dimethylfluorene or N-methylcarbazole analogues resulted in significantly higher conductance (3.82 and 3.27 nS, respectively). These other analogues were synthesised by Dr Wang in our laboratory.

The study of conductance of compounds 59 (RJ 40Ac), 58 (RJ 41Ac) and CSW 558 by *I(s)* methods.

The electronic properties of molecular junctions of **59 (RJ 40Ac)**, **58 (RJ 41Ac)** and **CSW 558** with *I(s)* methods were determined by our collaborators at Liverpool University.

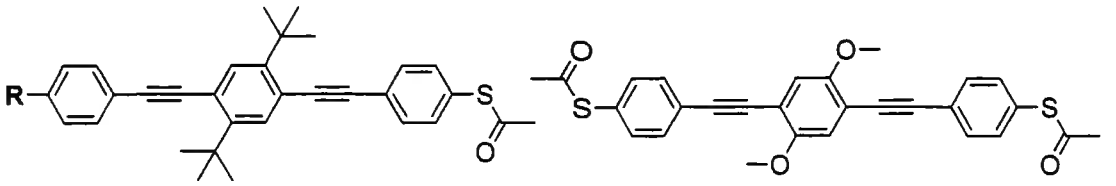

R = H; 59 (RJ 40Ac)

R = SCOMe; 58 (RJ 41Ac)

CSW 558

Figure 34. The structures of **59** (**RJ 40Ac**), **58** (**RJ 41Ac**) and **CSW 558**.

The *I(s)* results suggested that molecular wire **58** (**RJ 41Ac**) has one group signal (**A**) at ~ 1.0 nA (Figure 35, left), whereas **CSW 558** shows two group signals at ~ 0.9 nA and ~ 0.4 nA in (Figure 35, right). From both results, it is likely that the same signals at ~ 0.9 nA are the conductance from a single-molecule spanning the molecular junction (Au-S-OPEs-S-Au) and at ~ 0.4 nA from **CSW 558** is the signal from an intermolecular π–π stacking interaction between two phenyl rings (Figure 11). **58** (**RJ 41Ac**) has no π–π stacking signal (~ 0.4 nA) which we can be explain by the bulky *tert*-butyl group preventing the aromatic stacking of two adjacent molecules.

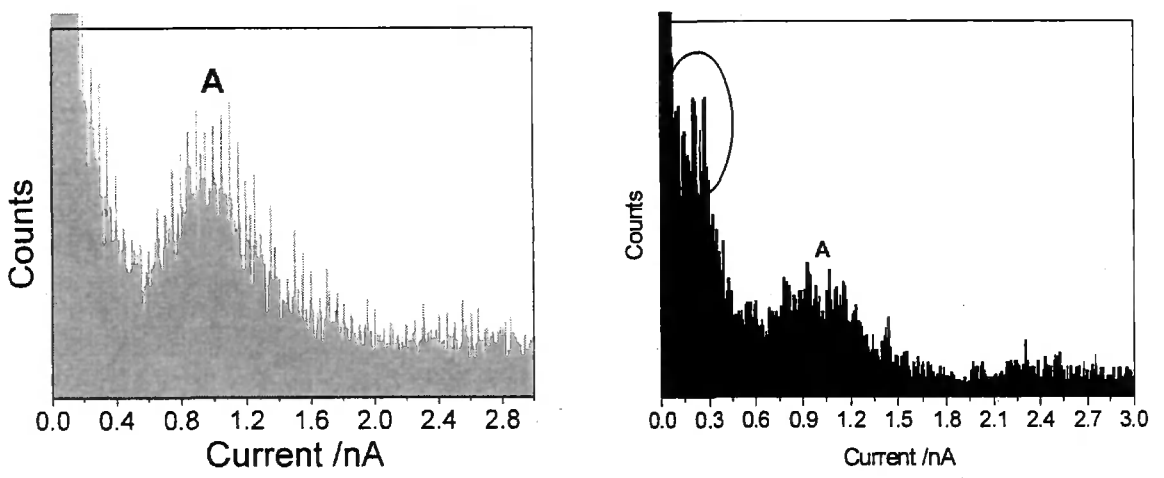

Figure 35. Conductance histograms for **58** (**RJ 41Ac**) (left) and **CSW 558** (right) molecules.

To test this suggestion, **59** (**RJ 40Ac**), which has only one terminal thiol and bulky *tert*-butyl groups to prevent π–π stacking, was synthesised, and its conductance has been measured. The result is shown in Figure 36. As expected, the conductance

histogram of **59** (**RJ 40Ac**) has no signal corresponding to those found in the case of **58** (**RJ 41Ac**) and **CSW 558**.

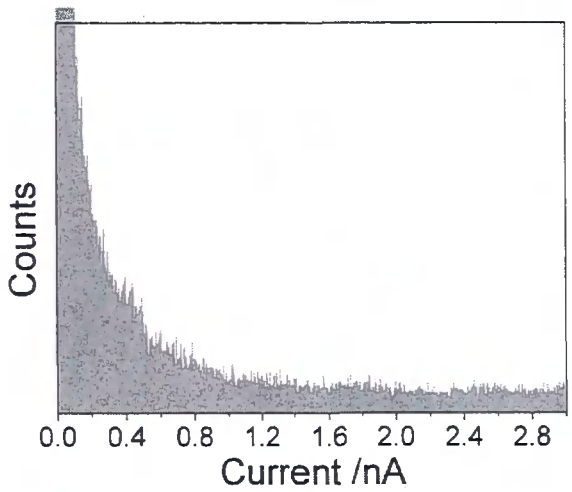

Figure 36. Conductance histograms for **59** (**RJ 40Ac**).

The study of 35 (RJ 8Ac) by mechanically controllable break junction (MCBJ) techniques.

Our molecules were studied using the MCBJ technique at the University of Basel. The results show that **35** (**RJ 8Ac**) can be inserted into the MCBJ device to form Au-Wire-Au contacts, as represented in Figure 37. The detail of the experiment is explained here. To assess the conductance G of a particular molecule, the junction is periodically opened and closed in the presence of a 0.25 mM solution of **35** (**RJ 8Ac**) in a mixture of THF/mesitylene (1:4 v/v-ratio) to which 15 μM tetrabutylammonium hydroxide (TBAH) was added to remove the acetyl protection groups *in-situ* in the liquid cell. During the measurements, the solution was kept under Ar atmosphere to prevent the deprotected bifunctional molecules from polymerisation *via* disulfide bond formation. The junction was opened until the conductance value G is below the resolution limit and it was closed until a Au-Au contact was re-established, identified by $G > G_0$ ($= 10G_0$). During opening and closing, G is continuously recorded for which the MCBJ data of **35** (**RJ 8Ac**) is ca. $1.2 (\pm 0.1) \times 10^{-4}$ G_0. (Figure 38).

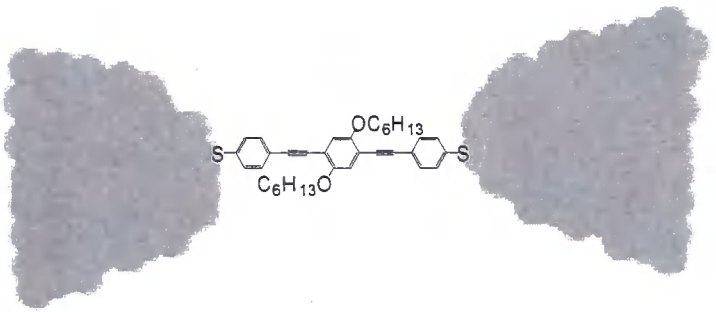

Figure 37. The molecular junction of deprotected **35** (**RJ 8Ac**) with gold contacts.

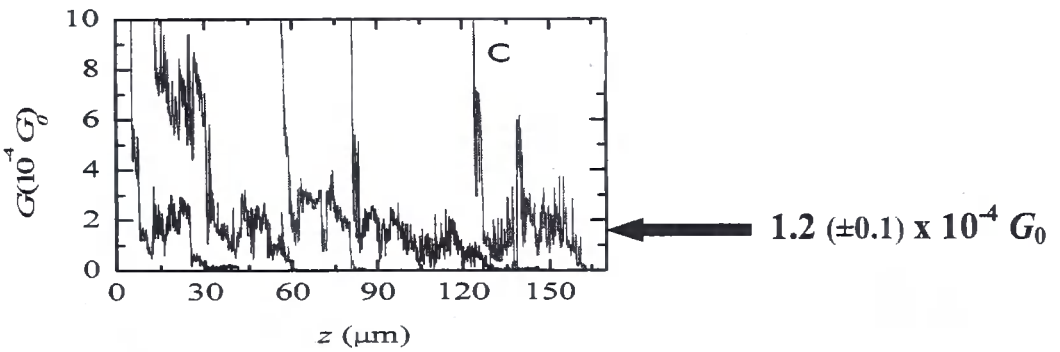

Figure 38. Variation of conductance during the breaking process of a junction of deprotected **57** (**RJ 8Ac**). The results of 5 different experiments are shown with the traces shifted horizontally for clarity.

Moreover, the comparative conductance histogram data of three OPEs, specifically, the parent OPE with no side-chain (**RJ 16Ac**), methoxy (**CSW 558**) and hexyloxy side chains (**35** (**RJ 8Ac**)) obtained from MCBJ technique, show that all OPEs yield essentially identical single-molecule conductance values of G = 1.2 x10^{-4} G_0, suggesting that the solubilising side groups do not affect the single-molecule conductance data. (Figure 39). An oligo(phenylenevinylene) (OPV) derivative (synthesised at the University of Basel) studied by the same technique has significantly higher conductance (G = 2.0 (±0.2) x10^{-4} G_0) which can be explained by the HOMO-LUMO gap (E_g) of the molecules. UV-vis adsorption spectra show that OPV has a significantly smaller energy gap (E_g = 3.2 eV) than OPE (E_g ≈3.5 eV).

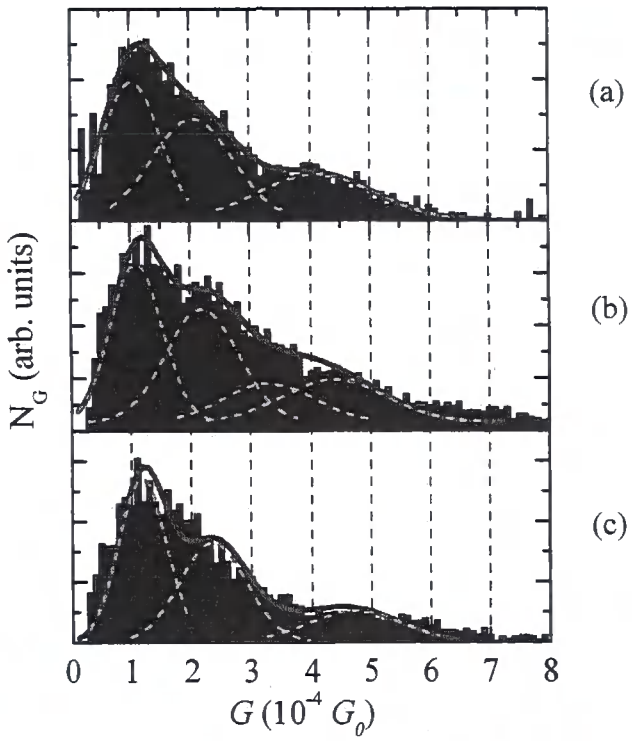

Figure 39. Histogram plot of conductance data during the breaking process of OPE derivatives (a) no side chain (**RJ 16Ac**) (b) methoxy side chains (**CSW 558**) and (c) hexyloxy side chains (**35 (RJ 8Ac)**).

Conclusions

We have synthesised and characterised a range of oligo(aryleneethynylene) derivatives end-capped with cyanoethylthio and acetylthio groups which are molecules designed as molecular wires for conductance studies, including single-molecule conductance using STM and break junction techniques. The results of STM studies in Professor Ashwell's group show symmetrical *I–V* characteristics (**35 (RJ 8)**, **41 (RJ 11)**, **43 (RJ 12)** and **47 (RJ 14)**). Preliminary STM results of **41 (RJ 11)** and **47 (RJ 14)** show length-independent current jumps. We believe that the molecules are being contacted by the STM tip along the backbone, not at the terminal sulfur. Most of the STM experiments show a single current jump, consistent with one molecule being contacted. However, some experiments with **43 (RJ 12)** show double or even triple current jumps, suggesting

simultaneous contact to two and three molecules. The conductance study of compound **RJ 32** with *I(t)*, *I(s)* and *BJ* techniques in Professor R. Nichols' group shows that the differing techniques favour differing current peaks, with the *BJ* technique leading to more higher current peaks, while the *I(t)* and *I(s)* method favour the lower current. A study using MCBJ experiments in Professor C. Schonenberger's group show that OPE derivatives have lower conductance than OPV analogues, and alkoxy side chains on OPEs do not affect the single-molecule conductance.

This work demonstrates the potential for OAE systems to act as molecular wires. In the future, OAE derivatives may be integrated into functioning device architectures.

Chapter 2

The synthesis and properties of ionic iridium(III) phenanthroline and bipyridine complexes for organic light emitting cell (LEC) applications.

Abstract

We report the synthesis, characterisation, photophysical and electrochemical properties of a series of cationic cyclometalated Ir(III) complexes of general formula $[Ir(ppy)_2(bpy)]^+$ and $[Ir(ppy)_2(phen)]^+$ where ppy, bpy and phen are 2-phenylpyridine, 6,6'-dimethylbipyridine and substituted phenanthroline ligands, respectively, with anions (BF_4 or PF_6). The single-crystal X-ray diffraction study of several complexes revealed an octahedral coordination of the Ir atom with the metalated C atoms of the ppy ligands in *trans* positions. The complexes exhibit strong absorption bands in the UV region in solution spectra, due to spin-allowed ligand-centred (LC) $^1\pi$-π^* transitions. Weaker absorption bands at longer wavelengths (in the range of 300-450 nm) have been attributed to metal-to-ligand charge transfer (MLCT). The photoluminescence spectra of all the complexes were characterised by a combination of ^{3}MLCT and $^3\pi\rightarrow\pi^*$ states. We have successfully tuned the emission colour in solution from blue to red (465–595 nm). The varied HOMO-LUMO gap of the complexes is supported by solution electrochemical data. Spin-coated light-emitting cells (LECs) fabricated with the device structures ITO/PEDOT:PSS/Ir complex/Al show that devices emit from green-blue to red (513–610 nm). Moreover, we have found that the maximum brightness (ca. 1000 cd m^{-2} at 3 V) was obtained for **96 (OLED 3)** which demonstrates a beneficial effect of bulky substituents.

Introduction

Organic Light Emitting Diodes (OLEDs) have been made and studied during recent years motivated by their potential for applications in display technology to replace liquid-crystal displays (LCDs). The term "OLED" is used as a general abbreviation for LEDs composed of organic materials. Recently, organic display materials have appeared on the market. Examples include: Kodak LS633, BenQ-Siemens S88, Nokia 6215i and Sony XEL-1 shown in Figure 40.

2003, Kodak LS633

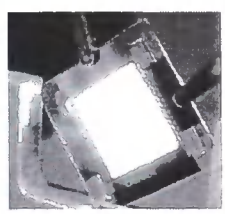

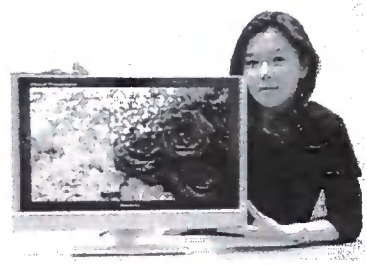

2005, 21'' OLED TV

2008, OSRAM white lighting panel

2006, BenQ-Siemens S88

2006, Nokia 6215i

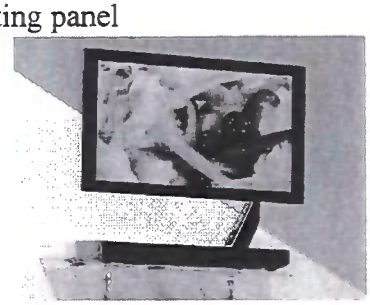

2007, Sony XEL-1: 2,500$

Figure 40. Examples of displays using organic materials.

For success in the consumer market, blue-, green- and red-light emitters are required. New organic materials are also need to achieve higher efficiencies, enhanced brightness, and improved lifetime of optoelectronic devices. Therefore, intensive research efforts in organic materials design and device architectures are ongoing. Many classes of compounds have been studied for organic displays, namely, small-molecule organics, [123-126] small-molecule organometallics, [127-131] polymeric systems, [132-135] and organic dendrimers,[136] some of which are shown below, in Figure 41-44.

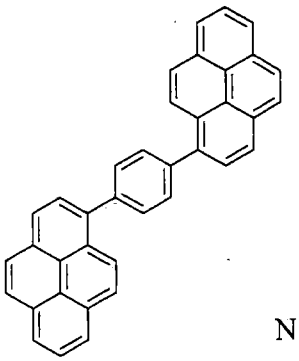

1,4-dipyrenylbenzene(DPB)

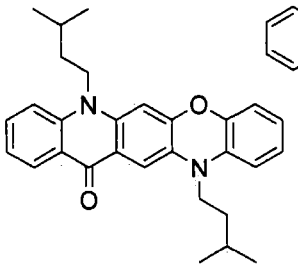

N,N'-di-isoamylquinacridone(DIQA)

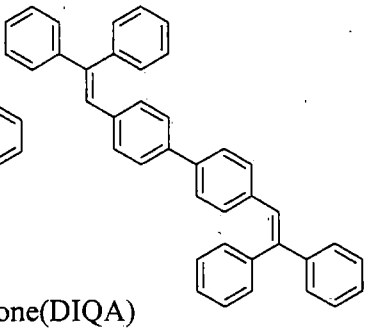

4,4'-bis(2,2'-diphenylvinyl)-1,1'-biphenyl (DPPVBi)

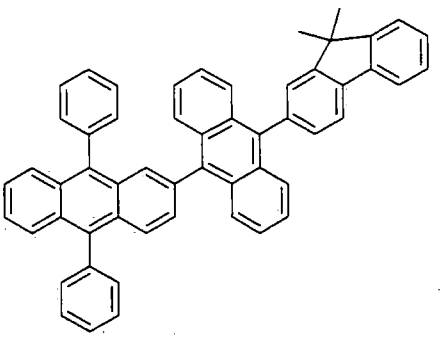

10'-(9,9-dimethyl-9*H*-fluoren-2-yl)-9,10-diphenyl-2,90-bianthracene (FADPA)

Figure 41. Example of organic small-molecules used in OLEDs.

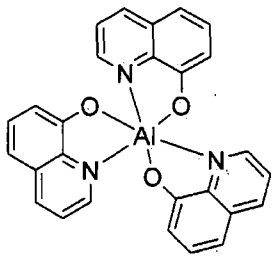

8-hydroxyquinoline aluminum (Alq_3)

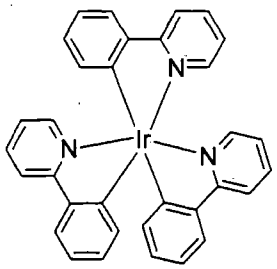

tris(2-phenylpyridine)iridium ($Ir(ppy)_3$)

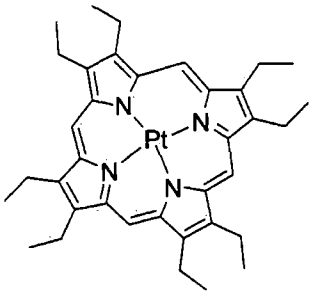

platinum octaethylporphyrin (PtOEP)

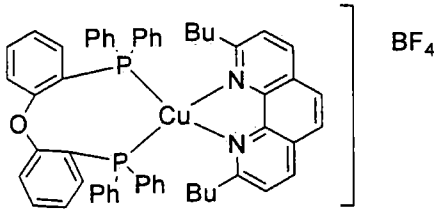

Cu(dnbp)(DPEphos)](BF_4)

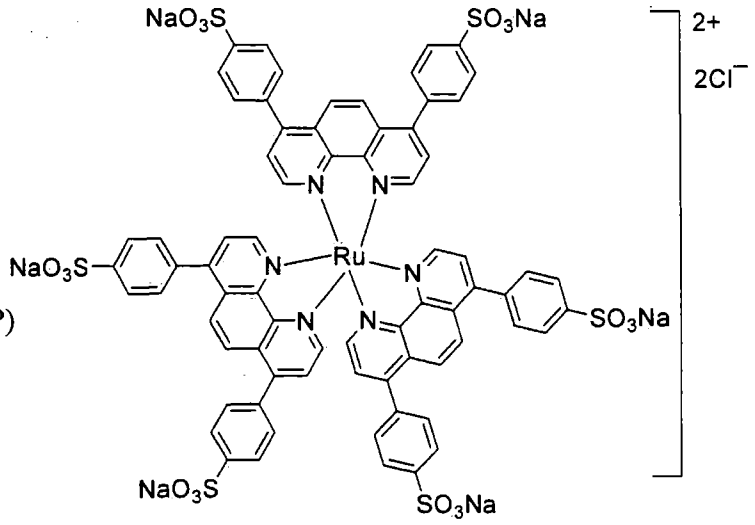

tris(phenanthroline)ruthenium ($Ru(Phen)_3^{2+}$)

Figure 42. Example of organometallic small-molecules used in OLEDs.

poly(phenylenevinylene) (PPV)

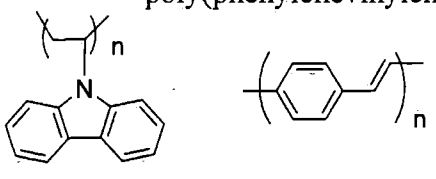

poly(vinylcarbazole) (PVK)

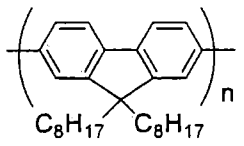

poly(9,9-dioctylfluorene) (PFO)

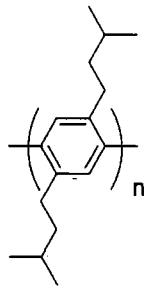

poly(3,6-dialkyl-p-phenylene)

Figure 43. Example of polymeric-molecules used in OLEDs

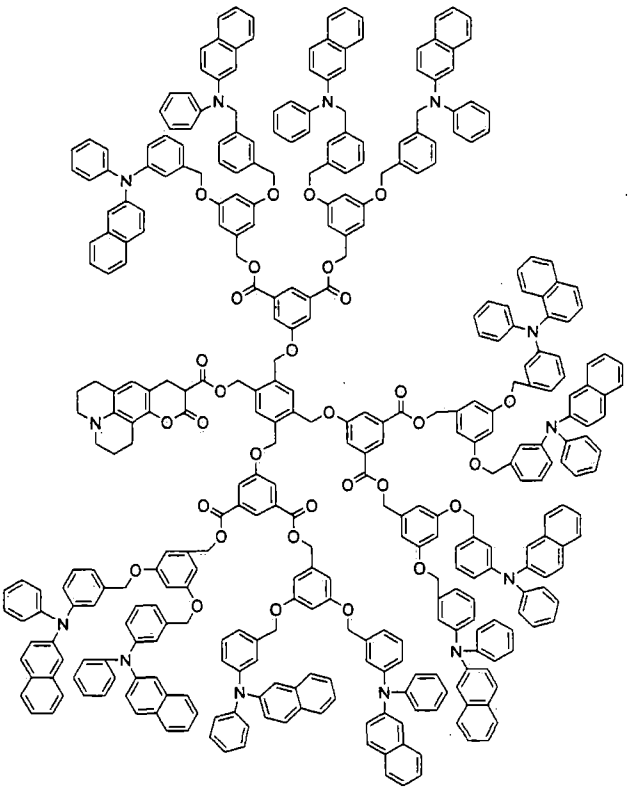

Figure 44. Example of a dendrimeric molecule used in OLEDs.

In this Chapter, the focus is on small organometallic molecules, specifically ionic iridium(III) complexes. The iridium(III) complexes containing 2-phenylpyridine, benzoquinoline, 2-phenylbenzothiazole, or their derivatives are well known materails which exhibit high triplet quantum yield due to the mixing of the singlet and triplet excited states *via* spin-orbit coupling, enhancing the triplet state, which, in turn, lead to high phosphorescence efficiencies. Moreover, the reversible electrochemistry, synthetic versatility, and robust nature of iridium(III) complexes render them appealing materials for OLED applications.[137-142,5,143-145] The effectiveness of a complex in a specific role is determined by its excited-state properties which can be manipulated through synthetic modifications. Early work in this field focused predominantly on homoleptic tris-iridium(III) complexes (e.g., [*fac*-Ir(ppy)$_3$]),[137] shown in Figure 45.

In 1984, Watts reported that the tris(phenylpyridine) iridium(III) complex :(Ir(ppy)$_3$) was obtained as a side product during the preparation of the chloro-bridged

phenylpyridine Ir(III) dimer $[Ir(ppy)_2\text{-}\mu\text{-}Cl]_2$ (where ppy = phenylpyridine).[146] The procedure involves refluxing iridium trichloride hydrate in the presence of 2-phenylpyridine in 2-ethoxyethanol under an inert atmosphere. Later, the same group reported a methodology for only $Ir(ppy)_3$ by using $Ir(acac)_3$, as a suitable precursor, and 2-phenylpyridine as a cyclometalating ligand in high yields as shown in Scheme 16 .[147]

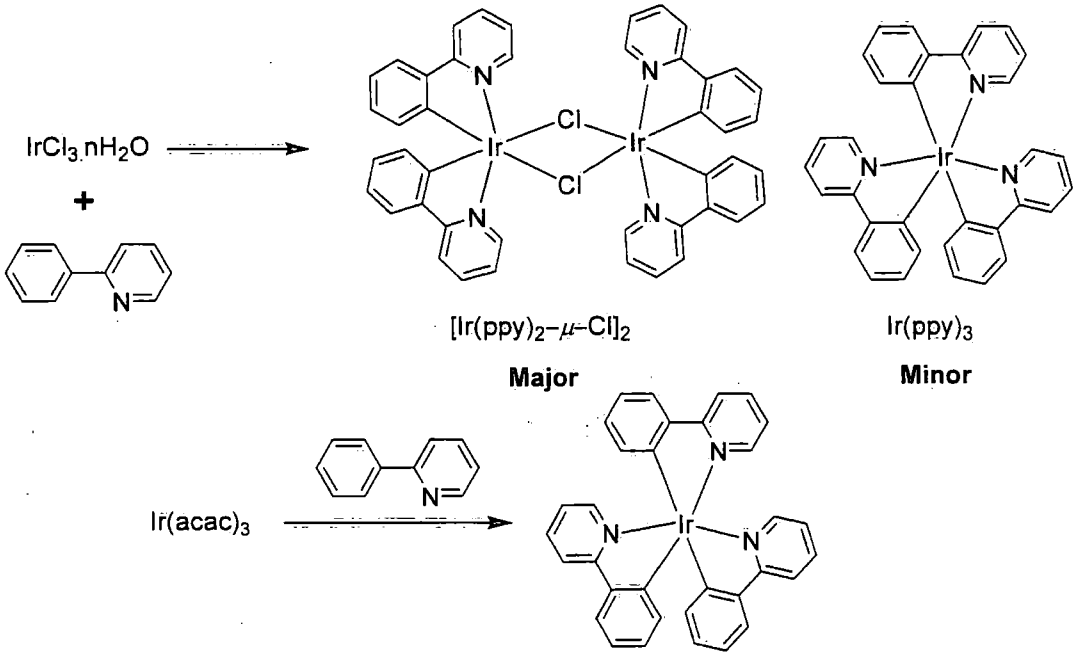

Scheme 16. Two synthetic methods to $Ir(ppy)_3$ by Watts' group.

Colombo and co-workers described a new synthesis to obtain tris-complexes in good yields by using silver triflate while performing the respective ligand-exchange reaction of chloro-bridged phenylpyridine Ir(III) dimer and phenylpyridine ligand, Scheme 17.[148]

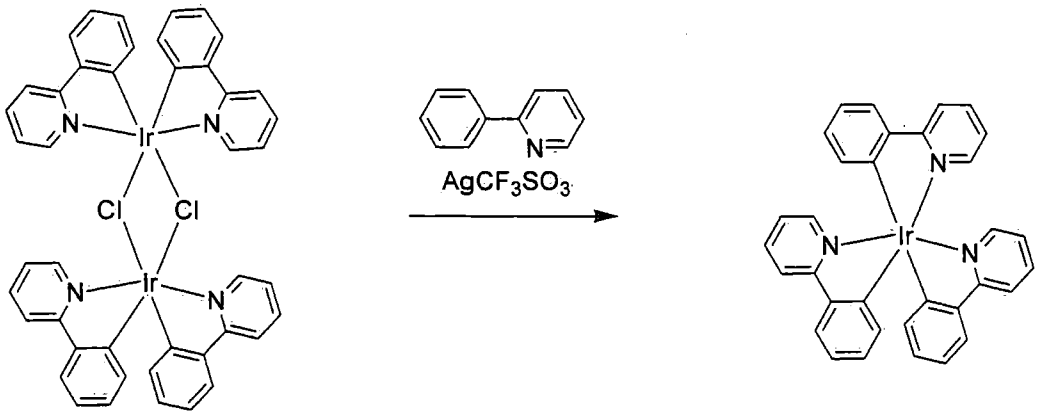

Scheme 17. The synthesis of $Ir(ppy)_3$ by Colombo's group.

Thompson and co-workers[149] reported three different synthetic procedures for the preparation of two isomers of tris-iridium(III) complexes containing heterocyclic phenylpyridine derivatives (Scheme 18). It was found that these different approaches, lead to different coordination isomers, namely facial (*fac*) and meridional (*mer*) complexes. Figure 45 presents the three dimensional structures of *fac* and *mer* $Ir(ppy)_3$. They conclude that higher reaction temperatures (~200 °C) used in methods A and B led to the thermodynamically favoured *fac* isomers, whereas method C (~140 °C) led to the kinetically favoured *mer* isomer. They also reported that methods B and C resulted in higher yields than method A.

Method A

$$Ir(acac)_3 + 3HC\hat{}N \xrightarrow[\text{reflux, } N_2]{\text{glycerol}} \textit{fac}\text{-}Ir(C\hat{}N)_3$$

Method B

$$(C\hat{}N)_2Ir(O\hat{}O) + HC\hat{}N \xrightarrow[\text{reflux, } N_2]{\text{glycerol}} \textit{fac}\text{-}Ir(C\hat{}N)_3$$

Method C

$$[(C\hat{}N)_2Ir(Cl)]_2 + 2HC\hat{}N \xrightarrow[\text{reflux, } N_2]{\text{glycerol, } K_2CO_3} 2\ \textit{mer}\text{-}Ir(C\hat{}N)_3$$

Scheme 18. The synthesis of *fac* and *mer* homoleptic iridium(III) complexes by Thompson's group.

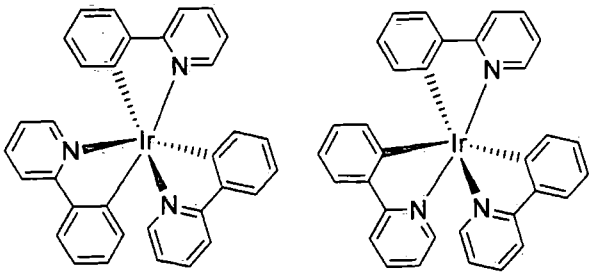

fac-Ir(ppy)$_3$ *mer*-Ir(ppy)$_3$

Figure 45. Facial and meridional isomers of Ir(ppy)$_3$.

Recenly, Shouquan *et al.* have reported a highly efficient method based on the transmetallation of iridium with an organozinc reagent for synthesis of only the meridional isomer of homo- and heteroleptic tris-cyclometalated iridium complexes.[150]

All methods which are shown above yield neutral iridium(III) complexes. The first report of charged iridium(III) complexes was by Watts' group. Introduction of 2,2'-bipyridines (bpy) utilising the bridge-splitting method of the respective chloro-bridged iridium(III) dimer produced the charged iridium(III) complexes in Figure 19.[151] More recently, Bernhard and co-workers have synthesised a library of charged irdium(III) complexes by using combinatorial synthetic techniques.[152]

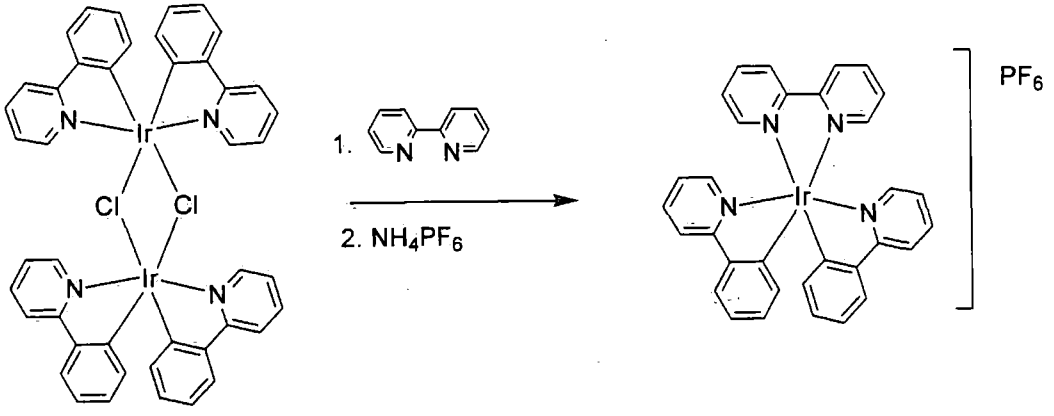

Scheme 19. The synthetic method to give charged iridium(III) complexes by Watts.

In this thesis, we focus on the synthesis of new charged iridium(III) complexes based on phenanthroline and bipyridine, building on synthetic strategies reported by our group.[153]

Electronic excitations and excited states of organometallic complexes

In general, photoluminescence properties are largely determined by the nature of the molecular orbitals (MOs) that are mainly responsible for the electronic ground state and the lowest excited state, called "frontier orbitals". Here, there are three important principal transitions that are observed

1) ligand-centred (LC) excitation, e.g. π-π^* character
2) metal-centred (MC) excitation, e.g. d-d* character
3) metal-to-ligand charge transfer (MLCT) excitation, e.g. d-π^* character

Ligand-centred (LC) transitions

This transition is found in a series of π-conjugated organic ligand compounds. The lowest excited states are predominantly determined by MOs which can be well described by the π-HOMO and the π^*-LUMO of the organic ligands, since MOs of other than π and π^* character lie at significantly lower and higher energies, respectively. For most ligand molecules, which are of interest here, the HOMO is occupied by two electrons and the compound is diamagnetic, i.e., the two electrons carry opposite spins (α and β spins). This situation is described by an electron configuration of π^2 where the resulting state, the ground state, is a spin singlet S_0 ($^1\pi^2$) (Figure 46, **A**). When, after a HOMO-LUMO excitation, the spins are also taken into account, one obtains the excited state configuration $^1\pi\pi^{*1}$ under four different situations (Figure 46, **B** and **C**). An excitation without a spin flip gives an excited singlet (Figure **B**), while an excitation with a spin flip gives a triplet due to three different possible spin orientations (Figure **B**).

From spectroscopic investigations, it is known that the splitting between the excited singlet state and the excited triplet state is usually significant. This results in the energy state as depicted in Figure 46, **D**. A quantum mechanical consideration shows that the triplet state T_1 (or $^3\pi\pi^*$), consisting of three substates, is stabilized with lower energy, while the singlet state S_1 (or $^1\pi\pi^*$) is destabilized and is higher energy relative to the triplet state.

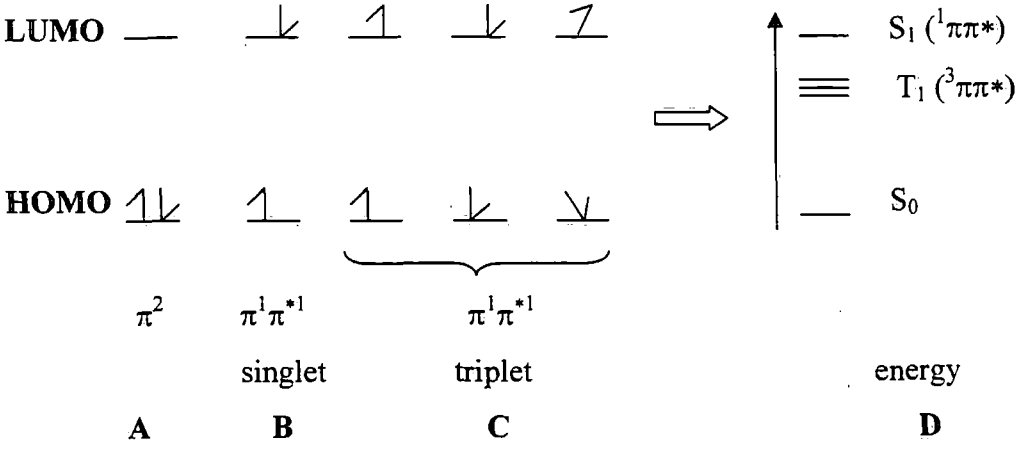

Figure 46. The schematic energy diagram of ground state (π^2) and excited state ($^1\pi\pi^*$ and $^3\pi\pi^*$) of a π- conjugated organic molecule.

Metal-centred (MC) transitions.

The absorption properties of inorganic non-conjugated compounds for example, $[PdCl_4]^{2-}$, $[MnCl_4]2^-$, $[Co(CN)_6]^{3-}$ and $[PtCl_4]^{2-}$ are determined by metal-centred excitations.[154] Usually, they occur by d-d transition states which are described by using group theory and the symmetry of the complex. From this point, only those compounds having central metal ions with a d^6 configuration, such as Ir^{3+}, Ru^{2+}, Os^{2+}, Re^+, and W^0, will be discussed as examples. These metals/ions tend to prefer a six-fold coordination which includes bidentate and tridentate chelating ligands. In a simple approach, the complexes can be described in an octahedral symmetry (O_h) of the first coordination-sphere around the central metal. In this symmetry, the d-orbitals are split into two sets of orbitals which are t_{2g} and e_g state (Figure 47). The magnitude of this splitting is given by the ligand field strength.

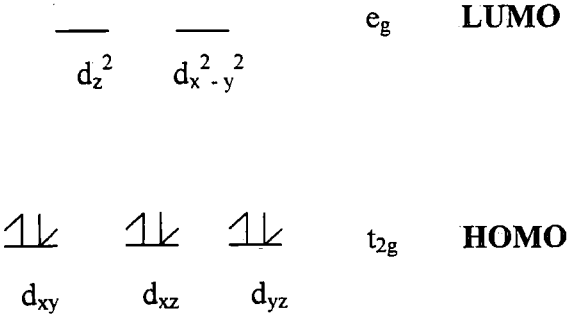

Figure 47. Splitting of d-orbitals in an octahedral ligand field with O_h symmetry.

Metal-to-ligand charge transfer (MLCT) transitions

A metal-to-ligand charge transfer transition is the transition from a d orbital of the metal to a π* orbital of organic ligand. Prime examples are complexes in which the ligands have empty π antibonding orbitals. The examples of ligands are carbon monoxide, pyridine, bipyridine, pyrazine, and phenanthroline.[155] Figure 48 shows this type of transition from d to π*.

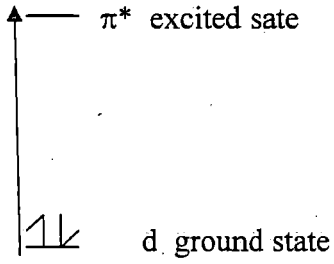

Figure 48. The metal-to-ligand charge transfer transitions from d to π* (MLCT).

From LC, MC and MLCT transitions of an organometallic complex, the simplified MO diagram showing how the MOs relate to the energy states is illustrated in Figure 49

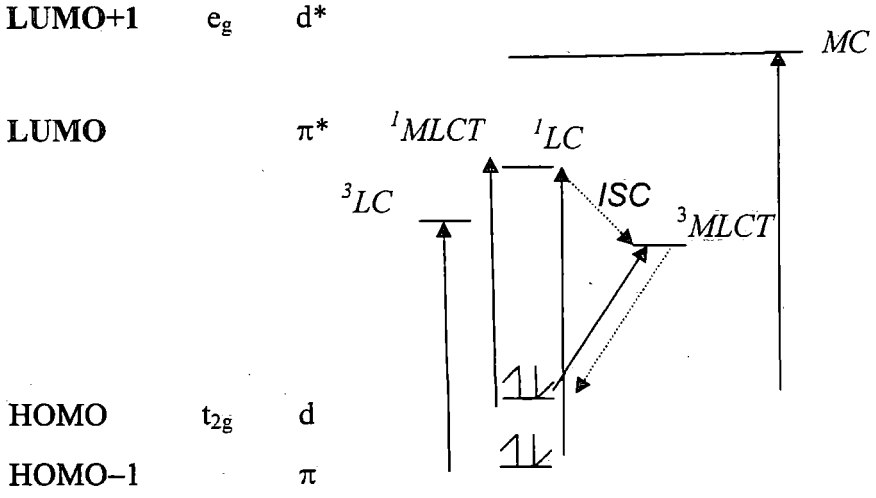

Figure 49. Introductory MO model for a compound with single π, d, and π* orbitals and the respective MLCT, LC and MC transitions.

In this simple model, one single ligand π-orbital (**HOMO-1**) and one metal d-orbital (**HOMO**) are considered as the occupied frontier orbitals with both of these being occupied by two electrons. The lowest unoccupied orbital (**LUMO**) is given by a single π*-MO and an additional unoccupied d*orbital (**LUMO+1**) also displayed in Figure 49. In model, there are three possible types of excited states.

(a) Ligand-centred states that are π-π* transitions. This transition from π orbitals to π* orbitals without spin change is allowed, called singlet-singlet absorption (^1LC). This transition is identified by a large extinction coefficient of absorption. Conversely, singlet-triplet absorption (^3LC) is identified by a weak extinction coefficient.

(b) Metal-to-ligand charge transfer states in which an electron is excited from metal t_{2g} orbitals into empty ligand orbitals (π*). Similar to *LC* transitions, MLCT shows two states. The transition without spin change is allowed, called singlet-singlet absorption (^{1}MLCT), while transitions with spin change are called singlet-triplet absorption (^{3}MLCT). In this model, the excited singlet state may undergo a spin flip, resulting in an excited triplet state. This process is called intersystem crossing and occurs due to strong spin-orbit coupling. The radiative process of a triplet excited state to a singlet ground state is termed phosphorescence.

(c) Metal-centred excited states occur with the promotion of an electron from t_{2g} to e_g orbitals. However, it is assumed that this energy level (**LUMO+1**) and those of the resulting states are too high to be important for the organometallic transitions here. For this reason, the three transition orbital model is characterised by just two excitations; LC and MLCT transitions.

Several research groups have used high-resolution spectroscopy to study the excited state properties of cyclometallated transition metal(III) complexes.[156-158] Their work has established that luminescence from these complexes originates from a lowest excited state that is best described as a ligand centred triplet (^{3}LC) with singlet and triplet metal-to-ligand-charge-transfer (^{3}MLCT) character mixed through spin-orbit coupling. Strong spin-orbit coupling from the iridium(III) centre facilitates intersystem crossing to energetically similar triplet states and enables the formation of an emissive, mixed triplet excited state [**T**; Eq (1)] in which the coefficients *a* and *b* refer to the contributions of the

^{3}MLCT and ^{3}LC states, respectively. An excited state manifold ($a \approx b$) is presented in Figure 50.

$$\Psi_T = a\Psi_{MLCT} + b\Psi_{LC} \qquad \text{Eq (1)}$$

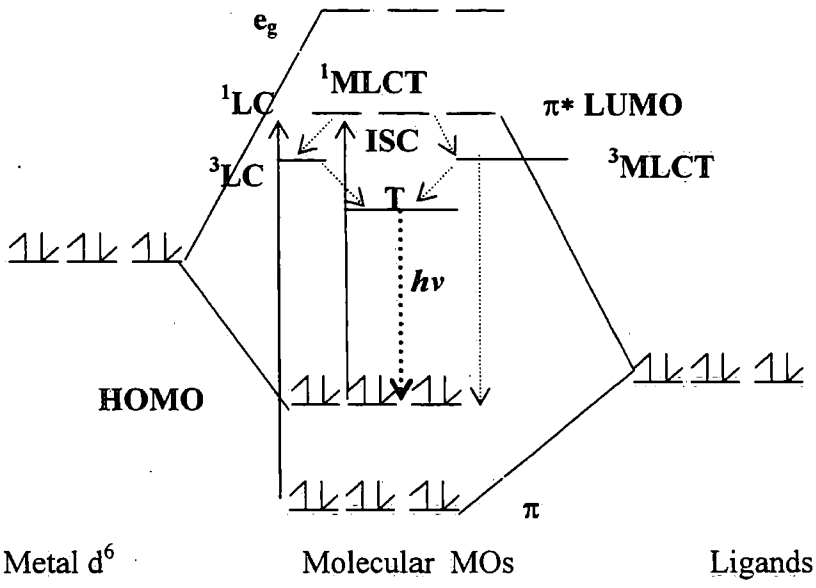

Figure 50. Schematic and simplified molecular orbital diagram for an octahedral d^6 metal complex involving 2-phenylpyridine (C_3 symmetry) type ligands in which various possible transitions are indicated.

From Figure 50, it can be seen that excited-state mixing occurs when sufficient overlap is present between the ^{3}LC and ^{3}MLCT states. Thus, it is possible to control the energy of the lowest excited state by deliberately adjusting the energy of metal and ligand orbitals, which can be achieved through substituent effects or by changing the parent ligand structure entirely. In such cases, the excited state can be tuned directly through ligand modifications, because each ligand is linked to a different energy transition. By monitoring the effect of various ligand permutations within the coordination sphere, it is possible to gain insight into the factors that govern the photophysical and electrochemical behaviour of iridium(III) complexes, and to tailor materials with specific excited-state properties.

Tuning of emission colours in neutral iridium complexes

Watts *et al.*,[147] have synthesised several substituted 2-phenylpyridine-based neutral iridium complexes **I-1**, **I-2**, **I-3** and *fac* Ir(ppy)$_3$ for studying their photophysics. The parent compound *fac*-Ir(ppy)$_3$ shows phosphorescence at λ_{max} 494 nm, measured at 77 K in ethanol/methanol glass (1:1 volume). The structures of the complexes are shown in Figure 51.

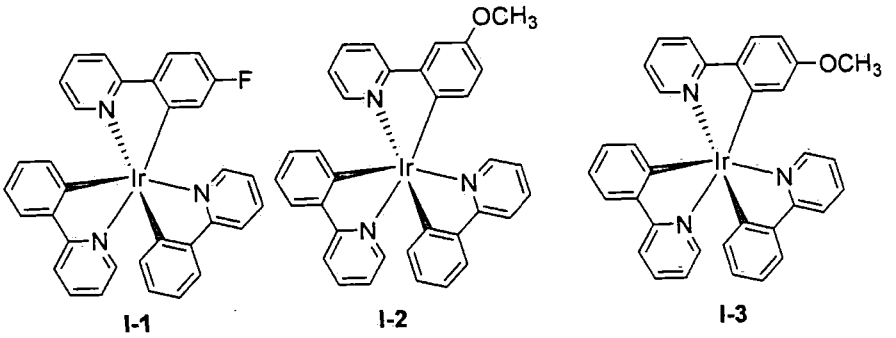

	I-1	I-2	I-3
λ_{max} Emission (nm) at 77 K in ethanol/methanol glass (1:1 volume)	465	539	481
$E_{1/2ox}$ (V) in CH_3CN (vs SCE)	0.97	0.55	0.75

Figure 51. Emission wavelength and solution electrochemical data of homoleptic iridium(III) complexes by Watts.[147]

All the complexes in Figure 51 show strong phosphorescence from a ^{3}MLCT excited state, and the phosphorescence lifetime of these complexes is in the range of 2-3 μs in nitrogen-saturated acetonitrile at room temperature. The photophysical and electrochemical data demonstrate the influence of ligands bearing electron-withdrawing and electron-donating substituents. Compound **I-1** with an electron-withdrawing group (F) exhibits a 29 nm blue-shift compared to Ir(ppy)$_3$. In the opposite way, **I-2** with its electron-donationg group (OCH_3) shows a 45 nm red-shift. It is interesting to note the difference between the complexes **I-2** and **I-3**, which is simply the effect of the position of the electron-donating substitution on the phenyl ring. In complex **I-2**, the electron-donating group is substituted at the *para*-position with respect to the iridium centre. Therefore, incorporation of an electron-donating substituent *para* to the iridium-carbon

bond decreases the emission energy due to a mesomeric effect (oxygen lone pair donation to the aromatic π orbitals) which is confirmed by the electrochemical data of the complexes shown in Figure 51. It is evident that the less positive oxidation potential values result from ligands with electron-donating substituents at the *para*-position, and more positive values result from ligands at the *meta*-position (with respect to the iridium centre).

In particular, electronic effects have been considered due to their profound influence on orbital energies as well as the relative ease with which electron-withdrawing (e.g., -F, $-CF_3$) and electron-donating (e.g., $-C(CH_3)_3$, $-OCH_3$) groups can be incorporated into the ligand structure. Electron-withdrawing substituents tend to stabilize the HOMO by removing electron density from the metal, whereas donating groups have an inverse effect. This relationship is convoluted by the fact that withdrawing groups may also lower the energy of the LUMO (i.e., increasing the electron affinity of the parent ligand).

Further investigation into tuning the emission colour of homoleptic iridium(III) complexes has been carried out by Thompson's group.[149] Representative structures are shown in Figure 52.

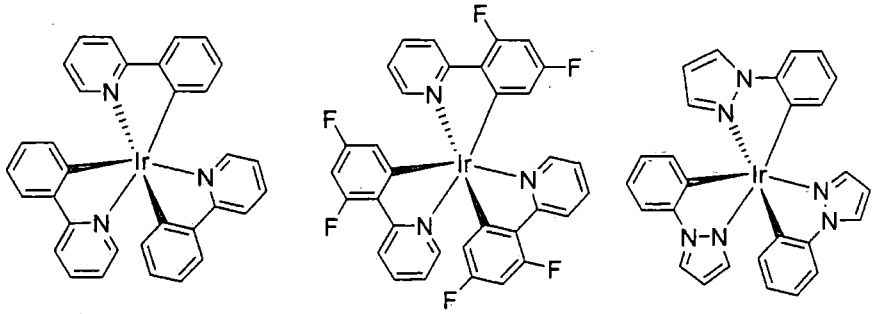

λ_{max} Emission (nm) at 77 K in 2-methyltetrahydrofuran	492	450	414

Figure 52. Tuning emission wavelength of neutral iridium complexes.[149]

The difluoro-substituted analogue, *fac*-Ir(46dfppy)$_3$, has a blue-shifted emission (λ_{max} = 450 nm) compared with *fac*-Ir(ppy)$_3$ (λ_{max} = 492 nm). The large hypsochromic shift caused by 4,6-difluoro substitution is consistent with the behaviour seen in **I-1**. Substitution of the phenyl hydrogens with inductively electron-withdrawing fluorine

atoms, particularly on the 4'- and 6'-positions, stabilizes the HOMO more than the LUMO, thus increasing the triplet energy gap.

Interestingly, the highly structured emissions of the facial phenylpyrazolyl (ppz)-based complexes occur at higher energies than the phenylpyridyl-based analogues. As shown in Figure 52, at 77 K, the emission for *fac*-Ir(ppz)$_3$ has λ_{max} = 414 nm. This phenomenon can be explained by a strongly perturbed ligand-centred transition in the phenylpyrazolyl derivatives. As can be seen in Figure 50, the emission wavelength can be controlled by the triplet excited state containing both MLCT and intra-ligand ($\pi \rightarrow \pi^*$) triplet character. This reports mentions that the triplet energy of phenylpyrazole (378 nm) is greater than that of phenylpyridine (430 nm) therefore, a phenylpyrazolyl-based cyclometalate is expected to have a higher emission energy than a related phenylpyridyl-based complex.[149] However, the facial isomers of the phenylpyrazolyl-based compounds are all very weak emitters at room temperature ($\Phi < 0.1\%$), but are intensely luminescent at 77 K. This report also shows that the addition of electron-withdrawing fluorine substituents on the phenyl ring of ppz gives a blue-shift (λ_{max} at 390 nm) yielding the first Ir(III) tris-cyclometalate that emits in the ultraviolet region (below 400 nm).

Dedeian and co-workers[159] have prepared several homo- and heteroleptic tris-cyclometalated iridium compounds (Figure 53) with systematic changes in their ligand systems. The mixed cyclometalates comprise the ligands 2-phenylpyridine and 1-phenylpyrazole (ppz) which feature the pyridine ring being replaced by pyrazole. Room-temperature emissions are observed and each replacement of pyridine by pyrazole results in a blue shift of 5 and 9 nm in the series Ir(ppy)$_3$ → Ir(ppy)$_2$(ppz) → Ir(ppy)(ppz)$_2$. (Figure 53).

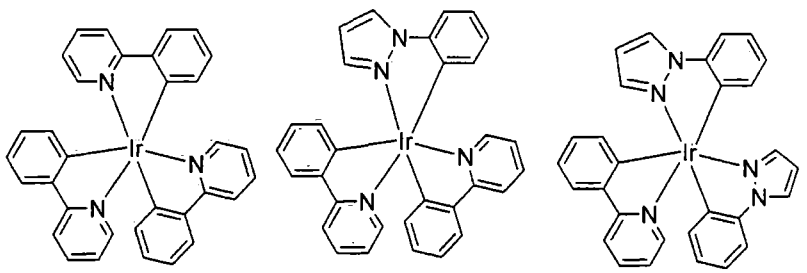

	Ir(ppy)$_3$	Ir(ppy)$_2$(ppz)	Ir(ppy)(ppz)$_2$
λ_{max} Emission (nm) at 298 K	509	504	495

Figure 53. Tuning emission wavelength of neutral iridium complexes by Dedeian.[159]

Park and You[160] demonstrated that using the cyclometalating ligand 2-(2,4-difluorophenyl)pyridine (**46dfppy**) enables control of emission in the blue to red range of heteroleptic iridium complexes by changing the ancillary ligands. The structures and λ_{max} emissions are shown in Figure 54.

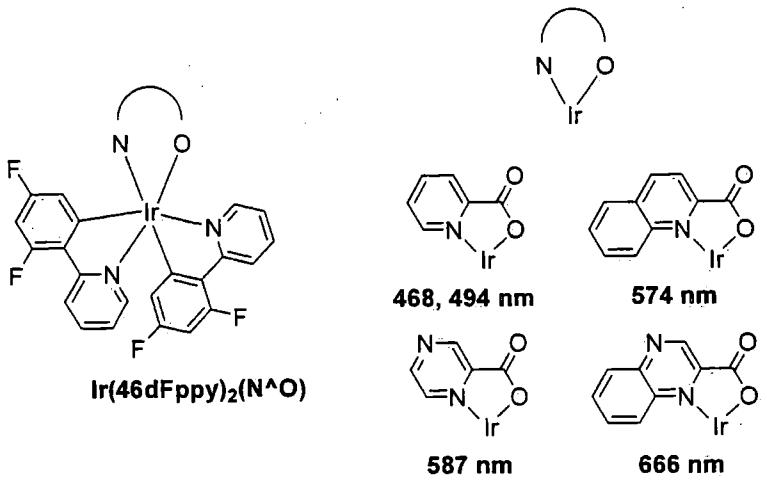

Figure 54. Tuning λ_{max} emission of heteroleptic iridium complexes by Park.[160]

It is clearly noted that the emission colour is controlled from sky blue (468 nm) to red (666 nm). On the basis of these experimental observations, the most probable mechanism of phosphorescence emission from the heteroleptic iridium complex is shown in Figure 55. After the ^{1}MLCT excitation from iridium to dfppy in the singlet manifold, highly efficient inter-system crossing to ^{3}MLCT occurs due to strong spin-orbit coupling. Then inter-ligand energy transfer (ILET) occurs to the ^{3}N^O state of the ancillary ligand (N^O ligand) followed by phosphorescent decay. This mechanism can occur only when the level of ^{3}N^O is lower than that of ^{3}MLCT.

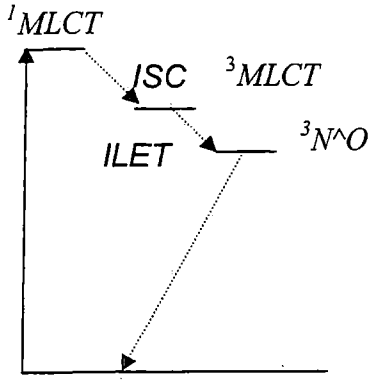

Figure 55. Mechanism of colour tuning from inter-ligand energy transfer (ILET) by Park.

MO analysis of cyclometallated iridium(III) complexes

For understanding the nature of iridium(III) complex, the density functional theory (DFT) calculations for *fac*-Ir(ppy)$_3$ and (ppy)$_2$Ir(acac) were carried out by Hay. The HOMO and LUMO orbitals of those complexes are shown in Figure 56.[161]

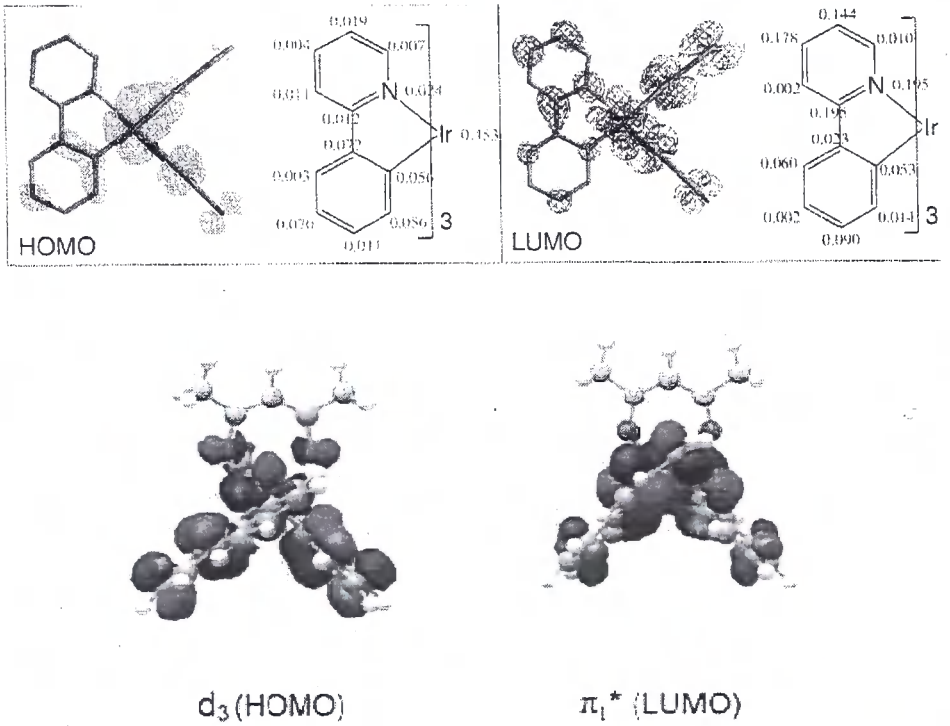

Figure 56. DFT derived orbitals of *fac*-Ir(ppy)$_3$ (top) and (ppy)$_2$Ir(acac) (bottom). (from reference 160)

Hay found that both *fac*-Ir(ppy)$_3$ and (ppy)$_2$Ir(acac) present the similar position of HOMO and LUMO orbitals. Figure 56 shows HOMO orbitals located on the iridium metal and phenyl ring, whereas the LUMO is localised on the ppy ligand, with a predominant contribution on the pyridyl ring and little metal character.

Interestingly, calculations for the heteroleptic iridium complex (ppy)$_2$Ir(acac) show that an ancillary acac ligand does not contribute substantially to either the HOMO or LUMO orbitals. This results in the absorption and emission spectra of the *fac*-Ir(ppy)$_3$ and (ppy)$_2$Ir(acac) complexes being nearly identical. This finding confirms that the acac ligand does not perturb the photophysical properties of the cyclometallated moiety.

Tuning of phosphorescence colours in cationic iridium complexes

One approach to tuning the emission colour of charged iridium(III) complexes has been established by Nazeeruddin by considering the following complexes: **I-4**, **I-5** and **I-6** in Figure 57.[162,163]

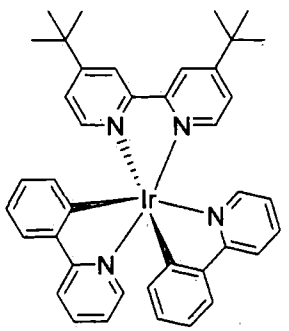

I-4

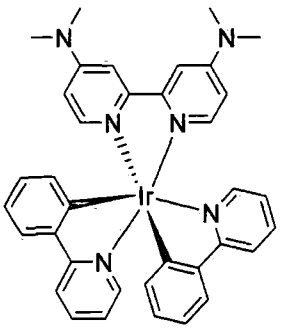

I-5

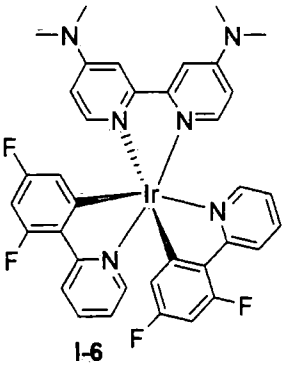

I-6

λ_{max} Emission (nm) at 298 K	581	491, 520	463, 493
$E_{1/2ox}$ (V) in CH_3CN vs Fc	0.83	0.72	1.00
$E_{1/2red}$ (V) in CH_3CN vs Fc	-1.88	-2.17, -2.61, -2.87	-2.13, -2.49, -2.77

Figure 57. Emission wavelength (DCM) and electrochemical data of charged iridium(III) complexes by Nazeeruddin (all complexes have PF_6 as counter anion).[162,163]

The emission colour of the charged complexes was tuned from 463 nm to 581 nm, a result which was consistent with cyclic voltammetry results. The cyclic voltammogram of complex **I-5**, measured in acetonitrile shows a reversible wave at 0.72 V (vs. Fc) due to oxidation of iridium(III/IV), which is cathodically shifted by 0.1 V compared to the complex **I-4** due to the increased donor strength of 4,4'-dimethylamino-2,2'-bipyridine. The three reversible reduction waves at -2.17 and -2.61, and -2.87 V (vs. Fc) are assigned to the reduction of 4,4'-dimethylamino-2,2'-bipyridine and the two 2-phenylpyridine ligands, respectively. It is interesting to note that the ligand-based reduction potential of **I-5** is significantly shifted cathodically (0.29 V) compared to the complex **I-4**. This demonstrates that the destabilisation of the LUMO orbitals of 4,4'-dimethylamino-2,2'-bipyridine offsets any destabilisation of the iridium HOMO orbitals caused by the donor 4,4'-dimethylamino-2,2'-bipyridine ligand. This ensures an increase in the gap between the HOMO and the LUMO of **I-5** compared to complex **I-4**. The cyclic voltammogram of

complex **I-6** shows a reversible couple at 1.0 V (vs. Fc) due to the oxidation of iridium(III/IV). The HOMO orbitals in **I-6** are stabilised upon insertion of fluoride substituents onto the phenylpyridine ligands, thus increasing the HOMO-LUMO gap of **I-6** compared to **I-4** and **I-5**. The largest HOMO-LUMO energy gap for **I-6** was confirmed by the emission colour, measured by excitation at 298 K within the π-π* or MLCT absorption bands, which shows λ_{max} at 463 and 493 nm, blue shifted compared to **I-4** and **I-5**.

The electronic structures of these complexes based on DFT calculations, together with plots of selected molecular orbitals, are shown in Figure 58. The HOMO in these complexes is an antibonding combination of Ir(t_{2g}) and ppy(π) orbitals. The LUMO is a π* orbital localized on the bipyridine ligand. The calculations show that energy gaps are 3.16, 3.47 and 3.85 eV for **I-4, I-5** and **I-6**, respectively.

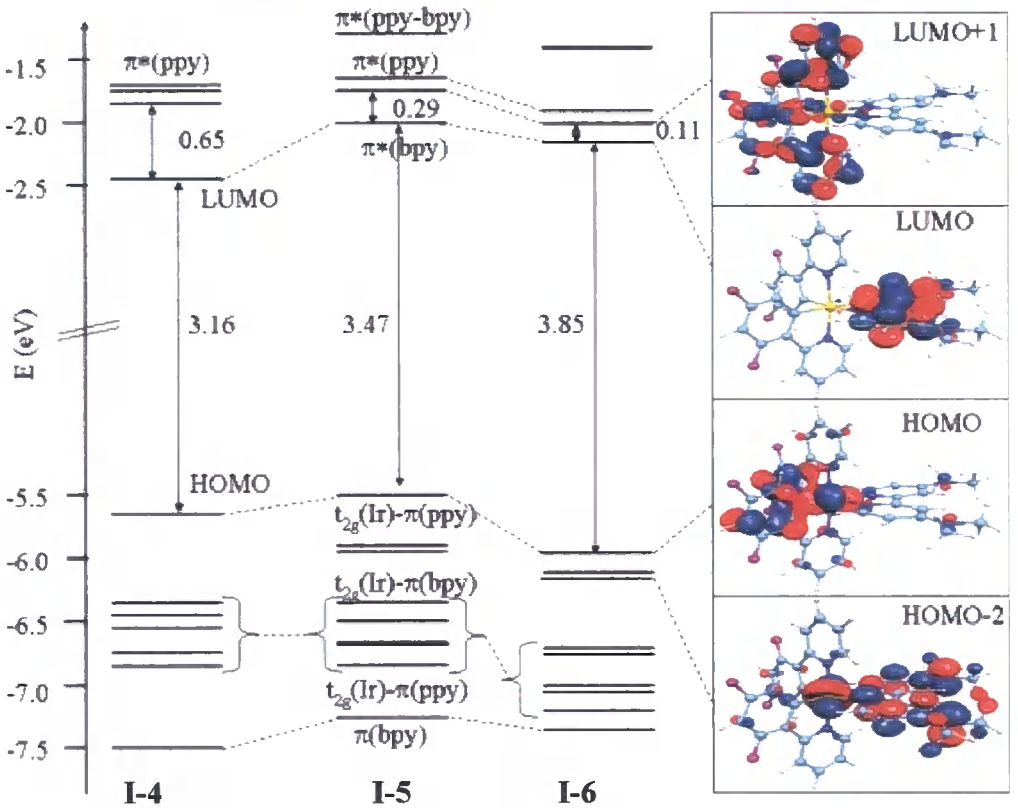

Figure 58. The calculated electronic structure of **I-4**, **I-5** and **I-6** by Nazeeruddin. (from reference 161)

Thompson and co-workers[164] have characterised a series of cationic Ir(III) complexes with the general formula $(C^N)_2Ir(N^N)^+PF_6^-$ featuring bis-ppz (C^N) and neutral diimine (N^N, e.g., bpy) ligands shown in Figure 59. The complexes display intense luminescence in fluid solution at 298 K that is assigned to emission from a triplet metal-ligand-to-ligand CT (^{3}MLLCT) excited state. These emission colors varied from red to blue which can be explained by density functional theory (DFT) calculations that indicate the HOMO of the compounds is comprised of a mixture of Ir d and phenylpyrazolyl-based orbitals, while the LUMO has predominantly diimine character.

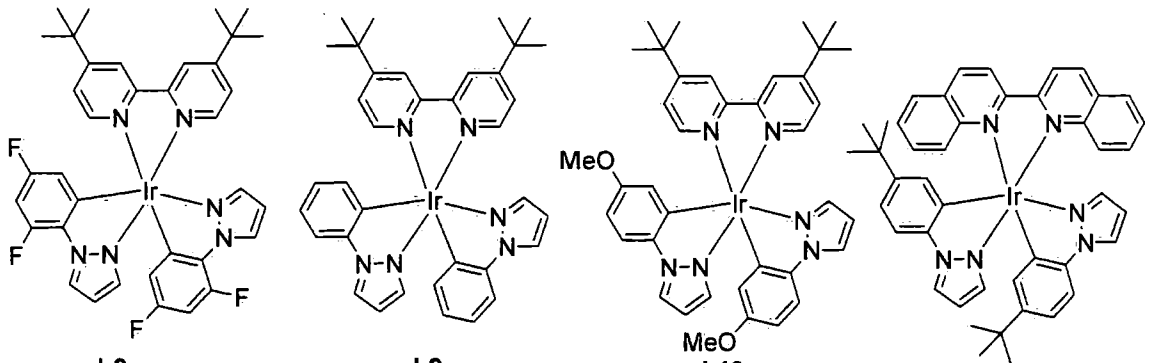

Figure 59. Tuning λ_{max} emission of charged iridium complexes by Thompson (all complexes have PF_6 as counter anion).[164]

Figure 60 shows schematically the concept of HOMO level tuning in iridium pseudohalogen complexes of the type $[Ir(ppy)_2(CN)_2]$ TBA (**I-12**), $[Ir(ppy)_2(NCS)_2]$ TBA (**I-13**) and $[Ir(ppy)_2(NCO)_2]$ TBA (**I-14**) by Nazeeruddin. The emission colours and structures are shown in Figure 61.[165]

Figure 60. Tuning λ_{max} emission of charged iridium complexes by Nazeeruddin (all complexes have TBA as counter cation).

The difference in the emission maxima is due to the difference in the ligand field strength of the pseudohalogen ligands (CN^-, NCS^- and NCO^-). Introducing ligands such as CN^- increases the gap between the LUMO of the phenylpyridine ligand and the metal t_{2g} orbitals, resulting in a blue shift of the lowest MLCT and the emission maxima. Moreover, the NCO^- ligand was introduced in order to reduce the gap between the LUMO of the phenylpyridine ligand and the metal t_{2g} orbitals, effectively red-shifting the emission because of the weak ligand field strength of NCO^- ligands (Figure 61).

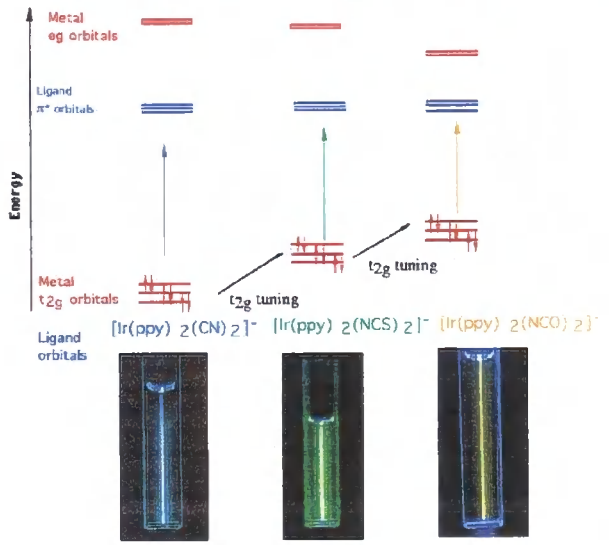

Figure 61. Schematic drawing of HOMO and LUMO orbitals for complexes $[Ir(ppy)_2(CN)_2]$ TBA (**I-12**), $[Ir(ppy)_2(NCS)_2]$ TBA (**I-13**) and $[Ir(ppy)_2(NCO)_2]$ TBA (**I-14**) (from reference 164).

Organic light-emitting device

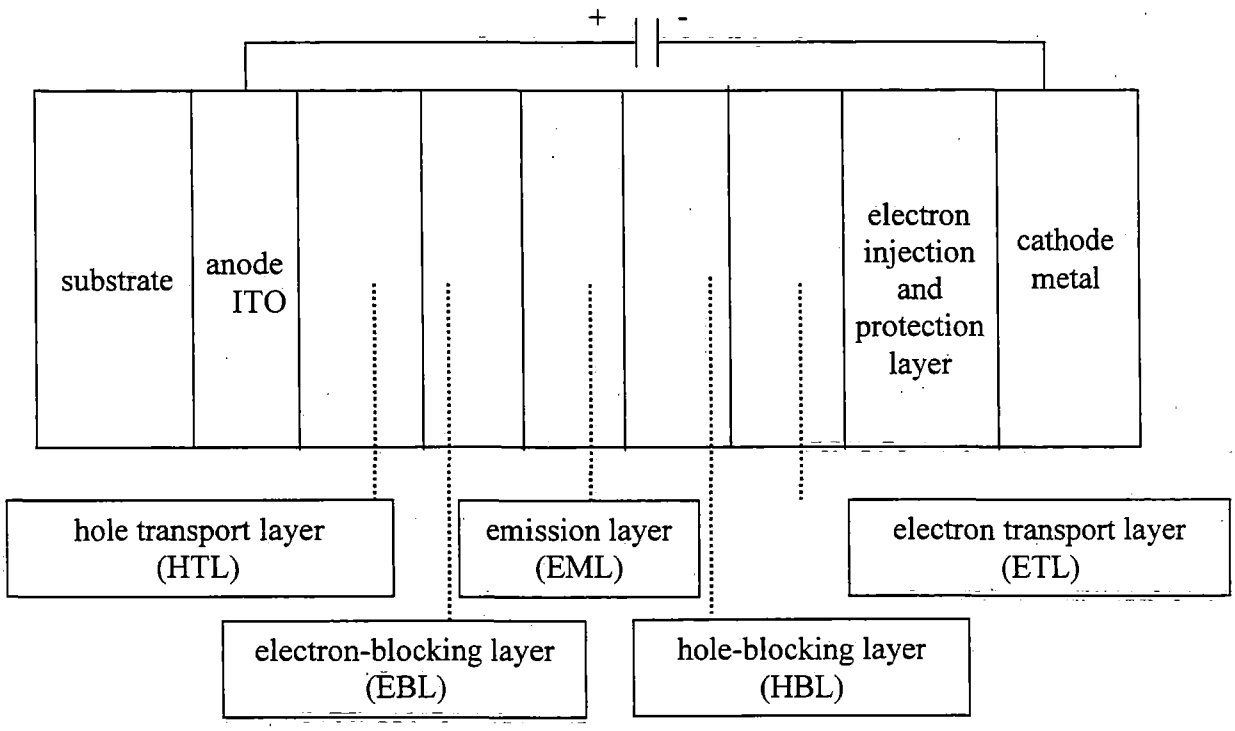

Figure 62. Multilayer structure of an organic light- emitting diode (OLED).

Organic light-emitting diodes (OLEDs) are now considered viable candidates for displays due to their colour versatility, low operating voltages, and good efficiencies. The first complex-based OLED was assembled by Tang and VanSlyke in 1987 containing an Alq_3 chromophore (q = 8-hydroxyquinoline) that emits green light (550 nm) from a singlet excited state. For improving the efficiency, multilayer devices have been fabricated as shown in Figure 62.

In a typical device architecture, a conducting transparent electrode such as indium tin oxide (ITO) [SnO_2 (10-20%) and In_2O_3 (90-80%)] is coated with a hole-conducting polymer such as poly(3,4-ethylenedioxythiophene)/poly(styrene sulfonate) (PEDOT:PSS). Secondly, a thin organic injection/transport layer (HTL) e.g. carbazole derivatives, 4,4'-bis(*N*-naphthyl-*N*-phenylamino)biphenyl (α-NPD), 4,4'-N,N'-dicarbazole-biphenyl (CBP), or triarylamines, is applied to facilitate hole-transport into the EML. Next, the emission layer (EML), such as Pt^{II} or Ir^{III} complexes, is assembled. In some case, an organic light-emitting host-guest layer of comparable thickness is

deposited. The choice of the host material is important since the transfer of triplet excitons from the phosphorescent emitter to the host material has to be prevented. Generally, the triplet energy levels of the host material need to be higher than those of the triplet emitters employed. Recently, studies by Thompson, Forrest and co-workers showed that the use of electron-blocking layers (EBLs) consisting of Ir(III) complexes with picolinate ligands produced improved colour purities in the case of blue-light-emitting devices.[166] These additional layers prevent electrons from crossing and leaving the EML without electron-hole recombination. As a result, the device efficiency can be distinctly increased. However, such blocking layers may lead to the build-up of high charge densities at the interfaces, with unfavourable consequences for the device lifetime. Next, a hole-blocking layer (HBL) was applied to prevent hole leakage from the emission layer. Many types of hole blocking material have been reported, for example bathocuproine (BCP), (biphenyloxaloaluminium(III) bis[2-methylquinolinateo(phenylphenolate)] (BAlq), fluorinated phenylenes, oxadiazole and triazole containing molecules such as the trimer of *N*-arylbenzimidazole (TPBi), 2-*tert*-butylphenyl-5-biphenyl-1,3,4-oxadiazole (PBD), 3-phenyl-4-(1'-naphthyl)-5-phenyl-1,2,4-triazole (TAZ) and 1,8-naphthalimides.

The next layer, an electron-transporting layer (ETL) e.g. Alq_3 is applied. Finally, cathode deposition completes the assembly of the device. Suitable cathode materials include calcium, aluminium, or an alloy such as magnesium-silver, which can be deposited onto the ETL surface. It has been shown that an additional, very thin layer of LiF, NaF or CsF (0.5 to 1 nm) strongly reduces the injection barrier and also protects the ETL from chemical reactions with the cathode material.

Hole transport materials

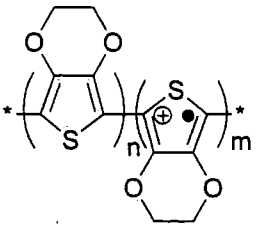

PEDOT

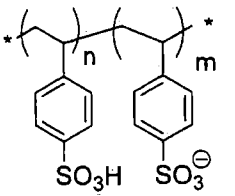

PSS

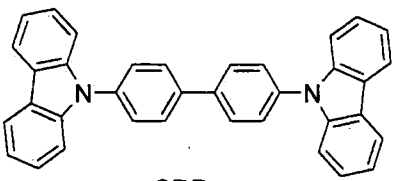

CBP

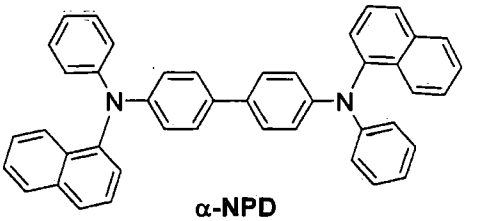

α-NPD

Hole blocking materials

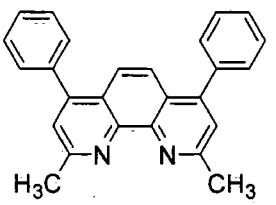

BCP

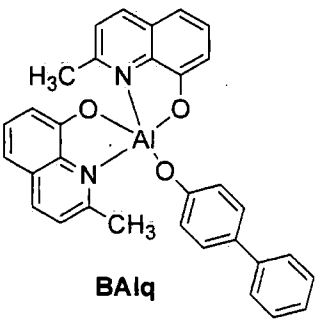

BAlq

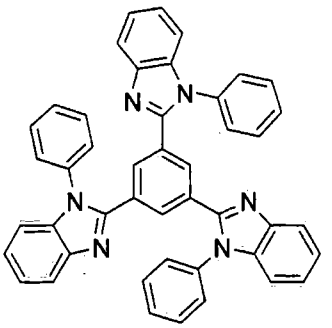

TPBI

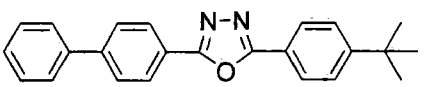

PBD

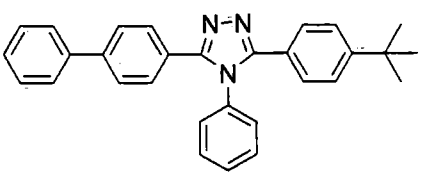

TAZ

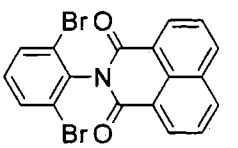

1,8-naphthalimide

The materials used for an OLED device must fulfil a series of requirements, such as suitability for a specific fabrication procedure (e.g., spin-coating, inkjet printing, vacuum deposition), good film-forming properties, sufficiently high glass transition temperature to avoid crystallisation of the material within the desired lifetime of the device and chemical and photochemical stability. Moreover, hole and electron injection barriers must be low and the mobilities, as well as the HOMO and LUMO energies of all the layers, must closely match the neighbouring layers as shown in Figure 63.

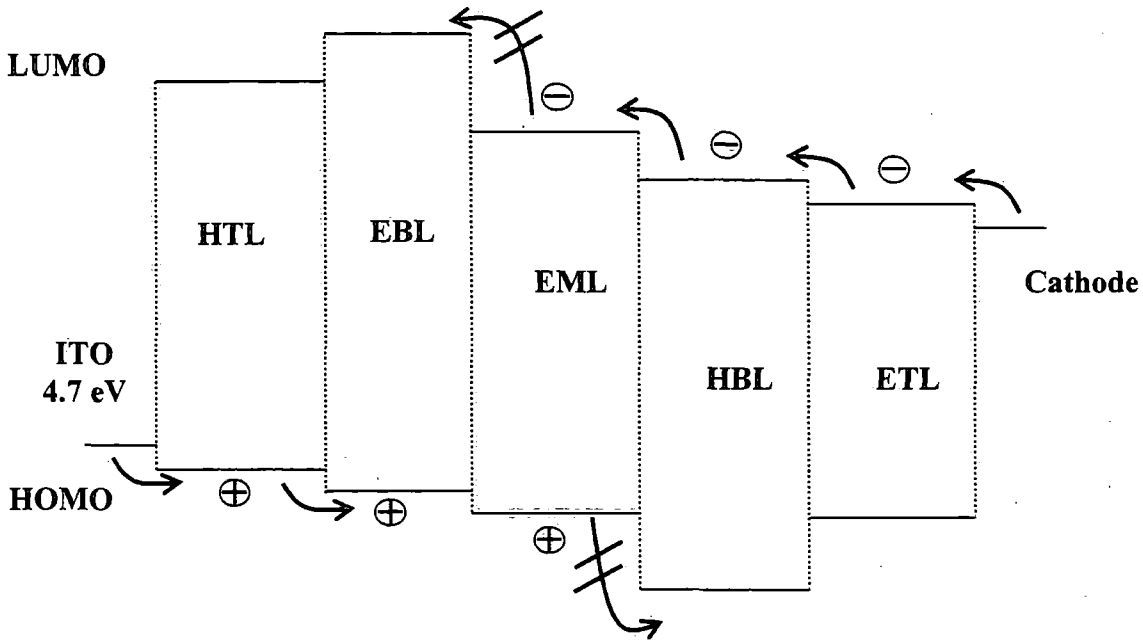

Figure 63. Schematic energy-level diagram of high-efficiency multilayer electrophosphorescent OLEDs.

Recently, light-emitting electrochemical cells (LECs) have been developed which provide an alternative to OLEDs due to their simple design. Early LECs were presented by Heeger et al.[167] which contained a blend of a semiconducting polymer admixed with a polyelectrolyte. Typically consisting of a complex of poly(ethyleneoxide) (PEO) and lithium trifluoromethanesulfonate (triflate), in a sandwich configuration between ITO and aluminum electrodes, these cells exhibit in situ formation of a light-emitting p-n junction.

Unlike conventional OLEDs, these devices exhibit some unique features, in particular antisymmetric current voltage characteristics (no rectification) and light emission with similarly low threshold voltages under forward as well as under reversed

bias. Moreover, the onset voltage was found to be almost independent of the film thicknesses. LECs exhibited significantly improved electroluminescence efficiencies compared with analogous conventional OLEDs and proved to be fairly insensitive to the electrode work-function.

The operating mechanism for polymeric LECs was explained by an electrochemical two-step process, shown in Figure 64.[168] The semiconducting polymer and the polyelectrolyte form an intimate blend with a phase-separated bicontinuous network morphology in which both ionic and electronic charge-carriers are mobile (Figure 64a). When a sufficiently high voltage is applied across the layer, the conjugated polymer is oxidized at the anode and reduced at the cathode. Maintaining charge neutrality, the p-type and n-type doped layers, formed during this initial step, are stabilised by the provision of counterions that are available in the ion-conducting phase (Figure 64b). Under the influence of the applied field these regions extend towards the centre of the layer, forming an electrochemically induced p-n junction, where the p-type carriers (holes) and n-type carriers (electrons) meet and recombine with the emission of photons (Figure 64c).

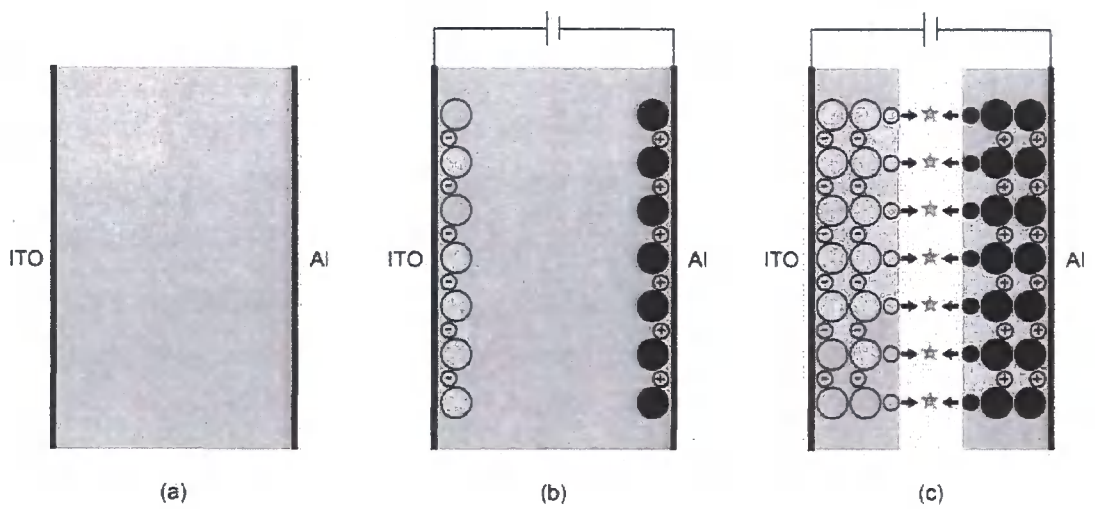

Figure 64. Schematic diagram of the electrochemical processes in a solid-state light-emitting electrochemical cell comprising oxidised molecules (large open circles), reduced molecules (large closed circles), anions (circled minus), cations (circled plus), holes (small open circles), electrons (small closed circles) and photons (stars) (from reference 167).

It has been shown by Rubner and Bard that tris(2,2'-bipyridyl)ruthenium(II) complexes such as $[Ru(bpy)_3]^{2+}$ can be employed in solid-state organic light-emitting devices.[1,169] What makes this class of materials different from previous organic semiconductors typically used in solid-state electroluminescent devices is the presence of mobile ions: $[Ru(bpy)_3]^{2+}$ carries a $^{2+}$ net positive charge, which is balanced by two negative counterions, such as PF_6^-. These counterions drift under the influence of an applied bias, leading to accumulation of negative ionic charge near one electrode and depletion near the other electrode which is similar to LECs. This ionic space charge creates high electric fields at the electrodes, which enhances electronic charge injection into the transition metal complexes. As a result, devices based on a single layer of such transition-metal complexes operate at a low voltage and have been shown to be insensitive to the choice of electrode material, allowing the use of air-stable anodes and cathodes. However, all single-layer devices from ruthenium chromophores reported thus far emit in the orange-red part of the spectrum.

The first LECs of charged iridium(III) complexes were demonstrated by Slinker's group.[170] [Ir(2-phenylpyridine)$_2$ (4,4'-*tert*-butyl-2,2'-bipyridine)]PF_6 (**I-4**) has been used as a multifunctional chromophore for single-layer electroluminescent devices which emit yellow light with a brightness that exceeds 300 cd/m^2 and a luminous power efficiency that exceeds 10 lm/W at only 3 V.

In this thesis, we focus on new charged iridium(III) complexes for devices which operate by the LEC process.

General aim

The goal was to synthesise heteroleptic charged iridium(III) phenanthroline and bipyridine complexes with varied aryl or heteroaryl ligands for studying their photophysics and redox chemistry. The target complexes are shown in Figure 65 and the general synthetic pathway is shown in Scheme 20.

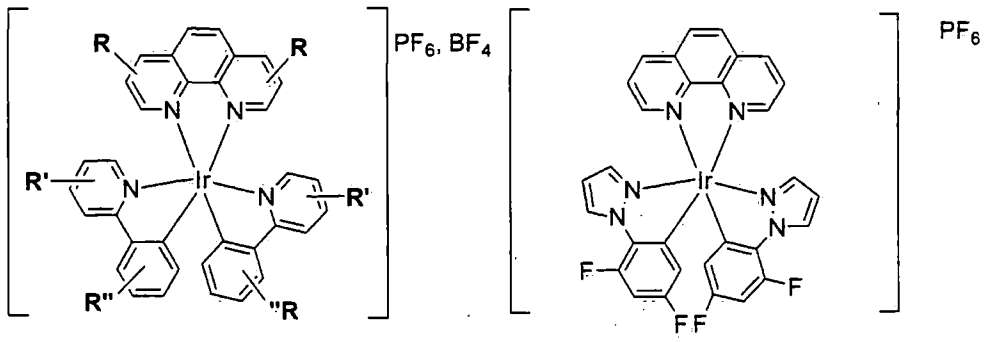

R = 2, 9-diMe or 4, 7-diMe or 3, 8-difluorene or 4, 7-dipyrole

R' = 4'-Me or 4'-CF_3 or 5'-CF_3

R'' = 2, 4-diF

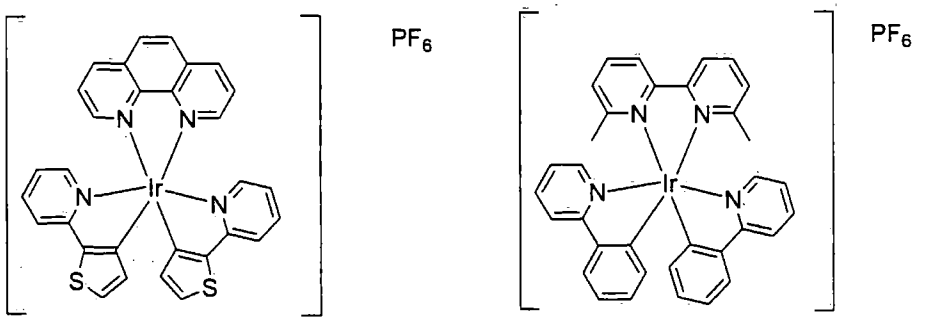

Figure 65. Target heteroleptic charged iridium(III) complexes.

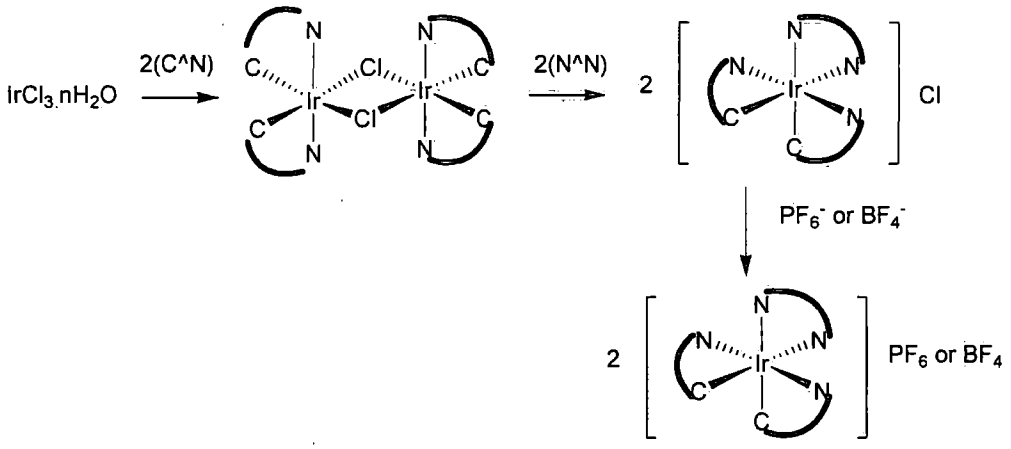

Scheme 20. The general synthesis of charged iridium(III) complexes

Results and Discussion

Neutral ligands (N^N)

The neutral N^N ligands which we have used in the synthesis of charged iridium(III) complexes are shown in Figure 66.

Commercial N^N ligands

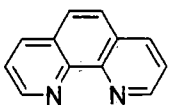

Phen

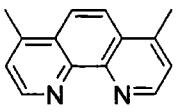

4,7-MePhen

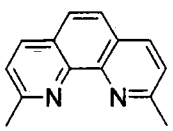

2,9-MePhen

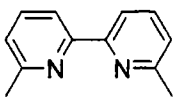

Mebpy

Synthesised N^N ligands

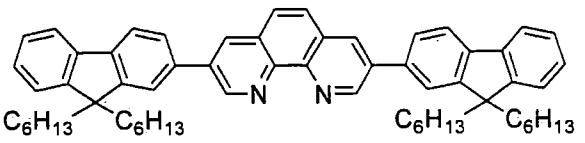

FluPhen[153]

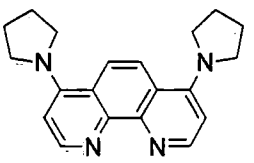

PyPhen

Figure 66. The structures of our neutral N^N ligands

The synthesis of 3-(9,9-dihexyl-9H-fluoren-2-yl)-8-(9,9-dihexyl-9H-fluoren-7-yl)-1,10-phenanthroline (**66**; **FluPhen**)[153]

Compound **66** (**FluPhen**) had been synthesised previously by Dr X. Zeng in our laboratory. More sample was needed for photophysical and device studies of the derived Ir complex **96** (**OLED 3**), so the synthesis was repeated. Bromination of 1,10-phenanthroline monohydrochloride monohydrate **64** as described in the literature[153] yielded the dibromo product **65**, then a standard Suzuki coupling reaction provided the final target product **66** in 63% yield.

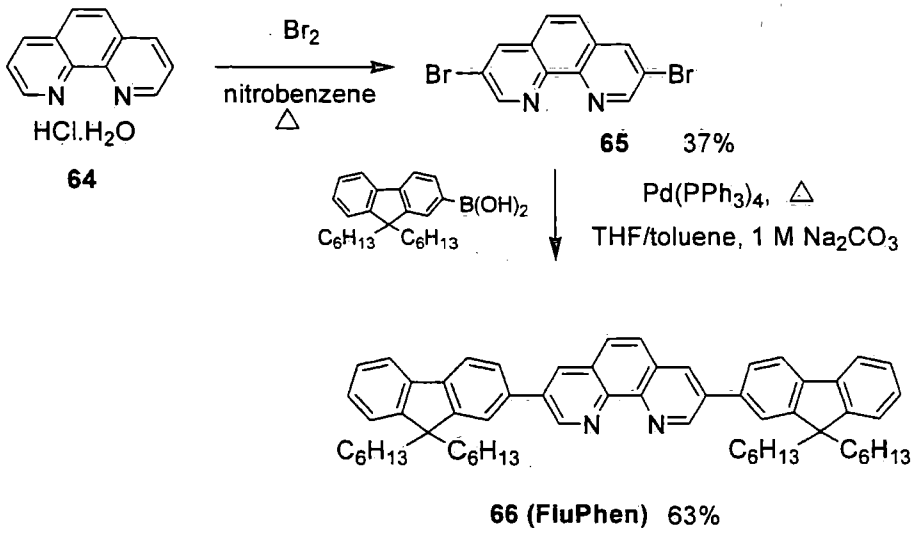

Scheme 21. The synthesis of **66** (**FluPhen**) ligand.

The synthesis of 4,7-di(pyrrolidin-1-yl)-1,10-phenanthroline (**69**; **PyPhen**)

PyPhen was synthesised by chlorination of commercial dihydroxyphenanthroline **67** to give **68**[171], followed by nucleophilic substitution by excess pyrrolidine to give the target product **69** (**PyPhen**) in 75% yield.

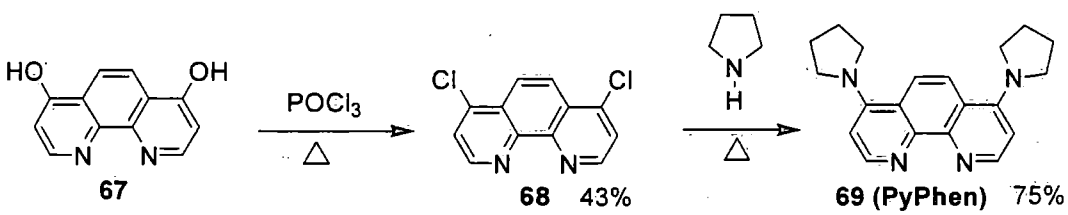

Scheme 22. The synthesis of **69** (**PyPhen**) ligand.

Cyclometalated ligand (C^N)

The cyclometalating ligands which were used in the synthesis of our charged iridium(III) complexes are shown in Figure 67.

Commercial N^N ligands *Synthesised N^N ligands*

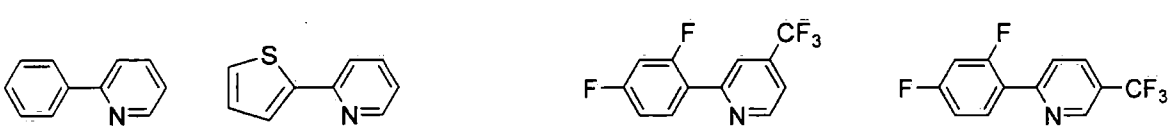

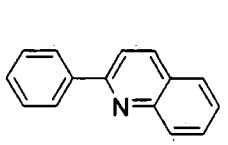

bq

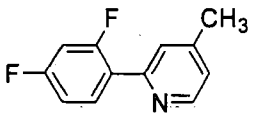

4Meppy[173]

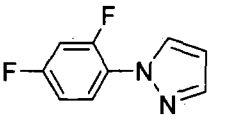

Fppz[174,175]

Figure 67. The structures of the C^N ligands for cyclometalation.

The synthesis of 4-(trifluoromethyl)-2-(2,4-difluorophenyl)pyridine (**72**; **4CF3ppy**), *2-(2,4-difluorophenyl)-4-methylpyridine* (**75**; **5CF3ppy**)[172] and *5-(trifluoromethyl)-2-(2,4-difluorophenyl)pyridine* (**78**; **4Meppy**)[173]

The syntheses were achieved by standard Suzuki-Miyaura reactions between difluorobenzene boronic acid **70** and 2-halopyridine derivatives **71**, **74** and **77** to give **72** (**F4CF3ppy**), **75** (**F5CF3ppy**) and **78** (**F4Meppy**) in 67, 85 and 88 % yields, respectively.

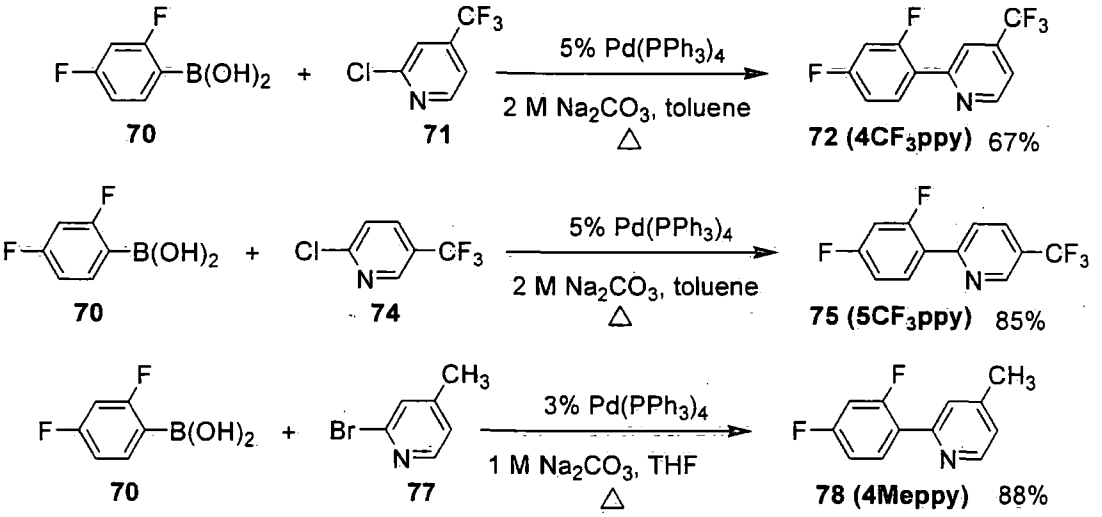

Scheme 23. The synthesis of **72** (**4CF3ppy**), **75** (**5CF3ppy**) and **78** (**4Meppy**)

The synthesis of 1-(2,4-difluorophenyl)-1H-pyrazole (**81**; **Fppz**) from acid cyclisation.[174]

Finar and Rackham reported the synthesis of **81** (**Fppz**) *via* acid protonated cyclisation of phenylhydrazine **79** and compound **80** in high yield (Scheme 24).

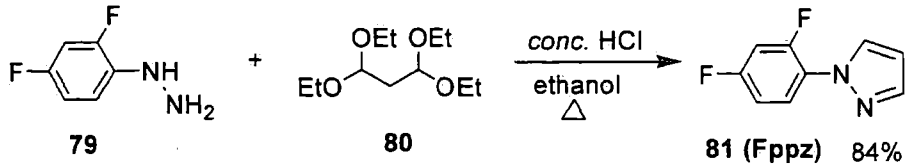

Scheme 24. The synthesis of **81** (**Fppz**) from acid cyclisation.

We also tried an alternative route to **81** (**Fppz**) involving the copper-catalysed arylation of pyrazole – a method which has been reported to be efficient for pyrazole derivatives by Taillefer's group.[176] Therefore, we adopted Taillefer's conditions to couple compound **82** with pyrazole in the presence of copper(I) and salicylaldoxime. However, the reaction gave **81** (**Fppz**) in only 13% yield together with products **83**, **84** and **85**. All of these compounds were smoothly separated by column chromatography. At this point in the project we recognised that a wider exploration of the *N*-arylation reactions of reagent **82** with heterocycles (with and without copper catalysis) would be of fundamental interest. This study is described in detail in Chapter 3.

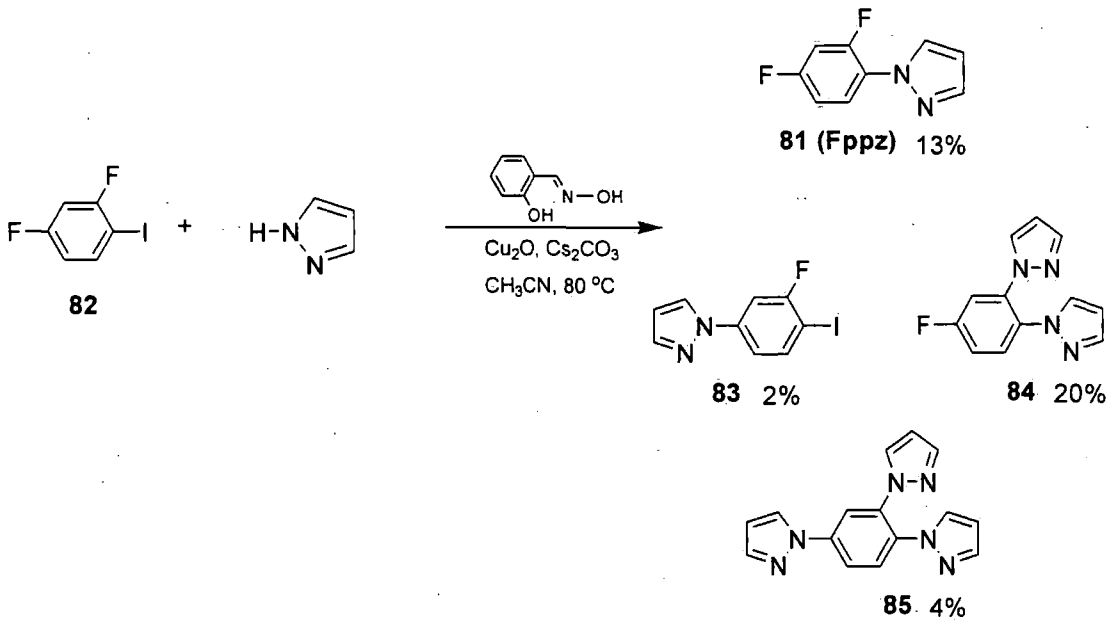

Scheme 25. The synthesis of **81** (**Fppz**) by copper(I) catalysis.

The synthesis of iridium(III) dimer complexes

The syntheses of iridium(III) dimer complex involving $IrCl_3.nH_2O$ were carried out in an inert atmosphere despite the stabilities of the compounds in air, with the main concern being the possible oxidative and thermal sensitivity of the intermediate complexes at the high temperature used in the reactions. Cyclometalated Ir(III) dichloro-bridged dimers of the general formula $(C^N)_2Ir(\mu\text{-}Cl)_2Ir(C^N)_2$ were synthesised by the method reported by Watts,[177] in which $IrCl_3.nH_2O$ and 2-2.5 equiv of cyclometalating ligand are heated in a 3 :1 mixture of 2-ethoxyethanol and deionised water to 110 °C. The general formulae and yields of iridium(III) dimer complexes are shown in Table 4 .

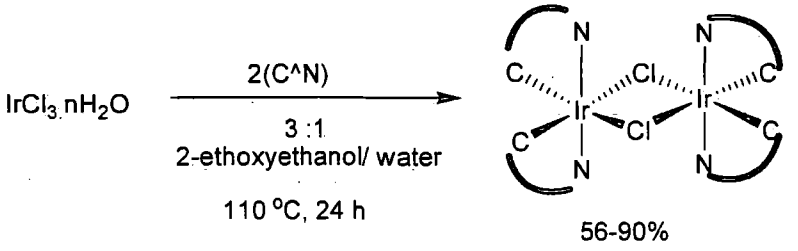

Scheme 26. The general synthesis of iridium(III) dimer complexes

Table 4. Summary of iridium(III) dimer complexes synthesised in the present work

	Code	C^N ligand	% yield
86	**$[(ppy)_2IrCl]_2$**	**ppy**	90
87	**$[(4Meppy)_2IrCl]_2$**	**4Meppy**	86
88	**$[(4CF_3ppy)_2IrCl]_2$**	**$4CF_3ppy$**	62
89	**$[(5CF_3ppy)_2IrCl]_2$**	**$5CF_3ppy$**	75
90	**$[(bq)_2IrCl]_2$**	**bq**	60
91	**$[(thpy)_2IrCl]_2$**	**thpy**	56
92	**$[(Fppz)_2IrCl]_2$**	**Fppz**	58

Single crystals of the chloro-bridged dimer, **89**; **[(5CF$_3$ppy)$_2$IrCl]$_2$**, were grown from CD_2Cl_2 and the X-ray molecular structure is shown in Table 5. The result shows that the nitrogen atoms were confirmed to be mutually *trans* to each other. The Ir-C, Ir-N, and Ir-Cl bond lengths for this complex are given in Table 5. The bond lengths are similar to those of analogues found in the literature.[178]

Table 5. The molecular structure and selected bond distances for **89**; **[(5CF$_3$ppy)$_2$IrCl]$_2$**.

Crystal structure*	3-D structure	Selected bond lengths (Å)
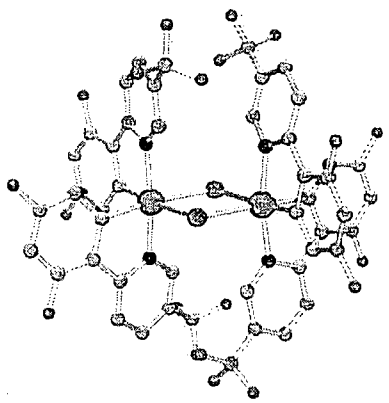	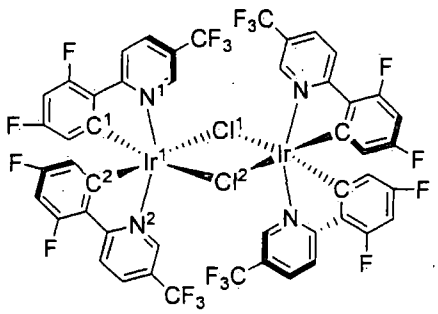	Ir^1-C^1= 2.001(4) Ir^1-C^2= 1.995(4) Ir^1-N^1= 2.049(3) Ir^1-N^2= 2.044(3) Ir^1-Cl^1= 2.5046(9) Ir^1-Cl^2 =2.5265(10)

* CD_2Cl_2 was omitted for clarity

The synthesis of charged iridium(III) complexes

The syntheses of charged iridium(III) complexes from iridium(III) dimer complexes were carried out in an inert atmosphere and no light or air following the method reported by our group (Scheme 27).[153] $(C^N)_2Ir(\mu\text{-}Cl)_2Ir(C^N)_2$ and an excess of N^N ligands were heated in a 1 :1 mixture of DCM and methanol to 80 °C followed by anion exchange using KPF_6 or KBF_4. The structures and yields of charged iridium(III) complexes are shown in Table 6.

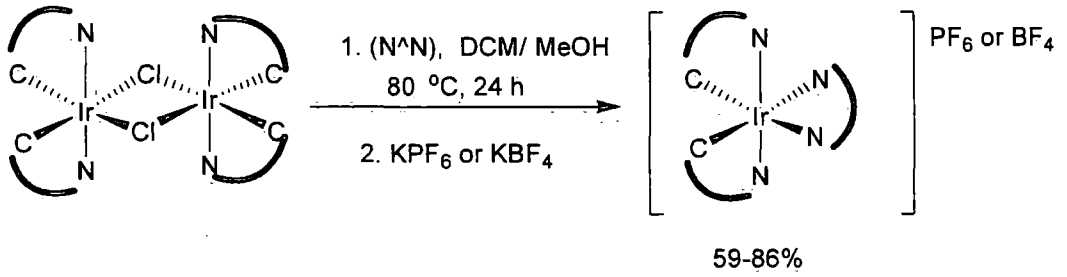

Scheme 27. The general synthesis of charged iridium(III) complexes.

Following the successful synthesis of **95** (**OLED 2**) and **101** (**OLED 7**), we decided to use **2,9 MePhen** ligand (N^N) in **95** (**OLED 2**) and **89** (**$[(5CF_3ppy)_2IrCl]_2$**) (C^N) in **101** (**OLED 7**). Unfortunately, the separated product obtained from column chromatography did not contain the **2,9 MePhen** unit. The ^1H NMR and mass spectroscopic characterisation showed that the product is the neutral iridium complex **93** (**OLED 12**) which is shown in Scheme 28. This is probably due to the steric bulk of the 2,9 MePhen unit.

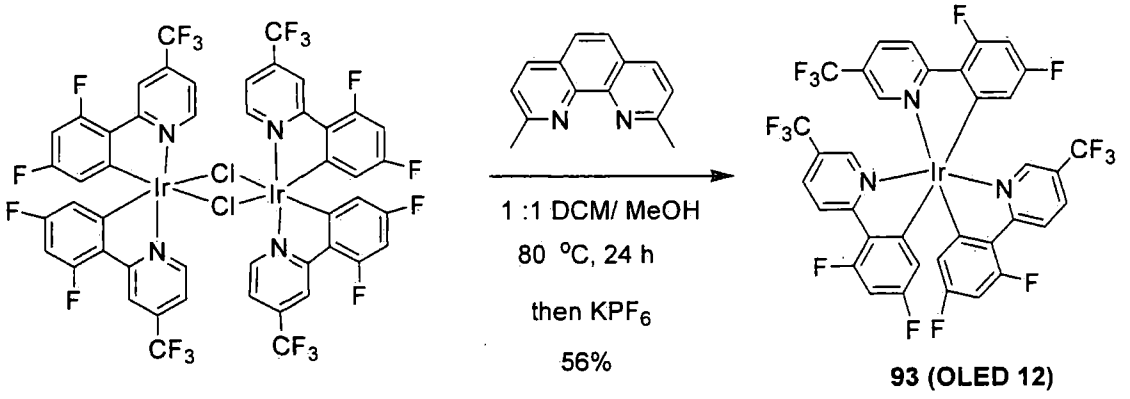

Scheme 28. Unexpected synthesis of **93** (**OLED 12**).

Table 6. Code, structure and isolated yield of charged iridium(III) complexes

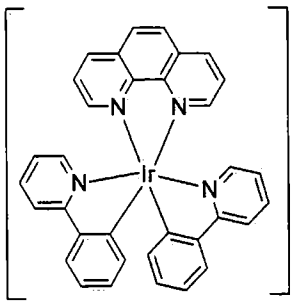 **94 (OLED 1)** (80 %)	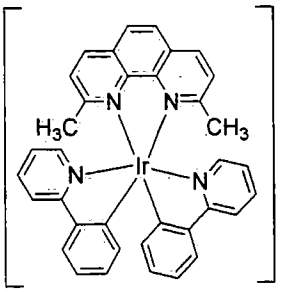 **95 (OLED 2)** (73 %)
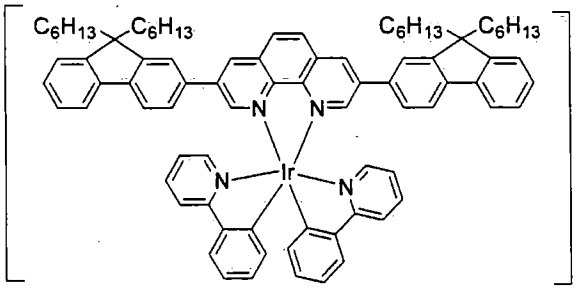 **96 (OLED 3)** (70 %)	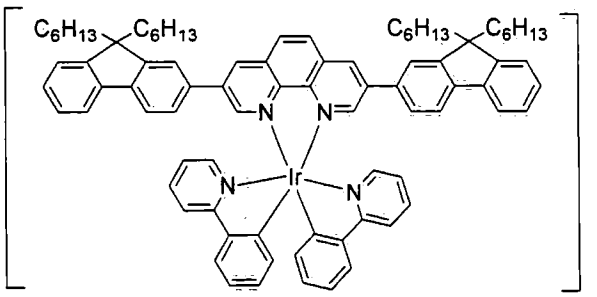 **97 (OLED 3-BF_4)** (70 %)
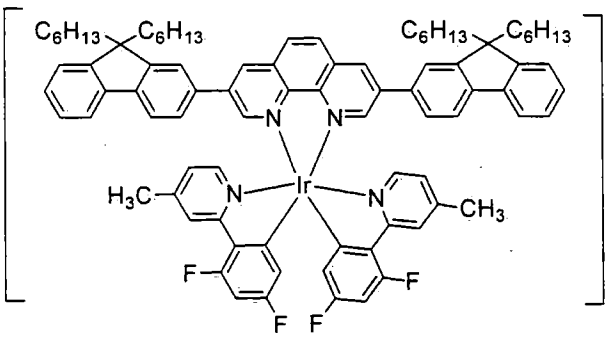 **98 (OLED 4)** (75 %)	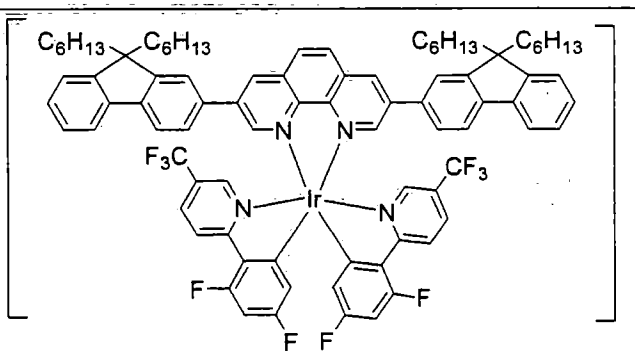 **99 (OLED 5)** (76 %)
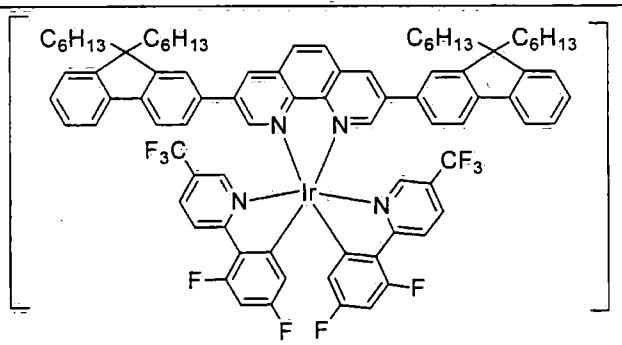 **100 (OLED 6)** (76 %)	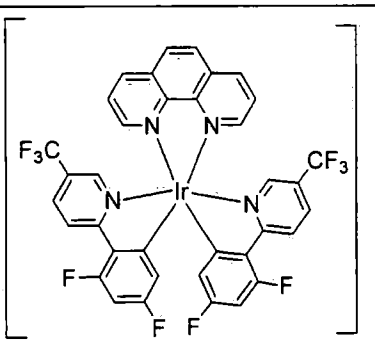 **101 (OLED 7)** (80 %)

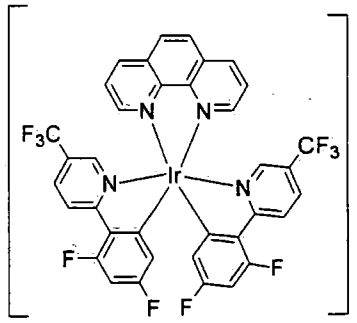

102 (OLED 8) (82 %)

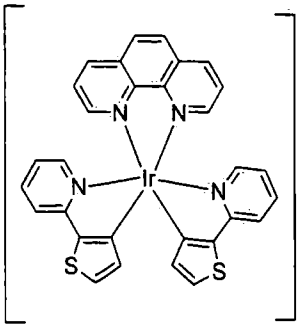

103 (OLED 9) (75 %)

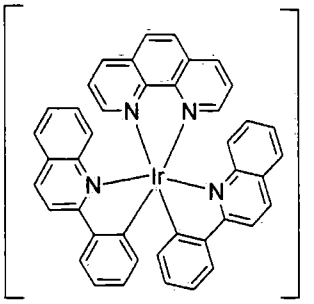

104 (OLED 10) (65 %)

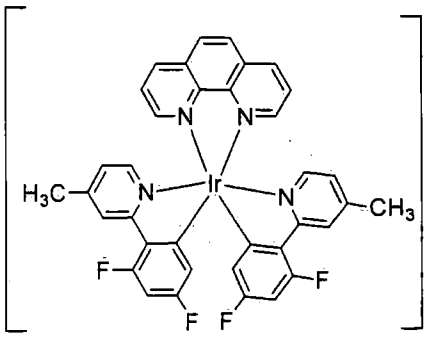

105 (OLED 11) (86 %)

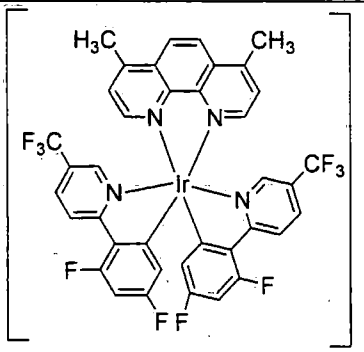

106 (OLED 13) (81 %)

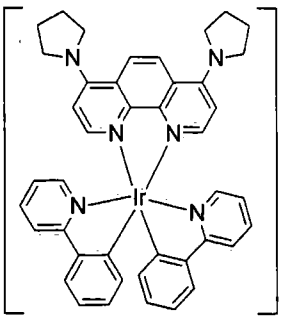

107 (OLED 14) (59 %)

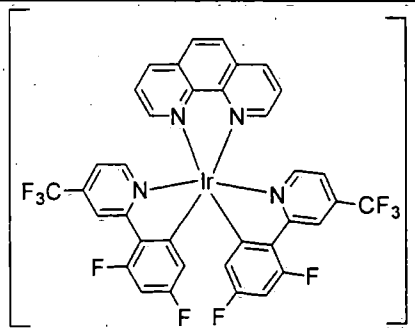

108 (OLED 15) (68 %)

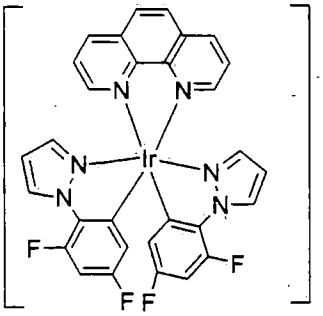

109 (OLED 16) (70 %)

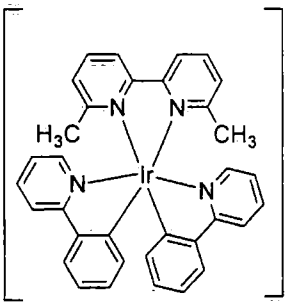

110 (OLED 18) (75 %)

Characterisation of charged iridium(III) complexes

The charged iridium(III) complexes were characterised by ^{1}H, ^{13}C and ^{19}F NMR spectroscopy, mass spectrometry using ES^{+}, ES^{-} and, where applicable, MALDI-TOF techniques and by CHN analysis.

NMR Characterisation.

The solution NMR spectra were carried out in either $CDCl_3$ or $CDCl_2$ depending on the solubility of the complex. Each complex shows C_2 symmetry and a first-order NMR spectrum, which makes spectral interpretation for these complexes relatively straightforward. Due to the C_2 symmetry, the number of resonances observed is half that of the protons in the complex; each resonance is equivalent to two protons in equivalent magnetic environments. For example, the proton assignment of **101** (**OLED 7**) is shown in (Figure 68, top). Nine distinct aromatic proton resonances are displayed, in parts of **75** (**5CF$_3$ppy**) and **Phen** ligands (Figure 68, top). Five aromatic resonances labeled H_1, H_2, H_3, H_4 and H_6 for protons of **75** (**5CF$_3$ppy**) ligand (δ = 5.85, 6.77, 8.53, 8.05 and 7.42 ppm, respectively), and four protons for **Phen** ligand at 8.39, 8.00, 8.81 and 8.32 ppm, labeled as H_A, H_B, H_C and H_D, respectively. It is interesting to note that the PF_6 and BF_4 anion salts forms of the complexes are distinguishable by ^{1}H NMR spectroscopy. A specific example is shown for **101** (**OLED 7**) and **102** (**OLED 8**). The solution ^{1}H NMR spectra of both complexes in CD_2Cl_2 at room temperature are presented in Figure 68. Moreover, the identification of the anions has been confirmed by ES^{-} mass spectrometric techniques which show the mass of PF_6 and BF_4 for **101** (**OLED 7**) and **102** (**OLED 8**), respectively.

The chemical shifts of the Phen protons are changed more than the ppy protons by the different anion, suggesting that the anion is located near the Phen ligand in solution.

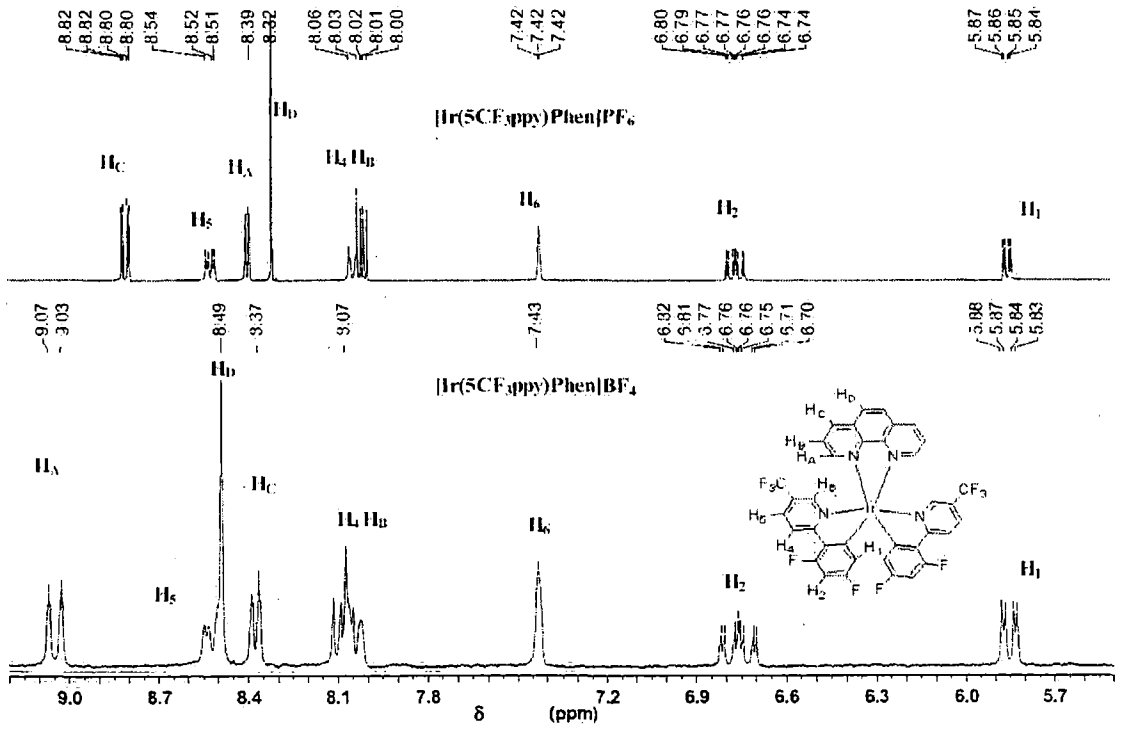

Figure 68. ^{1}H NMR spectra for **101** (**OLED 7**) PF_6 salt (top) and **102** (**OLED 8**) BF_4 salt (bottom) using 400 and 200 MHz, respectively, at room temperature in CD_2Cl_2. Includes proton assignment and structure of complexes as insert.

X-ray Crystallography.

Single crystals of **OLEDs 2, 3, 7, 9, 15, 16** and **18** were grown by allowing slow evaporation of their solutions in the NMR tube and they were characterised using X-ray crystallography. The molecular structures are given in Table 7. In addition, the crystal data are shown in Table 7.

The structures for **OLEDs 2, 3, 7, 9, 15, 16** and **18** show that the C-C and C-N intraligand bond lengths and angles are within normal ranges expected for cyclometalated Ir(III) complexes and are similar to the values of charged iridium(III) complexes previously reported in the literatures.[163,164,179-182] However, the Ir-N bond lengths for **OLEDs 2** and **18** differ markedly in detail *vide infra*.

All of the complexes examined here have the three cyclometalating ligands in a pseudooctahedral coordination geometry around the metal center. The two Ir–C bonds are situated *cis* to each other and *trans* to the Ir–N(phen or bpy) bonds. Interestingly, the Ir–N_1 and N_2 bonds are significantly longer than the Ir– N_3 and N_4 bonds (by ~ 0.1 Å) which

is consistent with the stronger *trans* influence of a phenyl group relative to a pyridyl group.

It is also interesting to compare **OLEDs 2** and **18** with **OLEDs 3, 7, 9, 15,** and **16**. The Ir–N_1 and N_2 bond lengths of **OLEDs 2** and **18** (average 2.19 Å) are significantly longer than the Ir– N_1 and N_2 bonds length of **OLEDs 3, 7, 9, 15,** and **16** (average 2.13 Å). A likely explanation for this is the steric repulsion of the iridium centre with the methyl groups on the phenanthroline unit.

Table 7. The molecular structure, solvent system and selected bond distance of charged iridium complexes.

Crystal structure**	3-D structure	Selected bond lengths (Å)
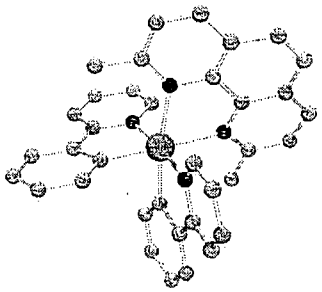 **95 (OLED 2)**	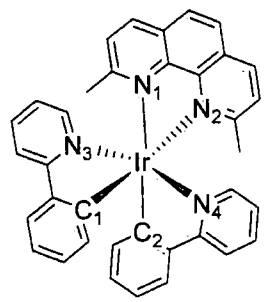	Ir-N_1 = 2.193(3) Ir-N_2 = 2.197(3) Ir-N_3 = 2.032(3) Ir-N_4 = 2.053(3) Ir-C_1 = 2.010(3) Ir-C_2 = 2.016(3)
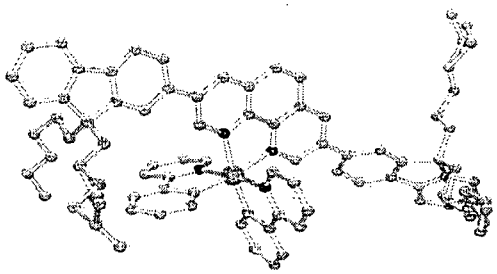 **96 (OLED 3)**	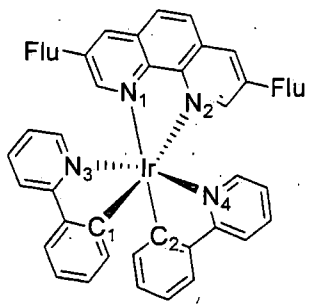	Ir-N_1 = 2.143(3) Ir-N_2 = 2.163(3) Ir-N_3 = 2.049(3) Ir-N_4 = 2.052(3) Ir-C_1 = 2.003(4) Ir-C_2 = 2.011(4)

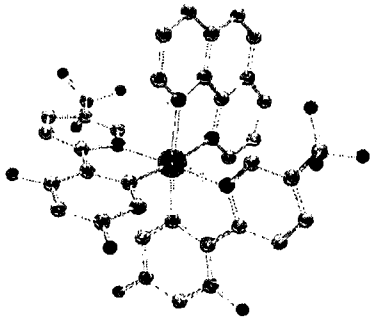 **101 (OLED 7)***	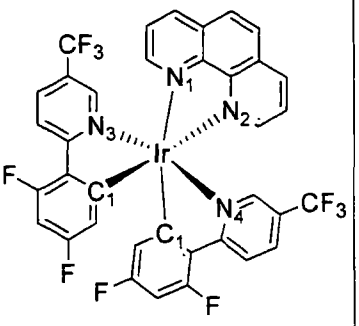	$Ir\text{-}N_1 = 2.119$ $Ir\text{-}N_2 = 2.119$ $Ir\text{-}N_3 = 2.044$ $Ir\text{-}N_4 = 2.044$ $Ir\text{-}C_1 = 2.014$ $Ir\text{-}C_2 = 2.014$
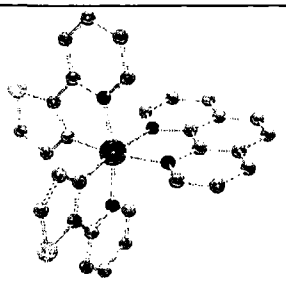 **103 (OLED 9)**	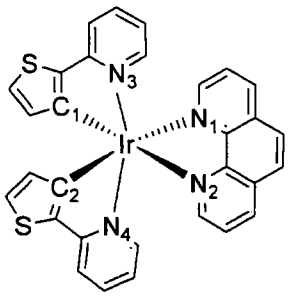	$Ir\text{-}N_1 = 2.130$ $Ir\text{-}N_2 = 2.128$ $Ir\text{-}N_3 = 2.085$ $Ir\text{-}N_4 = 2.061$ $Ir\text{-}C_1 = 2.007$ $Ir\text{-}C_2 = 1.972$
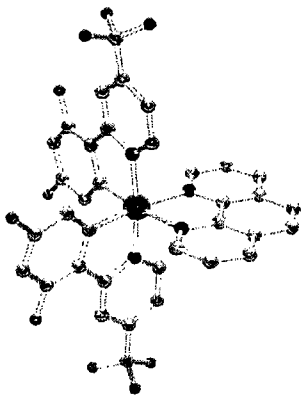 **108 (OLED 15)**	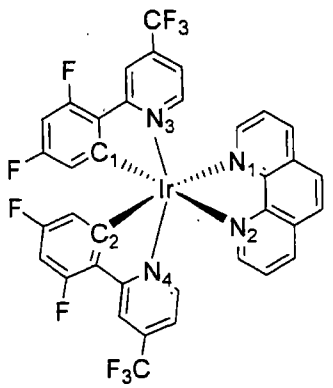	$Ir\text{-}N_1 = 2.141(2)$ $Ir\text{-}N_2 = 2.139(3)$ $Ir\text{-}N_3 = 2.041(2)$ $Ir\text{-}N_4 = 2.038(2)$ $Ir\text{-}C_1 = 2.015(2)$ $Ir\text{-}C_2 = 2.010(2)$
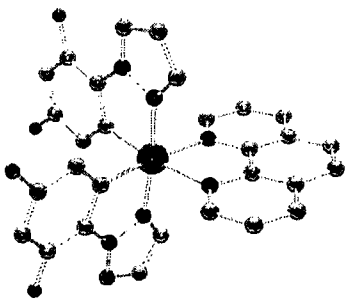 **109 (OLED 16)**	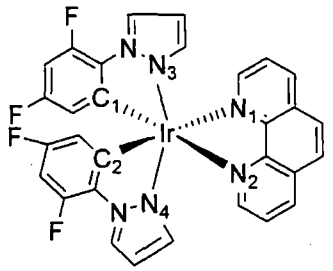	$Ir\text{-}N_1 = 2.128(2)$ $Ir\text{-}N_2 = 2.125(2)$ $Ir\text{-}N_3 = 2.016(3)$ $Ir\text{-}N_4 = 2.013(2)$ $Ir\text{-}C_1 = 2.023(3)$ $Ir\text{-}C_2 = 2.012(3)$

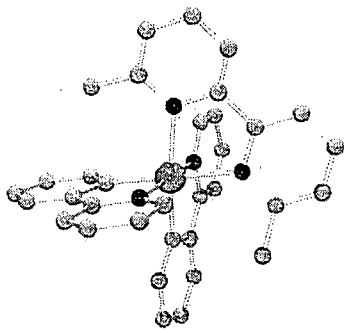 **110 (OLED 18)**	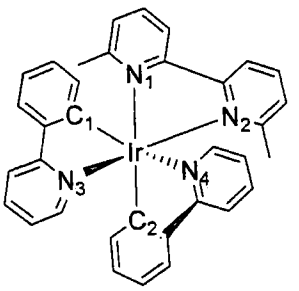	$Ir\text{-}N_1 = 2.205(3)$ $Ir\text{-}N_2 = 2.205(3)$ $Ir\text{-}N_3 = 2.045(4)$ $Ir\text{-}N_4 = 2.053(3)$ $Ir\text{-}C_1 = 2.008(4)$ $Ir\text{-}C_2 = 2.008(4)$

* The counterion for **101** (**OLED 7**) was found to be chloride, presumably from the dichloro-bridged precursor **89**.

** The solvent molecules and PF_6 anions were omitted for clarity.

Solution-state photophysical properties

Absorption.

The absorption spectra of charged iridium(III) complexes were recorded in DCM at 298 K. The λ_{max} values are shown in Table 8. All the complexes display strong absorption bands between 250 and 300 nm (not shown in Figure 69) which can be attributed to π-π^* ligand-centred (LC) transitions typically involving the excitation of electrons from filled π to vacant π^* orbitals of the cyclometalated ppy and phen ligands. Weaker absorption bands at longer wavelengths (in the range of 300-450 nm) can be attributed to metal-to-ligand charge transfer (MLCT, arising from the excitation from a filled t_{2g} orbital of Ir(III) to a vacant π^* orbital of the phenanthroline or bpy ligand acting as acceptor). These features are consistent with the literature data for related charged iridium(III) complexes.[163,164,179-182]

The spectra for **OLEDs 1, 2** and **3** are shown in Figure 69. It is interesting to note that **96** (**OLED 3**) show a red-shift which is explained by the increased conjugation length of phenanthroline with two fluorene substituents. It is also noteworthy that extinction coefficients increased as the conjugation length increased. The weak shoulders, as evident from their low energy and low extinction coefficients, seen at > 420 nm and extending towards the red region are assigned to both spin-allowed metal to

ligand charge-transfer (^{1}MLCT) transitions and spin-orbit coupling enhanced ^{3}LC and ^{3}MLCT transitions.

Table 8. The maxima for absorption and emission of complexes in DCM at 298 K.

Compound	λ_{abs}(nm)	λ_{em}(nm)
94 (OLED 1)	380	580
95 (OLED 2)	375	532
96 (OLED 3)	397	564, 610
98 (OLED 4)	411	566, 612
99 (OLED 5)	412	573, 616
100 (OLED 6)	411	573, 615
101 (OLED 7)	382	465, 498
102 (OLED 8)	381	464, 498
103 (OLED 9)	389	595

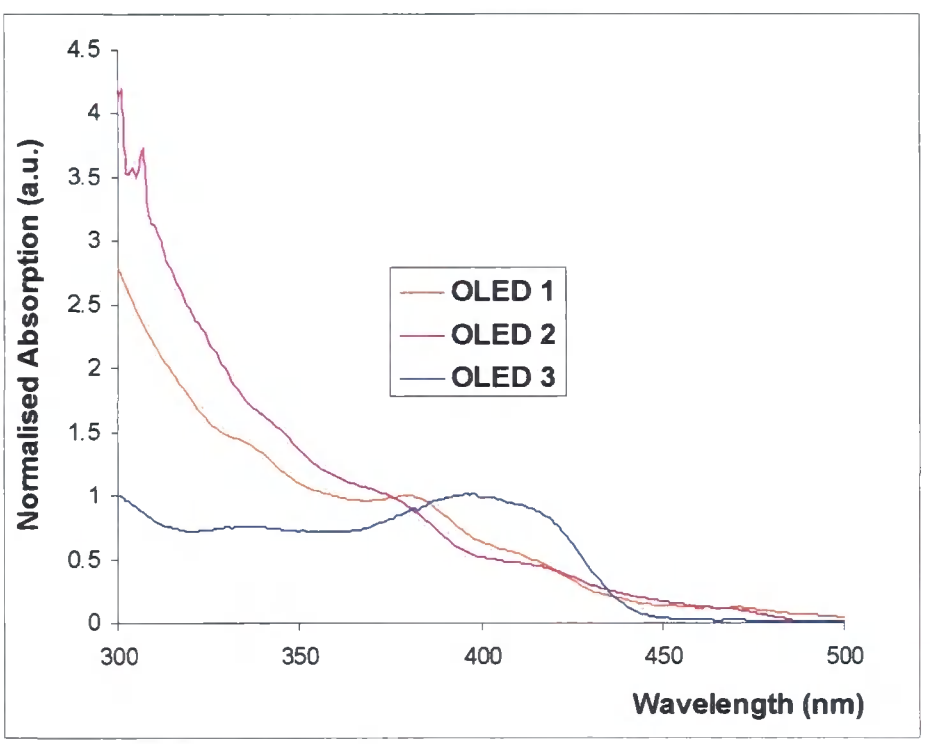

Figure 69. Absorption spectra of **OLEDs 1**, **2** and **3** in DCM at 298 K

Emission.

The λ_{max} emission data of the complexes in DCM at 298 K are shown in Table 9. The spectra of **OLEDs 1**, **2**, **3**, 7 and **9** are shown in Figure 71. Intensive luminescence was observed for the iridium complexes with λ_{max} ranging from 465-595 nm. The known complexes show similar λ_{max} values as our results. Specifically **94 (OLED 1)** shows 580 nm while the literature reported 575 (in DCM)[183] and 579 (in MeCN).[184] Moreover, **95 (OLED 2)** shows 532 nm, compared with 534 nm previously reported.[183]

It is noteworthy that **95 (OLED 2)** shows significantly blue-shifted emission compared with **94 (OLED 1)**. We believe that steric effects of the two methyl groups are responsible for this, as also seen in the longer bond length Ir-N1 and N2 (Table 7). The most hypsochromic shift in this series can be seen by adding electron withdrawing groups (two F atoms and one CF_3) to **101 (OLED 7)** and **102 (OLED 8)** which show the emission peak at 465 nm. As expected the different counter anions have no effect on the emission colour. Surprisingly, an increase in conjugation length of the phenanthroline ligand in **94 (OLED 1)** to **96 (OLED 3)** shifts the λ_{max} emission to the blue (by 16 nm). However, **96 (OLED 3)** shows a red-shifted emission shoulder (by 30 nm) compared with λ_{max} of the parent complex, **94 (OLED 1)**.

The bathochromic shift (15 nm) from the emission of **94 (OLED 1)** can be observed by changing ppy ligand to thpy ligand in **OLED 9** which contains the electron donating thiophene unit in place of ppy.

From this series, we have successfully tuned the emission colour in solution from blue to orange (465-595 nm) as shown in Figures 70 and 71.

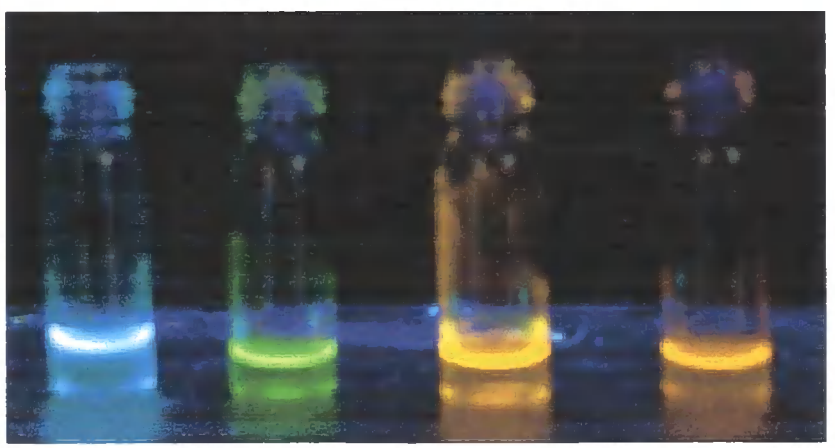

Figure 70. Emission colour of DCM solutions of **OLEDs 7, 2, 1** and **3** (left to right)

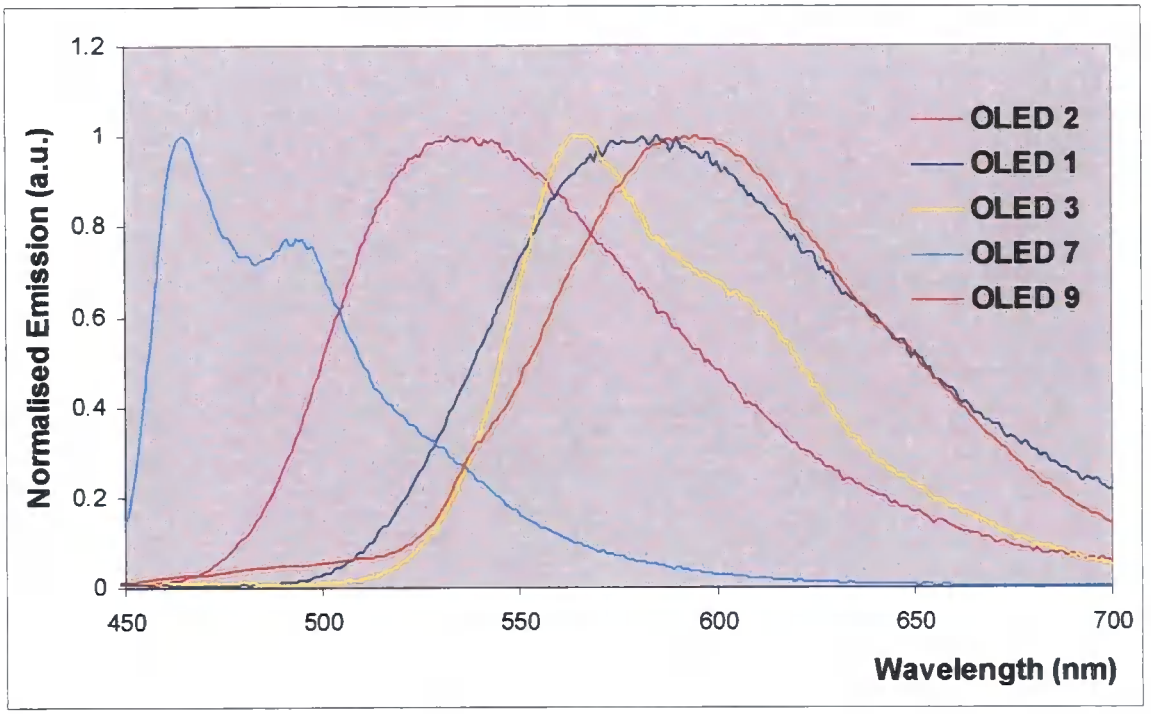

Figure 71. Emission spectra of **OLEDs 1, 2, 3, 7** and **9** in DCM at 298 K.

Table 9. Summary of the PLQY data of **OLEDs 1, 2, 3, 7, 9, 13** and **16**.[♣]

Compound	PLQY solution (toluene)	PLQY solution (CH_3CN)	PLQY film (toluene)	PLQY film (CH_3CN)
94 (OLED 1)	0.13	0.04	0.06	0.40
95 (OLED 2)	0.23	0.01	0.71	0.20
96 (OLED 3)	0.02	0.01	0.04	0.36
101 (OLED 7)	0.05	0.14	0.12	0.13
103 (OLED 9)	0.02	0.003	0.01	0.02
106 (OLED 13)	0.33	0.05	0.08	0.07
109 (OLED 16)	0.23	0.03	0.69	0.005

Table 9 shows preliminary PLQY data of **OLEDs 1, 2, 3, 7, 9, 13** and **16** in both solution (toluene and CH_3CN) and thin film (from toluene and CH_3CN). All complexes

[♣] Data from Mr. Khalid Abdullah in the Department of Physics, Durham University.

show low PLQY in solution (toluene and CH_3CN). Generally, in non-polar toluene the PLQYs are higher which suggests that the photophysical properties are modified by ionic solute-solvent interactions with more polar acetonitrile which reduce the PLQY. Surprisingly, most of the PLQYs in films are higher than in solution. More interestingly, **95** (**OLED 2**) and **109** (**OLED 16**) show high PLQY in film (from toluene) of 0.71 and 0.69, respectively. However, the reasons for this are not clear at present.

Solution Electrochemical Studies

Cyclic voltammetric (CV) studies were carried out at 298 K using $Ag/AgNO_3$ (CH_3CN) as a reference electrode and ferrocene/ferrocenium (Fc/Fc^+) couple as a secondary reference. Dichloromethane solutions of the complexes containing 0.1 M tetra(*n*-butyl)ammonium hexafluorophosphate (*n*-Bu_4NPF_6) as the supporting electrolyte were scanned at 100 mV/s. The oxidation and 1st reduction potentials of the **OLEDs 1**, **2**, **3**, **7**, **9**, **13** and **15** are summarised in Table 1 and the CV traces of **94** (**OLED 1**) are shown in Figure 2. The CVs of the complexes displayed chemically quasi-reversible oxidations. Quasi-reversible and irreversible waves have been observed on reduction scans as shown in Figure 72.

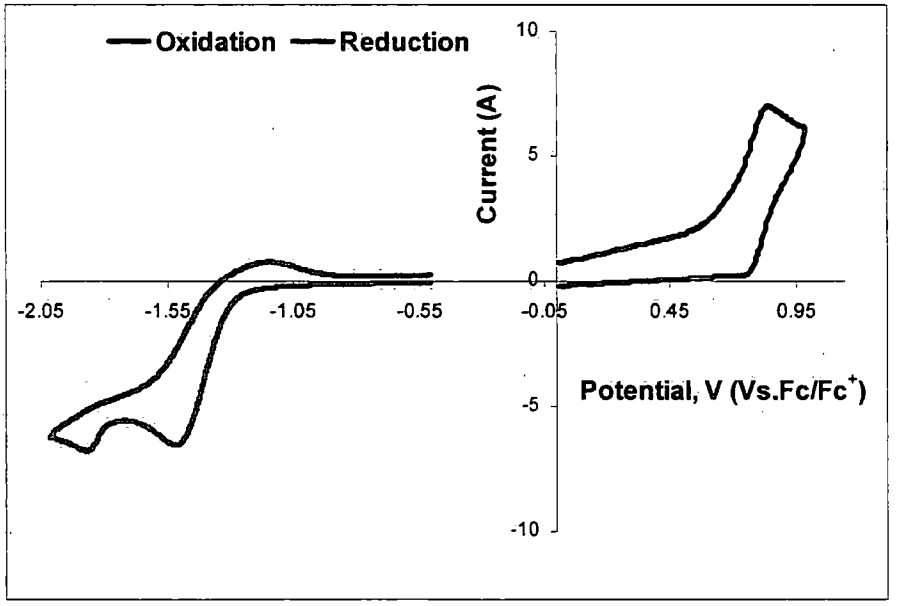

Figure 72. Cyclic voltammograms of **94** (**OLED 1**) showing both oxidation and reduction waves in 0.1 M *n*-Bu_4NPF_6 dichloromethane solution at 298 K, scan rate 100 mV s^{-1}, relative to Fc/Fc^+.

Table 10. Summary of the oxidation (E_{ox}) and reduction (E_{red}) potentials obtained by cyclic voltammetry for **OLEDs 1, 2, 3, 7, 9, 13, 15, 16** and **18**.

Compound	E_{ox} (V) [a]	E_{red} (V) [a]	ΔE (V) [b]
94 (OLED 1)	0.85	−1.54, −1.89	2.39
95 (OLED 2)	0.92	−1.74, −1.95	2.66
96 (OLED 3)	0.88	−1.66, −1.74	2.54
101 (OLED 7)	1.34	−1.60, -1.79	2.94
103 (OLED 9)	0.75	−1.52, −1.83	2.27
106 (OLED 13)	1.29	−1.66, −1.86	2.96
108 (OLED 15)	1.32	−1.57, −1.73	2.90
109 (OLED 16)	1.44	−1.70	3.14
110 (OLED 18)	0.98	−1.37, -1.87	2.35

[a] Oxidation and reduction potential with Ag/Ag^+, 0.1 M Bu_4NPF_6 in CH_3CN at 298 K, scan rate =100 mV s^{-1}, the values are reported relative to Fc/Fc^+, [b] $\Delta E = E_{ox} - 1^{st} E_{red}$.

It is notable that the oxidation potential of **OLEDs 7, 13, 15** and **16** (1.29–1.34 V) is significantly higher than those of the complexes **OLEDs 1, 2, 3** and **18** (0.85–0.98 V). As revealed by previous electrochemical studies and theoretical calculations,[163,164,179,180] of charged iridium(III) complexes, the one-electron oxidation of such d^6 metal complexes will mainly occur at the metal site, together with a minor contribution from the surrounding chelates. Thus, the higher oxidation potential of **OLEDs 7, 13, 15** and **16** is attributed to the diF and CF_3 groups in the ppy ligand, which stabilise the metal d orbitals *via* withdrawing electrons from the metal. Conversely, **103 (OLED 9)** (0.75 V) shows the oxidation potentials are relatively lower than those of the complexes **OLEDs 1, 2** and **3**. Upon switching to the reduction sweep, the similar results were observed for the 1^{st} E_{red} (−1.60 to −1.52 V). This wave is assigned to the reduction of the phenanthroline segment, which is observed in **OLEDs 1, 9, 7** and **15**. The result suggested that the highest destabilized LUMO among all the complexes is for the 2,9-dimethylphenanthroline ligand **95 (OLED 2)**. These data are in good agreement with the blue shift for their

emission signals. On the other hand, **96** (**OLED 3**) has the lowest 1st E_{red} at -1.66 V for which the conjugated fluorene is responsible. Most of the complexes show a second reduction wave which is assigned to the ppy unit.

A comparison of 2,9-dimethylphenanthroline with 2,9-dimethylbipyridine shows that the complex with 2,9-dimethylphenanthroline **95** (**OLED 2**) has a bigger energy gap than the complex with 2,9-dimethylbipyridine **110** (**OLED 18**). This is consistent with the reduction potentials in Table 10, i.e. –1.74 and –1.37 V for **95** (**OLED 2**) and **110** (**OLED 18**).

The redox chemistry results suggest that the highest energy gap is found for **OLEDs 7, 13** and **15** (2.90-2.96 V). Conversely, **103** (**OLED 9**) shows the lowest energy gap (2.27 V). It should be noted that the variation in the energy gap is consistent with the different emission colours, shown in Table 8. The consistency of the emission spectroscopic measurements with the energy gaps from cyclic voltammetry data is shown in Figure 73.

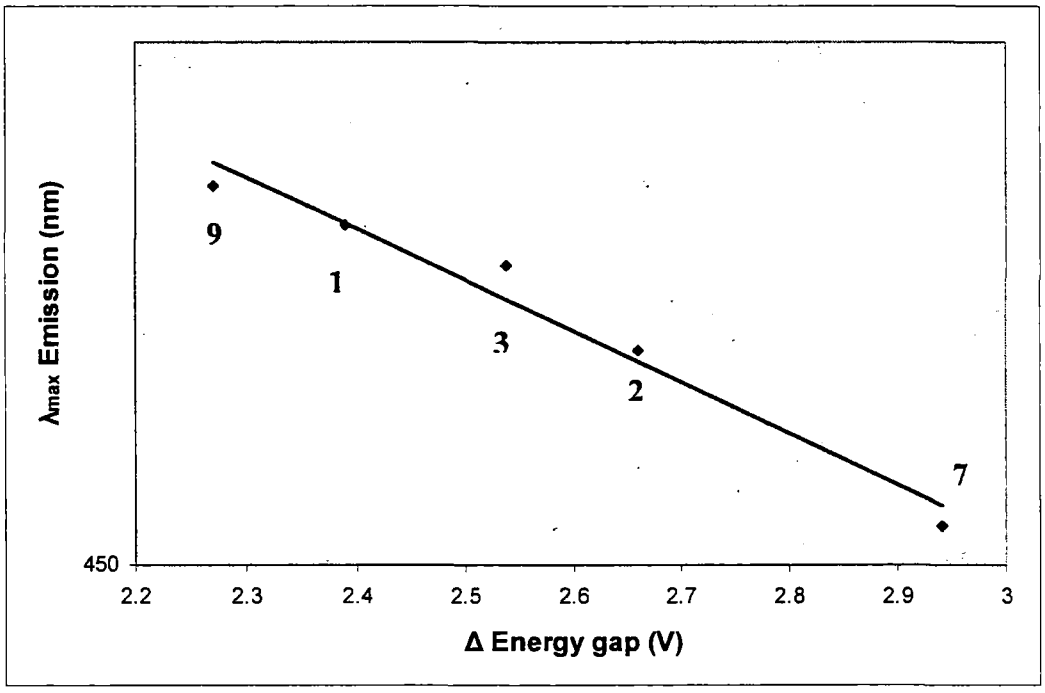

Figure 73. The correlation of the maximum emission wavelengths and the energy gaps from cyclic voltammetry data of **OLEDs 1, 2, 3, 7** and **9.**

Theoretical studies

The geometries and electronic structures of **96 (OLED 3)** were calculated by Dr I. F. Perepichka in our group using density functional theory (DFT) methods.[153] To decrease the computation time calculations were performed for analogues of **96 (OLED 3)**, in which CH_3 substituents replaced the C_6H_{13} chains (denoted as **96 (OLED 3')**).

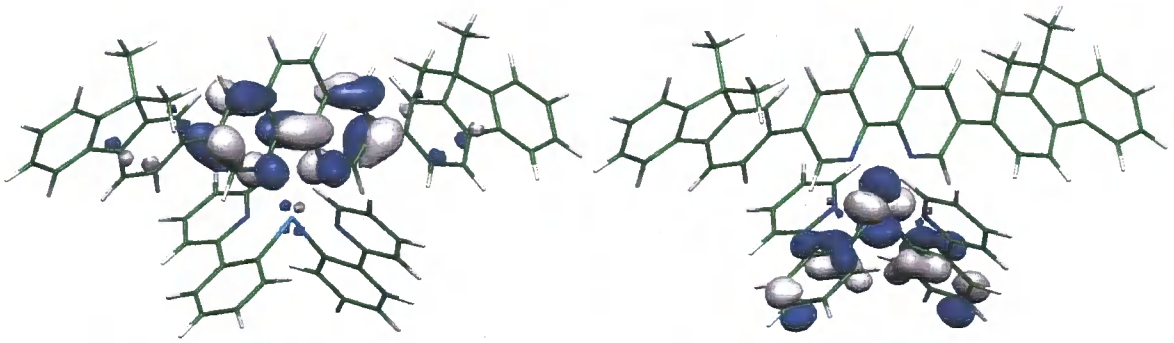

LUMO **HOMO**

Figure 74. Isocontour plots (0.04 e $bohr^{-3}$) calculated for the HOMO and the LUMO orbitals of **96 (OLED 3')** (from reference 153).

Figure 74 shows the atomic orbital composition calculated for the frontier molecular orbitals of complex **96 (OLED 3')** in the S_0 state. The HOMO (that is, the orbitals into which holes are injected, and which are involved in the hole injection process in light-emitting electrochemical cell (LEC) operation; see below) are distributed between the Ir atom and the benzene rings of the ppy ligands. The LUMOs (the orbitals into which electrons are injected in the LEC) are mainly located on the pyridine rings of the phenanthroline ligand, with only minor extension to the outer fluorene moieties.

Light-Emitting Cells (LECs)

The study of light-emitting cells of charged iridium(III) complexes with bulky side group

LEC studies of **OLEDs 1**, **3** and **31**[153] were chosen to probe the effect of the number of fluorene units on device properties. The device studies were performed in Professor Monkman's group in the Department of Physics, Durham University. Bulky 9,9-dihexylfluorene side groups were attached to phenanthroline ligands of **96 (OLED 3)** and **OLED 31** at sites where they have little effect on the electronic properties of the

complex while providing the benefit of enhanced steric hindrance which reduces concentration quenching. The structure of **OLED 31**[153] which was synthesised in our group by Dr. Xianshun Zeng is shown in Figure 75 .

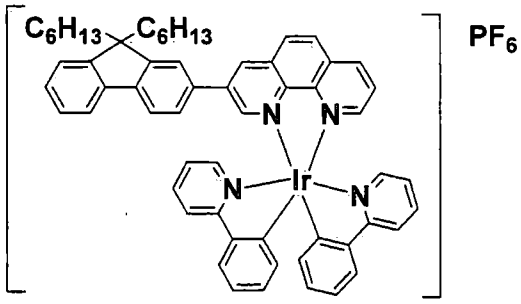

OLED 31

Figure 75. The structure of **OLED 31** synthesised by Dr. Xianshun Zeng

To assess the effective steric hindrance due to the fluorenyl substituents, the X-ray crystal structure of **96** (**OLED 3**) was obtained. The Ir atom has a distorted octahedral geometry (Figure 76).

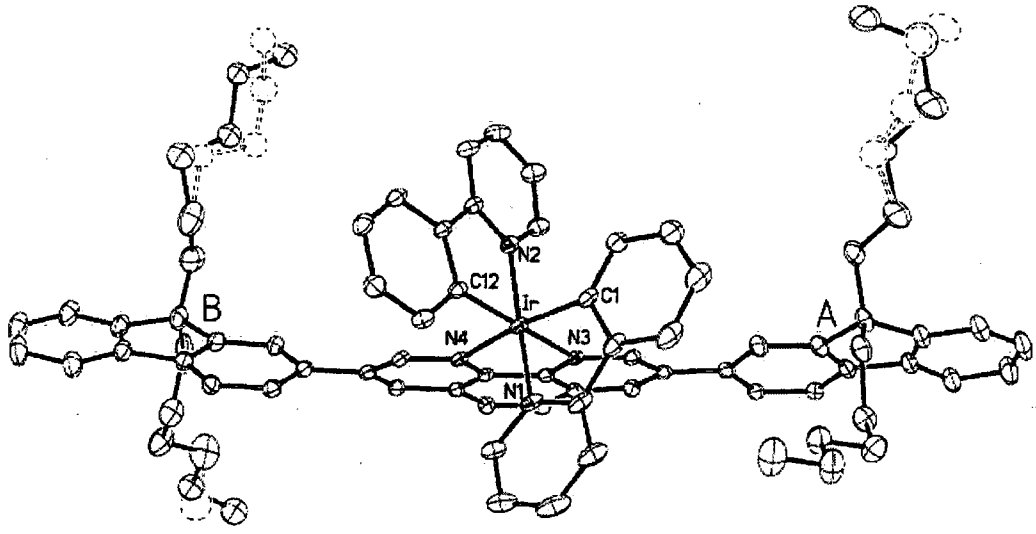

Figure 76. Cation in the crystal of **96** (**OLED 3**) .CH_2Cl_2 showing the disorder of hexyl chains. Thermal ellipsoids are drawn at the 30% probability level, hydrogen atoms are omitted. Bond distances (Å): Ir–N(1) 2.049(3), Ir–N(2) 2.052(3), Ir–N(3) 2.143(3), Ir–N(4) 2.163(3), Ir–C(1) 2.003(4), Ir–C(12) 2.011(4).

The two Ir–C bonds are situated *cis* to each other and *trans* to the Ir–N(phen) bonds, which are 0.1 Å longer than the Ir–N(ppy) bonds due to a *trans*-influence. The planar fluorene moieties A and B are inclined to the central phenanthroline plane by 9 and 43°, respectively, and to each other by 51°. The alkyl substituents of moiety A are in the *syn*-orientation with respect to the metal center, and those of moiety B are close to the *anti*-orientation. Three out of four hexyl chains are disordered, while large atomic displacement parameters of the anion and the DCM molecule also imply disorder which we could not rationalize. The cations related via an inversion center ($0\ 1/2\ 1/2$) have substantial overlap between their near-planar cores (comprising phenanthroline and fluorene A moieties), the interplanar separation between which (3.49 Å) is close to the normal van der Waals contact distance. However, these dimers are interspersed with anions and DCM molecules and do not form any continuous stacking motif (Figure 77). The shortest Ir....Ir distances in the structure (9.08 and 8.94 Å) are similar to those observed in a sterically hindered 4,5-diaza-9,9'-spirobifluorene (sb) complex $[Ir(ppy)_2sb]PF_6$ (9.21 and 8.62 Å).[181] They occur between molecules which are related via inversion centers ($0\ 0\ 1/2$) and ($0\ 1/2\ 1/2$) and form a chain parallel to the crystallographic y-axis.

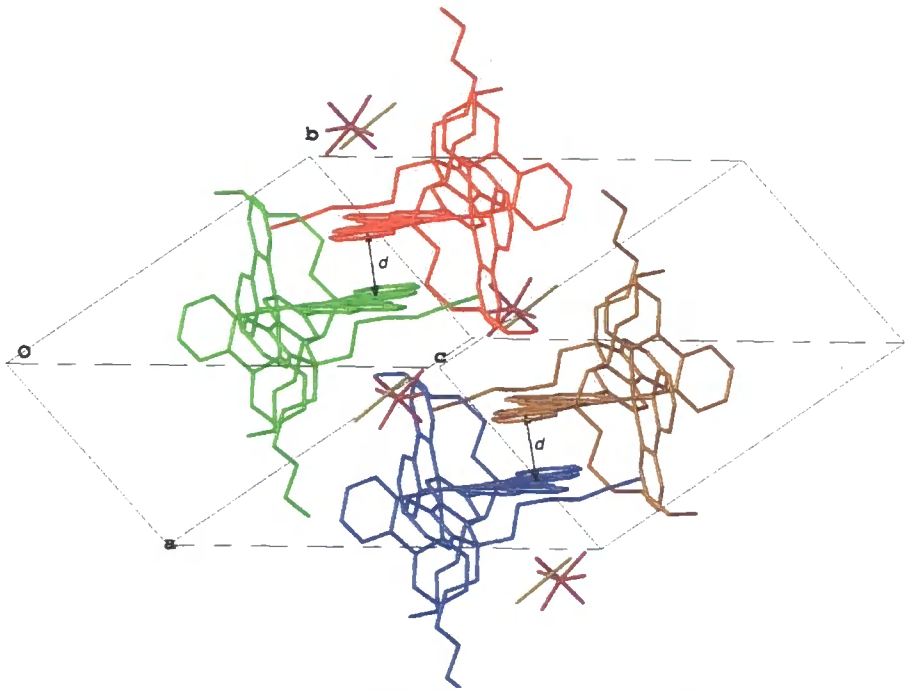

Figure 77. Crystal packing of **96** (**OLED 3**).CH_2Cl_2. Note the overlap between planar molecular cores (d =3.49 Å).

The following LEC device architecture was used: ITO/PEDOT:PSS/Ir complex/Al. LECs results are presented in Figure 78 which compares **OLEDs 1**, **3** and **31** in the term of the charging time and brightness. It is well-known that solid-state LECs exhibit a significant charging time because electroluminescence can only occur after the ionic double layers have been built up at the electrode interfaces. Because in this case only the PF_6^- anion is mobile, the double layers are formed by accumulation and depletion of PF_6^- at the anode and cathode, respectively. The device with **OLED 31** (one fluorene substituent) initially exhibits a higher current which slowly increases with time. In contrast, the current of the bulkier **96 (OLED 3)** starts from a lower value but increases more steeply. For the parent **94 (OLED 1)** (no fluorenes) the charging time is reduced. Compared to these three complexes, the largest complex in this series, **96** (**OLED 3**), required 3 V for more than 20 min before reaching maximum brightness. Thus, we conclude that using exactly the same device structure, the more bulky complexes require longer times to attain their maximum brightness. However, it is noteworthy that the maximum brightness of this series was obtained for **96 (OLED 3)**

(ca. 1000 cd m^{-2} at 3 V) which demonstrates a beneficial effect of the bulky substituents. From these observations, we realise that the diffusion of the counter ions is reduced with increasing size of the side-groups, which is consistent with findings by Handy et. al.[169]

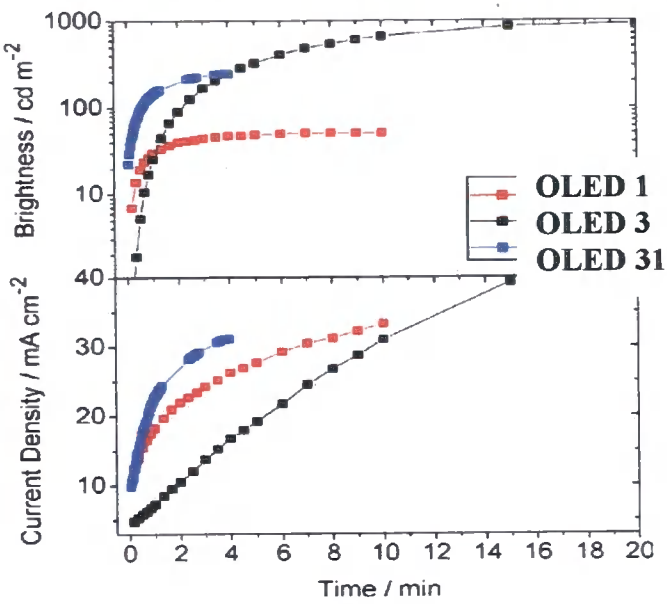

Figure 78. Linear logarithmical presentation of the brightness and current density as a function of time for LECs of **OLEDs 1**, **3** and **31** driven at an applied bias of 3 V: device architecture ITO/PEDOT:PSS/complex/Al.

Tuning the emission colour of LECs of charged iridium(III) complexes

Using the simple device configuration ITO/PEDOT:PSS/Ir(III)complex/Al **OLEDs 1**, **2**, **3**, 7 and **9** were studied and the emission wavelengths are shown in Figure 79. The electroluminescence spectra show that in this series emission can be tuned from green-blue to red emission (ca. 513 to 610 nm). With PL spectra (Figure 71) and EL spectra (Figure 79) in hand, we have found that all of the complexes show different emission wavelengths in solution and solid state. **OLEDs 2**, **3** and 7 show red-shifted emission with $\Delta\lambda_{max}$ = 23, 16 and 48 nm, respectively which may be explained by charge trapping and subsequent recombination at sites which are lower in energy. However, **94** (**OLED 1**) and **103** (**OLED 9**) show inversely blue-shifts with 10 and 15 nm, respectively.

Studies of the completed device structures are in progress to improve the efficiency in Professor Monkman's group in the Department of Physics, Durham University.

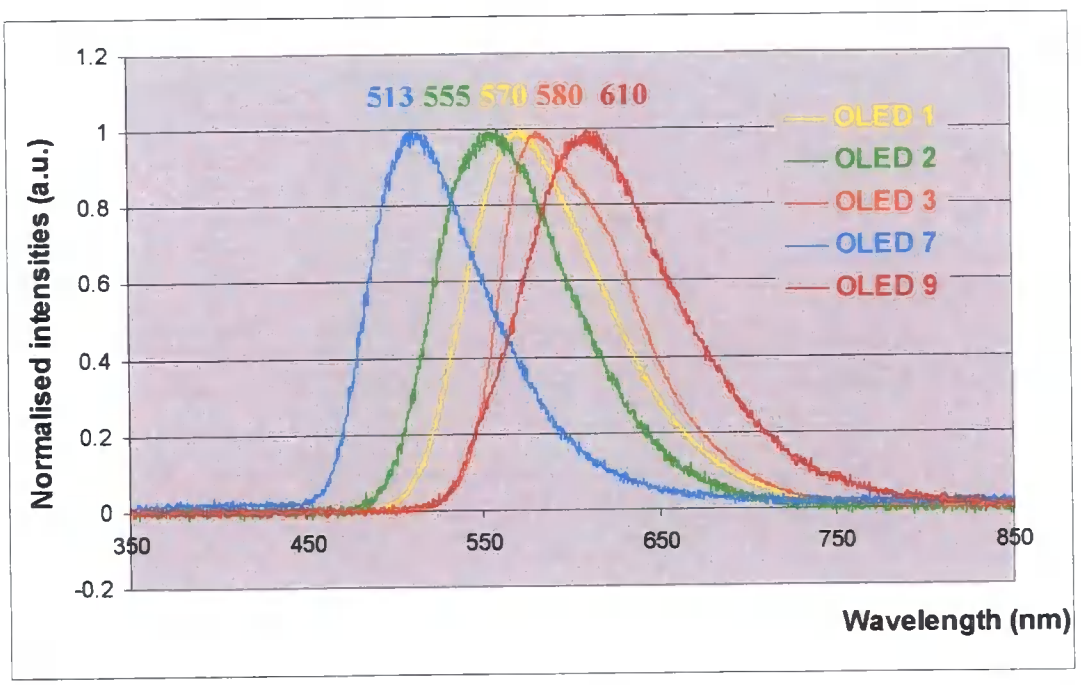

Figure 79. Tuning the emission colour of charged iridium(III) complexes from light-emitting cells, λ_{max} values are stated.

Future work

For the fabrication of OLEDs two approaches are currently in the focus, namely vapor-deposition and solution processing. Vapor deposition is a relatively costly process and is limited to small and thermally stable molecules. On the other hand, it enables the manufacture of complicated and well-defined device architectures, yielding devices with high efficiencies. In contrast, solution-based deposition methods are cost-effective and there are in principle no molar mass limitations for the used compounds. However, the realization of defined multi-layer architectures for solution-processed OLEDs is still limited by the need for orthogonal solvents or the design of polymers with alternating solubility, not influencing the electro-optical properties. Another approach to achieve multi-layer architectures via solution processing is realized by converting a soluble precursor into an insoluble polymer film after the deposition. Nuyken and Meerholz introduced a concept based on triarylamine-hole-transport materials equipped with oxetane moieties as polymerizable units (X-HTL).[185-189] These oxetane-bearing systems can be crosslinked photo-chemically by cationic ring opening polymerization (CROP), which results in nonsoluble networks and enables simple multi-layer fabrication from solution. Highly efficient solution processed multi-layer devices combining graded hole-transport-layers with a triplet emissive layer (EML) were presented recently.

More recently, Meerholz and Schubert's group reported on the combination of the oxetane-approach with phosphorescent Ir(III) emitters for application in OLEDs, which enabled the solution-based fabrication of multiple-layer devices in which the EML is crosslinked and sandwiched between hole-transport and electron-transport layers (HTL and ETL, respectively). In that orange-emitting device, they achieved internal QEs of 60–70%.[187]

For that reason, we propose the synthesis and characterization of oxetane-bearing, charged Ir(III) complexes for which the synthetic pathway is shown in Scheme 29.

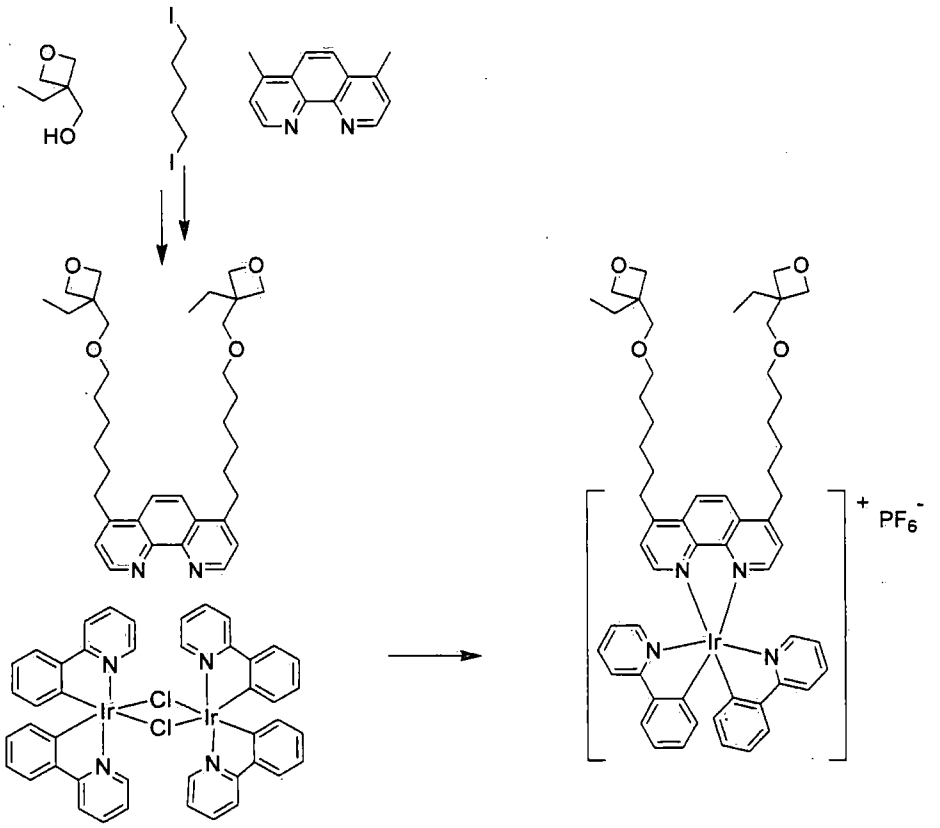

Scheme 29. The synthetic pathway to future target complex

Conclusions

A series of ionic cyclometalated Ir(III) complexes have been synthesised and characterised spectroscopically and for several derivatives by single-crystal X-ray diffraction. We have successfully tuned the emission colour in solution from blue to red (465–595 nm). The emission data, i.e colour tuning, is supported by the varying energy gap of the complexes studied by solution electrochemical techniques. Spin-coated light-emitting cells (LECs) fabricated with the device architecture ITO/PEDOT:PSS/Ir complex/Al show that devices have emission colours varying from green-blue to red (513–610 nm). Moreover, we found that the maximum brightness (ca. 1000 cd m^{-2} at 3 V) was obtained for **96** (**OLED 3**) which demonstrates a beneficial effect of two bulky fluorene substituents.

Chapter 3.

N-Arylation of nitrogen heterocycles with 2,4-difluoroiodobenzene

Abstract

Arylation reactions of NH-heterocycles [specifically, pyrazole, 3-(trifluoromethyl)pyrazole, imidazole and pyrrole] with 2,4-difluoroiodobenzene in the absence and presence of copper catalysis are described. The combination of fluoro and iodo substituents in the same aryl substrate has facilitated both S_NAr reactions at the C-F bonds and copper-catalysed Ullmann-type coupling reactions at the C-I bond. Products arising from regioselective reactions and multiple substitutions have been isolated, providing a range of new *N*-arylated pyrazole, imidazole and pyrrole derivatives.

Introduction

As shown in Scheme 25, we found that the coupling reaction of **82** with pyrazole proceeds at both iodine and fluorine sites, consistent with competing Ullmann-type coupling reaction and S_NAr reactions. We therefore decided to study this process in more detail by reacting a range of NH heterocycles (viz. pyrazoles, imidazole and pyrrole) with 2,4-difluoroiodobenzene **82** in the absence and presence of copper catalysis. The rationale was that the C-I bond should readily participate in Ullmann-type coupling reactions, whereas the C-F bonds would activate the system to S_NAr reactions. Using 2,4-difluoroiodobenzene **82** as a substrate also enabled the regioselectivity of the S_NAr processes to be explored.[190] It was also of interest to see if a second S_NAr reaction would occur on the initial S_NAr products which would be deactivated by the electron-donating *N*-heteroaryl substituent. To our knowledge, reactions of 2,4-difluoroiodobenzene **82** have not been studied previously in this context. These results are presented in this short Chapter.

Arylated nitrogen heterocycles are common motifs in biological and pharmaceutical science.[191-196] For example, a range of arylpyrazole[197,198] and arylimidazole derivatives[199,200] have promising medicinal properties; specifically, compounds **111** and **112** have been studied recently for their gene-activating properties on estrogen receptor alpha positive MCF-7 breast cancer cells. Arylazoles are also valuable building blocks in materials science due to their fluorescence properties: for example, pyrazole derivative **Fppz** (which was a target that inspired the present study) is a ligand for blue-emitting iridium complexes.[159] There is, therefore, broad interest in developing methods for the synthesis and modification of such compounds.

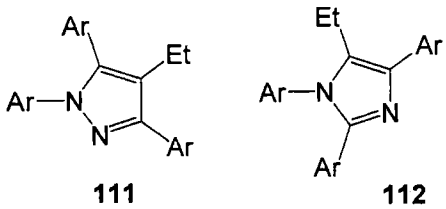

111 **112**

Ar = 4-OH-C_6H_4-

Aryl substrates which possess both fluoro and iodo substituents offer unique scope for both S_NAr reactions at the C-F bond(s) and Ullmann-type coupling reactions at the C-I bond(s) – a scenario that has not been widely explored. S_NAr reactions where the nucleophile is an *N*-heteroatom generally require activated aryl halides (halogen = F or Cl), electron-withdrawing substituents and/or quite forcing reaction conditions.[201,202] The copper-promoted Ullmann reaction is most efficient for aryl iodides. The scope of this reaction has recently been enhanced by the addition of ligands, such as diamines,[203,204,176,205,206] pipecolinic acid,[207] sterically-hindered phosphines,[208] a mixture of 1,10-phenanthroline and dibenzylideneacetone,[209] 4,7-dimethoxy-1,10-phenanthroline,[171] (*S*)-pyrrolidinylmethylimidazole,[210] *N*-hydroxyimides,[211] ninhydrin,[212] benzotriazole,[213] D-glucosamine,[214] hippuric acid[215] and (–)-sparteine.[216] Arylbromides and electron-deficient arylchlorides can also be substrates under these conditions,[215] although high selectivity in favour of displacement of iodide is generally observed, e.g. for 4-bromo-iodobenzene.[205] You et al. have shown that imidazoles can be *N*-arylated with aryl halides in the presence of base and a catalytic amount of CuI: the imidazole substrate may also function as a ligand in this process.[217] The CuOAc-mediated *N*-arylation of indoles and carbazole with aryl iodides under base-free and ligandless conditions has been developed.[218] These metal-catalyzed processes have recently been extended to *N*-heteroarylations to obtain bi(heteroaryl) systems.[219]

Results and Discussion

We initially studied the S_NAr reactions of **82** with pyrazole, 3-(trifluoromethyl)pyrazole, imidazole and pyrrole under basic conditions using 1.5 equivalents of the heterocycle. The results are shown in Table 11. Under these conditions, all the reactions (entries 1-4, conditions b) yielded mixtures of products which were generally straightforward to separate by column chromatography. In all cases the S_NAr reaction occurred preferentially at C-2 rather than C-4 (based on both ^1H NMR analysis of the crude mixtures and the relative yields of purified isomers). It is interesting to note that the di(pyrazolyl) product **114** was also isolated in 22% yield (entry 1) whereas analogous disubstituted products were not observed with the less nucleophilic reagents (entries 2-4). The electron-withdrawing effect of the trifluoromethyl group reducing the nucleophilicity of the pyrazole nitrogen accounts for the lack of disubstituted product in entry 2. Using 3.0 equivalents of pyrazole increased the yield of **114** to 56%. Using 1.0 equivalents of pyrazole raised the yield of **113** to 50%. ^{19}F NMR spectra were especially useful in assigning the regiochemistry of the mono-substituted product – with additional confirmation from the X-ray crystal structure of **125** (see below, Figure 82). The fluorine *ortho* to the iodine substituent was observed in the range δ_F -90 to -98 ppm (compounds **113**, **115**, **117** and **119**); *para* to the iodine at δ_F ca. -112 ppm (compounds **83**, **116**, **118** and **120**). Analysis of the ^1H and ^{19}F NMR spectra of compound **83** and **113** are shown in Table 12, Figure 80 and Figure 81.

Table 11. Arylation of *N*-heterocycles with **82** without Cu(I) catalysis

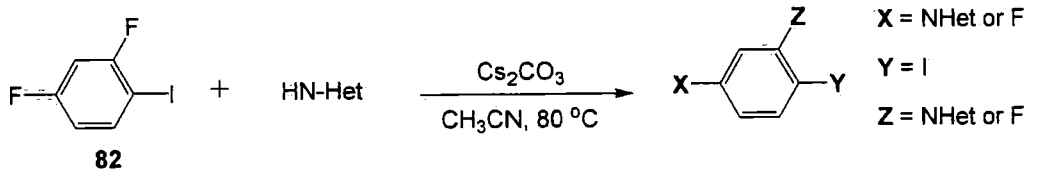

Entry	HN-Het	Product	Yield (%)[a]	Entry	HN-Het	Product	Yield (%)[a]
1		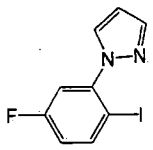 **113**	34[b] 50[c,d] 16[c,e]	3		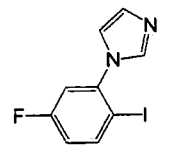 **117**	66[b]
		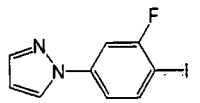 **83**	18[b] 15[c,d] 2[c,e]			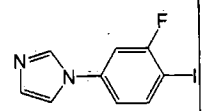 **118**	4[b]
		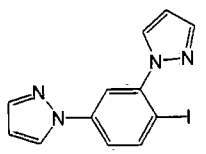 **114**	22[b] 15[c,d] 56[c,e]				
2	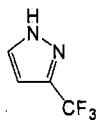	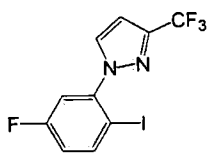 **115**	45[b]	4		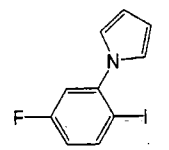 **119**	55[b]
		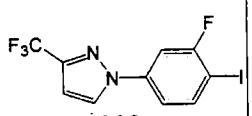 **116**	6[b]			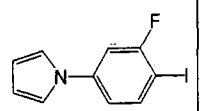 **120**	10[c]

[a] Isolated yield of product, unless otherwise noted. [b] Standard conditions: compound **82** (1.0 eq.), the N-heterocycle (1.5 eq.) and Cs_2CO_3 (2 eq.) in CH_3CN at 80 °C, 12 h. [c] Yield based on ^1H NMR analysis of the product mixture after column chromatography. [d] Pyrazole (1.0 equiv.) 80 °C, 12 h. [e] Pyrazole (3.0 equiv.), 80 °C, 24 h.

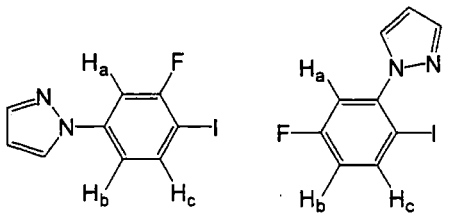

83 **113**

Table 12. The assignment of ^{1}H and ^{19}F NMR spectra of products **83** and **113**[a]

compound	δ H_a (ppm) J (Hz)	δ H_b (ppm) J (Hz)	δ H_c (ppm) J (Hz)	δ F (ppm)
83	7.48 J_{Hab} = 2.5 J_{HaF} = 9.0	7.17 J_{Hab} = 2.5 J_{Hbc} = 8.5	7.76 J_{Hbc} = 8.5 J_{HcF} = 7.0	-91.7
113	7.13 J_{Hab} = 3.0 J_{HaF} = 9.2	6.85 J_{Hab} = 3.0 J_{Hbc} = 8.8 J_{HbF} = 11.6	7.81 J_{Hbc} = 8.8 J_{HcF} = 5.8	-112.1

[a] ^{1}H at 400 MHz and ^{19}F at 376 MHz in $CDCl_3$.

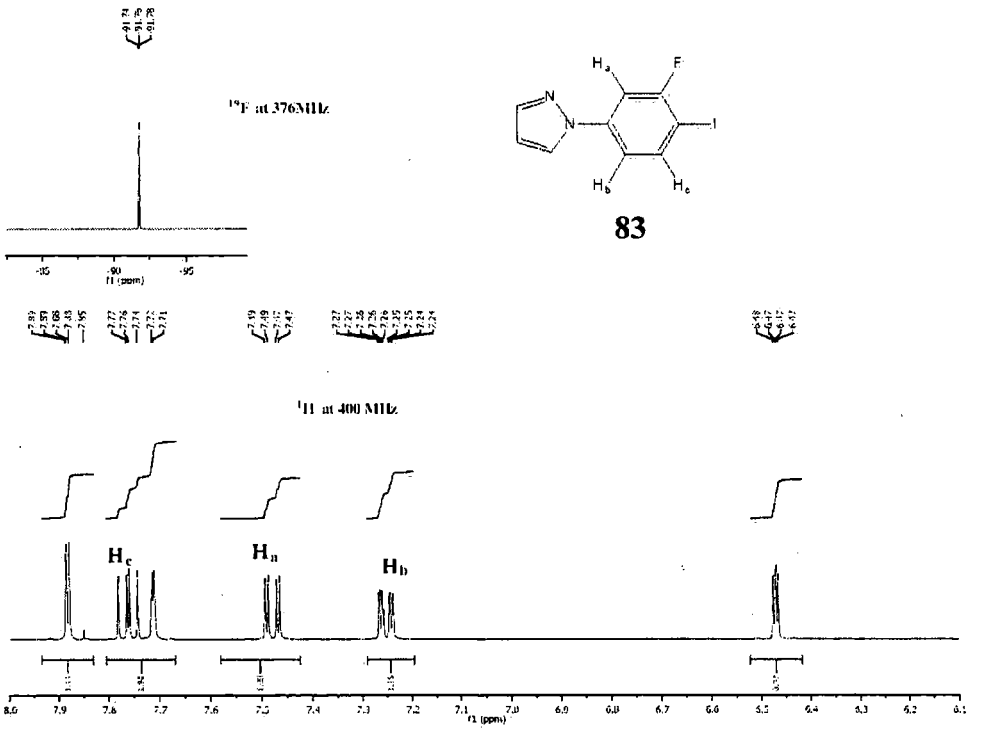

Figure 80. ^{19}F and ^{1}H NMR spectra of **83**.

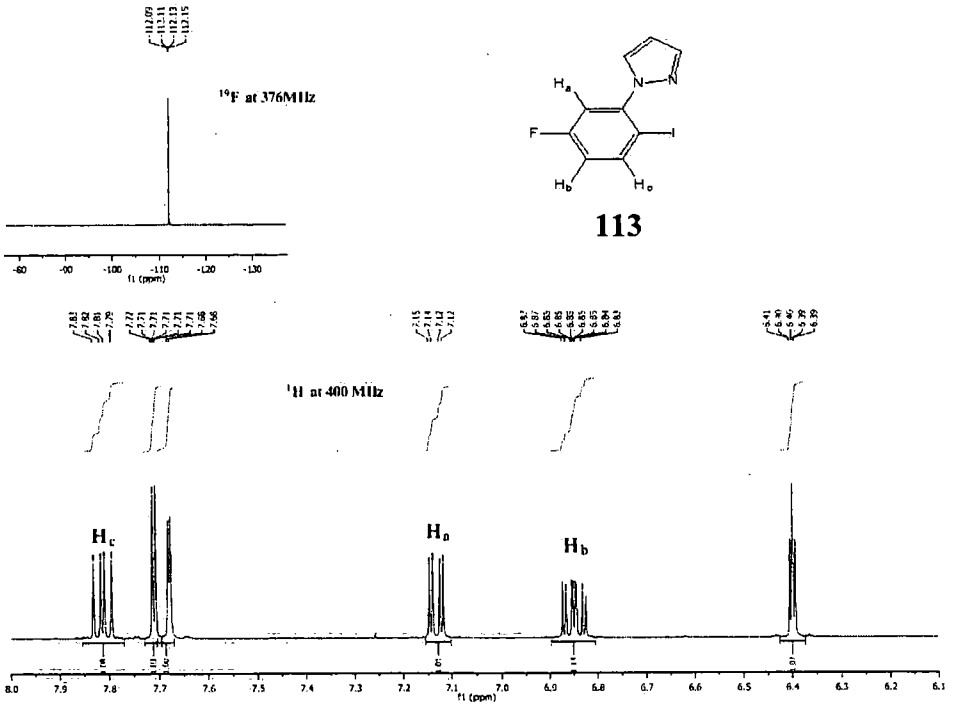

Figure 81. ^{19}F and ^{1}H NMR spectra of **113**.

To study the copper-catalyzed *N*-arylation, we adopted the conditions reported by Taillefer et al., viz. Cu_2O (5 mol%) 20% salicylaldoxime (20 mol%) and Cs_2CO_3 (2 equiv.) in acetonitrile.[176] The results are shown in Table 13.

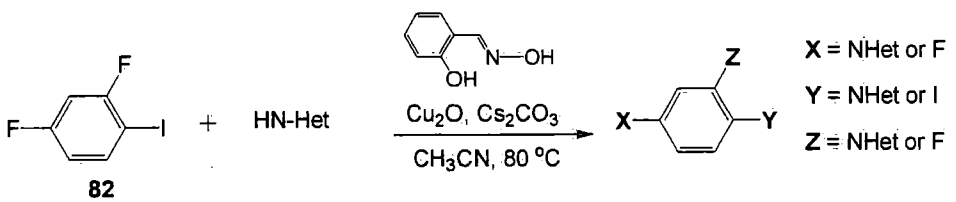

Table 13. Arylation of *N*-heterocycles with **82** with Cu(I) catalysis

Entry	HN-Het	Product	Yield (%)[a]	Entry	HN-Het	Product	Yield (%)[a]
1		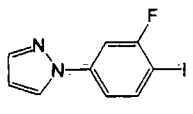 **83**	2[b] 0[c,d]	3		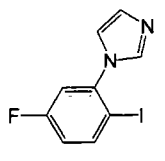 **117**	20[b]

		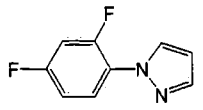 **81 (Fppz)**	13^{b} $0^{c,d}$			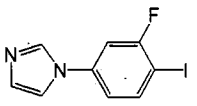 **118**	3^{b}
		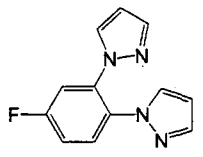 **84**	20^{b} $35^{c,d}$			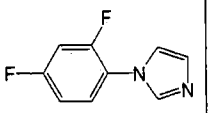 **123**	32^{b}
		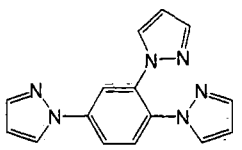 **85**	4^{b} $13^{c,d}$				
2	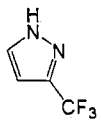	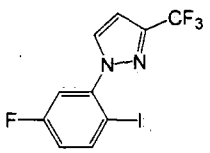 **115**	5^{b}	4		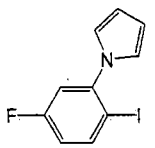 **119**	20^{c}
		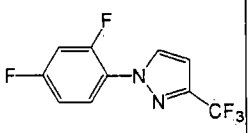 **121**	10^{b}			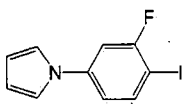 **120**	5^{c}
		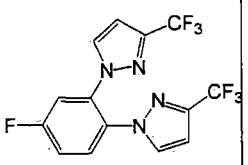 **122**	41^{b}			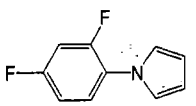 **124**	35^{b}

[a] Isolated yield of product, unless otherwise noted. [b] Standard conditions: compound **50** (1.0 eq.), the N-heterocycle (1.5 eq.), Cs_2CO_3 (2.0 eq.), salicylaldoxime (20%) and CuO_2 (5%) in CH_3CN at 80 °C, 12 h.

[c] Yield based on ^1H NMR analysis of the product mixture after column chromatography.

[d] Pyrazole (3.5 equiv.) at 80 °C, 24 h.

For all the systems studied, when using 1.5 equivalents of the heterocycle competing substitution at C-I and C-F sites was observed, with C-I substitution being the major product (entries 1-4). Moreover, disubstituted products (**84** and **122**) and trisubstituted product **85** were also isolated from the pyrazole reactions (entries 1 and 2). An X-ray crystal structure (see below) confirmed unambiguously the structure of product **122**. Using 3.5 equivalents of pyrazole increased the yields of **84** and **85** to 35% and 13%, respectively.

The ratio of products did not change significantly when a mixture of pyrazole (1.5 equiv.), Cu_2O and salicylaldoxime was stirred for 10 min at 20 °C (to preform the catalyst) before adding reagent **82**.

The general trend seen in Table 13 is consistent with the order of reactivity observed previously in Ullmann-type reactions in the azole series with aryl iodides, viz. pyrazole > imidazole > pyrrole.[205]

To extend the application of our methodology, product **83** was reacted further in a Suzuki-Miyaura reaction with *p*-tolueneboronic acid to obtain the linear triaryl product **125** in high yield (Scheme 1). The X-ray crystal structure of **125** (Figure 1) provided additional support for the NMR assignment of the structure of regioisomer **83** discussed earlier.

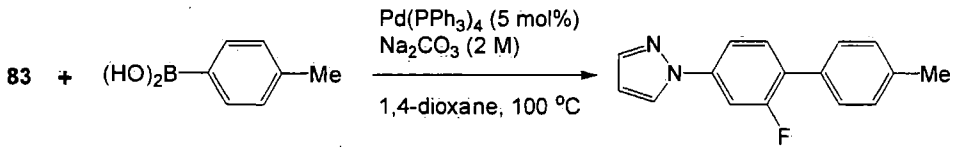

125 83%

Scheme 30. Suzuki-Miyaura reaction of **83**.

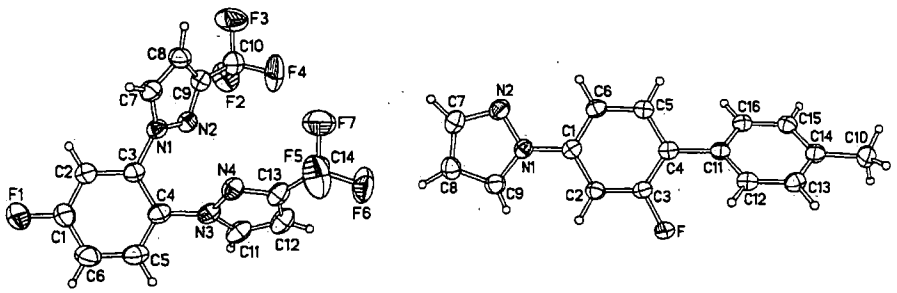

Figure 82. X-ray molecular structures of compounds **122** at room temperature (left) and **125** at 120 K (right). Thermal ellipsoids are drawn at the 30% (**122**) and 50% (**125**) probability levels; rotational disorder of CF_3 groups is not shown.

Conclusions

The functionalisation of aryl halides is a key topic in modern aromatic chemistry. In this context 2,4-difluoroiodobenzene **82** has been exploited as a substrate for both S_NAr reactions at the C-F bond(s) and copper-catalysed coupling reactions at the C-I bond. In this context NH heterocycles (specifically, pyrazoles, imidazole and pyrrole) have been reacted with **82** in the absence and presence of copper catalysis to afford *N*-heterocycles bearing iodoaryl and fluoroaryl substituents. The general trend in reactivity in both these processes is pyrazole > imidazole > pyrrole. Regioselectivity in the S_NAr reactions and, in some cases, multiple substitutions have been observed. These products offer scope for drug discovery and materials chemistry applications. The combination of a C-N coupling and a subsequent Suzuki-Miyaura reaction has led to compound **125** which illustrates that such protocols can provide a diversity of functionalised aryl/heteroaryl products. There is considerable scope for extension to other mixed-halogen substrates and optimisation of the selectivity of the reactions by using different nucleophiles, metal catalysts and ligands. Compounds synthesised by this methodology may be used in future as ligands for iridium complexes similar to those reported in chapter 2.

Chapter 4

Experimental

Tetrahydrofuran (THF) and triethylamine were dried over sodium metal and freshly distilled under argon before use. THF, acetonitrile and toluene were purified using a PureSolv solvent purification system. Flasks used to carry out Sonogashira couplings and basic deprotections were flame-dried and all reactions were protected with an argon atmosphere.

$IrCl_3$ hydrate was purchased from Precious Metals Online, 2,4-difluoroiodobenzene, pyrazole, 3-(trifluoromethyl)pyrazole, imidazole, pyrrole salicylaldoxime and Cs_2CO_3 (anhydrous, 99%) from Alfa Aesar, copper(I) iodide was from Avocado (98%+ grade) and copper(I) oxide from Aldrich which were used without further purification. Dichlorobis(triphenylphosphine)palladium(II) and tetrakis(triphenylphosphine)palladium(0) were prepared by the reported method.[220] Most ^1H and ^{13}C NMR spectra were recorded either on a Varian Unity-300 spectrophotometer operating at 299.91 MHz for ^1H and 75.41 MHz for ^{13}C or on a Bruker Avance 400 spectrophotometer operating at 400.13 MHz for ^1H and 100.61 MHz for ^{13}C, respectively. ^{19}F NMR spectra were recorded on a Varian Unity-400 spectrometer operating at 376.33 MHz. Chemical shifts are quoted downfield from TMS. Electron Impact (EI) mass spectra were recorded on a Micromass AutoSpec spectrometer operating at 70 eV. Gas Chromatography Mass Spectra were recorded on a Finnigan Trace GC spectrometer, at 70 eV. Elemental analyses were obtained on an Exeter Analytical Inc. CE-440 elemental analyser. Melting points were measured in open-end capillaries using a Stuart Scientific SMP3 melting point apparatus. The temperatures at the melting points were ramped at 2.5 /min and were uncorrected.

Chapter 4.1.

The synthesis of Oligo(aryleneethynylenes) (OAE)s for molecular wire applications.

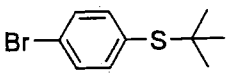

2

1-Bromo-4-(*t*-butylsulfanyl)benzene (2).[221] 4-Bromothiophenol (16.0 g, 85 mmol) was dissolved in *t*-butyl chloride (75 ml). To the stirred solution at r.t. $AlCl_3$ powder (16.5 g) was added slowly in small fractions to afford an orange slurry. The mixture was left standing overnight then poured into ice (ca. 200 g). The organic layer was extracted into diethyl ether-hexane (1:1 v/v, 2 x 50 ml) then dried over $MgSO_4$. The solution was evaporated then columned (silica, hexane) to yield **2** as a pale-yellow oil (18.1 g, 88%). ^{1}H NMR was identical with the literature.[221]

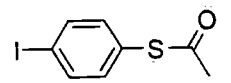

4

Thioacetic acid *S*-(4-iodophenyl) ester (4).[222] Under Ar, to a solution of 1-bromo-4-(*t*-butylsulfanyl)benzene (**2**) (11.3 g, 46 mmol) in dry THF (100 ml) cooled in a dry-ice-acetone bath was added dropwise *n*-butyllithium solution (2.5 M in hexane) (20 ml, 50.6 mmol). The solution was stirred for 2 h at low temperature followed by the addition of solid iodine (14.1 g, 55.2 mmol). The mixture was stirred for 5 h while the temperature was allowed to rise naturally to r.t. The solvents were removed by vacuum evaporation. Diethyl ether (15 ml) was added to the oily residue and the mixture was washed twice with saturated Na_2SO_3 solution (2 x 30 ml). The ether solution was dried over anhydrous $MgSO_4$ then filtered to remove the drying agent. Vacuum evaporation of the solution yielded a white solid.

The crude product in dry dichloromethane (100 ml) was syringed dropwise into a dichloromethane solution of BBr_3 (1.0 M, 55 ml). The resultant brownish solution was stirred for 2 h at r.t. after the addition. Acetyl chloride (35 ml) was added dropwise and the mixture was stirred for 1.5 h at r.t. prior to pouring onto crushed ice (~250 g). The DCM solution was separated then washed with water (2 × 200 ml) dried with anhydrous $MgSO_4$, filtered and vacuum evaporated. The solid residue was further purified on a silica column eluted with DCM-hexane (1:1, v/v) to afford compound **4** as an off-white solid (10.0 g, 79% for 2 steps). mp: 57.0 – 58.0 °C ; MS (EI): *m/z* (%) = 278 (M^+, 24), 236 (100). ^{1}H NMR ($CDCl_3$, 300 MHz): δ = 2.43 (s, 3H), 7.13 (d, *J* = 8.4 Hz, 2H), 7.74

(d, J = 8.4 Hz, 2H). ^{13}C NMR ($CDCl_3$, 75 MHz): δ = 30.2, 95.9, 127.7, 135.9, 138.3, 193.1.

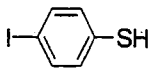

5

4-Iodothiophenol (5).[222] The *S*-ester (**4**) (10.0 g, 36 mmol) was dissolved in methanol (60 ml). The solution was degassed by bubbling argon through for 15 min. KOH pellets (6.0 g, 108 mmol) were added in one portion and the mixture was stirred at r.t. for 1 h, then 50 °C for 0.5 h under argon atmosphere. Concentrated hydrochloric acid was added to make the pH *ca.* 1, followed by slow addition of ice-water (~200 ml) with constant stirring. The precipitated pale-yellow crystals were collected by suction filtration and dried under vacuum to yield 4-iodothiophenol (**5**) (8.2 g, 96%), ^{1}H NMR ($CDCl_3$, 300 MHz): δ = 3.43 (s, 1H), 7.01 (d, J = 8.4 Hz, 2H), 7.54 (d, J = 8.4 Hz, 2H). ^{13}C NMR ($CDCl_3$, 75 MHz): δ = 90.1, 130.9, 131.1, 138.0.

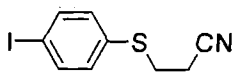

6

1-(2-Cyanoethylsulfanyl)-4-iodobenzene (6).[23] 4-Iodothiophenol (8.2 g, 29.4 mmol) and 3-bromopropionitrile (7.4 ml, 88.2 mmol) were dissolved in anhydrous DMF (70 ml) and the solution was degassed by bubbling argon through for 0.5 h. Finely-ground potassium carbonate powder (14.4 g, 88.2 mmol) was added and the mixture was heated to 105 °C and stirred for 3.5 h under argon. The cooled mixture was suction filtered to remove the solids and the filtrate was vacuum evaporated to dryness. The residual pale-yellow oil was dissolved in methanol (50 ml) followed by the addition of water (*ca.* 100 ml) slowly with constant shaking. Suction filtration and washing with a methanol-water mixture (1:2 v/v) gave white shiny plates of compound **6** (9.2 g, 98%); mp: 55.0-56.0 °C. Anal. calcd for C_9H_8INS: C, 37.39; H, 2.79; N, 4.84; found: C, 37.40; H, 2.78; N, 4.85%. ^{1}H NMR ($CDCl_3$, 300 MHz): δ 2.59 (t, J = 7.4 Hz, 2H), 3.12 (t, J = 7.2 Hz, 2H), 7.14 (d, J = 8.4 Hz, 2H), 7.66 (d, J = 8.4 Hz, 2H). ^{13}C NMR ($CDCl_3$, 75 MHz): δ 18.2, 30.0, 93.1, 117.7, 132.8, 133.2, 138.4. MS (EI) *m/z* (%): 289 (M^+, 100).

1-(2-Cyanoethylsulfanyl)-4-(trimethylsilylethynyl)benzene (7) from **6**.[23] To a stirred mixture of compound **6** (7.0 g, 24.2 mmol), $Pd[PPh_3]_2Cl_2$ (0.5 g), CuI (0.23 g) in dry THF (100 ml) was added

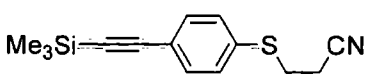

7

triethylamine (10 ml). After 5 min stirring at r.t., trimethylsilylacetylene (4 ml, 6.9 g, 36.3 mmol) was added with a syringe (5 × 2 ml portions, leaving 10 min intervals between each addition), with stirring in an argon atmosphere. The resultant mixture was stirred for an additional 1 h to yield a brown suspension. The solids in the suspension were removed by suction filtration (washed with diethyl ether) and the filtrate was vacuum evaporated to remove the solvents. The reddish-brown oily residue was dissolved in dichloromethane-hexane (3:1 v/v) then purified by chromatography on silica using the same solvent mixture as eluent, followed by crystallisation from hexane to yield compound **7** as off-white needles (5.9 g, 94%) mp: 60.3-62.0 °C. Anal. calcd for $C_{14}H_{17}NSSi$: C, 64.81; H, 6.60; N, 5.40 found: C, 64.68, H, 6.57; N, 5.49%. ^{1}H NMR ($CDCl_3$, 300 MHz): δ 0.25 (s, 9 H), 2.60 (t, J = 7.4 Hz, 2H), 3.14 (t, J = 7.4 Hz, 2H), 7.30 (d, J = 8.7 Hz, 2H), 7.42 (d, J = 8.4 Hz, 2H). ^{13}C NMR ($CDCl_3$, 75 MHz): δ -0.1, 18.1, 29.6, 95.7, 104.0, 117.7, 122.2, 130.1, 132.7, 134.0. MS (EI) *m/z* (%): 259 (M^+, 64), 244 (100).

1-(2-Cyanoethylsulfanyl)-4-(trimethylsilylethynyl)benzene (7) from **9.**

To a stirred mixture of compound **9** (21.5 g, 89.2 mmol), $Pd[PPh_3]_2Cl_2$ (3.0 g), CuI (1.7 g), triphenylphosphine (4.7 g), in dry THF (75 ml) was added triethylamine (75 ml) in an argon atmosphere. After 5 min stirring at r.t., trimethylsilylacetylene (10 ml) was added with a syringe in an argon atmosphere. The resultant mixture was stirred at 50 °C for an additional 1 day to yield a brown suspension. The next portion of trimethylsilylacetylene (5 ml) was added. The mixture was stirred for an additional 12 h. The solids in the suspension were removed by suction filtration (washed with diethyl ether) and the filtrate was vacuum evaporated to remove the solvents. The reddish-brown oily residue was dissolved in EtOAc-hexane (1:4 v/v) then purified by chromatography on silica using the same solvent mixture as eluent, followed by crystallisation from hexane to yield compound **7** as off-white needles (20.1 g, 87%). Spectroscopic data were identical with those of **7** prepared from **6**.

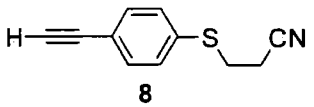

8

4-(2-Cyanoethylsulfanyl)phenylacetylene (8).[23] Compound **7** (10.9 g, 41.86 mmol) was dissolved in a mixture of dichloromethane (80 ml) and methanol (40 ml). Finely-ground potassium carbonate

powder (2.1 g) was added in one portion and the mixture was stirred at r.t. for 75 min. The resultant suspension was suction filtered through a Celite pad to remove the solid. Acetic acid (2 ml) was added to the filtrate to ensure that no deprotection of the cyanoethyl group occurred, followed by vacuum evaporation to remove the solvents. The yellow oily residue was then purified by column chromatography (silica, eluent dichloromethane-hexane 4:1 v/v) to afford **8** as a pale-yellow oil (6.9 g, 88%). The oil solidified into crystals upon standing at r.t., mp: 46.4-47.7 °C. Anal. calcd for $C_{11}H_{19}NS$: C, 70.55; H, 4.84; N, 7.48; Found: C, 70.56, H, 4.94; N, 7.44%. ^{1}H NMR ($CDCl_3$, 300 MHz): δ 2.61 (t, J = 7.2 Hz, 2H), 3.13 (s, 1H), 3.16 (t, J = 7.2 Hz, 2H), 7.33 (d, J = 8.4 Hz, 2H), 7.45 (d, J = 8.4 Hz, 2H). ^{13}C NMR ($CDCl_3$, 75 MHz): δ 18.2, 29.6, 78.4, 82.7, 106.5, 117.7, 121.1, 130.1, 132.9, 134.6. MS (EI) *m/z* (%): 147 (100), 187 (M^+, 89).

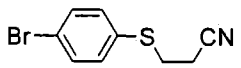

9

1-(2-Cyanoethylsulfanyl)-4-bromobenzene (9).[223] 4-bromothiophenol (22.83 g, 0.12 mol) and 3-bromopropionitrile (15 ml, 0.18 mol) were dissolved in anhydrous DMF (100 ml) and the solution was degassed by bubbling. Finely-ground potassium carbonate powder (25 g, 0.18 mol) was added and the mixture was heated to 105 °C and stirred for 3.5 h under argon. The cooled mixture was suction filtered to remove the solids and the filtrate was vacuum evaporated to dryness, then purified by column chromatography (silica, eluent ethyl acetate-hexane 1:2 v/v) to afford white shiny plates of compound **9** (27.8 g, 94%); mp: 57-58 °C. Anal. calcd for C_9H_8BrNS: C, 44.64; H, 3.33; Br, 33.00; N, 5.78; found: C, 44.76; H, 3.29; N, 5.82%. ^{1}H NMR ($CDCl_3$, 500 MHz): δ 2.60 (t, J = 7.0 Hz, 2H), 3.12 (t, J = 7.0 Hz, 2H), 7.29 (d, J = 8.5 Hz, 2H), 7.47 (d, J = 8.5 Hz, 2H). ^{13}C NMR ($CDCl_3$, 125 MHz): δ 18.5, 30.5, 118.0, 122.2, 132.6, 132.7, 133.2. MS (EI) *m/z* (%): 241 (M^+, 98), 243 (M^+, 100).

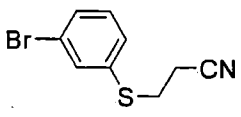

11

1-(2-Cyanoethylsulfanyl)-3-bromobenzene (11). 4-Bromothiophenol (5.0 g, 26 mmol) and 3-bromopropionitrile (7.0 ml, 84 mmol) were dissolved in anhydrous DMF (50 ml) and the solution was degassed by bubbling argon. Finely-ground potassium carbonate powder (10.0 g, 0.72 mmol) was added and the mixture was heated to 105 °C

and stirred for 3.5 h under argon. The cooled mixture was suction filtered to remove the solids and the filtrate was vacuum evaporated to dryness, then purified by column chromatography (silica, eluent ethyl acetate-hexane 1:2 v/v) to afford a colourless liquid of compound **11** (6.23 g, 97%); ^{1}H NMR (400 MHz, $CDCl_3$) δ 2.59 (t, J = 7.2, 3H), 3.11 (t, J = 7.2, 3H), 7.17 (t, J = 7.9, 1H), 7.29 (ddd, J = 1.0, 1.8, 7.9), 7.37 (ddd, J = 1.0, 1.8, 7.9, 1H), 7.50 (t, J = 1.8, 1H), 1H). ^{13}C NMR (101 MHz, $CDCl_3$) δ 18.5, 30.2, 117.9, 123.4, 129.6, 130.9, 133.5, 135.9. MS (EI) *m/z* (%): 241 (M^+, 98), 243 (M^+, 100).

1-(2-Cyanoethylsulfanyl)-3-(trimethylsilylethynyl)benzene (12). To a stirred mixture of compound **11** (5.00 g, 21 mmol), $Pd[PPh_3]_4$ (0.71 g, 0.62 mmol, 3 mol %), CuI (0.2 g, 1.0 mmol, 5 mol %) in dry THF (50 ml) was added triethylamine (5 ml) in an argon atmosphere. The mixture was then degassed for 10 min at r.t., and trimethylsilylacetylene (3.0 ml, 31 mmol) was added with a syringe in an argon atmosphere. The resultant mixture was stirred at 80 °C overnight. The solids in the suspension were removed by suction filtration (washed with diethyl ether) and the filtrate was vacuum evaporated to remove the solvents. The reddish-brown oily residue was dissolved in diethyl ether-hexane (1:1 v/v) then purified by chromatography on silica using the same solvent mixture as eluent, to yield compound **12** as an orange oil (4.79 g, 90%); ^{1}H NMR (400 MHz, $CDCl_3$) δ 0.18 (s, 9H), 2.49 (t, J = 7.3, 2H), 3.03 (t, J = 7.3, 2H), 7.18 (t, J = 8.0, 1H), 7.30 – 7.25 (m, 2H), 7.41 (t, J = 1.5, 1H). ^{13}C NMR (101 MHz, $CDCl_3$) δ 0.0, 18.3, 30.1, 95.7, 103.8, 117.9, 124.5, 129.2, 131.2, 131.3, 134.2. MS (EI) *m/z* (%): 259 (M^+, 50), 244 (M^+-CH_3, 100).

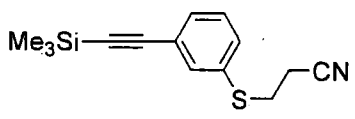

12

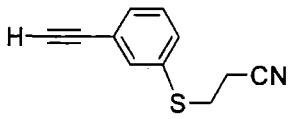

13

3-(2-Cyanoethylsulfanyl)phenylacetylene (13). Compound **12** (2.70 g, 41.86 mmol) was dissolved in a mixture of dichloromethane (20 ml) and methanol (20 ml). Finely-ground potassium carbonate powder (0.7 g) was added in one portion and the mixture was stirred at r.t. for 75 min. The resultant suspension was suction filtered through a Celite pad to remove the solid. Acetic acid (2 ml) was added to the filtrate to ensure that no deprotection of the cyanoethyl group occurred, followed by vacuum evaporation to

remove the solvents. The yellow oily residue was then purified by column chromatography (silica, eluent dichloromethane-hexane 4:1 v/v) to afford **13** as a pale-yellow oil (1.8 g, 92%). ^{1}H NMR (400 MHz, $CDCl_3$) δ 2.65 (t, J = 7.2, 2H), 3.18 (t, J = 7.2, 2H), 3.19 (s, 1H), 7.34 (t, J = 8.5, 1H), 7.44 (d, J = 8.5, 2H), 7.57 (s, 1H). ^{13}C NMR (101 MHz, $CDCl_3$) δ 18.3, 30.0, 78.5, 82.6, 117.9, 123.5, 129.3, 131.3, 131.5, 133.8, 134.2. MS (EI) *m/z* (%): 147 (100), 187 (M^+, 85).

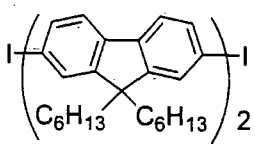

20

9,9,9',9'-Tetrahexyl-7,7'-diiodo-[2,2']bifluorenyl (20)

Under Ar gas to a solution of **25** (1.10 g, 1.35 mmol) in dry CH_2Cl_2 (20 ml), ICl (0.55 g, 3.39 mmol) was slowly added at 0 °C and the mixture was stirred at this temperature for 20 min, then stirred for a further 1 h at room temperature. The reaction was quenched with an aqueous $Na_2S_2O_3$ solution (10% wt) which was added dropwise until discolouration was observed. After extraction with dichloromethane and solvent evaporation, the crude residue was purified by chromatography (silica gel, eluent hexane) to yield compound **20** (1.05 g, 84%) as a white solid ; mp: 133.5-134.5 °C. ^{1}H NMR (500 MHz, $CDCl_3$) δ: 0.69 (p, J = 7.5 Hz, 4H), 0.77 (t, J = 7.5 Hz, 1H), 1.06-1.15 (m, 12H), 1.95-2.05 (m, 4H), 7.48 (d, J = 8.0 Hz, 1H), 7.56 (s, 1H), 7.63 (d, J = 8.0 Hz, 1H), 7.67 (d, J = 8.0 Hz, 1H), 7.68 (s, 1H), 7.74 (d, J = 8.0 Hz, 1H) ; ^{13}C NMR (125 MHz, $CDCl_3$) δ: 14.25, 22.8, 23.9, 29.8, 31.6, 40.4, 55.7, 92.7, 120.3, 211.6, 121.7, 126.5, 132.3, 136.1, 139.6, 140.6, 141.2, 151.1, 153.6. MS (MALDI-TOF) *m/z* (%) 918.3 (M^+, 100)

9,9,9',9',9'',9''-Hexahexyl-7,7''-diiodo-9H,9'H,9''H-[2,2']-[7',2'']trifluorenyl (21)[224]

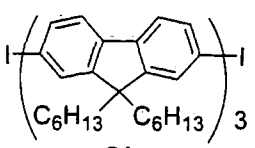

21

Under Ar gas to a solution of **27** (2.0 g, 1.7 mmol) in dry CH_2Cl_2 (40 ml), ICl (0.70 g, 4.3 mmol) was slowly added at 0 °C and stirred at this temperature 20 min, and then for a further 1 h at room temperature. The reaction was quenched with an aqueous $Na_2S_2O_3$ solution (10% wt) which was added dropwise until discolouration was observed. After extraction with dichloromethane and solvent evaporation, the crude residue was purified by chromatography (silica gel, DCM: hexane, 1/1 v/v) to yield compound **21** (1.54 g,

70%) as a white solid; mp: 78-79 °C. ^{1}H NMR (500 MHz, $CDCl_3$) δ: 0.82-0.67 (m, 15H), 1.07-1.16 (m, 18H), 1.96-2.12 (m, 6H), 7.49 (d, J = 8 Hz, 1H), 7.60-7.70 (m, 6H), 7.76 (d, J = 8 Hz, 1H), 7.82 (d, J = 8 Hz, 1H); ^{13}C NMR (125 MHz, $CDCl_3$) δ: 14.3, 22.7, 22.8, 23.9, 24.0, 29.9, 31.6, 31.7, 40.5, 40.6, 55.6, 55.7, 92.7, 120.2, 120.3, 121.6, 121.7, 121.8, 126.4, 126.5, 132.3, 136.1, 139.5, 140.3, 140.5, 140.7, 141.4, 151.2, 152.0, 153.7.; Anal. calcd for $C_{75}H_{96}I_2$: C, 71.99; H, 7.73. Found: C, 72.19; H, 7.83.

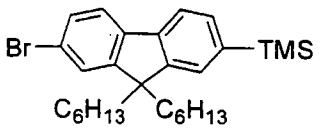

23

7-Bromo-9,9-dihexyl-2-trimethylsilyl-fluorene (23)[224]

A solution of *n*-BuLi in hexanes (2.5 M, 2.0 ml, 5.0 mmol) was added slowly to a solution of **22** (2.46 g, 5.0 mmol) in dry THF (20 ml) at -78 °C. The mixture was stirred for 1 h at this temperature, and then chlorotrimethylsilane (1.0 ml, 7.9 mmol) was added. The mixture was stirred for 30 min at 20 °C, and then poured into distilled water (20 ml). After the organic products were extracted into petroleum-ether, the combined extracts were dried over $MgSO_4$, filtered and concentrated in vacuo. Purification on a silica column (eluent: petroleum-ether) yielded **23** (2.1 g, 85%) as a clear oil. ^{1}H NMR (500 MHz, $CDCl_3$) δ: 0.33 (s, 9H), 0.56-0.72 (m, 4H), 0.79 (t, J = 7.2 Hz, 6H), 1.02-1.18 (m, 12H), 1.88-2.03 (m, 4H), 7.44-7.53 (m, 4H), 7.57 (d, J = 7.9 Hz, 1H), 7.66 (d, J = 7.5 Hz, 1H); ^{13}C NMR (125 MHz, $CDCl_3$) δ: .0.6, 14.3, 22.8, 23.9, 29.9, 31.7, 40.4, 55.6, 119.3, 121.4, 121.4, 126.5, 127.9, 130.2, 132.3, 140.0, 140.4, 141.0, 149.8, 153.5; MS (EI) *m/z* (%) 487 (M^+, 38), 486 (M^+, 80), 485 (M^+, 38), 484 (M^+, 76), 73 (100); HRMS calculated for $C_{28}H_{41}BrSi$ (M^+): 484.21609 found 484.21632.

9,9-Dihexyl-7-trimethylsilyl-fluorenyl-2-boronic acid (24)[121]

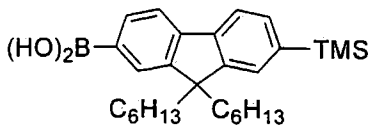

24

A solution of *n*-BuLi in hexanes (2.5 M, 2.5 ml, 6.25 mmol) was added slowly to a solution of **23** (2.0 g, 4.1 mmol) in dry THF (20 ml) at -78 °C. The mixture was stirred for 1 h at this temperature, and then (i-PrO)$_3$B (3 ml, 13 mmol) was added. The mixture was stirred for 21 h whilst gradually warming to 20 °C. The mixture was then poured into 100 ml of distilled water. The

organic products were extracted into diethyl ether. The combined organic layers were dried over $MgSO_4$, filtered and concentrated under reduced pressure to give a crude product. This was purified on a silica gel column, eluent petroleum-ether and ethyl acetate (7:3 v/v) to give **24** (1.0 g, 58%) as a white foamy solid. ^{1}H NMR (500 MHz, $CDCl_3$) δ: 0.38 (s, 9H), 0.59-0.85 (m, 4H), 0.80 (t, J = 7.0 Hz, 6H), 1.02-1.22 (m, 12H), 2.04-2.22 (m, 4H), 7.58 (s, 1H), 7.59 (d, J = 7.6 Hz, 1H), 7.83 (d, J = 7.6 Hz, 1H), 7.93 (d, J = 7.5 Hz, 1H), 8.27 (s, 1H), 8.35 (d, J = 7.5 Hz, 1H); ^{13}C NMR (125 MHz, $CDCl_3$) δ: 0.5, 14.4, 22.8, 24.1, 30.0, 31.8, 40.5, 55.3, 119.7, 120.0, 128.1, 129.4, 130.1, 134.9, 140.6, 141.7, 145.9, 150.7, 151.1; MS (EI) *m/z* (%) 423 (M^+-2xCH_3, 20), 422 (M^+-2xCH_3, 55), 406 (M^+-$B(OH)_2$, 27), 407 (M^+-$B(OH)_2$, 16).

9,9,9',9'-Tetrahexyl-7,7'-bis-trimethylsilyl-[2,2']bifluorenyl (25). A mixture of TMS-FlB$(OH)_2$ **24** (0.9 g, 2.0 mmol,), Br-Fl-Br **23** (1.94 g, 4.0 mmol) and $Pd(PPh_3)_4$ (70 mg) was partitioned between toluene (20 ml) and aqueous Na_2CO_3 (2 M, 3.5 ml). The mixture was degassed several times and then heated at 90 °C for 2 days under argon. The reaction mixture was cooled to r.t., and then diluted with petroleum-ether (30 ml). The organic layer was washed with distilled water (3 x 30 ml), dried over $MgSO_4$, filtered and concentrated in vacuo to give a pale orange liquid. Purification on a silica column, eluent petroleum-ether and ethyl acetate (9:1 v/v) gave **25** (1.10 g, 68%) as a clear oil. ^{1}H NMR (300 MHz, $CDCl_3$) δ: 0.41 (s, 9H), 0.83-0.95 (m, 12H), 1.16-1.17 (m, 12H), 2.05-2.07 (m, 4H), 7.58-7.60 (m, 2H), 7.69-7.73 (m, 2H), 7.79 (d, J = 7.5 Hz, 1H), 7.85 (d, J = 8.4 Hz, 1H).

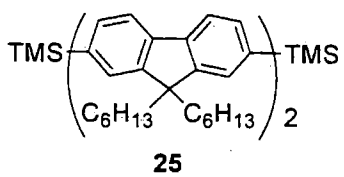

25

9,9-Dihexyl-fluorenyl-2,7-diboronic acid (26).[225] To a stirred solution of 2,7-dibromo-9,9'-dihexylfluorene (2.00 g, 4.00 mmol) in dry THF (20 ml) under argon, a solution of 2.5 M *n*-BuLi in hexane (4 ml, 10 mmol) was added dropwise at -78 °C. The mixture was stirred at this temperature for 6 h to give a white suspension. Triisopropylborate (3 ml, 13 mmol) was added quickly and the mixture was stirred overnight allowing the temperature to rise gradually to room temperature. 20 %

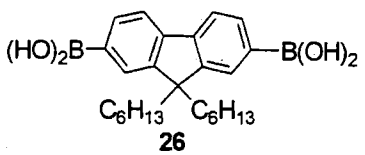

26

aqueous HCl (30 ml) was then added and the mixture was stirred at r.t. overnight. The organic solvents were removed in vacuo, water (20 ml) was added and the mixture was acidified to pH 1 with concentrated HCl. The product was collected by filtration to afford **26** (1.6 g, 94 %) as a white powder. ^{1}H NMR (400 MHz, acetone-d_6); δ= 7.99 (2H,dd), 7.9 (2H, dd, J =7.6, 3.6 Hz), 7.8 (2H, dd, 7.6,0.6 Hz), 7.19 (4H, s), 2.0-2.1 (4H, m), 0.9-1.2 (12H, m), 0.74 (6H, t, J = 7.2 Hz), 0.5-0.6 (4H, m). ^{13}C NMR (100 MHz acetone-d_6); δ = 14.21, 23.16, 24.57, 30.39, 32.27, 41.09, 55.50, 119.92, 129.39, 133.87, 144.09, 150.87.

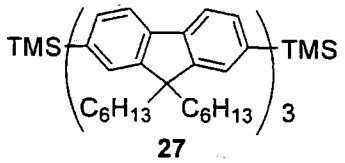

27

9,9,9',9',9'',9''-Hexahexyl-7,7''-bis-trimethylsilanyl-9H,9'H,9''H-[2,2']-[7',2'']trifluorenyl (27).[224] A mixture of compound **26** (1.0 g, 2.37 mmol,), bromofluorene **23** (2.53 g, 5.2 mmol) and $Pd(PPh_3)_4$ (82 mg) was partitioned between toluene (30 ml) and aqueous Na_2CO_3 (2 M, 5 ml) The mixture was degassed several times and then heated at 90 °C for 2 days under argon. The reaction mixture was cooled to r.t., and then diluted with petroleum-ether (30 ml). The organic layer was washed with distilled water, dried over $MgSO_4$, filtered and concentrated in vacuo to give a pale orange liquid. Purification on a silica column by elution with petroleum-ether and ethyl acetate (9:1 v/v) gave **27** (2.0 g, 74%) as a clear oil. ^{1}H NMR (300 MHz, $CDCl_3$) δ: 0.40 (s, 9H), 0.84-0.94 (m, 15H), 1.19 (b, 18H), 2.11-2.17 (b, 6H), 7.60-7.62 (m, 2H), 7.74-7.80 (m, 5H), 7.87-7.89 (m, 2H). MS (MALDI-TOF) *m/z* (%) 1142.8 (M^+, 100).

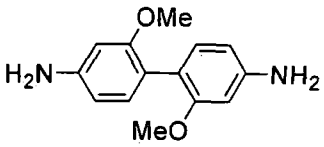

29

2,2'-Dimethoxy-4,4-diaminobiphenyl (29).[119] To a suspension of $NaBH_4$ (2.5 g, 66 mmol) and DMSO (50 ml) in a 3-necked flask 3-nitroanisole (4.0 g, 26 mmol) was added under argon gas. The mixture was heated while the temperature of the oil bath was raised gradually to 110 °C. The dark brown mixture was heated at 110 °C overnight. TLC confirmed the hydrazo derivative was the main product. The dark brown solution was cooled to r.t. and diluted with ethanol (20 ml), ether (10 ml) and water (10 ml). The mixture was cooled to 0 °C with an ice bath. A dropping funnel charged with HCl (180 ml) was fitted to the flask. The HCl was added slowly to destroy

the unreacted $NaBH_4$ until the foaming ceased. H_2O (20 ml) was poured into the mixture, which was stirred for a while then cooled to 0 °C. The remaining HCl was then added dropwise during 1 h. After the addition, the mixture was stirred at r.t. overnight. The precipitate was filtrated off and washed thoroughly with ethanol. The off-white solid thus obtained was purified by dissolving it in water. After filtration, the water solution was taken with NaOH solution to pH > 12. The product **29** (1.37 g, 22 %) was collected by filtration and washed with water (ca. 100 ml) and dried.

4,4'-Dibromo-2,2'-dimethoxybiphenyl (30). To **29** (1.56 g, 6.38 mmol) in a 100 ml conical flask in an ice bath was added HBr (conc.) (5 ml) / H_2O (5 ml). The resulting suspension was cooled thoroughly. $NaNO_2$ (1.0 g) was dissolved in H_2O (5 ml) and chilled in the ice bath. The cold $NaNO_2$ solution was added to the suspension dropwise (slowly) with stirring. The mixture was stirred in the ice bath for an additional 1 h, then urea (0.5 g) was added, followed by a cold solution of CuBr (2.3 g) in H_2O (5 ml). The mixture was stirred at r.t. overnight. Then the solid was filtered off, washed with water and dissolved in ethyl acetate. The organic layer was separated and dried with $MgSO_4$. The brown crude product was purified by silica column chromatography with ethyl acetate: hexane (1:9 v/v) as the eluent. Product **30** was collected as a colourless solid (0.65 g, 43%), mp 107.4-108.5 °C. Anal. calcd for $C_{14}H_{12}Br_2O_2$: C, 45.20; H, 3.25; found: C, 45.10; H, 3.20. ^1H NMR ($CDCl_3$, 500 MHz): δ 3.76 (s, 3H), 7.06 (d, J = 8.0 Hz, 1H), 7.09 (d, J = 1.5 Hz, 1H), 7.14 (dd, J = 8.0 Hz, J = 1.5, 1H). ^{13}C NMR ($CDCl_3$, 125.6 MHz): δ 56.2, 114.9, 122.4, 123.7, 125.9, 132.6, 157.7. MS (EI) *m/z* (%): 372 (M^+, 100).

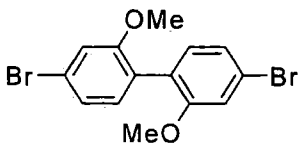

30

4,4'-Bis(diazonium)-2,2'-dimethoxybiphenyl bis(tetrafluoroborate) (31). To **29** (1.0 g, 4 mmol) cooled with an ice bath, was added HCl (conc.) (10 ml) / H_2O (10 ml). A cold aqueous $NaNO_2$ solution (1.0 g in water, 10 ml) was added to the suspension dropwise (slowly) with stirring. The mixture was stirred in the ice bath for an additional 1 h, urea (4.0 g) was added, followed by a saturated solution of $NaBF_4$ (10 ml) over 30 min. The solution was left at

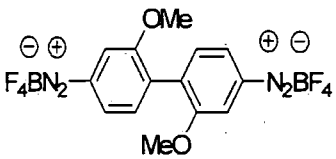

31

r.t. for 1 h. Then the solid was filtered off, washed with cold water, and the solid product was dried in an oven at ca. 30 °C to give the diazonium salt **31** for use in the next step without further purification.

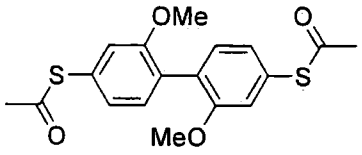

32

4,4'-Di(acetylsulfanyl)-2,2'-dimethoxybiphenyl (32).

To a solution of salt **31** (1.0 g, 2.3 mmol) in DMSO (6 ml) was slowly added a solution of potassium thiocaboxylate salt (0.65 g, 5.7 mmol) in DMSO (12 ml) under Ar. The mixture was stirred at r.t. for 1 h then the solvent was removed and the residue purified by column chromatography with eluent ethyl acetate : hexane (1/4 v/v) to give **32** as a white solid (312 mg, 30%); mp 93.5-94.6 °C. HRMS calcd. for $C_{18}H_{18}O_4S_2$ (M^+) 362.0647; found: 362.0647. ^{1}H NMR ($CDCl_3$, 400 MHz): δ 2.45 (s, 3H), 3.77, (s, 3H), 7.02 (d, J = 1.2 Hz, 1H), 7. 33 (dd, J = 8 Hz, J = 1.2 Hz, 1H), 7.28 (d, J = 8.4 Hz, 1H). ^{13}C NMR ($CDCl_3$, 100 MHz): δ 30.5, 56.0, 117.0, 126.4, 128.3, 128.4, 132.1, 157.4, 194.4. MS (EI) *m/z* (%): 362 (M^+, 33), 278 (100).

4,4'-Diiodo-2,2'-dimethoxybiphenyl (33).[119] To **33** (1.37 g, 5.6 mmol) cooled in an ice bath was added HCl (conc.) (5 ml) / H_2O (5 ml). The resulting suspension was cooled to 0 °C. $NaNO_2$ (1.3 g) was dissolved in H_2O (5 ml) and chilled in the ice bath. The cold $NaNO_2$ solution was added to the suspension dropwise (slowly) with stirring. The mixture was stirred in the ice bath for an additional 1 h, during which time the suspension became clear orange. To a cold solution of KI (4.0 g) in H_2O (5 ml) the orange diazo solution was added dropwise with vigorous stirring. After the addition, a mixture of HCl (conc.) (5 ml) and / H_2O (5 ml) (pre-cooled in the ice bath) was added to the reaction mixture, which turned into a brown thick suspension. Then the ice bath was removed and ether (5 ml) was added. The mixture was stirred at r.t. overnight. Then the solid was filtered off, washed with water and dissolved in ethyl acetate. The organic layer was separated and dried with $MgSO_4$. The brown crude product was purified by silica column chromatography with ethyl acetate: petroleum-ether (1:9 v/v) as the eluent. Product **33** was collected as a colourless solid (644 mg, 43%). ^{1}H NMR ($CDCl_3$, 300 MHz): δ 3.75

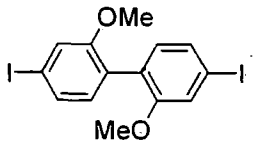

33

(s, 3H), 6.91 (d, J = 7.8 Hz, 1H), 7.26 (d, J = 1.5 Hz, 2H), 7.34 (dd, J = 8.5 Hz, J = 1.5 Hz, 1H); MS (EI) *m/z* (%): 466 (M^+, 100).

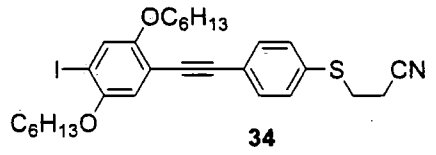

34

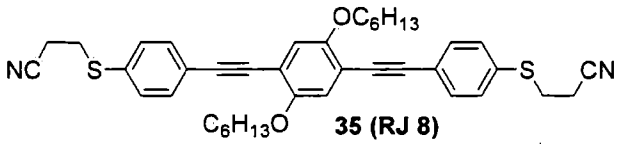

35 (RJ 8)

1-Iodo-4-[4-(2-cyanoethylsulfanyl)phenylethynyl]-2,5-dihexyloxybenzene (41) and **1,4-Bis[4-(2-cyanoethylsulfanyl)phenylethynyl]-2,5-dihexyloxybenzene (35; RJ 8)**. Compound **8** (0.65 g, 3.47 mmol) and 1,4-diiodo-2,6-dihexyloxybenzene (0.79 g, 1.59 mmol) were dissolved in dry THF (5 ml). $Pd[PPh_3]_2Cl_2$ (37 mg) and CuI (10 mg) were added with stirring followed by the addition of triethylamine (30 ml). The mixture was stirred under Ar at 50 °C for 4 h. The solution was cooled to r.t., resulting in a yellow suspension. The solids were removed by suction filtration (washed with diethyl ether) and the filtrate was vacuum evaporated to remove the solvents. Then chromatography on silica (eluent DCM-ethyl acetate-hexane 1:5:15 v/v) afforded compound **34** as an orange solid (0.04 g, 4 %);mp: 46-47 °C, ^{1}H NMR ($CDCl_3$, 500 MHz): δ 0.90 (t, J = 6H), 1.34-1.37 (m, 8H), 1.38-1.53 (m, 4H), 1.81-1.84 (m, 4H), 2.62 (t, J = 7.0 Hz, 2H), 3.16 (t, J = 7.0 Hz, 2H), 3.98 (q, J = 8.0 Hz, 4H), 6.90 (s, 1H), 7.30 (s, 1H), 7.35 (d, J = 8.0 Hz, 2H), 7.47 (d, J = 8.0 Hz, 2H). ^{13}C NMR ($CDCl_3$, 125 MHz): δ 14.3, 18.4, 22.8, 22.9, 25.9, 26.0, 29.3, 29.5, 30.0, 31.7, 31.8, 70.0, 70.3, 87.1, 88.1, 93.5, 113.4, 116.1, 118.0, 122.9, 124.0, 130.6, 132.5, 133.9, 152.0, 154.6; MS (MALDI-TOF) *m/z* (%): 589.2 (M^+, 35), 279.1 (100). The next product to elute was **35; RJ 8** as a pale-yellow solid (0.93 g, 88%) mp: 81-82 °C. HRMS calcd. for $C_{40}H_{44}N_2O_2S_2$ (M^+) 648.2844; found: 648.2844. ^{1}H NMR ($CDCl_3$, 200 MHz): δ 0.89 (t, J = 7.2 Hz, 3H), 1.33-1.36 (m, 4H), 1.50-1.56 (m, 2H), 1.81-1.85(m, 2H), 2.63 (t, J = 7.6 Hz, 2H), 3.17 (t, J = 7.6 Hz, 2H), 4.02 (d, J = 6.4 Hz, 2H), 7.00 (s, 1H), 7.36 (d, J = 8.4 Hz, 2H), 7.48 (d, J = 8.4 Hz, 2H). ^{13}C NMR ($CDCl_3$, 75 MHz): δ 14.0, 18.2, 22.6, 25.73, 29.3, 29.7, 30.1, 30.3, 31.5, 69.6, 87.2, 94.1, 113.9, 116.9, 122.6, 130.6, 131.8, 133.9, 132.7, 153.7. MS (EI) *m/z* (%): 648.1 (M^+, 100).

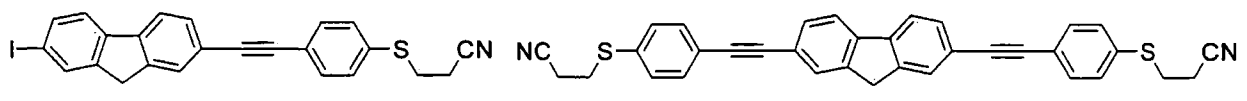

36

37 (RJ 9)

2-Iodo-7-[4-(2-cyanoethylsulfanyl)phenylethynyl]-fluorene (36) and

2,7-Bis[4-(2-cyanoethylsulfanyl)phenylethynyl]-fluorene (37; RJ 9). Compound **8** (0.500 g, 2.67 mmol) and 2,7-diiodofluorene (0.507 g, 1.2 mmol) were dissolved in dry THF (20 ml). $Pd[PPh_3]_2Cl_2$ (25 mg) and CuI (7 mg) were added with stirring followed by the addition of triethylamine (20 ml). The mixture was stirred under Ar at 50 °C for 4 h. The solution was cooled to r.t., resulting in a yellow suspension. The yellow suspension was mixed with DCM then filtered with a silica pad (washed with a small amount of DCM). The filtrate was partially vacuum evaporated to remove some of the solvents to give a yellow solid which was filtered from the remaining solvent to give solid fraction 1 (impure **37 (RJ 9)**), which was washed with a small amount of DCM. The solvent was removed from the filtrate and then chromatographed on silica (eluent DCM), to afford compound **36** (1st band) as a yellow solid (0.045 g, 7 %), mp: 211-212 °C. Anal. calcd for $C_{24}H_{16}INS$: C, 60.39; H, 3.38; N, 2.93. Found: C, 60.02; 3.24; N, 2.55. ^1H NMR ($CDCl_3$, 300 MHz): δ 2.63 (t, J = 7.4 Hz, 2H), 3.89 (s, 2H), 7.35-7.92 (m, 10H). ^{13}C NMR ($CDCl_3$, 75 MHz): δ 18.2, 29.7, 29.8 ,36.4, 88.96, 91.3, 92.5, 117.8, 120.0, 121.6, 121.7, 122.6, 128.1, 130.5, 130.7, 131.8, 132.3, 133.7, 134.2, 136.0, 140.6, 141.1, 142.7, 145.7. MS (EI) *m/z* (%): 476.8 (M^+, 100) and a yellow solid (2nd band); (solid fraction 2; impure **37 (RJ 9)**). Combined solid fractions 1 and 2 were recrystallised with DCM and hexane (ca. 9:1 v/v) to give compound **37; RJ 9** as a pale yellow solid (0.589 g, 91%), mp: 229-230 °C. ^1H NMR ($CDCl_3$, 500 MHz): δ 2.65 (t, J = 7.0 Hz, 4H), 3.19 (t, J = 7.0 Hz, 4H), 3.95 (s, 2H), 7.40 (d, J = 8.0 Hz, 4H), 7.53 (d, J = 8.0 Hz, 4H), 7.59 (d, J = 8.0 Hz, 2H), 7.73 (s, 2H), 7.78 (d, J = 8.0 Hz, 2H). ^{13}C NMR ($CDCl_3$, 125 MHz): δ 18.4, 29.8, 30.2, 36.8, 89.2, 91.6, 117.7, 120.3, 121.8, 123.0, 128.4, 130.8, 130.9, 132.6, 134.1, 141.6, 143.8. HRMS calcd for $C_{35}H_{24}N_2S_2$ 536.1381; found: 536.1380. MS (EI) *m/z* (%): 535.9 (M^+, 100).

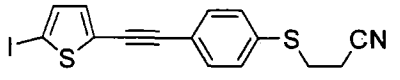

38

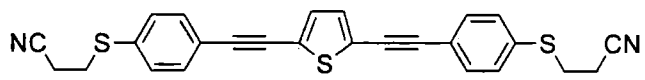

39 (RJ 10)

2-Iodo-5-[4-(2-cyanoethylsulfanyl)phenylethynyl]-thiophene (38) and **2,5-Bis[4-(2-cyanoethylsulfanyl)phenylethynyl]-thiophene (39; RJ 10).** Compound **8** (0.65 g, 3.47 mmol) and 2,5-diiodothiophene (0.53 g, 1.58 mmol) were dissolved in dry THF (20 ml). $Pd[PPh_3]_2Cl_2$ (33 mg) and CuI (9 mg) were added with stirring followed by the addition

of triethylamine (20 ml). The mixture was stirred under Ar at 50 °C for 4 h. The resulting yellow suspension was evaporated under vacuum and the dark yellow residue was chromatographed on silica (eluent dicholomethane), to afford compound **38** as a pale-yellow solid (0.37 mg 6 %) mp: 93-94 °C; ^{1}H NMR ($CDCl_3$, 300 MHz): δ 2.63 (t, *J* = 7.4 Hz, 2H), 3.17 (t, *J* = 7.4 Hz, 2H), 6.93 (d, *J* = 3.9, 1H), 7.14 (d, *J* = 3.9, 1H), 7.34 (d, *J* = 8.8, 1H), 7.45 (d, *J* = 8.8 Hz, 2H). ^{13}C NMR ($CDCl_3$, 100.6 MHz): δ 18.2, 29.6, 82.6, 94.0, 117.7, 121.7, 129.1, 131.5, 131.7, 132.2, 133.4, 134.5, 137.2. MS (EI) *m/z* (%): 394.7 (M^+, 100). Next to elute was compound **39; RJ 10** as a pale-orange solid (0.65 g, 90%), mp: 126-128 °C. ^{1}H NMR ($CDCl_3$, 300 MHz): δ 2.64 (t, *J* = 7.5 Hz, 2H), 3.18 (t, *J* = 7.5 Hz, 2H), 7.17 (s, 1H), 7.36 (d, *J* = 8.4 Hz, 2H), 7.48 (d, *J* = 8.4 Hz, 2H). ^{13}C NMR ($CDCl_3$, 125 MHz): δ18.4, 29.8, 83.7, 93.7, 117.9, 121.8, 124.8, 130.4, 132.4, 132.5, 134.7. MS (EI) *m/z* (%):72.9 (100), 454 (M^+, 26).

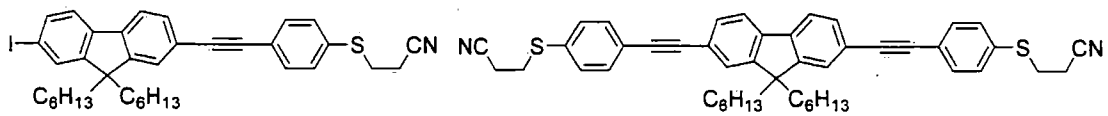

40 **41 (RJ 11)**

2-Iodo-7-[4-(2-cyanoethylsulfanyl)phenylethynyl]-9,9-dihexylfluorene (40) and **2,7-Bis[4-(2-cyanoethylsulfanyl)phenylethynyl]-9,9-dihexylfluorene (41; RJ 11).** Compound **8** (0.56 g, 3.00 mmol) and 2,7-diiodo-9,9-dihexylfluorene[118] (0.80 g, 1.38 mmol) were dissolved in dry THF (30 ml). $Pd[PPh_3]_2Cl_2$ (54 mg) and CuI (17 mg) were added with stirring followed by the addition of triethylamine (30 ml). The mixture was stirred under Ar at 50 °C for 4 h. The solution was cooled to r.t. resulting in a yellow suspension. The solids in the suspension were removed by suction filtration (washed with diethyl ether) and the filtrate was vacuum evaporated to remove the solvents. Chromatography of the residue on silica (eluent DCM-hexane 1:1 v/v) afforded compound **40** as a white solid (0.12 g, 13%); mp: 89-90 °C. ^{1}H NMR ($CDCl_3$, 200 MHz): δ 0.56 (m, 4H), 0.77 (t, *J* = 7.4 Hz, 6H), 1.05 (m, 12H), 1.95 (m, 4H), 2.63 (t, *J* = 7.4 Hz, 2H), 3.18 (t, *J* = 7.4 Hz, 2H), 7.35-7.68 (m, 10H). ^{13}C NMR ($CDCl_3$, 100 MHz)): δ 13.9, 18.2, 22.5, 23.6, 29.6, 29.8, 31.4, 40.2, 55.4, 88.9, 91.6, 93.2, 117.7, 119.8, 121.7, 121.8, 122.6, 125.9, 130.4, 130.8, 132.1, 132.3, 133.7, 136.0, 140.0, 140.6, 150.2, 153.4. MS (EI) *m/z* (%): 644.8 (M^+, 100). Next to elute was compound **41; RJ 11** as an orange oil

(0.61 g 63 %); ^{1}H NMR ($CDCl_3$, 400 MHz): δ 0.61 (b, 2H), 0.77 (t, J = 7.2 Hz, 3H), 1.10 (m, 6H), 2.20 (m, 2H), 2.63 (t, J = 7.0 Hz, 2H), 3.17 (t, J = 7.0 Hz, 2H), 7.37 (d, J = 8.76 Hz, 2H), 7.50-7.53 (m, 4H), 7.67 (d, J = 8.0 Hz, 1H). ^{13}C NMR ($CDCl_3$, 100 MHz) : δ 14.0, 18.2, 22.6, 23.7, 29.7, 29.8, 31.5, 40.4, 55.3, 89.0, 91.7, 117.8, 120.1, 121.7, 122.6, 125.9, 130.0, 130.4, 130.8, 132.3, 133.2, 133.8, 140.8, 151.2. MS (MALDI-ToF) *m/z* (%): 704.4 (M^+, 100).

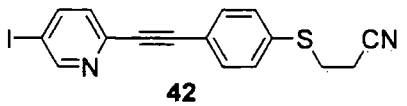

42

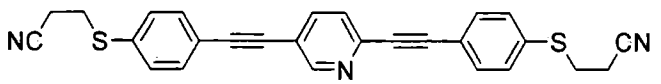

43 (RJ 12)

5-Iodo-1-[4-(2-cyanoethylsulfanyl)phenylethynyl]-pyridine (42) and **2,5-Bis[4-(2-cyanoethylsulfanyl)phenylethynyl]-pyridine (43; RJ 12).** Compound **8** (0.84 g, 4.49 mmol) and 2,5-diiodopyridine (0.67 g, 2.02 mmol) were dissolved in dry THF (30 ml). $Pd[PPh_3]_2Cl_2$ (46 mg) and CuI (11 mg) were added with stirring followed by the addition of triethylamine (30 ml). The mixture was stirred under Ar at 50 °C for 4 h. The solution was cooled to r.t., resulting in a yellow suspension. The yellow suspension was mixed with DCM then filtered with a silica pad (washed with small amount of DCM). The filtrate was partially vacuum evaporated to remove some of the solvents to give a yellow solid which was filtered from the remaining solvent to give solid fraction 1 (impure **43 (RJ 12)**; solid fraction 1), which was washed with a small amount of DCM. The solvent was removed from the filtrate and then chromatographed on silica (eluent DCM), to afford compound **42** (1st band) as a pale-yellow solid (0.07 g, 9%); mp: 148-150 °C. ^{1}H NMR ($CDCl_3$, 300 MHz): δ 2.65 (t, J = 7.0 Hz, 2H), 3.19 (t, J = 7.0 Hz, 2H), 7.31 (d, J_{12} = 8.5 Hz, 1H), 7.37 (d, J = 8.5 Hz, 2H), 7.55 (d, J = 8.5 Hz, 2H), 8.00 (dd, J_{12} = 8.5 Hz, J_{23} = 1.5 Hz, 1H), 8.84 (d, J_{23} = 1.5 Hz, 1H), ^{13}C NMR ($CDCl_3$, 125 MHz): δ 18.5, 29.6, 89.1, 90.1, 92.8, 117.9, 119.6, 121.1, 128.7, 130.1, 133.0, 135.2, 142.0, 144.7, 156.4 and a yellow solid (2nd band; impure **43 (RJ 12)**); (solid fraction 2). Mixed solid fractions 1 and 2 were recrystallised with DCM and hexane (ca. 9:1 v/v) to give compound **43; RJ 12** (0.80 g, 88 %); mp: >165 °C (decomposed). ^{1}H NMR ($CDCl_3$, 500 MHz): 2.65 (t, J = 7.5 Hz, 4H), 3.19 (t, J = 7.5 Hz, 4H), 7.35-7.38 (m, 4H), 7.49-7.51 (m, 3H), 7.56 (d, J = 8.0 Hz, 2H), 7.79 (dd, J_{13} = 1.5 Hz, J_{23} = 8.0 Hz, 1H), 8.75 (d, J_{13} = 1.5 Hz, 1H). ^{13}C NMR ($CDCl_3$, 125 MHz)): δ 18.5, 29.6, 29.7, 87.3, 89.8, 90.6, 93.9, 117.9, 119.6, 121.1,

211.5, 126.7, 130.1, 130.3, 132.7, 133.0, 135.2, 135.6, 138.7, 142.0, 152.7. MS (MALDI-TOF) *m/z* (%) 449.1 (M^+, 93), 333.1 (100).

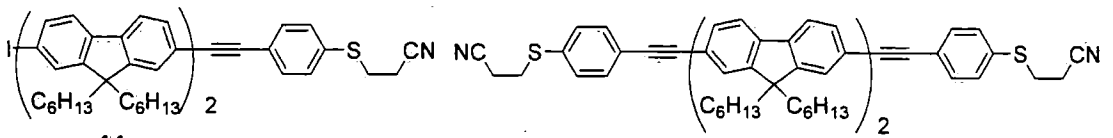

44 **45 (RJ 13)**

2-Iodo-7'-[4-(2-cyanoethylsulfanyl)phenylethynyl]-9,9,9',9'-tetrahexyl-[2,2']bifluorenyl (44) and **2,7'-Bis[4-(2-cyanoethylsulfanyl)phenylethynyl]- 9,9,9',9'-tetrahexyl-[2,2']bifluorenyl (45; RJ 13)**.

Compounds **8** (0.30 g, 1.6 mmol) and **20** (0.67 g, 0.73 mmol) were dissolved in dry THF (15 ml). $Pd[PPh_3]_2Cl_2$ (15 mg) and CuI (5 mg) were added with stirring followed by the addition of triethylamine (15 ml). The mixture was stirred under Ar at 50 °C for 4 h. The solution was cooled to r.t., resulting in a yellow suspension. The solids in the suspension were removed by suction filtration (washed with diethyl ether) and the filtrate was vacuum evaporated to remove the solvents. Chromatography on silica (eluent DCM-hexane 1:1 v/v) afford compound **44** as orange solid (0.12 g, 17 %). ^1H NMR ($CDCl_3$, 200 MHz): δ 0.76-1.11 (m, 44H), 2.06 (b, 8H), 2.64 (d, J = 7.2 Hz, 2H), 3.18 (d, J = 7.2 Hz, 2H), 7.40 (d, J = 8.4 Hz, 3H), 7.52-7.78 (m, 14H); MS (MALDI-TOF) *m/z* (%) 977.5(M^+, 60), 857.6 (100). Next to elute was compound **45; RJ 13** as a pale-yellow solid (0.47 g, 62%), mp: 45-47 °C. ^1H NMR ($CDCl_3$, 500 MHz): δ 0.72-0.80 (m, 10H), 1.10-1.15 (m, 12H), 2.06-2.07(m, 4H), 2.66(t, J = 7.5 Hz, 2H), 3.20 (t, J = 7.5 Hz, 2H), 7.40 (d, J = 8 Hz, 2H), 7.55-7.57 (m, 4H), 7.64 (s, 1H), 7.68 (d, J = 8 Hz, 1H), 7.74 (d, J = 8 Hz, 1H), 7.82 (d, J = 7 Hz, 1H). ^{13}C NMR ($CDCl_3$, 125 MHz): δ 14.3, 18.5, 22.8, 24.0, 29.9, 30.0, 31.7, 40.6, 55.6, 88.9, 92.2, 118.1, 120.0, 120.6, 121.3, 121.7, 122.9, 126.2, 126.6, 130.7, 131.0, 132.6, 133.9, 139.9, 141.1, 141.6, 151.4, 152.1. MS (MALDI-TOF) *m/z* (%) 1036.6 (M^+, 100).

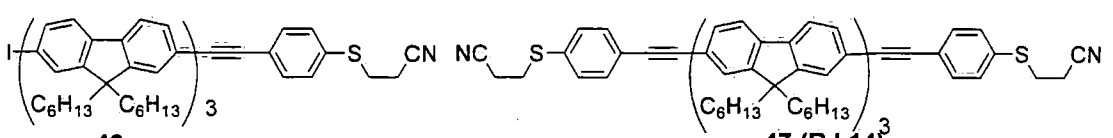

46 **47 (RJ 14)**

2-Iodo-7''-[4-(2-cyanoethylsulfanyl)phenylethynyl]- 9,9,9',9',9'',9''-hexahexyl-[2,2']-[7',2'']trifluorenyl (47) and 2,7''-Bis[4-(2-cyanoethylsulfanyl)phenylethynyl]-9,9,9',9',9'',9''-hexahexyl-[2,2']-[7',2'']trifluorenyl (47; RJ 14).

Compounds **8** (0.16 g, 0.85 mmol) and **21** (0.50 g, 0.40 mmol) were dissolved in dry THF (15 ml). $Pd[PPh_3]_2Cl_2$ (10 mg) and CuI (3 mg) were added with stirring followed by the addition of triethylamine (15 ml). The mixture was stirred under Ar at 50 °C for 4 h. The solution was cooled to r.t., resulting in a yellow suspension. The solids in the suspension were removed by suction filtration (washed with diethyl ether) and the filtrate was vacuum evaporated to remove the solvents. After that, chromatography on silica (eluent DCM-hexane 1:1 v/v), afforded compound **47** as an orange solid (0.15 g, 28 %). ^{1}H NMR ($CDCl_3$, 400 MHz): δ 0.67-1.17 (m, *J* = 66H), 1.35-1.84 (m, 12H), 2.61 (d, *J* = 7.2 Hz, 2H), 3.15 (d, *J* = 7.2 Hz, 2H), 7.16 (s, 1H), 7.30 (d, *J* = 8.0 Hz, 2H), 7.39-7.75 (m, 21H). MS (MALDI-TOF) *m/z* (%) 1309.7 (M^+, 100). Compound **47; RJ 14** as a pale-yellow solid (0.32 g, 59%), mp: 86-87 °C. ^{1}H NMR ($CDCl_3$, 500 MHz): δ 0.78-0.82 (m, 15H), 1.10-1.17 (m, 18H), 2.02-2.19 (m, 6H), 2.66 (t, *J* = 7.0 Hz, 2H), 3.20 (t, *J* = 7.0 Hz, 2H), 7.41 (d, *J* = 7.0 Hz, 1H), 7.56-7.58 (m, 4H), 7.67-7.71 (m, 4H), 7.75 (d, *J* = 8.0 Hz, 1H), 7.82 (d, *J* = 8.5 Hz, 1H), 7.86 (d, *J* = 8.0 Hz, 1H). ^{13}C NMR ($CDCl_3$, 125 MHz): δ 14.3, 18.5, 22.8, 22.8, 24.0, 29.9, 30.0, 31.7, 31.8, 40.6, 55.5, 55.6, 88.9, 92.2, 118.0, 120.0, 210.3, 120.6, 121.3, 121.7, 121.8, 123.0, 126.3, 126.5, 126.6, 130.7, 131.0, 132.6, 133.9, 139.8, 140.3, 140.6, 141.3, 141.6, 151.4, 152.1, 152.1. MS (MALDI-TOF) *m/z* (%) 1369.9 (M^+, 100).

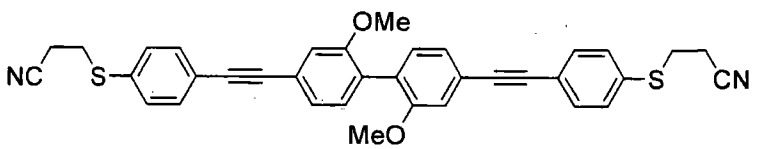

49 (RJ 17)

4,4'-Bis[4-(2-cyanoethylsulfanyl)phenylethynyl]-2,2'-dimethoxybiphenyl (49; RJ 17). Compound **8** (0.20 g, 1.00 mmol) and diiodobiphenyl **33** (0.54 g, 1.16 mmol) were dissolved in dry THF (25 ml). $Pd[PPh_3]_2Cl_2$ (21 mg) and CuI (10 mg) were added with stirring followed by the addition of triethylamine (15 ml). The mixture was stirred under Ar at 50 °C for 4 h. The solution was cooled to r.t., resulting in a yellow suspension. The

solids in the suspension were removed by suction filtration (washed with diethyl ether) and the filtrate was vacuum evaporated to remove the solvents. After that chromatography on silica (eluent DCM-hexane 1:1 v/v), afford compound **49** (**RJ 17**) as a yellow solid (0.61 g, 90 %); mp: 146-148 °C, ^{1}H NMR ($CDCl_3$, 500 MHz): δ 2.63 (t, J = 7.5 Hz, 2H), 3.18 (t, J = 7.5 Hz, 2H), 3.82 (s, 3H), 7.13 (d, J_{12} = 1.2 Hz, 1H), 7.19 (dd, J_{12} = 1.2 Hz, 2H, J_{13} = 7.6 Hz, 1H), 7.24 (d, J_{13} = 7.6 Hz, 1H), 7.37 (d, J = 8.4 Hz, 2H), 7.51 (d, J = 8.4 Hz, 2H). ^{13}C NMR ($CDCl_3$, 125 MHz): δ 18.5, 30.0, 56.0, 88.8, 91.0, 114.2, 118.0, 122.7, 123.5, 124.2, 130.7, 131.6, 132.6, 134.0, 156.9 ; MS (MALDI-TOF) *m/z* (%) 584.2 (M^+, 100).

1,3-Bis[4-(2-cyanoethylsulfanyl)phenylethynyl]-2,5-dimethoxybenzene (50; RJ 39).

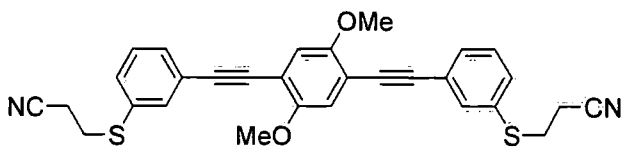

50 (RJ 39)

Compound **13** (0.33 g, 1.76 mmol) and 1,4-diiodo-2,6-dimethoxybenzene (0.31 g, 0.79 mmol) were dissolved in dry THF (15 ml). $Pd[PPh_3]_2Cl_2$ (17 mg) and CuI (8 mg) were added with stirring followed by the addition of triethylamine (15 ml). The mixture was stirred under Ar at 50 °C for 4 h. The solution was cooled to r.t., resulting in a yellow suspension. The solids in the suspension were removed by suction filtration (washed with diethyl ether) and the filtrate was vacuum evaporated to remove the solvents. After that chromatography on silica (eluent ethyl acetate-hexane 2:8 v/v), afford compound **50 (RJ 39)** as a white solid (0.35 g , 87 %) ; mp: 99-101 °C, ^{1}H NMR (400 MHz, $CDCl_3$) δ 2.60 (t, J = 7.2, 2H), 3.14 (t, J = 7.2, 2H), 3.90 (s, 3H), 7.02 (s, 1H), 7.31 (t, J = 7.7, 1H), 7.37 (dt, J = 1.6, 7.7, 1H), 7.46 (dt, J = 1.4, 7.7, 1H), 7.59 (t, J = 1.6, 1H). ^{13}C NMR (101 MHz, $CDCl_3$) δ 18.5, 30.3, 56.7, 86.9, 94.2, 113.4, 115.8, 118.0, 124.7, 129.5, 131.1, 131.4, 133.8, 134.1, 154.1. MS (MALDI-TOF) *m/z* (%): 508.3 (M^+, 100); Crystals for X-ray analysis were grown from slowly evaporating a solution of **50** (**RJ 39**) in ethyl acetate-hexane.

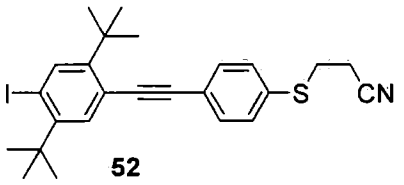

52

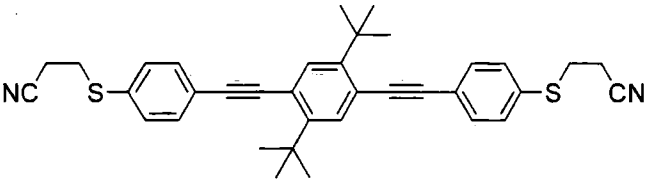

51 (RJ 41)

3-**[4-(2-(2,5-Di-*tert*-butyl-4-iodophenyl)ethynyl)phenylthio]propanenitrile (52)** and **1,4-bis[4-(2-cyanoethylsulfanyl)phenylethynyl]-2,5-di-*tert*-butylbenzene (51; RJ 41)**. Compound **8** (0.50 g, 1.1 mmol) and 1,4-diiodo-2,6-di-*tert*-butylbenzene (**36**) (0.22 g, 1.2 mmol) were dissolved in dry THF (30 ml). $Pd[PPh_3]_2Cl_2$ (17 mg) and CuI (10 mg) were added with stirring followed by triethylamine (30 ml). The mixture was stirred under Ar at 50 °C for 4 h. The solution was cooled to r.t., resulting in a yellow suspension. The solids in the suspension were removed by suction filtration (washed with diethyl ether) and the filtrate was vacuum evaporated to remove the solvents. After that chromatography on silica (eluent ethyl acetate-hexane 2:8 v/v), afford compound **52** as a white solid (0.20 g, 35 % from 59 % conversion) ; mp: 97-101 °C, ^{1}H NMR (400 MHz, $CDCl_3$) δ 1.49 (s, 9H), 1.51 (s, 9H), 2.61 (t, J = 7.3, 2H), 3.15 (t, J = 7.3, 2H), 7.36 (d, J = 8.6, 2H), 7.47 (d, J = 8.6, 2H), 7.51 (s, 1H), 7.95 (s, 1H). ^{13}C NMR ($CDCl_3$, 100.6 MHz): δ 18.2, 29.8, 29.9, 34.1, 35.1, 36.2, 92.0, 96.5, 117.8, 125.5, 129.9, 130.6, 133.3, 141.2, 147.6, 150.2; MS (MALDI-TOF) *m/z* (%): 501.1 (M^+, 100). Next to elute was **51; RJ 41** as a white solid (0.10 g, 16% from 59 % conversion) mp: 103-104.5 °C. ^{1}H NMR (400 MHz, $CDCl_3$) δ 1.55 (s, 9H), 2.63 (t, J = 7.3, 2H), 3.17 (t, J = 7.3, 2H), 7.39 (d, J = 8.3, 2H), 7.50 (d, J = 8.3, 2H), 7.55 (s, 1H); ^{13}C NMR (101 MHz, $CDCl_3$) δ 18.2, 29.7, 29.8, 29.9, 35.4, 92.6, 95.0, 117.7, 121.1, 130.6, 131.8, 132.4, 148.6; MS (MALDI-TOF) *m/z* (%): 560.3 (M^+, 100). From the final fraction **56** (0.20 g) was recovered. Crystals of for X-ray analysis were grown from slowly evaporating a solution of **51 (RJ 41)** in ethyl acetate-hexane, *Crystal data*: Triclinic ($P\ \bar{1}$), a= 6.6930(14), b= 13.459(3), c= 16.804(3) Å, α= 95.46(3), β= 92.07(3), γ= 98.41(3)°.

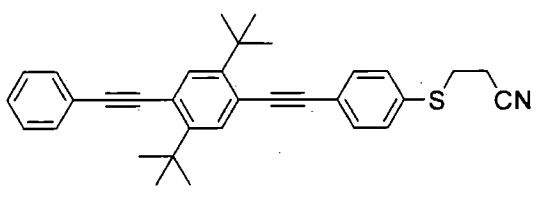

53 (RJ 40)

3-[4-(2-(2,5-Di-*tert*-butyl-4-(2-phenylethynyl)phenyl)ethynyl)phenylthio]propanenitrile (53; RJ 40). Compound **37**

(0.29 g, 0.57 mmol) and phenylacetylene (0.12 g, 1.2 mmol) were dissolved in dry THF (15 ml). $Pd[PPh_3]_4$ (20 mg) and CuI (6 mg) were added with stirring followed by the addition of triethylamine (15 ml). The mixture was stirred under Ar at 50 °C overnight. The solution was cooled to r.t., resulting in a yellow suspension. The solids in the suspension were removed by suction filtration (washed with diethyl ether) and the filtrate was vacuum evaporated to remove the solvents. After that, chromatography on silica (eluent DCM-ethyl acetate-hexane 1:5:15 v/v), afford compound **53; RJ 40** as a white solid (0.18 g, 66%) ; mp: 106-110 °C, ^{1}H NMR (400 MHz, $CDCl_3$) δ 1.56 (s, 9H), 1.57 (s, 9H), 2.63 (t, J = 7.3, 1H), 3.17 (t, J = 7.3, 1H), 7.42 – 7.35 (m, 5H), 7.51 (d, J = 8.5, 2H), 7.59 – 7.54 (m, 4H). ^{13}C NMR (101 MHz, $CDCl_3$) δ 28.6, 28.8, 29.2, 34.3, 90.2, 92.0, 93.9, 94.9, 119.7, 120.5, 122.6, 123.9, 126.9, 127.2, 127.4, 130.0, 130.5, 131.3, 131.4, 133.3, 147.5, 147.6; MS (MALDI-TOF) *m/z* (%): 475.2 (M^+, 100). Crystals for X-ray analysis were grown from slowly evaporating a solution of **53** (**RJ 40**) in ethyl acetate-hexane.

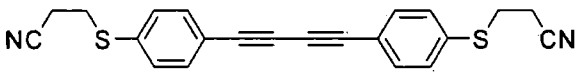

54

1,4-Bis[4-(2-cyanoethylsulfanyl)-phenyl]-1,3-butadiyne (54). This compound was sometimes isolated in <5% yield as the oxidative self-coupled product from Sonogashira cross-coupling reactions involving **8**. A white solid mp: 137-139 °C. ^{1}H NMR ($CDCl_3$, 500 MHz): δ 2.64 (t, J = 7.0 Hz, 2H), 3.18 (t, J = 7.0 Hz, 2H), 7.33 (d, J = 8.5 Hz, 2H), 7.45 (d, J = 8.5 Hz, 2H); ^{13}C NMR ($CDCl_3$, 125 MHz): δ 18.4, 29.5, 75.1, 81.6, 117.9, 120.7, 129.9, 133.5, 133.8; MS (MALDI-TOF) *m/z* (%) 372.1 (M^+, 100).

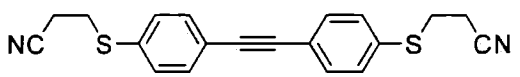

55

Bis[4-(2-cyanoethylsulfanyl)-phenyl]-ethyne (55). Compound **8** (0.35 g, 1.87 mmol) and iodobenzene **6** (0.60 g, 2.07 mmol) were dissolved in dry THF (15 ml). $Pd[PPh_3]_2Cl_2$ (33 mg) and CuI (10 mg) were added with stirring followed by the addition of triethylamine (15 ml). The mixture was stirred under Ar at 50 °C for 4 h. The solution was cooled to r.t., resulting in a yellow suspension. The solids in the suspension were removed by suction filtration (washed with diethyl ether)

and the filtrate was vacuum evaporated to remove the solvents. Then chromatography on silica (eluent DCM), afford compound **55** as an orange solid (0.62 g, 93 %); mp: 144-145 °C, ^{1}H NMR ($CDCl_3$, 200 MHz): δ 2.63 (t, J = 7.2 Hz, 2H), 3.17 (t, J = 7.2 Hz, 2H), 7.36 (d, J = 8.5 Hz, 2H), 7.49 (d, J = 8.5 Hz, 2H); MS (MALDI-TOF) *m/z* (%) 348.1 (M^+, 100). Crystals for X-ray analysis were grown from slowly evaporating a solution of **55** in ethyl acetate-hexane.

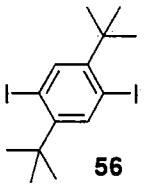
56

1,4-Di-*tert*-butyl-2,5-diiodobenzene (56) was synthesised as reported in literature in three steps.[120] 1st Step. A 250 ml round-bottomed flask equipped with a condenser, was charged with mercuric trifluoroacetate (30 g, 70 mmol) under argon, and was heated with stirring until the solid melted (180-190 °C). Then 2,5-di-*tert*-butylbenzene (6.08 g, 32.0 mmol) was added. The temperature was increased to 210 °C for 20 min, whereupon the melt solidified. The resulting white solid was collected on a sintered disc filter funnel and was washed with water (300 ml) and methanol (300 ml). Vacuum drying afforded the product (24.7 g, 95%) as a white powder product; 1,4-bis[(trifluoroacetoxy)mercurio)]-2,5-di-*tert*-butylbenzene: ^{1}H NMR (400 MHz, acetone-D_6) δ 1.53 (s, 9H), 7.91 (s, 1H).

2nd Step. A mixture of 1,4-bis[(trifluoroacetoxy)mercurio)]-2,5-di-*tert*-butylbenzene (22.1 g, 27.1 mmol), sodium chloride (8.5 g, 145 mmol), water (200 ml), and methanol (200 ml) was refluxed for 2 days under argon. The resulting white powder was collected on a sintered disc filter funnel and was washed with hexane (300 ml), methanol (300 ml), and diethyl ether (300 ml). Vacuum drying afforded 1,4-bis(chloromercurio)-2,5-di-*tert*-butylbenzene as a white powder (17.0 g, 95%): ^{1}H NMR (400 MHz, $CDCl_3$) δ 1.32 (s, 9H), 7.32 (s, 1H).

3rd Step. To a suspension of 1,4-bis(chloromercurio)-2,5-di-*tert*-butylbenzene (5.4 g, 8.2 mmol) and 1,2-dimethoxyethane (120 ml) a solution of methylmagnesium chloride in tetrahydrofuran (3.0 M, 11 ml, 33 mmol) was added under argon. The mixture was refluxed for 17 h to afford a white suspension. Iodine (21 g, 82 mmol) was added at room temperature, and the solution was stirred for 1 h. The solvent was removed under reduced pressure, and the residue was extracted with hexane (50 ml). The hexane extract was passed through a 2 cm pad of silica gel on a course glass frit. Elution with hexane (50 ml), followed by removal of the solvent under reduced pressure and recrystallisation from

dichloromethane, afforded **36** (2.5 g, 70%): mp 137 °C; ^{1}H NMR (400 MHz, $CDCl_3$) δ 1.48 (s, 9H), 7.9 (s, 1H).

1,4-Bis[4-(2-acetylsulfanyl)phenylethynyl]-2,6-dihexyloxybenzene[226] **(57; RJ 8Ac)**

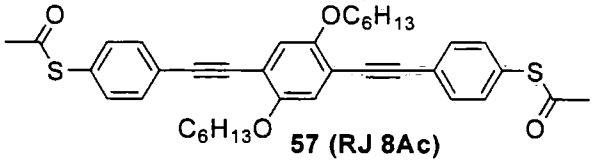

57 (RJ 8Ac)

To a degassed solution of **35; RJ 8** (0.25 g, 0.39 mmol) in dry THF (30 ml) was added sodium methoxide solution (25% in methanol, 0.5 ml). The mixture was stirred at r.t. under argon for 20 min to afford a thick yellow suspension. Acetic anhydride (1.0 ml) was added and the mixture was stirred for 0.5 h to afford a pale yellow solution. Solvents were removed by vacuum evaporation followed by the addition of dichloromethane (50 ml) to the solid residue. The mixture was sonicated for 2 min then suction filtered through a Celite pad. The filtrate was concentrated and chromatographed on silica (eluent hexane/ethyl acetate 11:4 v/v) to give **57; RJ 8Ac** as a yellow solid (0.17 g, 70%), mp: 110-111 °C. ^{1}H NMR ($CDCl_3$, 400 MHz): δ 0.82 (t, J = 7.3 Hz, 3H), 1.20-1.40 (m, 4H), 1.50 (m, 2H), 1.80 (m 2H), 2.36 (s, 3H), 3.95 (t, 3H, , J = 6 Hz), 6.93 (s, 1H), 7.32 (d, J = 8.0, 2H), 7.47 (d, J = 8 Hz, 2H). ^{13}C NMR ($CDCl_3$, 100.6 MHz): 14.0, 22.6, 25.7, 29.7, 30.6, 31.5, 69.7, 87.7, 94.1, 114.0, 117.0, 124.7, 128.7, 132.1, 134.2, 153.6, 193.4; MS (MALDI-TOF) *m/z* (%) 626.3 (M^+, 100). Crystals for X-ray analysis were grown from slowly evaporating a solution of **57** (**RJ 8Ac**) in ethyl acetate-hexane, *Crystal data*: triclinic ($P\bar{1}$), a= 5.9242(6), b= 11.2445(12), c= 13.1502(14) Å, α= 81.16(1), β= 82.54(1), γ= 75.46(1)°.

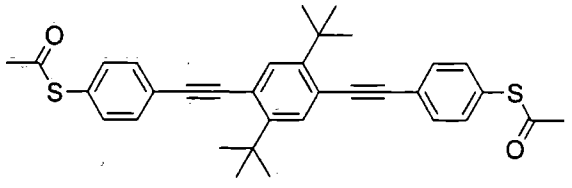

58 (RJ 41Ac)

1,4-Bis[4-(2-acetylsulfanyl)phenylethynyl]-2,5-di-*tert*-butylbenzene (58; RJ 41Ac). To a degassed solution of compound **51; RJ 41** (0.36 g, 0.64 mmol) in dry THF (30 ml) was added sodium methoxide solution (25% in methanol, 0.5 ml). The mixture was stirred at r.t. under argon for 20 min to afford a thick yellow suspension. Acetic anhydride (2.0 ml) was added and the mixture was stirred for

0.5 h to afford a pale-yellow solution. Solvents were removed by vacuum evaporation followed by the addition of dichloromethane (50 ml) to the solid residue. The mixture was sonicated for 2 min then suction filtered through a Celite pad. The filtrate was concentrated and chromatographed on silica (eluent hexane/ethyl acetate 8:2 v/v) to give **58; RJ 41Ac** as a white solid (0.31 g, 90%), mp: 129-132 °C. ^{1}H NMR (400 MHz, $CDCl_3$): δ 1.54 (s, 9H), 2.43 (s, 3H), 7.40 (d, J = 8.0, 2H), 7.55 (s, 1H), 7.56 (d, J = 8.0, 2H). ^{13}C NMR (101 MHz, $CDCl_3$) δ 29.9, 30.3, 35.4, 93.0, 95.1, 121.1, 124.9, 128.0, 131.6, 132.4, 134.3, 148.7, 193.5. MS (MALDI-TOF) *m/z* (%) 464.3 (M^+, 100). Crystals for X-ray analysis were grown from slowly evaporating a solution of **58** (**RJ 41AC**) in ethyl acetate-hexane.

1-Phenylethynyl,4-[4-(2-acetylsulfanyl)phenylethynyl]-2,5-di-*tert*-butylbenzene (59; RJ 40Ac). To a degassed solution of compound **53; RJ 40** (0.20 g, 0.42 mmol) in dry THF (30 ml) was added sodium methoxide solution (25% in methanol, 0.5 ml). The mixture was stirred at r.t. under argon for 20 min to afford a thick yellow suspension. Acetic anhydride (1.0 ml) was added and the mixture was stirred for 0.5 h to afford a pale-yellow solution. Solvents were removed by vacuum evaporation followed by the addition of dichloromethane (50 ml) to the solid residue. The mixture was sonicated for 2 min then suction filtered through a Celite pad. The filtrate was concentrated and chromatographed on silica (eluent hexane/ethyl acetate 8:2 v/v) to give **59; RJ 40Ac** as a white solid (0.19 g, 97%), mp: 108-111 °C. ^{1}H NMR (400 MHz, $CDCl_3$) δ 1.57 (s, 9H), 1.58 (s, 9H), 2.45 (s, 3H), 7.39 – 7.36 (m, 3H), 7.43 (d, J = 8.5, 2H), 7.61 – 7.54 (m, 6H). ^{13}C NMR (101 MHz, $CDCl_3$) δ 28.6, 28.8, 28.9, 29.2, 34.3, 90.2, 92.0, 93.9, 94.9, 119.7, 120.5, 122.6, 123.9, 126.9, 127.2, 127.4, 130.0, 130.5, 131.3, 131.4, 133.3, 147.5, 147.6, 192.5. MS (MALDI-TOF) *m/z* (%) 538.3 (M^+, 100). Crystals for X-ray analysis were grown from slowly evaporating a solution of **59** (**RJ 40Ac**) in ethyl acetate-hexane mixture. *Crystal data*: triclinic ($P\bar{1}$), a= 6.1691(6), b= 11.0563(10), c= 19.9938(18) Å, α= 95.555(9), β= 97.928(8), γ= 104.921(8)°.

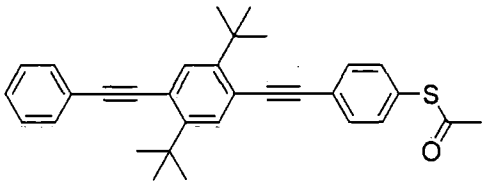

59 (RJ 40Ac)

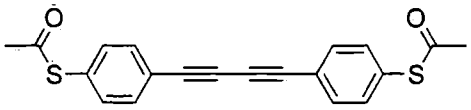

60

1,4-Bis[4-(2-acetylsulfanyl)-phenyl]-1,3-butadiyne (60). To a degassed solution of compound **37** (0.20 g, 0.54 mmol) in dry THF (30 ml) was added tetrabutylammonium hydroxide solution (1 M in methanol, 0.5 ml). The mixture was stirred at r.t. under argon for 20 min to afford a thick yellow suspension. Acetic anhydride (1.0 ml) was added and the mixture was stirred for 0.5 h to afford a pale yellow solution. Solvents were removed by vacuum evaporation, followed by the addition of DCM (30 ml) to the solid residue. The mixture was extracted with DCM (3 x 20 ml), dried with $MgSO_4$ and chromatographed on silica (eluent DCM) to give **60** as a yellow solid (0.15 g, 82%). ^{1}H NMR ($CDCl_3$, 500 MHz): δ 2.44 (s, 3H), 7.34, (d, J = 8.5 Hz, 2H), 7.55 (d, J = 8.5 Hz, 2H). ^{13}C NMR ($CDCl_3$, 125 MHz): δ 30.6, 75.5, 81.6, 122.9, 129.7, 133.3, 134.5, 193.3; MS (MALDI-TOF) *m/z* (%) 350.4 (M^+, 100).

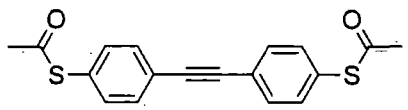

61

Bis[4-(2-acetylsulfanyl)-phenyl]-ethyne (61).[227]

To a degassed solution of compound **39** (0.20 g, 0.57 mmol) in dry THF (30 ml) was added sodium methoxide solution (25% in methanol, 0.1 ml). The mixture was stirred at r.t. under argon for 20 min to afford a thick yellow suspension. Acetic anhydride (1.5 ml) was added and the mixture was stirred for 1.5 h to afford a pale-yellow solution. Solvents were removed by vacuum evaporation followed by the addition of DCM (30 ml) to the solid residue. The mixture was extracted with DCM (3 x 20 ml), dried with $MgSO_4$ and chromatographed on silica (eluent DCM). The resulting yellow solid was recrystallised from chloroform-ethanol to afford yellow crystals of **61** (0.17 g, 92%). ^{1}H NMR ($CDCl_3$, 500 MHz): δ 2.52 (s, 3H), 7.48 (d, J = 8.5 Hz, 2H), 7.64 (d, J = 8.5 Hz, 2H). ^{13}C NMR ($CDCl_3$, 125 MHz): δ 30.5, 90.5, 124.4, 128.6, 132.5, 134.5, 193.7.

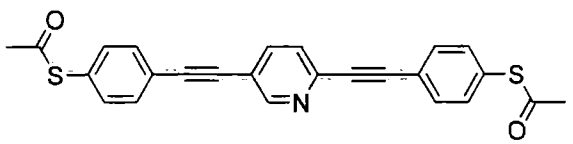

62 (RJ 12Ac)

1,4-Bis[4-(2-acetylsulfanyl)phenylethynyl]-2,6-pyridine (62; RJ 12Ac)

To a degassed solution of compound **43 (RJ 12)** (0.10 g, 0.22 mmol) in dry DMF (30 ml) was added $CsOH.H_2O$ (0.15 g, 0.89 mmol). The mixture was stirred at r.t. under argon for 20 min to afford a thick yellow suspension. Acetic anhydride (1.0 ml) was added and the mixture was stirred for 1 h to afford a pale-yellow solution. Solvents were removed by vacuum evaporation followed by the addition of dichloromethane (50 ml) to the solid residue. The mixture was sonicated for 2 min then suction filtered through a Celite pad. The filtrate was concentrated and chromatographed on silica (eluent DCM) to give **62 (RJ 12Ac)** as a yellow solid (80 mg, 83%), mp: 112-115 °C. ^{1}H NMR (400 MHz, $CDCl_3$) δ 2.41 (s, 6H), 7.42 – 7.37 (m, 4H), 7.49 (d, J = 8.2, 1H), 7.54 (d, J = 8.2, 2H), 7.60 (d, J = 8.1, 2H), 7.77 (dd, J = 2.2, 8.1, 1H), 8.73 (d, J = 2.2, 1H). ^{13}C NMR (101 MHz, $CDCl_3$) δ 30.3, 99.9, 119.5, 123.0, 123.3, 126.7, 129.1, 129.4, 132.2, 132.6, 134.2, 134.3, 138.9, 193.1, 193.2; No mass spectrum could be obtained by EI, ES or MALDI-ToF techniques; Anal. calcd for $C_{25}H_{17}NO_2S_2$: C, 70.23; H, 4.01; N, 3.28. Found: C, 70.22; H, 4.00; N, 3.28.

Chapter 4.2.

The synthesis of charged iridium (III) phenanathroline and bipyridine complexes for organic light emitting diode applications.

3,8-Bis[-(9,9-dihexylfluorenyl)]-phenanthroline 66; FluPhen.[153]

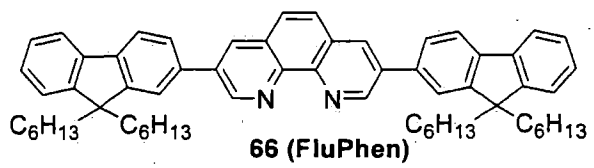

66 (FluPhen)

A mixture of dibromophenanthroline, **65** (1.6 g, 4.7 mmol), fluorenylboronic acid (4.0 g, 10.5 mmol), THF (40 ml), toluene (40 ml) and aqueous Na_2CO_3 (1 M, 15 ml) was purged with argon for 30 min, then $Pd(PPh_3)_4$ (0.3 g, 0.09 mmol) was added in one portion. The mixture was stirred at 88 °C for 72 h. The solvent was removed under reduced pressure. The residue was dissolved in dichloromethane (50 ml) and washed with water (2 ×50 ml). The organic phase was dried over anhydrous $MgSO_4$. The solvent was removed and the yellow residue was purified by column chromatography

(SiO_2, eluent dichloromethane/acetone gradient) to yield **66**; **FluPhen** as a white powder (2.5 g, 63% yield); mp: 99-101 °C; Anal. calcd for $C_{62}H_{72}N_2$: C, 88.10; H, 8.59; N, 3.31; Found: C, 88.18; H, 8.55; N, 3.27; ^{1}H NMR (400 MHz, $CDCl_3$): δ 0.62-0.72 (m, 10H), 0.96-1.05 (m, 12H), 1.91-2.01 (m, 4H), 7.26-7.31 (m, 3H), 7.66-7.77 (m, 3H), 7.78 (d, J = 7.6 Hz, 1H), 7.85 (s, 1H), 8.38 (d, J = 2.4 Hz, 1H), 9.45 (d, J = 2.4 Hz, 1H); ^{13}C NMR (100 MHz, $CDCl_3$): δ 13.97, 22.54, 23.82, 29.67, 31.46, 40.36, 55.36, 120.03, 120.42, 121.82, 123.00, 126.49, 126.94, 127.15, 127.51, 128.15, 128.59, 133.36, 136.21, 136.38, 140.36, 141.64, 149.63, 151.12, 152.01; MS (ES$^+$): *m/z* (%) 845.9 (MH^+, 100).

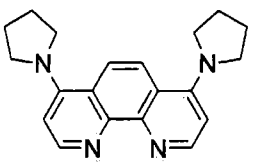

69 (PyPhen)

4,7-Dipyrrolidin-1-yl-[1,10]phenanthroline 69; PyPhen.

4,7-Dichlorophenanthroline (0.2 g, 0.8 mmol) was mixed with pyrrolidine (20 ml) and refluxed for 2 h under N_2. The reaction mixture was cooled down, the excess pyrrolidine was removed under reduced pressure and then the crude product was passed through a silica pad washed with DCM. The product **69** was obtained after recrystallisation with DCM/hexane, as a white solid (0.19 g, 75 %); mp 125-130 °C. ^{1}H NMR (200 MHz, $CDCl_3$): δ 2.05-2.18 (m, 4H), δ 3.78-3.88 (m, 4H), 6.66 (d, J = 6.2 Hz, 1H), 8.12 (s, 1H), 8.85 (d, J = 6.2 Hz, 1H); MS (EI) *m/z* (%): 318.2 (M^+, 100). ^{13}C NMR (100 MHz, $CDCl_3$): δ 26.1, 52.8, 118.5, 130.1, 150.5, 154.5.

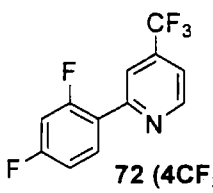

72 (4CF$_3$ppy)

2-(2,4-Difluorophenyl)-4-(trifluoromethyl)pyridine 72; 4CF$_3$ppy.

Following the procedure for **5CF$_3$ppy**, 2,4-difluorophenylboronic acid (0.5 g, 3.1 mmol), 2-chloro-4-trifluoromethyl-pyridine (0.52 g, 2.8 mmol), toluene (30 ml), Na_2CO_3 (aqueous 2 M, 8 ml) and $Pd(PPh_3)_4$ (0.1 mg, 5 mol%) gave a crude product which was purified by column chromatography (SiO_2, eluent ethyl acetate/hexane 2:9 v/v) to yield **72; 4CF$_3$ppy** as a white powder (0.51 g, 67%); mp: 62-63 °C. ^{1}H NMR (500 MHz, $CDCl_3$): δ 6.93 (ddd, J = 2.5 Hz, J_{HF} = 8.8 Hz, J_{HF} = 11.2 Hz, 1H), 7.02 (td, J = 8.8 Hz, J = 2.5 Hz, 1H), 7.46 (d, 4.5 Hz, 1H), 7.99 (s, 1H), 8.06 (td, J_{HF} = 6.3 Hz, J = 8.8 Hz, 1H), 8.86 (d, 4.5 Hz, 1H); ^{13}C NMR (125 MHz, $CDCl_3$): δ 104.5 (t, J_{CF} = 25.9 Hz), 112.1 (dd, J_{CF} = 3.8 Hz, J_{CF} =

21.1 Hz), 119.5, 122.8 (q, J_{CF} = 273.3 Hz), 128.4, 128.6 (d, J_{CF} = 20.1 Hz), 138.9 (q, J_{CF} = 34.5 Hz), 150.5, 151.4, 153.7 (d, J_{CF} = 1.9 Hz), 160.7 (dd, J_{CF} = 12.5 Hz, J_{CF} = 253.1 Hz), 163.6 (dd, J_{CF} = 11.5 Hz, J_{CF} = 252.2 Hz); ^{19}F NMR ($CDCl_3$, 376 MHz) : δ -112.8 (dd, J_{FC1} = 9.1 Hz, J_{FC2} = 21.3 Hz), -103.9 (q, J_{FC} = 9.1 Hz), -65.3. MS (EI): *m/z* (%): 259.9 (M^+, 100), 240.0 (M^+-F, 20), 189.9 (M^+-CF_3, 75).

2-(2',4'-Difluorophenyl)-5-(trifluoromethyl)pyridine 75; 5CF$_3$ppy.[172]

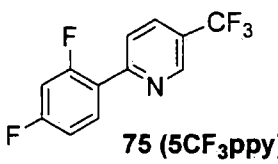

75 (5CF$_3$ppy)

A flask was charged with 2,4-difluorophenylboronic acid (1.57 g, 9.9 mmol), 2-chloro-5-(trifluoromethyl)pyridine (1.5 g, 8.2 mmol), toluene (30 ml) and Na_2CO_3 (aqueous 2 M, 20 ml). The mixture was degassed for 5 minute before $Pd(PPh_3)_4$ (0.48 mg, 5 mol %) was added and the mixture was stirred for 2 day at 100 °C. Upon cooling, the layers were separated and the aqueous layer was extracted with DCM. The combined organic layers were washed with brine and dried ($MgSO_4$), filtered and concentrated. The crude product was purified by column chromatography (SiO_2, eluent ethyl acetate/hexane 2:9 v/v) to yield **75; 5CF$_3$ppy** as a white powder (1.8 g, 85% yield); ^{1}H NMR ($CDCl_3$, 200 MHz): δ 6.77 (m, 2H), 7.81 (m, 3H), 8.95 (d, J = 1.5 Hz, 1H); ^{19}F NMR ($CDCl_3$, 188 MHz): δ -112.5, -107.6, -62.8; MS (EI) *m/z* (%): 259 (M^+, 100), 240 (M^+-F, 15), (M^+-CF_3, 45).

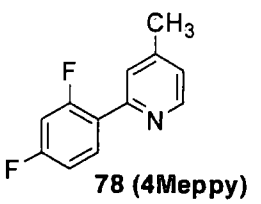

78 (4Meppy)

2-(2',4'-Difluorophenyl)-4-methylpyridine 78; 4Meppy.[173]

A flask was charged with 2,4-difluorophenylboronic acid (1.50 g, 9.50 mmol), 4-methyl-2-bromopyridine (0.9 ml, 8.1 mmol), Na_2CO_3 (aqueous 1M, 20 ml) and THF (40 ml). The mixture was degassed for 1 h before $Pd(PPh_3)_4$ (190 mg, 0.16 mmol) was added and the mixture was stirred for 65 h at 80 °C. Upon cooling, the layers were separated and the aqueous layer was extracted with ethyl acetate. The combined organic layers were washed with brine and dried ($MgSO_4$), filtered and concentrated. The crude product was purified by column chromatography (SiO_2, eluent ethyl acetate/DCM 1:9 v/v), then distillation in Kugelrohr apparatus at 145 °C and 26 mbar to yield **78; 4Meppy** as a pale pink oil that solidified to a white solid on standing (1.47 g, 88%); mp: 34.2 – 35.7 °C; ^{1}H ($CDCl_3$, 400 MHz) :

δ 2.42 (s, 3H), 6.91 (td, J = 8.9 Hz, J_{HF} = 2.6 Hz, 1H), 6.99 (td, J = 8.9 Hz, J_{HF} = 2.7 Hz, 1H), 7.09 (d, J = 5.8 Hz, 1H), 7.56 (s, 1H), 7.96 (m, 1H), 8.56 (d, J = 5.1 Hz, 1H); ^{13}C NMR ($CDCl_3$, 400 MHz) : 21.2, 104.3 (dd, J_{CF} = 27.1 Hz, J_{CF} = 24.9 Hz), 111.8, (dd, J_{CF} = 21.2 Hz, J_{CF} = 3.7 Hz), 123.5, 125.1 (d, J_{CF} = 8.8 Hz), 132.2 (dd, J_{CF} = 9.6 Hz, J_{CF} = 4.4 Hz), 147.8, 149.3, 152.3, 158.0, 161.9 (dd, J_{CF} = 251.0 Hz, J_{CF} = 12.5 Hz) 161.4 (dd, J_{CF} = 251.0 Hz, J_{CF} = 12.5 Hz); ^{19}F NMR ($CDCl_3$, 367 MHz) -113.27, -109.86; MS (EI) *m/z* (%): 205 (M^+, 100%).

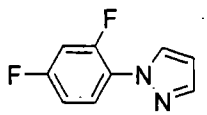

81 (Fppz)

2-(2',4'-Difluorophenyl)- 1*H* –pyrazole 81; Fppz by acid catalysis (Method **A**).[174]

2,4-Difluorophenyl hydrazine (2.0 g, 11 mmole) was added to a mixture of 1,1,3,3-tetraethoxypropane (1.85 ml, 11 mmole), conc. hydrochloric acid (2 ml), and ethanol (20 ml), and the mixture was refluxed for 2 h. The reaction mixture was cooled, then the solvent was removed in vacuo, and the residue column on silica eluting with DCM. Product **81; Fppz** was obtained as a colourless viscous liquid (1.67 g, 84 %); ^{1}H NMR ($CDCl_3$, 400 MHz): δ 6.45 (t, J = 1.5 Hz, 1H), 6.93-6.99 (m, 2H), 7.71 (d, J = 1.5 Hz, 1H), 7.83 (td, J_{HF} = 6.0 Hz, J = 8.0 Hz, 1H), 7.90 (t, J_{HF} = 2.4 Hz 1H); ^{13}C NMR ($CDCl_3$, 100 MHz): δ 105.0, (dd, J_{CF} = 24.9 Hz, J_{CF} = 26.3 Hz), 107.5, 112.1, (dd, J_{CF} = 21.9 Hz, J_{CF} = 4.4 Hz), 125.2 (dd, J_{CF} = 8.8 Hz, J_{CF} = 2.9 Hz), 125.6 (dd, J_{CF} = 7.3 Hz, J_{CF} = 10.2 Hz), 130.6 (d, J_{CF} = 8.7 Hz), 140.9, 151.7 (dd, J_{CF} = 251.8 Hz, J_{CF} = 11.7 Hz), 161.3 (dd, J_{CF} = 250.3 Hz, J_{CF} = 11.7 Hz); ^{19}F NMR ($CDCl_3$, 376 MHz): δ -121.2, -112.0; IR (neat) 3730, 3109, 2360, 1583, 1474, 1390, 1193, 863, 748 cm^{-1}; MS (EI) *m/z* (%): 180 (M^+, 100); MS (ES+) *m/z* (%): 181.1 (MH^+, 100); HRMS calcd. for $C_9H_7F_2N_2$ (MH^+) 181.05718; found: 181.05715.

The synthesis **81** by copper(I) catalysis (Method **B**). A mixture of pyrazole (0.85 g, 12.5 mmol), 2,4-difluoroiodobenzene **82** (1.0 ml, 8.3 mmol), salicylaldoxime (0.23 g, 1.67 mmol), Cs_2CO_3 (5.4 g, 16.7 mmol), Cu_2O (60 mg, 0.42 mmol) and anhydrous degassed acetonitrile (10 ml) was stirred and heated in an oil bath to 80 °C for 12 h, then cooled to room temperature and diluted with dichloromethane and water. The organic layer was washed with water and saturated NaCl solution and was then separated and

dried over $MgSO_4$. The solvent was removed in vacuo to yield the crude product, which was purified by column chromatography on silica Eluent ether/DCM, 0:1 to 1:5 v/v gave in order of elution:

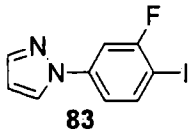

83

1-(3-Fluoro-4-iodophenyl)-1*H*-pyrazole; 83 (39 mg, 2%); a white solid; mp. 76.0-77.5 °C; ^{1}H NMR ($CDCl_3$, 400 MHz): δ 6.39 (dd, J = 1.5 Hz, 2.5 Hz, 1H), 7.17 (dd, J = 2.5 Hz, 8.5 Hz, 1H), 7.48 (dd, J = 2.5 Hz, J_{HF} = 9.0 Hz, 1H), 7.71 (d, J = 1.5 Hz, 1H), 7.76 (dd, J_{HF} = 7.0 Hz, J = 8.5 Hz, 1H), 7.88 (d, J = 2.5 Hz, 1H); ^{13}C NMR ($CDCl_3$, 100 MHz): δ 106, (d, J_{CF} = 27.8 Hz), 108.5, 115.9 (d, J_{CF} = 2.9 Hz), 126.7, 139.7, 139.8 (d, J_{CF} = 2.9 Hz), 141.6, 141.7 (d, J_{CF} = 9.0 Hz), 162.2 (d, J_{CF} = 246 Hz); ^{19}F NMR ($CDCl_3$, 376 MHz): δ -91.7; IR (neat) 3114, 2522, 2359, 1599, 1517, 1389, 1028, 752 cm^{-1}; MS (ES+) *m/z* (%): 288 (M^+, 100); HRMS calcd. for $C_9H_6FIN_2$ (MH^+) 288.96326; found: 288.96327; calcd. C, 37.53; H, 2.10; N, 9.72 found: C, 37.40; H, 2.09; N, 9.67%.

81 (Fppz) (0.25 g, 13%); spectroscopically identical with the product obtained from acid catalysis (Method **A**).

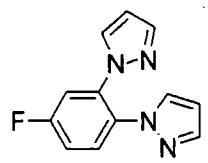

84

3,4-Di(1*H*-pyrazolyl)fluorobenzene; 84 (0.36 g, 20%); a colourless liquid; ^{1}H NMR ($CDCl_3$, 400 MHz): δ 6.25 (s, 1H), 6.31 (s, 1H), 6.82 (s, 1H), 7.08 (s, 1H), 7.15 (td, J = 8.8 Hz, 2.3 Hz, 1H), 7.50 (dd, J = 2.3 Hz, J_{HF} = 8.8 Hz, 1H), 7.58 (dd, J_{HF} = 5.5 Hz, J = 8.8 Hz, 1H), 7.67 (s, 1H), 7.70 (s, 1H); ^{13}C NMR (100 MHz, $CDCl_3$): δ 162.0 (d, J_{CF} = 250 Hz), 141.5, 141.3, 136.5 (d, J_{CF} = 11.0 Hz), 130.9, 130.2, 129.9 (d, J_{CF} = 3.7 Hz), 129.2 (d, J_{CF} = 9.5 Hz), 115.4 (d, J_{CF} = 17.7 Hz), 113.5 (d, J_{CF} = 26.0 Hz), 108.0, 107.7; ^{19}F NMR ($CDCl_3$, 376 MHz): δ -110.5; IR (neat) 3725, 3111, 2360, 1580, 1465, 1382, 1158, 870, 745 cm^{-1}; MS (ES+) *m/z* (%): 229.2 (MH^+, 100); HRMS calcd. for $C_{12}H_{10}N_4F$ (MH^+) 229.08840; found: 229.08848.

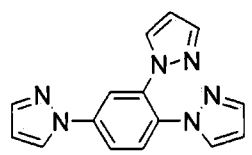

85

1,2,4-Tris(1*H*-pyrazolyl)benzene; 85 (80 mg, 4%); a colourless liquid; ^{1}H NMR ($CDCl_3$, 400 MHz): δ 6.26 (t, J = 2.5 Hz, 1H) , 6.28 (t, J = 2.0 Hz, 1H), 6.45 (t, J = 2.5 Hz, 1H), 6.95 (d, J = 2.5 Hz,

1H), 7.01 (d, J = 2.0 Hz, 1H), 7.67-7.71 (m, 4H), 7.83 (dd, J = 2.5 Hz, J = 8.5 Hz, 1H), 7.98 (d, J = 2.5 Hz, 1H), 8.02 (d, J = 2.5 Hz, 1H); ^{13}C NMR ($CDCl_3$, 100 MHz): δ 107.7, 107.8, 108.4, 116.6, 118.5, 126.9, 128.2, 130.4, 130.6, 131.8, 135.4, 140.0, 141.3, 141.4, 141.8; IR (neat) 3727, 2360, 1586, 1479, 1275, 1129, 865, 764 cm^{-1}; MS (ES+) *m/z* (%): 277.2 (MH^+, 32), 299.2 (M^++Na^+, 100); HRMS calcd. for $C_{15}H_{12}N_6$ (M^++Na^+) 299.10157; found: 299.10169.

Tetrakis-(2-phenylpyridine-C$^{2'}$,N)-(*p*-dichloro) diiridium 86; [Ir(ppy)$_2$Cl]$_2$.[177]

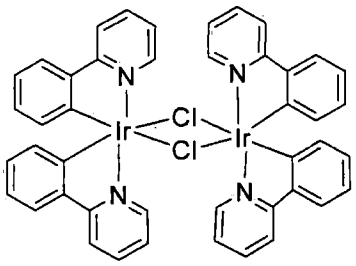

86 [(ppy)$_2$IrCl]$_2$

Iridium tri-chloride hydrate (1.1 g, 3.1 mmol) was combined with 2-phenylpyridine (2.0 g, 12.9 mmol), dissolved in a mixture of 2-ethoxyethanol (50 ml) and water (17 ml), and refluxed for 24 h. The solution was cooled to room temperature, and the yellow precipitate was collected on a glass filter frit. The precipitate was washed with ethanol and acetone and then dissolved in dichloromethane and filtered. The solvent was moved to give crystals of **86; [Ir(ppy)$_2$Cl]$_2$** (3.0 g, 90%); ^{1}H NMR (CD_2Cl_2, 200 MHz): δ 5.88 (dd, J = 1.0 Hz, J = 7.8 Hz, 1H), 6.62 (td, J = 7.4 Hz, J = 1.5 Hz, 1H), 6.79-6.87 (m, 2H), 7.57 (dd, J = 1.0 Hz, J = 7.8 Hz, 1H), 7.81 (td, J = 7.4 Hz, J = 1.5 Hz, 1H), 7.95 (d, J = 7.4 Hz, 1H), 9.26 (dd, J = 1.0 Hz, J = 5.8 Hz, 1H).

Tetrakis-(2-(2',4'-difluorophenyl)-4-methylpyridine –C$^{6'}$,N)-(*p*-dichloro) diiridium 87 ; [Ir(4Meppy)$_2$Cl]$_2$.

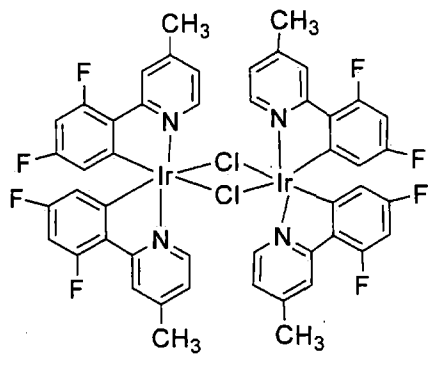

87 [(4Meppy)$_2$IrCl]$_2$

Following the procedure for **86; [Ir(ppy)$_2$Cl]$_2$**, **4Meppy** (1.0 g, 4.9 mmol), $IrCl_3.nH_2O$ (0.4 g, 1.26 mmol), 2-ethoxyethanol (30 ml) and water (10 ml) were refluxed for 24 h. After cooling to room temperature, work-up as for **86; [Ir(ppy)$_2$Cl]$_2$** gave **87; [Ir(4Meppy)$_2$Cl]$_2$** as a yellow powder (1.4 g, 86%); Anal. calcd for $C_{48}H_{32}Cl_2F_8Ir_2N_4$; C, 45.32; H, 2.54; N, 4.40; Found: C, 45.18; H, 2.56; N, 4.38; ^{1}H NMR ($CDCl_3$, 500 MHz): δ 2.71 (s,

3H), 5.33 (dd, J = 2.1 Hz, J_{HF} = 9.0 Hz, 1H), 6.36 (ddd, J = 2.1 Hz, J_{HF} = 9.0 Hz, J_{HF} = 11.5 Hz, 1H), 6.67 (dd, J_{HF} = 1.2 Hz, J = 5.8 Hz, 1H), 8.15 (s, 1H), 8.92 (d, J = 5.8 Hz, 1H); ^{19}F NMR ($CDCl_3$, 470 MHz) : δ -111.1 (t, J_{FC} = 9.9 Hz), -109.5 (dd, J_{FC} = 8.2 Hz, J_{FC} = 18.1 Hz); MS (MALDI-TOF) *m/z* (%): 1272.2 (M^+, 10), 636.2 (M^+/2, 100).

Tetrakis-(2-(2,4-Difluorophenyl)-4-methylpyridine-C^6,N')-(*p*-dichloro) diiridium; 88; [Ir(4CF$_3$ppy)$_2$Cl]$_2$.

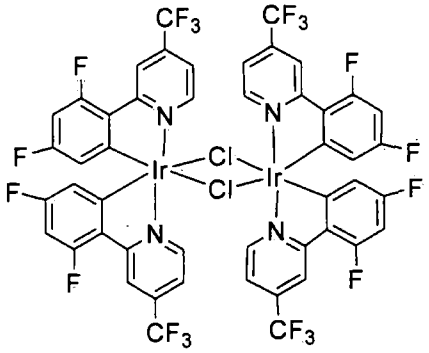

88 [(4CF$_3$ppy)$_2$IrCl]$_2$

Following the procedure for **86; [Ir(ppy)$_2$Cl]$_2$**, **4CF$_3$ppy** (0.51 g, 1.93 mmol), $IrCl_3.nH_2O$ (288 mg, 0.96 mmol), 2-ethoxyethanol (30 ml) and water (10 ml) were refluxed for 24 h. After cooling to room temperature, work-up as for **86; [Ir(ppy)$_2$Cl]$_2$** gave **88; [Ir(4CF$_3$ppy)$_2$Cl]$_2$** as a yellow powder (845 mg, 62%); ^{1}H NMR (CD_2Cl_2, 400 MHz): δ 5.28 (dd, J = 2.2 Hz, J_{HF} = 8.5 Hz, 1H), 6.45 (ddd, J = 2.2 Hz, J_{HF} = 9.1 Hz, J_{HF} = 12.5 Hz, 1H), 6.99 (dd, J = 2.0 Hz, J = 6.0 Hz, 1H), 8.55 (d, J = 2.0 Hz, 1H), 9.18 (d, J = 6.0 Hz, 1H); ^{19}F NMR (CD_2Cl_2, 376 MHz) : δ -108.9 (J_{FC} = 6.1Hz), δ -105.5 (dd, J_{FC} = 9 Hz, J_{FC} = 21.3 Hz), -65.8; MS (MALDI-TOF) *m/z* (%): 1488.0 (M^+, 5).

Tetrakis-(2-(2',4'-Difluorophenyl)-5-trifluoromethylpyridine-C$^{6'}$,N)-(*p*-dichloro) diiridium; 89; [Ir(5CF$_3$ppy)$_2$Cl]$_2$.[172]

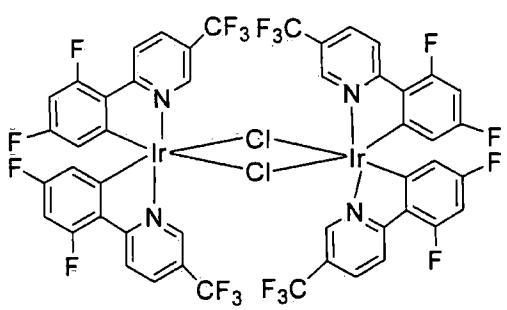

89 [(5CF$_3$ppy)$_2$IrCl]$_2$

Following the procedure for **86; [Ir(ppy)$_2$Cl]$_2$**, **5CF$_3$ppy** (1.23 g, 4.75 mmol), $IrCl_3.nH_2O$ (0.51 g, 1.58 mmol), 2-ethoxyethanol (30 ml) and water (10 ml) were refluxed for 24 h. After cooling to room temperature, work-up as for **86; [Ir(ppy)$_2$Cl]$_2$** gave **89; [Ir(5CF$_3$ppy)$_2$Cl]$_2$** as a yellow powder (1.76 g, 75%); Anal. calcd for $C_{48}H_{20}Cl_2F_{20}Ir_2N_4$; C, 38.74; H, 1.35; N, 3.77; Found: C, 38.64; H, 1.33; N, 3.69; ^{1}H NMR ($CDCl_3$, 500 MHz): δ 5.08 (dd, J = 2.1 Hz, J_{HF} = 9.0 Hz, 1H), 6.45 (td, J_{HF} = 12.2 Hz, J = 2.1 Hz, 1H), 8.06 (dd, J = 2.0 Hz, J = 8.8 Hz, 1H), 8.48 (dd, J_{HF} = 2.7 Hz, J = 8.8 Hz, 1H), 9.25 (d, J = 2.0 Hz, 1H); ^{13}C

NMR ($CDCl_3$, 125 MHz) : δ 99.2 (t, J_{CF} = 26.8 Hz), 112.6 (dd, J_{CF} = 2.9 Hz, J_{CF} = 19.2 Hz), 122.2 (q, J_{CF} = 272.3 Hz), 122.8 (d, J_{CF} = 20.1 Hz), 124.5 (q, J_{CF} = 34.5 Hz), 126.7 (dd, J_{CF} = 1.9 Hz, J_{CF} = 4.8 Hz), 136.0, 147.5, 148.1 (d, J_{CF} = 7.7 Hz), 161.5 (dd, J_{CF} = 13.4 Hz, J_{CF} = 261.7 Hz), 163.6 (dd, J_{CF} = 13.4 Hz, J_{CF} = 260.0 Hz), 169.0 (d, J_{CF} = 6.7 Hz); ^{19}F NMR ($CDCl_3$, 470 MHz) : δ -108.0 (t, J_{FC} = 11.5 Hz), -105.5 (dd, J_{FC} = 9.5 Hz, J_{FC} = 19.8 Hz), -62.4. MS (MALDI-TOF) *m/z* (%): 1487.9 (M^+, 5), 744.0 ($M^+/2$, 100). Crystals of **89; [Ir(5CF$_3$ppy)$_2$Cl]$_2$** for X-ray analysis were grown from slowly evaporated CD_2Cl_2 in an NMR tube; *Crystal data*: $C_{48}H_{20}Cl_2F_{20}Ir_2N_4.CD_2Cl_2$, *M*= 1574.92, monoclinic ($P2_1/n$), *a*=10.7904(10), *b*=22.406(2), *c*=20.3259(17) Å, α =90.00, β=90.74(2), γ=90.00°, *V*=4913.7(8) Å^3, Z=4.

Tetrakis-(2-phenylquinoline-C$^{2'}$,N)-(*p*-dichloro)diiridium; 90; [Ir(pq)$_2$Cl]$_2$.[177]

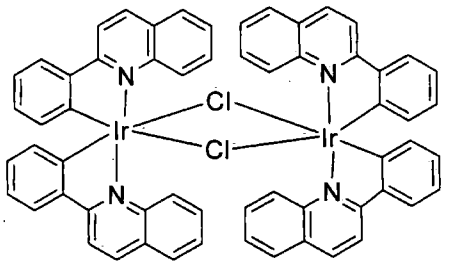

90 [(bq)$_2$IrCl]$_2$

Following the procedure for **86; [Ir(ppy)$_2$Cl]$_2$**, 2-phenylquinoline (0.41 g, 2.0 mmol), $IrCl_3.nH_2O$ (0.3 g, 0.95 mmol), 2-ethoxyethanol (30 ml) and water (10 ml) were refluxed for 24 h. After cooling to room temperature, work-up as for **86; [Ir(ppy)$_2$Cl]$_2$** gave **90; [Ir(pq)$_2$Cl]$_2$** as a red powder (0.72 g, 60%); ^{1}H NMR (200 MHz, $CDCl_3$): δ 6.28 (d, *J* = 8.0 Hz , 1H), 6.57 (d, *J* = 7.4 Hz, 1H), 6.93 (t, *J* = 7.8 Hz, 1H), 7.58-7.63 (m, 2H), 7.81 (d, 7.8 Hz, 1H), 7.92, (d, 8.5 Hz, 1H), 8.11 (d, 8.9 Hz, 1H), 8.32 (d, 8.9 Hz, 1H), 8.56 (d, *J* = 8.5 Hz, 1H); MS (MALDI-TOF) *m/z* (%): 1096.0 (M^+/2-Cl, 100).

Tetrakis-(2-(thiophen-2'-yl)-pyridine-C$^{5'}$,N)-(*p*-dichloro) diiridium; 91; [Ir(thpy)$_2$Cl]$_2$.[178]

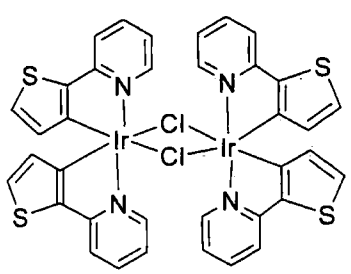

91 [(thpy)$_2$IrCl]$_2$

Following the procedure for **86; [Ir(ppy)$_2$Cl]$_2$**, 2-(2'-thienyl)pyridine (0.54 g, 3.35 mmol), $IrCl_3.nH_2O$ (0.5 g, 157 mmol), 2-ethoxyethanol (30 ml) and water (10 ml) were refluxed for 24 h. After cooling to room temperature, work-up as for **86; [Ir(ppy)$_2$Cl]$_2$** gave **91; [Ir(thpy)$_2$Cl]$_2$** as an orange powder (0.97 g, 56%); ^{1}H NMR (CD_2Cl_2, 400

MHz): δ 5.90 (d, J = 4.5 Hz, 1H), 6.67 (ddd, J = 1.5 Hz, J = 7.0 Hz, J = 8.0 Hz, 1H), 7.12 (d, J = 4.5 Hz, 1H), 7.57 (dd, J = 1.5 Hz, J = 8.0 Hz, 1H), 7.68 (td, J = Hz 8.0, J =1.5 Hz, 1H), 9.00 (dd, J = 1.5 Hz, J = 7.0 Hz, 1H); ^{13}C NMR (CD_2Cl_2, 100 MHz): δ 117.7, 119.9, 128.0, 129.6, 135.6, 137.6, 145.4, 151.9, 165.0; MS (MALDI-TOF) *m/z* (%): 1096.0 (M^+, 50), 548.0 ($M^+/2$, 100).

Tetrakis-(1-(2',4'-Difluoro-phenyl)-1*H*-pyrazole-C$^{6'}$,N^{2})-(*p*-dichloro) diiridium; 92; [Ir(Fppz)$_2$Cl]$_2$.

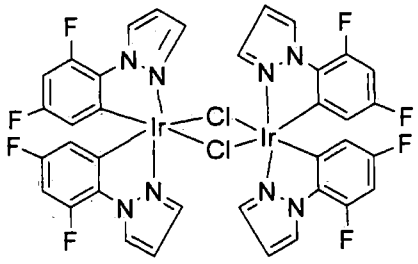

92 [(Fppz)$_2$IrCl]$_2$

Following the procedure for **86; [Ir(ppy)$_2$Cl]$_2$**, **Fppz** (1.0 g, 5.55 mmol), $IrCl_3.nH_2O$ (0.79 g, 2.49 mmol), 2-ethoxyethanol (30 ml) and water (10 ml) were refluxed for 24 h. After cooling to room temperature, work-up as for **86; [Ir(ppy)$_2$Cl]$_2$** gave **92; [Ir(Fppz)$_2$Cl]$_2$** as a white powder (1.7 g, 58%); ^{1}H NMR (CD_2Cl_2, 400 MHz): δ 5.38 (dd, J = 2.4 Hz, J_{HF} = 8.5 Hz, 1H), 6.65 (ddd, J = 2.4 Hz, J_{HF} = 8.8 Hz, J_{HF} = 12.0 Hz, 1H), 6.75 (t, J = 2.5 Hz, 1H), 7.76 (d, J = 2.4 Hz, 1H), 8.46 (d, J = 2.5 Hz, 1H); ^{19}F NMR (CD_2Cl_2, 376 MHz) : δ -125.7 (dd, J_{FC} = 6.1 Hz, J_{FC} = 12.2 Hz), δ -114.7 (dd, J_{FC} = 6.1 Hz, J_{FC} = 12.2 Hz); MS (MALDI-TOF) *m/z* (%): 1172.0 (M^+, 5), 586.0 ($M^+/2$, 100).

{(Phenanthroline-N-N')-bis-(2-phenylpyridine-C$^{2'}$,N)-iridium(III)} hexafluorophosphate; 94; OLED 1.[152,179,183]

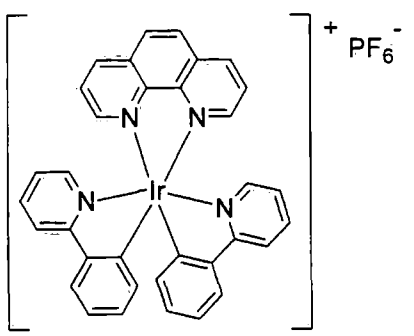

94 (OLED 1)

A solution of phenanthroline (36 mg, 0.2 mmol), and **86; [Ir(ppy)$_2$Cl]$_2$** (107 mg, 0.1 mmol) in dichloromethane (10 ml) and methanol (10 ml) was refluxed for 24 h in the dark. After cooling to room temperature, KPF_6 (0.4 g) was added and the mixture was stirred for 1 h at room temperature. The excess salt was removed by filtration, then solvent was removed under reduced pressure. The residue was purified by column chromatography (SiO_2, eluent DCM) to give **94; OLED 1** as a yellow powder (67 mg, 81%); ^{1}H NMR

(400 MHz, CD_2Cl_2): δ 6.42 (dd, J = 1.5 Hz, 7.5 Hz , 1H), 6.84 (td, J = 7.5 Hz, 1.5 Hz, 1H), 7.00 (td, J = 1.5 Hz, 7.5 Hz, 1H), 7.12 (td, J = 7.5 Hz, 1.5 Hz , 1H), 7.32 (dd, J = 1.5 Hz, 7.5 Hz, 1H), 7.73 (td, J = 7.5 Hz, 1.5 Hz, 1H), 7.83 (dd, J = 1.5 Hz, 7.5 Hz, 1H), 7.78 (dd, J = 5.0 Hz, J = 8.1 Hz , 1H), 7.96, (dd, J = 1.5 Hz, 7.5 Hz, 1H), 8.21 (s, 1H), 8.34 (dd, J = 1.5 Hz, J = 5.0 Hz, 1H), 8.63 (dd, J = 1.5 Hz, J = 8.1 Hz, 1H); ^{13}C NMR (100 MHz, $CDCl_3$): δ 120.2, 123.2, 123.5, 125.3, 127.0, 128.9, 131.1, 131.9, 132.2, 138.6, 138.9, 144.3, 147.2, 148.9, 151.5, 168.2; MS (ES+) *m/z* (%) 681.3 (M^+-PF_6, 100).

Hexakis-[2-(2',4'-difluorophenyl)-5-trifluoromethylpyridine–$C^{6'}$,N]-iridium (III); 93; OLED 12.

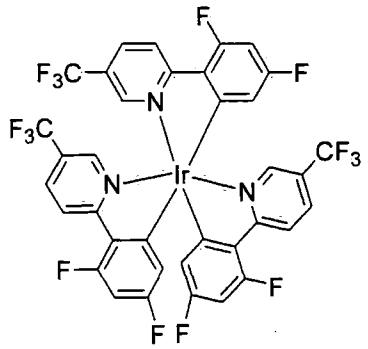

93 (OLED 12)

Following the procedure for **94; OLED 1**, **2,9-diMephen** (42 mg, 0.2 mmol), **89; $[Ir(5CF_3ppy)_2Cl]_2$** (150 mg, 0.1 mmol), dichloromethane (15 ml) and methanol (15 ml) were refluxed for 24 h in the dark. After cooling to room temperature, KPF_6 (0.4 g) was added and stirred for 1 h at room temperature. Work-up as for **94; OLED 1** and column chromatography (SiO_2, eluent DCM) gave **93; OLED 12** as a yellow powder (54 mg, 56%); ^1H NMR ($CDCl_3$, 200 MHz): δ 5.06 (dd, J = 2.0 Hz, J_{HF} = 9.0 Hz, 1H), 6.42 (ddd, J = 2.0 Hz, J_{HF} = 9.0 Hz, J_{HF} = 12.0 Hz, 1H), 8.04 (dd, J = 1.5 Hz, J = 8.5 Hz, 1H), 8.46 (dd, J_{HF} = 2.7 Hz, J = 8.5 Hz, 1H), 9.50 (d, J = 1.5 Hz, 1H). MS (MALDI-TOF) *m/z* (%): 967.1 (M^+, 5).

{(2,9-Dimethylphenanthroline-N-N')-bis-(2-phenylpyridine $C^{2'}$,N)-iridium(III)} hexafluorophosphate; 95; OLED 2.[21]

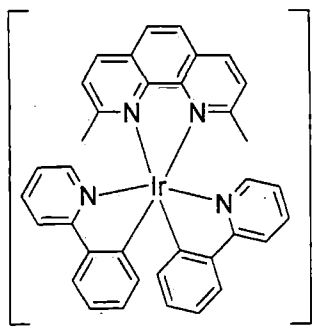

95 (OLED 2)

Following the procedure for **94; OLED 1**, 2,9-dimethylphenanthroline (117 mg, 0.56 mmol), **86; $[Ir(ppy)_2Cl]_2$** (300 mg, 0.28 mmol), dichloromethane (10 ml) and methanol (10 ml) were refluxed for 24 h in the dark. After cooling to room temperature, KPF_6 (0.4 g) was added and stirred for 1 h at room temperature. Work-up as for **94; OLED 1** and column

chromatography (SiO_2, eluent DCM) gave **95; OLED 2** as a yellow powder (179 mg, 75%); Anal. calcd for $C_{36}H_{28}F_6IrN_4P$; C, 50.64; H, 3.31; N, 6.56; Found: C, 50.37; H, 3.35; N, 6.40; ^{1}H NMR (700 MHz, $CDCl_3$): δ 2.13 (s, 3H), 6.11 (d, J = 7.5.0 Hz , 1H), 6.77 (d, J = 6.9 Hz 1H), 6.90-6.93 (m, 2H), 7.46 (d, J = 5.6 Hz, 1H), 7.61-7.63 (m , 2H), 7.73 (d, J = 7.7 Hz, 1H), 7.90 (d, J = 8.3 Hz, 1H), 8.02 (s, 1H), 8.47 (d, J = 8.3 Hz, 1H); ^{13}C NMR (175 MHz, $CDCl_3$): δ 27.8, 119.7, 122.5, 123.1, 124.8, 127.6, 128.2, 130.1, 130.5, 138.2, 139.5, 142.9, 148.0, 148.9, 165.0, 168.0; ^{19}F NMR (376 MHz, $CDCl_3$): δ -74.1, -73.0. MS (ES+) *m/z* (%) 709.3 (M^+-PF_6, 100). Crystals of **95; OLED 2** for X-ray analysis were grown from slowly evaporated $CDCl_3$ in an NMR tube; *Crystal data*: $C_{36}H_{28}IrN_4PF_6.2CDCl_3$, M= 1094.54, monoclinic ($P2_1/c$), a=12.0642(12), b=10.5616(11), c=31.526(3) Å, α=90.00, β=90.662(10), γ=90.00°, V=4016.7(7) Å^3, Z=4.

{(3,8-Bis[(9',9'-dihexylfluorenyl)]-phenanthroline-N-N')-bis-(2-phenylpyridine $C^{2'}$,N)-iridium(III)} hexafluorophosphate; 96; OLED 3.[153]

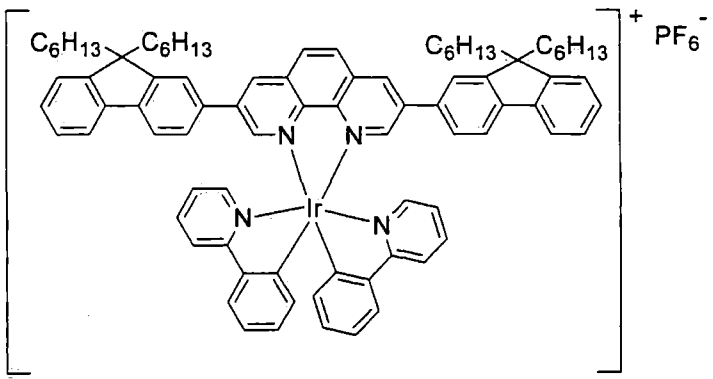

96 (OLED 3)

Following the procedure for **94; OLED 1, 66; FluPhen** (0.43 g, 0.50 mmol), **86; $[Ir(ppy)_2Cl]_2$** (0.27 g, 0.25 mmol), dichloromethane (30 ml) and methanol (30 ml) were refluxed for 24 h in the dark. After cooling to room temperature, KPF_6 (0.4 g) was added and stirred for 1 h at room temperature. Work-up as for **94; OLED 1** and column chromatography (SiO_2, eluent DCM/acetone, 100:3 v/v to 100:5) gave **96; OLED 3** as a orange-yellow powder (285 mg, 76%). mp 174-175 °C. Anal. calcd for $C_{84}H_{88}F_6IrN_4P$: C, 67.67; H, 5.95; N, 3.76; Found: C, 67.74; H, 5.95; N, 3.71. ^{1}H NMR (400 MHz, $CDCl_3$): δ 0.59-0.54 (m, 4H), 0.74 (t, J = 7.6 Hz, 6H), 1.16-0.99 (m, 12H), 2.08-1.92 (m, 4H), 6.56 (d, J = 7.6 Hz, 1H), 6.98 (td, J = 7.6 Hz, 1.2 Hz, 1H), 7.02 (td, J = 7.6 Hz, 1.2 Hz, 1H), 7.15 (td, J = 7.6 Hz, 0.8 Hz, 1H), 7.37-7.32 (m, 4H), 7.55 (dd, J = 7.4 Hz, 0.8 Hz, 1H), 7.61 (dd, J = 2.0 Hz , 8.0 Hz, 1H), 7.84-7.71 (m, 4H), 7.98 (d, J = 8.0 Hz, 1H), 8.33 (s, 1H), 8.53 (d, J = 2.0 Hz, 1H), 8.87 (d, J = 2.0 Hz,

1H); ^{13}C NMR (100 MHz, $CDCl_3$): δ, 14.0. , 22.6, 23.8, 29.7, 31.5, 40.3, 55.4, 119.7, 120.3, 120.9, 121.1, 123.1, 123.6, 124.7, 126.4, 127.0, 128.0, 129.4, 130.9, 131.6, 132.2, 133.32, 135.0, 138.4, 139.4, 139.9, 143.0, 144.0, 145.2, 148.9, 149.1, 149.9, 151.2, 152.3, 167.9; ^{19}F NMR (376 MHz, $CDCl_3$): δ -74.5, -72.6; MS (MALDI-TOF): *m/z* (%) 1345.6 (M^+-PF_6, 100). Crystals of **96; OLED 3** for X-ray analysis were grown from slowly evaporated CH_2Cl_2; *Crystal data*: $C_{84}H_{90}IrN_4PF_6.CH_2Cl_2$, *M*= 1577.70, triclinic ($P\bar{1}$), *a*=11.1499(6), *b*=16.8726(9), *c*=22.0126(13)Å, α =68.982(9), β=75.369(8), γ=73.785(12)°, *V*=3657.8(4) $Å^3$, Z=2.

{(3,8-Bis[(9',9'-dihexylfluorenyl)]-phenanthroline-N-N')-bis-(2-phenylpyridine C^2,N')-iridium(III)} tetrafluoroborate; 97; OLED 3-BF_4.

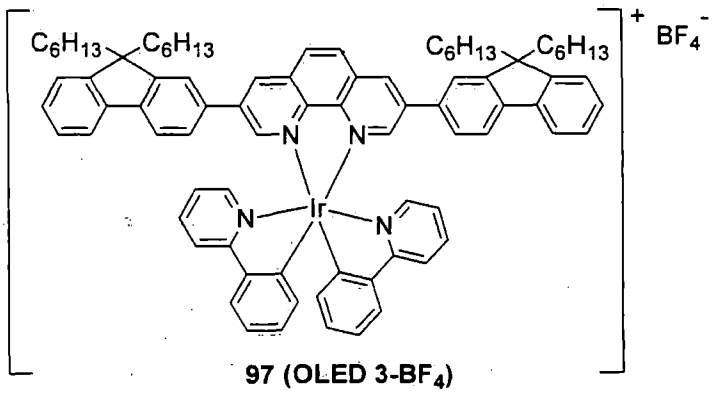

97 (OLED 3-BF_4)

Following the procedure for **94; OLED 1**, **66; FluPhen** ligand (0.43 g, 0.50 mmol), **86; $[Ir(ppy)_2Cl]_2$** (0.27 g, 0.25 mmol), dichloromethane (30 ml) and methanol (30 ml) were refluxed for 24 h in the dark. After cooling to room temperature, KBF_4 (1 g) was added and stirred for 1 h at room temperature. Work-up as for **94; OLED 1** and column chromatography (SiO_2, eluent DCM) gave **97; OLED 3-BF_4** as a yellow powder (274 mg, 76%); ^1H NMR (400 MHz, $CDCl_3$): δ 0.52-0.59 (m, 4H), 0.72 (t, *J* = 6.7 Hz, 6H), 1.01-1.10 (m, 12H), 1.87-2.04 (m, 4H), 6.53 (d, *J* = 7.6 Hz, 1H), 6.99 (t, *J* = 7.6 Hz, 1H), 7.01 (t, *J* = 7.6 Hz, 1H), 7.13 (t, *J* = 7.6 Hz, 1H), 7.32-7.37 (m, 4H), 7.49 (d, *J* = 6.1 Hz, 1H), 7.63 (d, *J* = 7.9 Hz, 1H), 7.69-7.81 (m, 4H), 7.96 (d, *J* = 8.2 Hz, 1H), 8.49 (s, 1H), 8.53 (s, 1H), 9.06 (s, 1H). ^{19}F NMR (376 MHz, $CDCl_3$): δ -153.8. MS (ES+): *m/z* (%) 1345.6 (M^+-BF_4, 100).

{(3,8-Bis[(9',9'-dihexylfluorenyl)]-phenanthroline-N-N')-bis-(2-(2',4'-difluorophenyl)-4-methylpyridine $C^{6'}$,N)-iridium(III)} hexafluorophosphate; 98; OLED 4.

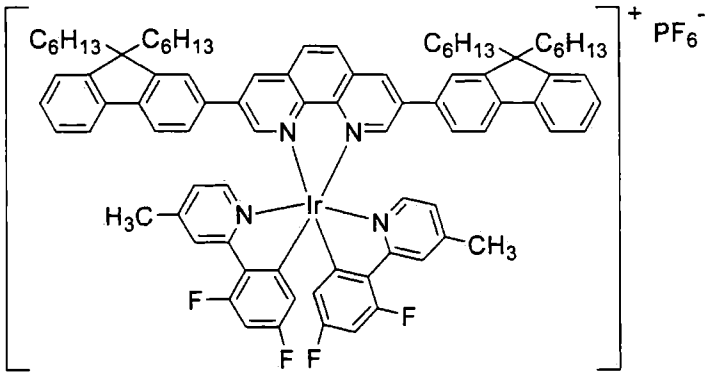

98 (OLED 4)

Following the procedure for **94; OLED 1**, **66; FluPhen** ligand (400 mg, 0.47 mmol), **$[Ir(4Meppy)_2Cl]_2$** (300 mg, 0.23 mmol), dichloromethane (10 ml) and methanol (10 ml) were refluxed for 24 h in the dark. After cooling to room temperature, KPF_6 (0.4 g) was added and stirred for 1 h at room temperature. Work-up as for **94; OLED 1** and column chromatography (SiO_2, eluent DCM) gave **98; OLED 4** as a yellow powder (281 mg, 75%); ^{1}H NMR (700 MHz, $CDCl_3$): δ 0.52-0.62 (m, 4H), 0.74-0.76 (t, , J = 8.0 Hz, 6H), 1.01-1.13 (m, 12H), 1.95-2.07 (m, 4H), 2.49 (s, 3H), 5.96 (dd, J = 2.4 Hz, J_{HF} = 8.2 Hz , 1H), 6.66 (dt, J = 2.4 Hz, J_{HF} = 11.3 Hz 1H), 7.84 (d, J = 6.2 Hz, 1H), 7.35-7.38 (m, 4H), 7.41, (s, 1H), 7.60 (d, J = 7.9 Hz, 1H), 7.75 (t, J = 4.1 Hz , 1H), 7.83 (d, J = 7.6 Hz, 1H), 8.17 (s, 1H), 8.36 (s, 1H), 8.49 (d, J = 1.3 Hz, 1H), 8.90 (d, J = 1.3 Hz, 1H); ^{13}C NMR (175 MHz, $CDCl_3$): δ 14.2, 21.8, 22.7, 22.8, 24.0, 24.1, 29.9, 31.7, 31.8, 40.4, 40.5, 55.6, 99.4, 114.7, 120.6, 121.2, 121.5, 123.3, 124.7, 124.8, 125.2, 126.7, 127.3, 128.1, 128.3, 129.8, 131.9, 133.4, 136.0, 139.9, 140.0, 142.3, 154.1, 148.5, 148.8, 151.3, 151.6, 152.7, 153.7, 161.5, 165.5, 164.6; MS (ES+) *m/z* (%) 1445.7 (M^+-PF_6, 100).

{(3,8-Bis[(9',9'-dihexylfluorenyl)]-phenanthroline-N-N')-bis-(2-(2',4'-difluorophenyl)-5-trifluoromethylpyridine $C^{6'}$,N)-iridium(III)} hexafluorophosphate; 99; OLED 5.

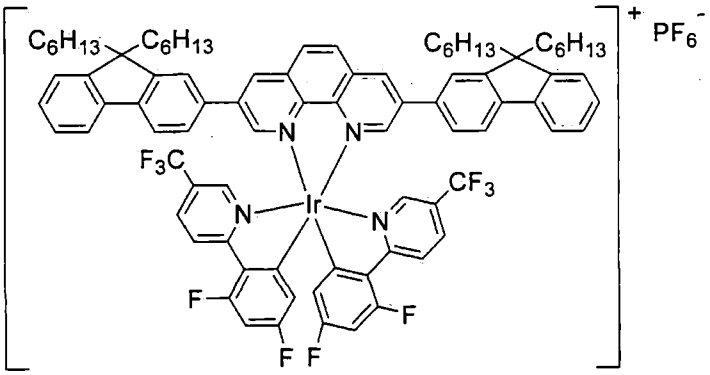

99 (OLED 5)

Following the procedure for **94; OLED 1**, **66; FluPhen**

ligand (250 mg, 0.28 mmol), **89; [Ir(5CF$_3$ppy)$_2$Cl]$_2$** (212 mg, 0.0.14 mmol), dichloromethane (15 ml) and methanol (15 ml) were refluxed for 24 h in the dark. After cooling to room temperature, KPF_6 (0.4 g) was added and stirred for 1 h at room temperature. Work-up as for **94; OLED 1** and column chromatography (SiO_2, eluent DCM) gave **99; OLED 5** as a yellow powder (184 mg, 76%); Anal. calcd for $C_{86}H_{82}F_{16}IrN_4P$; C, 60.80; H, 4.87; N, 3.30; Found: C, 61.14; H, 4.89; N, 3.34; ^{1}H NMR (400 MHz, $CDCl_3$): δ 0.59-0.62 (m, 4H), 0.71-0.77 (m, 6H), 1.00-1.14 (m, 12H), 1.95-2.08 (m, 4H), 5.87 (dd, J = 2.0 Hz, J_{HF} = 8.0 Hz , 1H), 6.74 (ddd, J = 2.0 Hz, J_{HF} = 8.6 Hz , J_{HF} = 13.0 Hz 1H), 7.36-7.39 (m, 3H), 7.48 (d, J = 2.0 Hz, 1H), 7.55 (dd, J = 2.0 Hz, 8.0 Hz , 1H), 7.62 (s, 1H), 7.75 (m, 1H), 7.85 (d, J = 8.0 Hz, 1H), 8.06 (dd, J = 1.5 Hz, 9.0 Hz , 1H), 8.51 (d, J = 2.0 Hz, 1H), 8.53 (s, 1H), 8.55 (dd, J = 3.0 Hz, 9.0 Hz , 1H), 9.09 (d, J = 2.0 Hz, 1H); ^{13}C NMR (125 MHz, $CDCl_3$): δ 13.9, 14.0, 22.5, 22.6, 23.8, 29.6, 29.7, 31.4, 31.5, 40.2, 40.3, 55.4, 100.2, 114.3, 120.2 120.4, 121.4, 122.4, 123.0, 123.7, 126.3, 126.6, 127.1, 128.2, 130.1, 132.0, 132.7, 136.7, 137.0, 139.5, 140.4, 143.4, 145.0, 148.8, 151.1, 152.7, 153.9, 162.4, 164.5, 167.8; ^{19}F NMR (376 MHz, $CDCl_3$): δ -106.1 (t, J_{FC} = 12.2 Hz), -101.3 (dd, J_{FC} = 9.1 Hz, J_{FC} = 21.4 Hz), -74.4, -72.4, -63.2; MS (ES+) *m/z* (%) 1553.6 (M^+-PF_6, 100); MS (ES-) *m/z* (%) 145.0 (PF_6, 100).

{(3,8-Bis[(9',9'-dihexylfluorenyl)]-phenanthroline-N-N')-bis-(2-(2',4'-difluorophenyl)-5-trifluoromethylpyridine C$^{6'}$,N)-iridium(III)} tetrafluoroborate; 100; OLED 6.

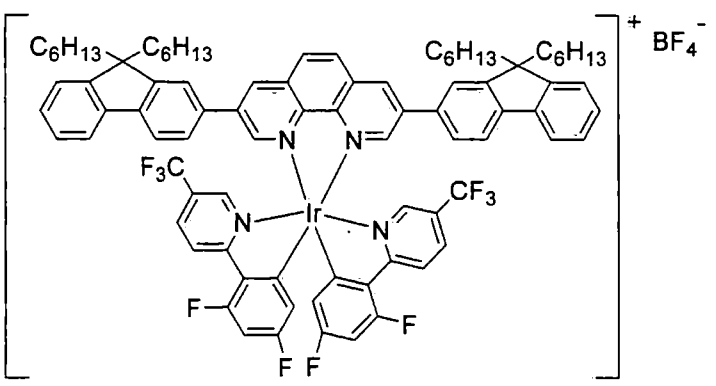

100 (OLED 6)

Following the procedure for **94; OLED 1**, **66; FluPhen** ligand (250 mg, 0.28 mmol), **89; [Ir(5CF$_3$ppy)$_2$Cl]$_2$** (212 mg, 0.0.14 mmol), dichloromethane (15 ml) and methanol (15 ml) were refluxed for 24 h in the dark. After cooling to room temperature, KBF_4 (0.4 g) was added and stirred for 1 h at room temperature. Work-up as for **94; OLED 1** and column chromatography (SiO_2, eluent DCM)gave **100; OLED 6** as a yellow powder (175 mg,

75%); ^{1}H NMR (400 MHz, $CDCl_3$): δ 0.59-0.62 (m, 4H), 0.70-0.77 (m, 6H), 1.00-1.10 (m, 12H), 1.96-2.08 (m, 4H), 5.88 (dd, J = 2.0 Hz, J_{HF} = 7.6 Hz , 1H), 6.74 (ddd, J = 2.0 Hz, J_{HF1} = 8.6 Hz , J_{HF2} = 12.5 Hz 1H), 7.36-7.39 (m, 3H), 7.47 (d, J = 1.0 Hz, 1H), 7.62 (dd, J = 1.5 Hz, 8.0 Hz , 1H), 7.64 (s, 1H), 7.75 (m, 1H), 7.89 (d, J = 8.0 Hz, 1H), 8.06 (dd, J = 1.5 Hz, 8.6 Hz , 1H), 8.50 (d, J = 2.0 Hz, 1H), 8.54 (dd, J = 3.0 Hz, 9.0 Hz , 1H), 8.60 (s, 1H), 9.16 (d, J = 2.0 Hz, 1H). ^{13}C NMR (125 MHz, $CDCl_3$): δ 14.0, 14.1, 22.6, 22.7, 23.9, 29.8, 29.9, 31.5, 31.6, 40.4, 40.5, 55.6, 100.4, 114.4, 120.5, 121.3, 121.6, 122.7, 123.3, 124.0, 126.4, 126.9, 127.3, 128.4, 130.5, 132.4, 133.0, 137.0, 137.4, 139.8, 140.6, 143.6, 144.7, 145.4, 148.9, 151.4, 152.9, 154.3, 162.5, 165.05, 168.2. ^{19}F NMR (376 MHz, $CDCl_3$): δ -153.1, -106.1 (t, J_{FC} = 12.2 Hz), -101.3 (dd, J_{FC} = 9.1 Hz, J_{FC} = 21.4 Hz), -63.2. MS (ES+) *m/z* (%) 1553.6 (M^+-BF_4, 100); MS (ES-) *m/z* (%) 86.9 (BF_4, 100).

{(Phenanthroline-N-N')-bis-(2-(2',4'-difluorophenyl)-5-trifluoromethylpyridine $C^{6'}$,N)-iridium(III)} hexafluorophosphate; 101; OLED 7.

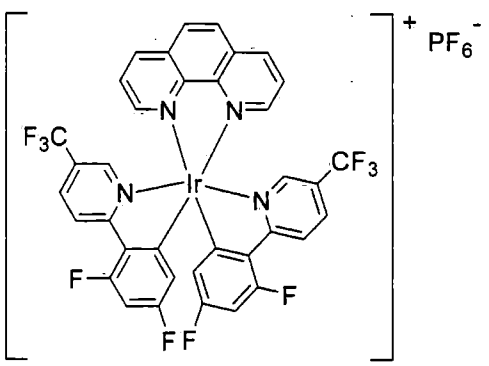

101 (OLED 7)

Following the procedure for **94; OLED 1**, phenanthroline (127 mg, 0.7 mmol), **89; $[Ir(5CF_3ppy)_2Cl]_2$** (500 mg, 0.34 mmol), dichloromethane (15 ml) and methanol (15 ml) were refluxed for 24 h in the dark. After cooling to room temperature, KPF_6 (1 g) was added and stirred for 1 h at room temperature. Work-up as for **94; OLED 1** and column chromatography (SiO_2, eluent DCM) gave **101; OLED 7** as a yellow powder (277 mg, 80%); Anal. calcd for $C_{36}H_{18}F_{16}IrN_4P$; C, 41.83; H, 1.76; N, 5.42; Found: C, 41.62; H, 1.86; N, 5.09; ^{1}H NMR (CD_2Cl_2, 400 MHz): δ 5.83(dd, J = 2.4 Hz, J_{HF} = 8.2 Hz, 1H), 6.75 (ddd, J = 2.4 Hz, J_{HF} = 9.1 Hz, J_{HF} = 12.5 Hz, 1H), 7.40 (d, J = 2.1 Hz, 1H), 8.00 (dd, J = 5.2 Hz, J = 8.2 Hz, 1H), 8.03 (dd, J = 2.1 Hz, J = 8.8 Hz, 1H), 8.30 (s, 1H), 8.39 (dd, J = Hz 1.5, J = 5.2 Hz, 1H), 8.51 (dd, J_{HF} = 3.3 Hz, J = 8.8 Hz, 1H), 8.79 (dd, J = 1.5 Hz, J = 8.2 Hz, 1H). ^{13}C NMR (CD_2Cl_2, 125 MHz) : δ 100.0 (t, J_{CF} = 26.8 Hz), 114.3 (dd, J_{CF} = 2.8 Hz, J_{CF} = 18.2 Hz), 121.3 (q, J_{CF} = 272.3 Hz), 123.8 (d, J_{CF} = 21.1 Hz), 125.7 (q, J_{CF} =

34.5 Hz), 126.5, 127.2, 128.9, 131.8, 136.6, 140.0, 144.4 (d, J_{CF} = 4.8 Hz), 145.9, 151.3, 153.0 (d, J_{CF} = 7.7 Hz), 162.5 (dd, J_{CF} = 12.5 Hz, J_{CF} = 262.7 Hz), 164.8.7 (dd, J_{CF} = 13.4 Hz, J_{CF} = 260.8 Hz), 167.8 (d, J_{CF} = 6.7 Hz); ^{19}F NMR (CD_2Cl_2, 376 MHz): δ -153.2, -106.5 (t, J_{FC} = 12.2 Hz), -102.8 (dd, J_{FC1} = 12.2 Hz, J_{FC2} = 21.3 Hz), -63.7. ^{19}F NMR (CD_2Cl_2, 376 MHz): δ -106.5 (t, J_{CF} = 12.2 Hz), -102.8 (t, J_{CF} = 9.1 Hz), -74.6, -72.8, -63.7; MS (ES+) *m/z* (%): 889.2 (M^+- PF_6, 100); MS (ES–) *m/z* (%): 145.1 (PF_6, 100). Crystals of **101 (OLED 3)** for X-ray analysis were grown from slowly evaporated CH_2Cl_2. The crystals were found to have the chloride counterion.

{(Phenanthroline-N-N')-bis-(2-(2',4'-difluorophenyl)-5-trifluoromethylpyridine $C^{6'}$,N)-iridium(III)} tetrafluoroborate; 102; OLED 8.

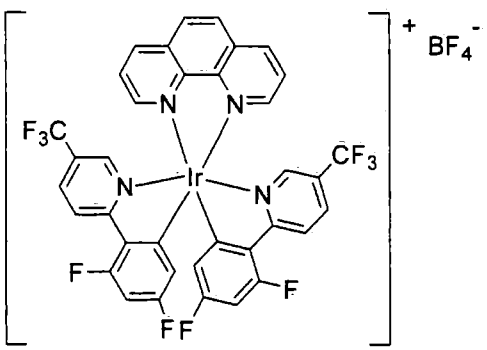

102 (OLED 8)

Following the procedure for **94; OLED 1**, phenanthroline (127 mg, 0.7 mmol), **89; $[Ir(5CF_3ppy)_2Cl]_2$** (500 mg, 0.34 mmol), dichloromethane (15 ml) and methanol (15 ml) were refluxed for 24 h in the dark. After cooling to room temperature, KBF_4 (1 g) was added and stirred for 1 h at room temperature. Work-up as for **94; OLED 1** and column chromatography (SiO_2, eluent DCM) gave **102; OLED 8** as a yellow powder (160 mg, 50%); ^{1}H NMR (CD_2Cl_2, 400 MHz): δ 5.84 (dd, *J* = 2.4 Hz, J_{HF} = 8.0 Hz, 1H), 6.75 (ddd, *J* = 2.4 Hz, J_{HF} = 9.0 Hz, J_{HF} = 12.6 Hz, 1H), 7.42 (d, *J* = 1.5 Hz, 1H), 8.03 (dd, *J* = 1.5 Hz, *J* = 9.0 Hz, 1H), 8.06 (dd, *J* = 5.0 Hz, *J* = 8.1 Hz, 1H), 8.37 (dd, *J* = 1.5 Hz, *J* = 5.0 Hz, 1H), 8.44 (s, 1H), 8.50 (dd, J_{HF} = 3.5 Hz, *J* = 9.1 Hz, 1H), 9.00 (dd, *J* = 1.5 Hz, *J* = 8.1 Hz, 1H); ^{13}C NMR (CD_2Cl_2, 125 MHz) : δ 101.9 (t, J_{CF} = 26.8 Hz), 116.4 (dd, J_{CF} = 2.8 Hz, J_{CF} = 17.2 Hz), 120.2 (q, J_{CF} = 272.3 Hz), 125.8(d, J_{CF} = 21.1 Hz), 127.7 (q, J_{CF} = 35.5 Hz), 128.5 (d, J_{CF} = 3.8 Hz), 129.3, 131.1, 133.9, 138.6, 142.4, 146.8 (d, J_{CF} = 4.8 Hz), 147.9, 155.2 (d, J_{CF} = 6.7 Hz), 164.5 (dd, J_{CF} = 13.4 Hz, J_{CF} = 263.7 Hz), 166.7 (dd, J_{CF} = 13.4 Hz, J_{CF2} = 261.8 Hz), 169.8 (d, J_{CF} = 6.7 Hz); ^{19}F NMR (CD_2Cl_2, 376 MHz): δ -153.2, -106.5 (t, J_{FC} = 12.2 Hz), -102.8 (dd, J_{FC} = 12.2 Hz, J_{FC} = 21.3 Hz), -63.7; MS (ES+) *m/z* (%): 889.2 (M^+- BF_4, 100). MS (ES–) *m/z* (%): 87.0 (BF_4, 40).

{(Phenanthroline-N-N')-bis-(2-thiophen-2'-yl-pyridine $C^{5'}$,N)-iridium(III)} hexafluorophosphate; 103; OLED 9.

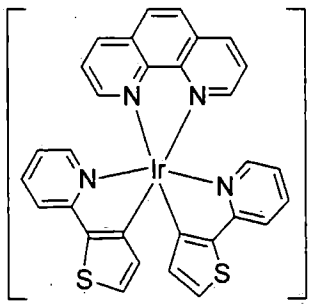

103 (OLED 9)

Following the procedure for **94; OLED 1**, phenanthroline (170 mg, 0.96 mmol), **91; $[Ir(thpy)_2Cl]_2$** (500 mg, 0.46 mmol), dichloromethane (15 ml) and methanol (15 ml) were refluxed for 24 h in the dark. After cooling to room temperature, KPF_6 (1 g) was added and stirred for 1 h at room temperature. Work-up as for **94; OLED 1** and column chromatography (SiO_2, eluent DCM) gave **103; OLED 9** as a orange powder (286 mg, 75%); Anal. calcd for $C_{30}H_{20}F_6IrN_4PS_2$; C, 43.01; H, 2.41; N, 6.69; Found: C, 43.17; H, 2.73; N, 6.47; ^{1}H NMR (CD_2Cl_2, 400 MHz): δ 6.41 (d, J = 5.0 Hz, 1H), 6.67 (t, J = 6.0 Hz, 1H), 7.24 (d, J = 6.0 Hz, 1H), 7.51 (d, J = 5.0 Hz, 1H), 7.58 (d, J = 6.0 Hz, 1H), 7.69 (t, J = 6.0 Hz, 1H), 7.87 (dd, J = 5.0 Hz, J = 8.5 Hz, 1H), 8.21 (s, 1 H), 8.29 (dd, J = 1.5 Hz, J = 5.0 Hz, 1H), 8.64 (dd, J = 1.5 Hz, J = 8.5 Hz, 1H); ^{13}C NMR (CD_2Cl_2, 100 MHz): δ 118.9, 120.7, 127.1, 128.8, 130.8, 131.0, 131.9, 137.6, 139.0, 139.1, 147.4, 149.3, 151.6, 152.1, 164.5; MS (ES+) *m/z* (%): 693.2 (M^+- PF_6, 100).

{(Phenanthroline-N-N')-bis-(2-phenylquinoline $C^{2'}$,N)-iridium(III)} hexafluorophosphate; 104; OLED 10.[21]

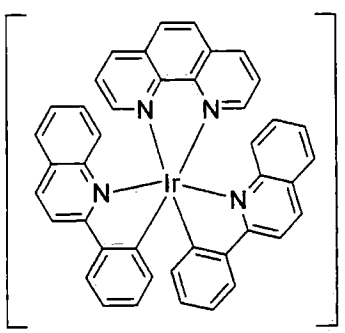

104 (OLED 10)

Following the procedure for **94; OLED 1**, phenanthroline (60 mg, 0.33 mmol), **90; $[Ir(bq)_2Cl]_2$** (200 mg, 0.16 mmol), dichloromethane (15 ml) and methanol (15 ml) were refluxed for 24 h in the dark. After cooling to room temperature, KPF_6 (0.5 g) was added and stirred for 1 h at room temperature. Work-up as for **94; OLED 1** and column chromatography (SiO_2, eluent DCM) gave **104; OLED 10** as a yellow powder (95 mg, 65%); ^{1}H NMR (CD_2Cl_2, 400 MHz): δ 6.61 (dd, J = 1.0 Hz, 7.5 Hz, 1H), 6.71 (ddd, J = 1.0 Hz, 6.5 Hz, 8.0 Hz, 1H), 6.84 (dd, J = 1.0 Hz, 7.5 Hz, 1H), 7.11-7.22 (m, 3H), 7.57 (dd, J = 1.5 Hz, 8.0 Hz, 1H), 7.77 (dd, J =

5.0 Hz, J = 8.0 Hz, 1H), 7.85 (s, 1H), 8.07 (dd, J = 1.0 Hz, 7.6 Hz, 1H), 8.15 (d, J = 8.7 Hz, 1H), 8.19 (d, J = 8.7 Hz, 1H), 8.41 (dd, J = 1.5 Hz, J = 8.0 Hz, 1H), 8.52 (dd, J = 1.5 Hz, J =5.0 Hz, 1H); ^{13}C NMR (CD_2Cl_2, 100 MHz) : δ 117.4, 123.0, 123.8, 126.0 126.4, 126.9, 127.8, 128.7, 130.5, 130.5, 130.6, 134.7, 138.2, 139.7, 145.5, 146.5, 147.4, 148.0, 150.0. MS (ES+) *m/z* (%): 781.3 (M^+- PF_6, 100).

{(Phenanthroline-N-N')-bis-(2-(2',4'-difluorophenyl)-4-methylpyridine $C^{6'}$,N)-iridium(III)} hexafluorophosphate; 105; OLED 11.

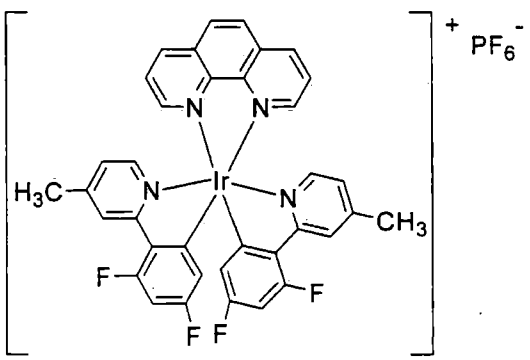

105 (OLED 11)

Following the procedure for **94; OLED 1**, phenanthroline (38 mg, 0.21 mmol), **87; $[Ir(4Meppy)_2Cl]_2$** (135 mg, 0.10 mmol), dichloromethane (10 ml) and methanol (10 ml) were refluxed for 24 h in the dark. After cooling to room temperature, KPF_6 (0.4 g) was added and stirred for 1 h at room temperature. Work-up as for **94; OLED 1** and column chromatography (SiO_2, eluent DCM) gave **105; OLED 11** as a yellow powder (85 mg, 86%); Anal. calcd for $C_{36}H_{24}F_{10}IrN_4P$; C, 46.71; H, 2.61; N, 6.05; Found: C, 46.26; H, 2.67; N, 6.00; ^{1}H NMR ($CDCl_3$, 400 MHz): δ 2.46 (s, 3H), 5.81(dd, J = 2.4 Hz, J_{HF} = 8.4 Hz, 1H), 6.60 (ddd, J = 2.4 Hz, J_{HF} = 9.0 Hz, J_{HF} = 12.5 Hz, 1H), 6.75 (dd, J_{HF} = 1.2 Hz, J = 6.4 Hz, 1H), 7.13 (d, J = 6.4 Hz, 1H), 7.87 (dd, J = 4.8 Hz, J = 8.4 Hz, 1H), 8.01 (s, 1H), 8.23 (s, 1H), 8.26 (dd, J = 1.4 Hz, J = 4.8 Hz, 1H), 8.70 (dd, J = Hz 1.4 J = 8.4 Hz, 1H); NMR ($CDCl_3$, 125 MHz) : δ 99.5, 114.04, 124.07, 125.0, 126.9, 127.9, 129.1, 132.0, 139.7, 146.6, 148.2, 150.6, 151.5, 153.4, 161.3, 163.8, 164.7; MS (ES+) *m/z* (%): 781.3 (M^+- PF_6, 100).

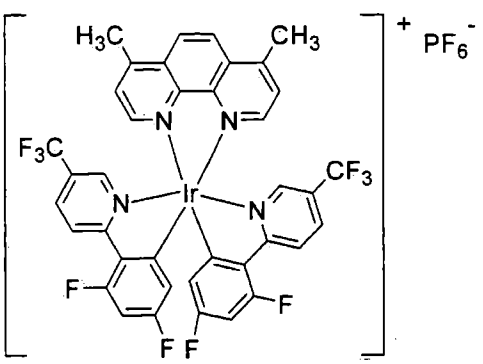

106 (OLED 13)

{(4,7-Dimehyl-phenanthroline-N-N')-bis-(2-(2',4'-difluorophenyl)-5-trifluoromethylpyridine $C^{2'}$,N)-iridium(III)} hexafluorophosphate; 106; OLED 13. Following the procedure for **94; OLED 1**, 4,7-

dimethylphenanthroline (63 mg, 0.3 mmol), **89; $[Ir(5CF_3ppy)_2Cl]_2$** (150 mg, 0.1 mmol), dichloromethane (15 ml) and methanol (15 ml) were refluxed for 24 h in the dark. After cooling to room temperature, KPF_6 (0.4 g) was added and stirred for 1 h at room temperature. Work-up as for **94; OLED 1** and column chromatography (SiO_2, eluent DCM) gave **106; OLED 13** as a yellow powder (95 mg, 88%); Anal. calcd for $C_{38}H_{22}F_{16}IrN_4P$; C, 42.99; H, 2.09; N, 5.28; P; Found: C, 42.98; H, 2.07; N, 5.25; ^1H NMR (CD_2Cl_2, 400 MHz): δ 3.02 (s, 3H), 5.83 (dd, J = 2.0 Hz, J_{HF} = 8.5 Hz, 1H), 6.73 (ddd, J = 2.0 Hz, J_{HF} = 9.0 Hz, J_{HF} = 12.0 Hz, 1H), 7.43 (d, J = 1.5 Hz, 1H), 7.75 (d, J = 5.0 Hz, 1H), 8.02 (dd, J = 1.5 Hz, J = 8.5 Hz, 1H), 8.20 (d, J = 5.0 Hz, 1H), 8.41 (s, 1H), 8.50 (dd, J_{HF} = 3.0 Hz, J = 8.5 Hz, 1H); ^{13}C NMR (CD_2Cl_2, 125 MHz) : δ 99.8 (t, J_{CF} = 26.8 Hz), 114.3 (dd, J_{CF} = 2.9 Hz, J_{CF} = 18.2 Hz), 121.5 (q, J_{CF} = 272.3 Hz), 123.7 (d, J_{CF} = 21.1 Hz), 125.0, 125.6 (q, J_{CF} = 33.5 Hz), 126.5, 127.6, 131.3, 136.5, 144.7 (d, J_{CF} = 4.8 Hz), 145.6, 150.6, 150.7, 153.9, (d, J_{CF} = 7.7 Hz), 162.5 (dd, J_{CF} = 13.4 Hz, J_{CF} = 260.8 Hz), 164.7 (dd, J_{CF} = 11.5 Hz, J_{CF} = 260.8 Hz), 167.9 (d, J_{CF} = 6.7 Hz); ^{19}F NMR (CD_2Cl_2, 376 MHz) : δ -107.7 (t, J_{FC} = 12.2 Hz), -103.9 (dd, J_{FC} = 9.1 Hz, J_{FC} = 21.3 Hz), -74.5, -72.7, -65.9; MS (ES+) *m/z* (%): 917.2 (M^+- PF_6, 100).

(4,7-Dipyrrolidinyl-phenanthroline-N-N')-bis-(2-phenyl-pyridine) $C^{2'},N$)-iridium(III)} hexafluorophosphate; 107; OLED 14.

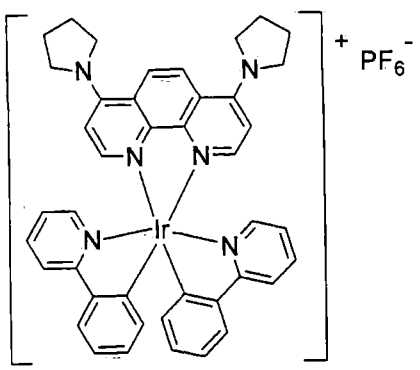

107 (OLED 14)

Following the procedure for **94; OLED 1**, **PyPhen** (70 mg, 0.22 mmol), **86; $[Ir(ppy)_2Cl]_2$** (107 mg, 0.1 mmol), dichloromethane (10 ml) and methanol (10 ml) were refluxed for 24 h in the dark. After cooling to room temperature, KPF_6 (0.4 g) was added and stirred for 1 h at room temperature. Work-up as for **94; OLED 1** and column chromatography (SiO_2, eluent DCM) gave **107; OLED 14** as a yellow powder (57 mg, 59%); ^1H NMR (CD_2Cl_2, 500 MHz): δ 3.82 (m, 4H), 2.10 (m, 4H), 6.41 (d, J = 8.0 Hz, 1H), 6.55 (d, J = 6.3 Hz, 1H), 6.86 (t, J = 8.0 Hz, 1H), 6.91 (t, J = 8.0 Hz, 1H), 7.04 (t, J = 8.0 Hz, 1H), 7.56 (d, J = 8.0 Hz, 1H), 7.66 (d, J = 6.3 Hz, 1H), 7.70 (d, J = 8.0 Hz, 1H), 7.73 (d, J = 8.0 Hz, 1H), 7.92 (d, J = 8.0 Hz, 1H), 8.32 (s, 1H). ^{13}C NMR (CD_2Cl_2, 125 MHz) : δ 26.1, 52.8,

106.7, 119.5, 121.3, 121.5, 122.0, 122.7, 124.8, 130.4, 132.1, 137.5, 144.3, 148.4, 148.7, 148.8, 152.4, 153.2, 168.5. ^{19}F NMR (CD_2Cl_2, 376 MHz) : δ -74.5, -72.7. MS (ES+) *m/z* (%): 819.4 (M^+- PF_6, 100).

(Phenanthroline-N-N')-bis-(2-(2',4'-difluorophenyl)-4-trifluoromethylpyridine C$^{6'}$,N)-iridium(III)} hexafluorophosphate; 108; OLED 15.

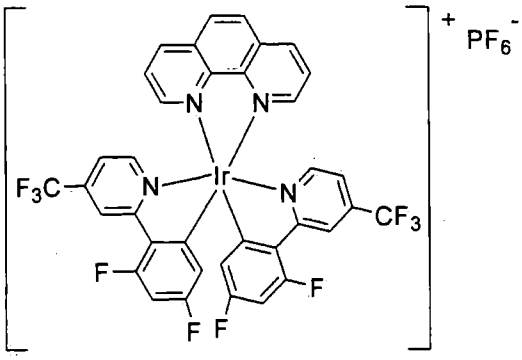

108 (OLED 15)

Following the procedure for **94; OLED 1**, phenanthroline (25 mg, 0.14 mmol), **88; [Ir(4CF$_3$ppy)$_2$Cl]$_2$** (100 mg, 0.07 mmol), dichloromethane (10 ml) and methanol (10 ml) were refluxed for 24 h in the dark. After cooling to room temperature, KPF_6 (0.5 g) was added and stirred for 1 h at room temperature. Work-up as for **94; OLED 1** and column chromatography (SiO_2, eluent DCM) gave **108; OLED 15** as a yellow powder (50 mg, 72%); Anal. calcd for $C_{36}H_{18}F_{16}IrN_4P$; C, 41.83; H, 1.76; N, 5.42; Found: C, 41.80; H, 1.77; N, 5.45; ^1H NMR (CD_2Cl_2, 400 MHz): δ 5.88 (dd, J = 2.5 Hz, J_{HF} = 8.5 Hz, 1H), 6.74 (ddd, J = 2.5 Hz, J_{HF} = 9.0 Hz, J_{HF} = 12.1 Hz, 1H), 7.13 (dd, J = 2.0 Hz, J = 6.0 Hz, 1H), 7.53 (d, J = 6.0 Hz, 1H), 7.94 (dd, J = 5.0 Hz, J = 8.5 Hz, 1H), 8.27 (s, 1H), 8.32 (dd, J = 1.5 Hz, J = 5.0 Hz, 1H), 8.52 (d, J = 2.0 Hz, 1H), 8.74 (dd, J = 1.5 Hz, J = 8.5 Hz, 1H). ^{13}C NMR (CD_2Cl_2, 125 MHz) : δ 100.1 (t, J_{CF} = 26.8 Hz), 114.7 (d, J_{CF} = 18.2 Hz), 119.8, 119.9, 122.1 (q, J_{CF} = 274.2 Hz), 127.1, 127.4, 129.1, 132.2, 140.2, 140.8 (q, J_{CF} = 35.5 Hz), 146.5, 150.3, 151.4, 153.0 (d, J_{CF} = 7.7 Hz), 162.4 (dd, J_{CF} = 12.5 Hz, J_{CF} = 261.8 Hz), 164.6 (dd, J_{CF} = 12.5 Hz, J_{CF} = 259.9 Hz), 166.0 (d, J_{CF} = 6.7 Hz); ^{19}F NMR (CD_2Cl_2, 376 MHz) : δ -107.7 (t, J_{FC} = 12.2 Hz), -103.9 (dd, J_{FC} = 9.1 Hz, J_{FC} = 21.3 Hz), -74.5, -72.7, -65.9; MS (ES+) *m/z* (%): 889.2 (M^+- PF_6, 100). Crystals of **108; OLED 15** for X-ray analysis were grown from slowly evaporated $CDCl_3$ in an NMR tube; *Crystal data*: $C_{36}H_{18}F_{10}IrN_4PF_6.2CDCl_3$, M= 1274.46, triclinic ($P\bar{1}$), a=10.9459(17), b=10.9554(17), c=18.973(3) Å, α =76.10(2), β=80.06(3), γ=76.85(3)°, V=2133.8(6) Å^3, Z=2.

{(Phenanthroline-N-N')-bis-(1-(2',4'-difluoro-phenyl)-1*H*-pyrazole $C^{6'},N^{2}$)-iridium(III)} hexafluorophosphate; 109; OLED 16.

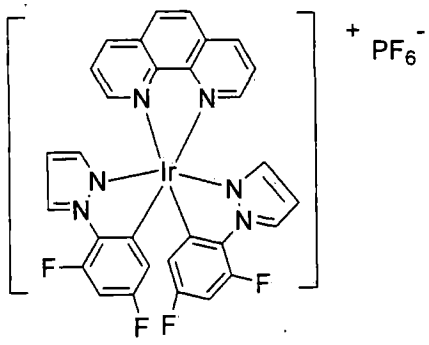

109 (OLED 16)

Following the procedure for **94; OLED 1**, phenanthroline (40 mg, 0.22 mmol), **92; $[Ir(Fppz)_2Cl]_2$** (117 mg, 0.1 mmol), dichloromethane (10 ml) and methanol (10 ml) were refluxed for 24 h in the dark. After cooling to room temperature, KPF_6 (0.5 g) was added and stirred for 1 h at room temperature. Work-up as for **94; OLED 1** and column chromatography (SiO_2, eluent DCM) gave **109; OLED 16** as a yellow powder (74 mg, 84%); Anal. calcd for $C_{30}H_{18}F_{10}IrN_6P$: C, 41.15; H, 2.07; N, 9.60 found: C, 40.62; H, 2.06; N, 9.50; ^1H NMR (CD_2Cl_2, 500 MHz): δ 5.89 (dd, J = 2.4 Hz, J_{HF} = 8.3 Hz, 1H), 6.51 (t, J = 2.4 Hz, 1H), 6.74 (d, J = 2.4 Hz, 1H), 6.77 (ddd, J = 2.4 Hz, J_{HF} = 8.8 Hz, J_{HF} = 12.2 Hz, 1H), 7.90 (dd, J = 4.9 Hz, J = 8.2 Hz, 1H), 8.24 (s, 1H), 8.38 (d, J = 2.4 Hz, 1H), 8.47 (dd, J = 1.5 Hz, J = 4.9 Hz, 1H), 8.71 (dd, J = 1.5 Hz, J = 8.2 Hz, 1H); ^{13}C NMR (CD_2Cl_2, 125 MHz) : δ 99.6 (dd, J_{CF} = 24.8 Hz, J_{CF} = 27.8 Hz), 108.7 (d, J_{CF} = 2.9 Hz), 115.2 (dd, J_{CF} = 2.9 Hz, J_{CF} = 19.2 Hz), 126.3, 127.1 (dd, J_{CFI} = 2.9 Hz, J_{CF} = 4.8 Hz), 128.4, 131.4, 131.6, 131.7, 135.3 (dd, J_{CF} = 2.9 Hz, J_{CF} = 6.7 Hz), 138.0, 139.2, 147.0, 149.4 (dd, J_{CF} = 253.1 Hz, J_{CF} = 12.5 Hz), 151.2, 160.3 (dd, J_{CF} = 2.9 Hz, J_{CF} = 4.8 Hz). ^{19}F NMR (CD_2Cl_2, 376 MHz) : δ -124.1 (dd, J_{FC} = 6.1 Hz, J_{FC} = 12.2 Hz), -112.7 (dd, J_{FC} = 6.1 Hz, J_{FC} = 12.2 Hz), -74.5, -72.7; MS (ES+) *m/z* (%): 731.1 (M^+- PF_6, 100). Crystals of **109; OLED 16** for X-ray analysis were grown from slowly evaporated CH_2Cl_2; *Crystal data*: $C_{30}H_{18}F_{10}IrN_6PF_6.CH_2Cl_2$, M= 960.60, monoclinic ($P2_1/n$), a=17.4740(15), b=12.7473(11), c=30.204(3) Å, α =90.00, β=105.283(11), γ=90.00°, V=6490.0(10) Å^3, Z=8.

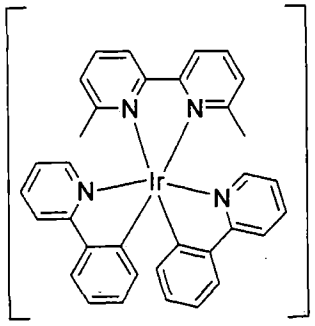

110 (OLED 18)

{(2,9-Dimethylbipyridine-N-N')-bis-(2-phenylpyridine $C^{2'},N$)-iridium(III)} hexafluorophosphate; **110**; **OLED 18**. Following the procedure for 94; OLED 1, 2,9-dimethylbipyridine (0.11 g, 0.59 mmol), 86;

$[Ir(ppy)_2Cl]_2$ (0.30 g, 0.28 mmol), dichloromethane (10 ml) and methanol (10 ml) were refluxed for 24 h in the dark. After cooling to room temperature, KPF_6 (0.5 g) was added and stirred for 1 h at room temperature. Work-up as for **94**; **OLED 1** and column chromatography (SiO_2, eluent DCM) gave 110; OLED 18 as a yellow powder (173 mg, 75%); Anal. calcd for $C_{34}H_{28}F_6IrN_4P$: C, 49.21; H, 3.40; N, 6.75 found: C, 49.22; H, 2.50; N, 6.70; ^{1}H NMR (400 MHz, $CDCl_3$) δ 1.86 (s, 3H), 6.07 (d, J = 6.9, 1H), 6.75 (dd, J = 1.2, 7.5, 1H), 6.91 (dd, J = 4.2, 10.9, 1H), 7.16 – 7.04 (m, 1H), 7.23 (d, J = 7.2, 1H),), 7.57 (dd, J = 1.1, 7.8, 1H), 7.79 (dd, J = 6.6, 8.6, 2H 7.92 – 7.87 (m, 1H), 7.99 (t, J = 7.9, 1H), 8.37 (d, J = 8.1, 1H); ^{13}C NMR (101 MHz, $CDCl_3$) δ 26.7, 119.4, 122.2, 123.1, 123.3, 124.5, 128.3, 130.1, 131.5, 138.1, 140.0, 142.6, 149.7, 163.1, 167.7; ^{19}F NMR (376 MHz, $CDCl_3$) δ -72.34, -74.24; MS (ES+) *m/z* (%): 685.2 (M^+- PF_6, 100). Crystals of **110**; **OLED 18** for X-ray analysis were grown from slowly evaporated $CHCl_3$; *Crystal data*: $C_{36}H_{28}IrN_4PF_6.2CHCl_3$, M= 1068.51, monoclinic ($P2_1/n$), a=15.8293(10), b=15.9663(8), c=16.4922(9) Å, α=90.00, β=109.28(1), γ=90.00°, V=3934.4(4) Å^3, Z=4.

Chapter 4.3.

N-Arylation of nitrogen heterocycles with 2,4-difluoroiodobenzene

General Procedure for the N-Arylation without Cu(I) catalysis

To a mixture of the *N*-heteroaromatic compound (1.5 eq.), Cs_2CO_3 (2.0 eq.) and 2,4-difluoroiodobenzene **82** (1.0 eq.) anhydrous degassed acetonitrile (10 ml) was added. The mixture was stirred and heated in an oil bath to 80 °C for 12 h, then cooled to room temperature and diluted with dichloromethane and water. The organic layer was washed with water and saturated NaCl solution and was then separated and dried over $MgSO_4$. The solvent was removed in vacuo to yield the crude product, which was purified by column chromatography on silica.

The reaction of pyrazole (0.85 g, 12.5 mmol), 2,4-difluoroiodobenzene **82** (1.0 ml, 8.3 mmol) and Cs_2CO_3 (5.4 g, 16.7 mmol) in acetonitrile (10 ml) and column

chromatography (SiO_2, eluent ether/DCM, 0:1 to 1:5 v/v) gave the following products in order of elution:

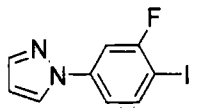

83

1-(3-Fluoro-4-iodophenyl)-1*H*-pyrazole; 83 (0.43 g, 18%); a white solid; mp. 76.0-77.5 °C; ^{1}H NMR ($CDCl_3$, 400 MHz): δ 6.39 (dd, J = 1.5 Hz, 2.5 Hz, 1H), 7.17 (dd, J = 2.5 Hz, 8.5 Hz, 1H), 7.48 (dd, J = 2.5 Hz, J_{HF} = 9.0 Hz, 1H), 7.71 (d, J = 1.5 Hz, 1H), 7.76 (dd, J_{HF} = 7.0 Hz, J = 8.5 Hz, 1H), 7.88 (d, J = 2.5 Hz, 1H); ^{13}C NMR ($CDCl_3$, 100 MHz): δ 106, (d, J_{CF} = 27.8 Hz), 108.5, 115.9 (d, J_{CF} = 2.9 Hz), 126.7, 139.7, 139.8 (d, J_{CF} = 2.9 Hz), 141.6, 141.7 (d, J_{CF} = 9.0 Hz), 162.2 (d, J_{CF} = 246 Hz); ^{19}F NMR ($CDCl_3$, 376 MHz): δ -91.7; IR (neat) 3114, 2522, 2359, 1599, 1517, 1389, 1028, 752 cm^{-1}; MS (ES+) *m/z* (%): 288 (M^+, 100); HRMS calcd. for $C_9H_6FIN_2$ (MH^+) 288.96326; found: 288.96327; calcd. C, 37.53; H, 2.10; N, 9.72 found: C, 37.40; H, 2.09; N, 9.67%.

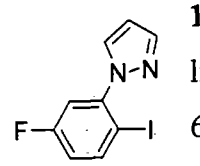

113

1-(5-Fluoro-2-iodophenyl)-1*H*-pyrazole; 113 (0.81 g, 34%); a colourless liquid; ^{1}H NMR ($CDCl_3$, 400 MHz): δ 6.40 (dd, J = 1.8 Hz, 2.4 Hz, 1H), 6.85 (ddd, J = 3.0 Hz, 8.8 Hz, J_{HF} = 11.6 Hz, 1H), 7.13 (dd, J = 3.0 Hz, J_{HF} = 9.2 Hz, 1H), 7.68 (d, J = 1.8 Hz, 1H), 7.71 (d, J = 2.4 Hz, 1H), 7.81 (dd, J_{HF} = 5.8 Hz, J = 8.8 Hz, 1H); ^{13}C NMR ($CDCl_3$, 100 MHz): δ 86.5, (d, J_{CF} = 4.4 Hz), 106.7, 115.5 (d, J_{CF} = 23.4 Hz), 117.1 (d, J_{CF} = 20.5 Hz), 130.8, 140.8 (d, J_{CF} = 8.8 Hz), 140.9, 144.2 (d, J_{CF} = 10.2 Hz), 162.5 (d, J_{CF} = 250 Hz); ^{19}F NMR ($CDCl_3$, 376 MHz): δ -112.1; IR (neat) 3726, 3102, 3102, 2360, 1583, 1468, 1191, 861, 749 cm^{-1}; MS (ES+) *m/z* (%): 289.1 (MH^+, 100); HRMS calcd. for $C_9H_6FIN_2$ (MH^+) 288.96326; found: 288.96333.

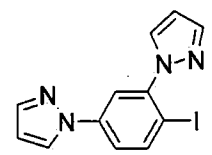

114

2,4-Di(1-1*H*-pyrazolyl)-iodobenzene; 114 (0.61 g, 22%); white solid; mp. 96.0-98.0 °C;[1] H NMR ($CDCl_3$, 400 MHz): δ 6.44 (dd, J = 1.5 Hz, 2.5 Hz, 1H), 6.46 (dd, J = 1.5 Hz, 2.5 Hz, 1H), 7.52 (dd, J = 2.5 Hz, 8.5 Hz, 1H), 7.69 (d, J = 1.5 Hz, 1H), 7.74 (d, J = 1.5 Hz, 1H), 7.75 (d, J = 2.5 Hz, 1H), 7.77 (d, J = 2.5 Hz, 1H), 7.91 (d, J = 2.5 Hz, 1H), 7.96 (d, J = 8.5 Hz, 1H); ^{13}C NMR ($CDCl_3$, 100 MHz): δ 89.4, 106.8, 108.4, 118.2, 120.2, 120.0, 126.6, 131.0, 140.7, 140.8, 141.0, 141.7, 144.0; IR (neat) 3735, 2360, 1524, 1267, 963, 847, 749

cm^{-1}; MS (ES+) *m/z* (%): 337.0 (MH^+, 100); HRMS calcd. for $C_{12}H_9IN_4$ (MH^+) 336.99448; found: 336.99447.

The analogous reaction using pyrazole (1.0 equiv.) gave **113** (50%), **83** (15%) and **114** (15%), using pyrazole (3.0 equiv.) at 80 °C for 24 h gave **113** (16%), **83** (2%) and **114** (56%).

The reaction of 3-(trifluoromethyl)pyrazole (1.7 g, 12.5 mmol), 2,4-difluoroiodobenzene **82** (1.0 ml, 8.3 mmol) and Cs_2CO_3 (5.4 g, 16.7 mmol) in acetonitrile (10 ml) and column chromatography (SiO_2, eluent DCM/hexane, 1:1 v/v) gave in order of elution:

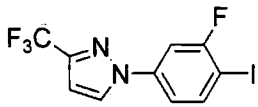

116

1-(3-Fluoro-4-iodophenyl)-4-trifluoromethyl-1*H*-pyrazole; 116 (0.18 g, 6%); a colourless liquid; ^1H NMR ($CDCl_3$, 400 MHz): δ 6.77 (dd, J_{HF} = 0.5 Hz, J = 2.4 Hz, 1H), 7.61 (dd, J_{HF} = 2.6 Hz, J = 8.6 Hz, 1H), 7.85 (dd, J = 0.5 Hz, J_{HF} = 8.8 Hz, 1H), 8.00-8.01 (m, 1H), 8.07 (dd, J = 0.5 Hz, 8.6 Hz, 1H); ^{19}F NMR ($CDCl_3$, 376 MHz): δ -97.8, -62.8; IR (neat) 3730, 2360, 1518, 1267, 845, 751 cm^{-1}; MS (EI) *m/z* (%): 356 (M^+, 100), 337 (M^+-F, 10), 229 (M^+-I, 100); MS (ES+) *m/z* (%): 356.8 (MH^+, 100); HRMS calcd. for $C_{10}H_6F_4I_2N_2$ (MH^+) 356.95064; found: 356.95063. ^1H NMR showed that **116** was not completely separated from traces of **115**.

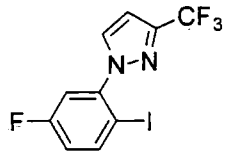

115

1-(5-Fluoro-2-iodophenyl)-3-trifluoromethyl-1*H*-pyrazole; 115 (1.33 g, 45%); a colourless liquid; ^1H NMR ($CDCl_3$, 400 MHz): δ 6.74 (dd, J_{HF} = 0.6 Hz, J = 2.4 Hz, 1H), 6.99 (ddd, J = 3.0 Hz, 8.8 Hz, J_{HF} = 11.9 Hz, 1H), 7.40 (dd, J = 3.0 Hz, J_{HF} = 8.5 Hz, 1H), 7.80 (qd, J_{HF} = 0.9 Hz, J = 2.4 Hz, 1H), 7.92 (dd, J = 8.8 Hz, J_{HF} = 5.8 Hz, 1H); ^{13}C NMR ($CDCl_3$, 125 MHz): δ 86.9, (d, J_{CF} = 3.8 Hz), 105.5 (q, J_{CF} = 1.9 Hz), 116.3 (d, J_{CF} = 24.9 Hz), 118.7 (d, J_{CF} = 22.0 Hz), 121.1 (q, J_{CF} = 270 Hz), 132.8, 141.3 (d, J_{CF} = 7.7 Hz), 143.6 (d, J_{CF} = 9.6 Hz), 144.7 (q, J_{CF} = 38.4 Hz), 162.9 (d, J_{CF} = 252 Hz); ^{19}F NMR ($CDCl_3$, 376 MHz): δ -111.6, -62.5; IR (neat) 3732, 2359, 1532, 1258, 968, 843, 747 cm^{-1}; MS (EI) *m/z* (%): 356 (M^+, 100), 337 (M^+-F, 10), 229 (M^+-I,

100); MS (ES+) *m/z* (%): 356.8 (MH^+, 100); HRMS calcd. for $C_{10}H_6F_4I_2N_2$ (MH^+) 356.95064; found: 356.95060.

The reaction of imidazole (0.85 g, 12.5 mmol), 2,4-difluoroiodobenzene **82** (1.0 ml, 8.3 mmol) and Cs_2CO_3 (5.4 g, 16.7 mmol) and column chromatography (SiO_2, eluent haxane/DCM, 4:1 to 1:1 v/v) gave in order of elution:

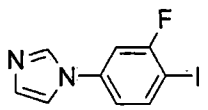

118

1-(3-Fluoro-4-iodophenyl)-1*H*-imidazole; 118 (80 mg, 4%); a white solid; mp. 106.5-108.0 °C; ^{1}H NMR ($CDCl_3$, 400 MHz): δ 6.98 (dd, J = 2.5 Hz, $^2J_{HF}$ = 9.0 Hz, 1H), 7.11 (dd, J = 2.5 Hz, 8.5 Hz, 1H), 7.19 (s, 1H), 7.24 (s, 1H), 7.81 (dd, J_{HF} = 7.0 Hz, J = 8.5 Hz, 1H), 7.84 (s, 1H); ^{13}C NMR ($CDCl_3$, 100 MHz): δ 78.9, (d, J_{CF} = 24.9 Hz), 109.0 (d, J_{CF} = 26.3 Hz), 117.8, 118.2 (d, J_{CF} = 4.4 Hz), 131.0, 135.2, 138.8 (d, J_{CF} = 8.8 Hz), 140.4, 162.2 (d, J_{CF} = 247 Hz); ^{19}F NMR ($CDCl_3$, 376 MHz) : δ -90.5; IR (neat) 2518, 2359, 1571, 1179, 852, 753 cm^{-1}; MS (EI) *m/z* (%): 287.9 (M^+, 100); 260.8 (M^+-I, 30); MS (ES+) *m/z* (%): 289.0 (MH^+, 100); HRMS calcd. for $C_9H_6FIN_2$ (MH^+) 288.96326; found: 288.96322.

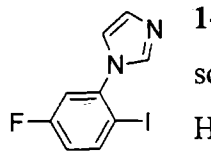

117

1-(5-Fluoro-2-iodophenyl)-1*H*-imidazole; 117 (1.8 g, 66%); a white solid; mp. 67.0-68.5 °C; ^{1}H NMR ($CDCl_3$, 400 MHz): δ 6.97 (ddd, J = 3.0 Hz, 8.5 Hz, J_{HF} = 11.6 Hz, 1H), 7.07 (d, J = 1.0 Hz, 1H), 7.08 (dd, J = 3.0 Hz, J_{HF} = 8.5 Hz, 1H), 7.21 (d, J = 1.0 Hz, 1H), 7.64 (s, 1H), 7.91 (dd, J_{HF} = 5.0 Hz, J = 8.5 Hz, 1H); ^{13}C NMR ($CDCl_3$, 100 MHz): δ 88.8, (d, J_{CF} = 2.9 Hz), 115.8 (d, J_{CF} = 23.4 Hz), 118.1 (d, J_{CF} = 21.9 Hz), 120.4, 129.9, 137.4, 141.1 (d, J_{CF} = 8.8 Hz), 141.5 (d, J_{CF} = 10.2 Hz), 162.9 (d, J_{CF} = 252 Hz); ^{19}F NMR ($CDCl_3$, 376 MHz): δ -111.7; IR (neat) 3733, 2360, 1496, 1243, 1189, 1051, 846, 748 cm^{-1}; MS (ES+) *m/z* (%): 289.0 (MH^+, 100); HRMS calcd. for $C_9H_6FIN_2$ (MH^+, 100); 288.96326; found: 288.96320.

The reaction of pyrrole (0.85 ml, 12.5 mmol), 2,4-difluoroiodobenzene **82** (1.0 ml, 8.3 mmol) and Cs_2CO_3 (5.4 g, 16.7 mmol) and column chromatography (SiO_2, eluent hexane) gave a mixture of **119** and **120** (1.55 g, 65%, ca. 5:1 ratio by ^{1}H NMR analysis of the crude mixture). Crystallisation of the mixture from hexane gave:

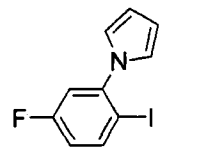

1-(5-Fluoro-2-iodophenyl)-1*H*-pyrrole; 119 (1.31 g, 55%) a white solid; mp. 70-71.5 °C; ^{1}H NMR ($CDCl_3$, 400 MHz): δ 6.34 (t, J = 2.0 Hz, 2H), 6.82 (t, J = 2.0 Hz, 2H), 6.89 (ddd, J = 3.0 Hz, 8.5 Hz, J_{HF} = 11.6 Hz, 1H), 7.06 (d, J = 3.0 Hz, J_{HF} = 9.0 Hz, 1H), 7.88 (dd, J_{HF} = 5.5 Hz, J = 8.5 Hz, 1H); ^{13}C NMR ($CDCl_3$, 125 MHz): δ 88.6 (d, J_{CF} = 3.8 Hz), 109.7 (2C), 115.8 (d, J_{CF} = 23.0 Hz), 116.9 (d, J_{CF} = 21.0 Hz), 122.1 (2C), 140.9 (d, J_{CF} = 8.6 Hz), 145.2 (d, J_{CF} = 10.5 Hz), 162.9 (d, J_{CF} = 250 Hz); ^{19}F NMR ($CDCl_3$, 376 MHz): δ -112.7 ; IR (neat) 3140, 2798, 1530, 1480, 1125, 768 cm^{-1}; MS (ES+) *m/z* (%): 287.1 (MH^+, 100); HRMS calcd. for $C_{10}H_7FIN$ (MH^+) 287.96801; found: 287.96825.

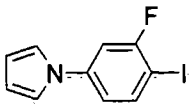
120

1-(3-Fluoro-4-iodophenyl)-1*H*-pyrrole; 120 (0.24 g, 10%) a colourless liquid; ^{1}H NMR ($CDCl_3$, 400 MHz): δ 6.39 (t, J = 2.1 Hz, 2H), 7.00 (t, J_{12} = 2.4 Hz, J_{13} = 8.5 Hz, 1H), 7.07 (t, J = 2.1 Hz, 2H), 7.14 (d, J_{12} = 2.4 Hz, $^2J_{HF}$ = 9.1 Hz, 1H), 7.77 (dd, $^3J_{HF}$ = 7.0 Hz, J_{13} = 8.5 Hz, 1H); ^{19}F NMR ($CDCl_3$, 376 MHz): δ -91.8; IR (neat) 3148, 2787, 1532, 1485, 1120, 765 cm^{-1}; MS (EI) *m/z* (%): 287 (M^+, 100); 160 (M^+-I, 100). ^{1}H NMR showed that **120** was not completely separated from traces of **119**.

General Procedure for the N-Arylation with Cu(I) catalysis

The procedure was the same as described above with the addition of Cu_2O (5 mol%) and salicylaldoxime (20 mol%) to the reaction mixture.

The reaction of pyrazole (0.85 g, 12.5 mmol), 2,4-difluoroiodobenzene **82** (1.0 ml, 8.3 mmol), salicylaldoxime (0.23 g, 1.67 mmol), Cs_2CO_3 (5.4 g, 16.7 mmol), Cu_2O (60 mg, 0.42 mmol) and column chromatography (SiO_2, eluent ether/DCM, 0:1 to 1:5 v/v) gave in order of elution: **83** (39 mg, 2%) spectroscopically identical with the sample above, **81 (Fppz)** (0.25 g, 13%); spectroscopically identical with the product from acid catalysis.

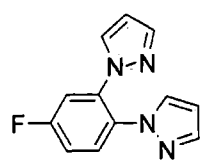
84

3,4-Di(1*H*-pyrazolyl)fluorobenzene; 84 (0.36 g, 20%); a colourless liquid; ^{1}H NMR ($CDCl_3$, 400 MHz): δ 6.25 (s, 1H), 6.31 (s, 1H), 6.82 (s, 1H), 7.08 (s, 1H), 7.15 (td, J = 8.8 Hz, 2.3 Hz, 1H), 7.50 (dd, J =

2.3 Hz, J_{HF} = 8.8 Hz, 1H), 7.58 (dd, J_{HF} = 5.5 Hz, J = 8.8 Hz, 1H), 7.67 (s, 1H), 7.70 (s, 1H); ^{13}C NMR (100 MHz, $CDCl_3$): δ 162.0 (d, J_{CF} = 250 Hz), 141.5, 141.3, 136.5 (d, J_{CF} = 11.0 Hz), 130.9, 130.2, 129.9 (d, J_{CF} = 3.7 Hz), 129.2 (d, J_{CF} = 9.5 Hz), 115.4 (d, J_{CF} = 17.7 Hz), 113.5 (d, J_{CF} = 26.0 Hz), 108.0, 107.7; ^{19}F NMR ($CDCl_3$, 376 MHz): δ -110.5; IR (neat) 3725, 3111, 2360, 1580, 1465, 1382, 1158, 870, 745 cm^{-1}; MS (ES+) *m/z* (%): 229.2 (MH^+, 100); HRMS calcd. for $C_{12}H_{10}N_4F$ (MH^+) 229.08840; found: 229.08848.

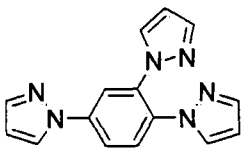

85

1,2,4-Tris(1*H*-pyrazolyl)benzene; 85 (80 mg, 4%); a colourless liquid; ^{1}H NMR ($CDCl_3$, 400 MHz): δ 6.26 (t, J = 2.5 Hz, 1H) , 6.28 (t, J = 2.0 Hz, 1H), 6.45 (t, J = 2.5 Hz, 1H), 6.95 (d, J = 2.5 Hz, 1H), 7.01 (d, J = 2.0 Hz, 1H), 7.67-7.71 (m, 4H), 7.83 (dd, J = 2.5 Hz, J = 8.5 Hz, 1H), 7.98 (d, J = 2.5 Hz, 1H), 8.02 (d, J = 2.5 Hz, 1H); ^{13}C NMR ($CDCl_3$, 100 MHz): δ 107.7, 107.8, 108.4, 116.6, 118.5, 126.9, 128.2, 130.4, 130.6, 131.8, 135.4, 140.0, 141.3, 141.4, 141.8; IR (neat) 3727, 2360, 1586, 1479, 1275, 1129, 865, 764 cm^{-1}; MS (ES+) *m/z* (%): 277.2 (MH^+, 32), 299.2 (M^++Na^+, 100); HRMS calcd. for $C_{15}H_{12}N_6$ (M^++Na^+) 299.10157; found: 299.10169.

The analogous reaction using pyrazole (3.5 equiv.) at 80 °C for 24 h gave **84** (35%) and **85** (13%).

The reaction of 3-(trifluoromethyl)pyrazole (1.7 g, 12.5 mmol), 2,4-difluoroiodobenzene **82** (1.0 ml, 8.3 mmol), salicylaldoxime (0.23 g, 1.67 mmol), Cs_2CO_3 (5.4 g, 16.7 mmol), Cu_2O (60 mg, 0.42 mmol) and column chromatography (SiO_2, eluent DCM/hexane, 1:1 v/v) gave in order of elution: Compound **115** (0.15 g, 5%) spectroscopically identical with the sample above, followed by:

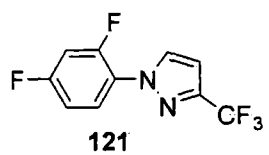

121

1-(2,4-Difluorophenyl)-3-trifluoromethyl-1*H*-pyrazole; 121 (0.2 g, 10%); a white solid; mp. 29-30 °C; ^{1}H NMR ($CDCl_3$, 200 MHz): δ 6.73 (d, J = 1.9 Hz, 1H), 6.97-7.01 (m, 2H), 7.85 (td, J_{HF} = 5.8 Hz, J = 8.1 Hz, 1H), 7.95 (d, J = 1.9 Hz, 1H); ^{13}C NMR ($CDCl_3$, 100 MHz): δ 105.4, (t, $^2J_{CF}$ = 26.9 Hz),106.0, 112.6 (dd, J_{CF1} = 22.2 Hz, J_{CF2} = 3.2 Hz), 121.4 (q, J_{CF} = 269.5 Hz), 124.5-124.6 (m), 126.4 (d, J_{CF} = 9.5 Hz), 132.4 (d, J_{CF} = 9.5 Hz), 144.4 (d, J_{CF} = 38.0 Hz), 154.4 (dd, J_{CF1} = 252.0 Hz, J_{CF2} = 12.7 Hz), 161.5 (dd, J_{CF1} = 252.0 Hz, $^3J_{CF2}$ = 11.0 Hz); ^{19}F NMR ($CDCl_3$, 376 MHz) : δ -120.9, -109.6, -62.7;

IR (neat) 3731, 3110, 2360, 1512, 1275, 1120, 861, 752 cm^{-1}; MS (EI) *m/z* (%): 248 (M^+, 100); 229 (M^+-F, 10), 179 (M^+-CF_3, 10); MS (ES+) *m/z* (%): 349.0 (MH^+, 100); HRMS calcd. for $C_{10}H_6F_5N_2$ (MH^+) 249.04511; found: 249.04515.

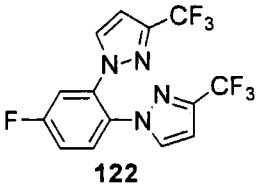

122

3,4-Bis(4-trifluoromethyl-1*H*-pyrazolyl)fluorobenzene; 122 (1.24 g, 41%); a white solid; mp. 83.4-84.0 °C; ^1H NMR ($CDCl_3$, 400 MHz): δ 6.58 (d, *J* = 2.5 Hz, 1H), 6.61 (d, *J* = 2.0 Hz, 1H), 7.14 (d, *J* = 2.0 Hz, 1H), 7.27 (d, *J* = 2.5 Hz, 1H), 7.31 (ddd, *J* = 2.5 Hz, 8.5 Hz, J_{HF} = 11.6 Hz , 1H), 7.50 (dd, *J* = 2.5 Hz, J_{HF} = 8.5 Hz, 1H), 7.67 (dd, J_{HF} = 5.0 Hz, *J* = 8.5 Hz, 1H); ^{13}C NMR ($CDCl_3$, 125 MHz): δ 106.3, (d, J_{CF} = 1.9 Hz), 114.5 (d, J_{CF} = 25.9 Hz), 117.1 (d, J_{CF} = 22.1 Hz), 119.8 (q, J_{CF} = 277 Hz), 121.9 (q, J_{CF} = 277 Hz), 129.5 (d, J_{CF} = 9.6 Hz), 130.1 (d, J_{CF} = 3.9 Hz), 132.1, 132.8, 136.1 (d, J_{CF} = 10.5 Hz), 144.7-145.2 (m, 2C), 162.6 (d, J_{CF} = 254 Hz); ^{19}F NMR ($CDCl_3$, 376 MHz): δ -107.9, -62.8, -62.7; IR (neat) 3730, 3115, 2360, 1512, 1272, 1130, 755 cm^{-1}; MS (EI) *m/z* (%): 364.0 (M^+, 100); 295.0 (M^+-CF_3, 70); MS (ES+) *m/z* (%): 365.1 (MH^+, 100); HRMS calcd. for $C_{14}H_7F_7N_4$ (M^++Na^+) 387.04512; found: 387.04505. Crystals of **122** for X-ray analysis were grown from slowly evaporated ethyl acetate-hexane mixture. *Crystal data*: $C_{14}H_7F_7N_4$, *M*=364.24, monoclinic (*C*2/*c*, no. 15), *a*=18.4627(15), *b*=9.8208(8), *c*=18.659(2) Å, *β*=112.86(2)°, *V*=3117.5(5) $Å^3$, Z=8, $R1[I>2\sigma(I)]$= 0.049, wR_2(all data)=0.133, CCDC-698164.

The reaction of imidazole (0.85 g, 12.5 mmol), 2,4-difluoroiodobenzene **82** (1.0 ml, 8.3 mmol), salicylaldoxime (0.23 g, 1.67 mmol), Cs_2CO_3 (5.4 g, 16.7 mmol), Cu_2O (60 mg, 0.42 mmol) and column chromatography (SiO_2, eluent ether/DCM, 0:1 to1:1 v/v) gave in order of elution: Compounds **117** (0.48 g, 20%) and **118** (70 mg, 3%) which were spectroscopically identical with the samples above, followed by:

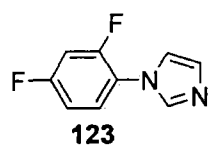

123

1-(2,4-Difluorophenyl)-1*H*-imidazole; 123 (0.48 g, 32%); a white solid; mp. 60.0-62.0 °C; ^1H NMR ($CDCl_3$, 400 MHz): δ 6.97-7.06 (m, 2H), 6.20 (s, 1H), 6.22 (s, 1H), 7.37 (td, J_{HF} = 6.1 Hz, *J* = 8.8 Hz 1H), 7.75 (s, 1H); ^{13}C NMR ($CDCl_3$, 175 MHz): δ 105.4 (dd, J_{CF} = 23.8 Hz, J_{CF} = 26.5 Hz), 112.1 (dd, J_{CF} = 3.9 Hz, J_{CF} = 22.5 Hz), 119.6 (d, J_C = 1.6 Hz), 121.8 (dd, J_{CF} = 3.9 Hz,

J_{CF} = 11.8 Hz), 126.2 (dd, J_{CF} = 1.9 Hz, J_{CF} = 9.9 Hz), 129.8, 136.9 (d, J_{CF} = 3.3 Hz), 155.3 (dd, J_{CF} = 12.3 Hz, J_{CF} = 254 Hz), 161.5 (dd, J_{CF} = 11.0 Hz, J_{CF} = 251 Hz); ^{19}F NMR ($CDCl_3$, 376 MHz): δ -119.7, -109.5; IR (neat) 3735, 3109, 2360, 1581, 1425, 1243, 1185, 1052, 823, 745 cm^{-1}; MS (EI) *m/z* (%): 180 (M^+, 100); MS (ES+) *m/z* (%): 181.1 (MH^+, 100); HRMS calcd. for $C_9H_6F_2N_2$ (MH^+) 181.05718; found: 181.05714.

The reaction of pyrrole (0.85 ml, 12.5 mmol), 2,4-difluoroiodobenzene **82** (1.0 ml, 8.3 mmol), salicylaldoxime (0.23 g, 1.67 mmol), Cs_2CO_3 (5.4 g, 16.7 mmol), Cu_2O (60 mg, 0.42 mmol) and column chromatography (SiO_2, eluent hexane) gave in order of elution: Compounds **119** and **120** (57 mg, 25%, 4:1 ratio by ^{1}H NMR) which were not separated, followed by:

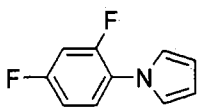

124

1-(2,4-Difluorophenyl)-1*H*-pyrrole; 124 (0.60 g, 35%); a colourless liquid; ^{1}H NMR ($CDCl_3$, 400 MHz): δ 6.43 (t, J = 2.0 Hz, 2H), 6.96-7.05 (m, 3H), 7.07-7.15 (m, 1H), 7.40 (td, J_{HF} = 5.7 Hz, J = 8.8 Hz, 1H); ^{13}C NMR ($CDCl_3$, 125 MHz): δ 105.6 (dd, J_{CF} = 24.2 Hz, J_{CF} = 26.3 Hz), 109.7, 112.7 (dd, J_{CF} = 3.9 Hz, J_{CF} = 21.5 Hz), 121.5, 123.2 (dd, J_{CF} = 2.0 Hz, J_{CF} = 8.9 Hz), 124.9 (d, J_{CF} = 10.5 Hz), 156.5 (dd, J_{CF} = 11.5 Hz, J_{CF} = 250 Hz), 161.0 (dd, J_{CF} = 10.1 Hz, J_{CF} = 251 Hz); ^{19}F NMR ($CDCl_3$, 376 MHz): δ -112.7, -120.6; IR (neat) 3138, 2854, 2755, 1540, 1482, 1124, 1075, 748 cm^{-1}; MS (ES+) *m/z* (%): 287.1 (MH^+, 100); HRMS calcd. for $C_{10}H_7F_2N$ (MH^+) 180.06248; found: 180.06240.

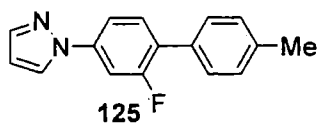

125

1-(2-Fluoro-4'-methylbiphenyl-4-yl)-1*H*-pyrazole; 125. A mixture of $Pd(PPh_3)_4$ (40 mg, 0.03 mmol), compound **6** (0.20 g, 0.69 mmol), Na_2CO_3 (2 M, 2.0 ml) and *p*-tolueneboronic acid (0.11 g, 0.83 mmol) in degassed 1,4-dioxane (20 ml) was stirred and heated in an oil bath at 100 °C overnight. The reaction mixture was cooled to room temperature, diluted with dichloromethane and water. The resulting organic layer was washed with water and saturated NaCl solution, separated and dried over $MgSO_4$. The solvent was removed in vacuo to yield the crude product, which was purified by column chromatography (SiO_2, eluent ether/DCM, 1:5 v/v) to give **21** (0.14 g, 83%); a white solid; mp. 115.5-117 °C; ^{1}H NMR ($CDCl_3$, 400 MHz): δ 2.41 (s, 3H), 6.50 (t, J = 2.4 Hz, 1H), 7.27 (d, J = 7.6 Hz,

2H), 7.46 (d, J = 2.0 Hz, 1H), 7.48 (d, J = 2.0 Hz, 1H), 7.52-7.60 (m, 3H), 7.44 (d, J = 2.4 Hz, 1H), 7.94 (d, J = 2.4 Hz, 1H); ^{13}C NMR ($CDCl_3$, 125 MHz): δ 107.4, (d, J_{CF} = 28.8 Hz), 108.2, 114.6 (d, J_{CF} = 3.8 Hz), 126.8, 127.0 (d, J_{CF} = 13.4 Hz), 128.8, 128.9, 129.4 (2C), 131.5 (d, J_{CF} = 4.8 Hz), 132.2, 137.9, 140.3 (d, J_{CF} = 10.5 Hz), 160.5 (d, J_{CF} = 248 Hz); ^{19}F NMR ($CDCl_3$, 376 MHz): δ -115.8; IR (neat) 3728, 2928, 2524, 2359, 1500, 1390, 1267, 1037, 850, 751 cm^{-1}; MS (ES+) *m/z* (%): 253.1 (MH^+, 100); HRMS calcd. for $C_{16}H_{14}FN_2$ (MH^+) 253.11355; found: 253.11351. Crystals of **125** for X-ray analysis were grown from slowly evaporated ethyl acetate-hexane mixture. *Crystal data*: M=252.28, orthorhombic (*Pbca*, no. 61), a=8.8599(7), b=16.5827(14), c=16.8780(15) Å, V=2479.7(4) Å^3, Z=8, $R_1[I>2\sigma(I)]$=0.051, wR_2(all data)=0.153, CCDC-698165.

References

1. Gao, F. G.; Bard, A. J. *J. Am. Chem. Soc.* **2000**, *122*, 7426-7427.
2. Tsuzuki, T.; Shirasawa, N.; Suzuki, T.; Tokito, S. *Adv. Mater.* **2003**, *15*, 1455-1458.
3. Jung, S.; Kang, Y.; Kim, H.-S.; Kim, Y.-H.; Lee, C.-L.; Kim, J.-J.; Lee, S.-K.; Kwon, S.-K. *Eur. J. Inorg. Chem.* **2004**, *17*, 3415-3423.
4. Ren, X.; Li, J.; Holmes, R. J.; Djurovich, P. I.; Forrest, S. R.; Thompson, M. E. *Chem. Mater.* **2004**, *16*, 4743-4747.
5. Holder, E.; Langeveld, B. M. W.; Schubert, U. S. *Adv. Mater.* **2005**, *17*, 1109-1121.
6. Lo, S.-C.; Anthopoulos, T. D.; Namdas, E. B.; Burn, P. L.; Samuel, I. D. W. *Adv. Mater.* **2005**, *17*, 1945-1948.
7. Veinot, J. G. C.; Marks, T. J. *Acc. Chem. Res.* **2005**, *38*, 632-643.
8. Chen, L.; You, H.; Yang, C.; Zhang, X.; Qin, J.; Ma, D. *J. Mater. Chem.* **2006**, *16*, 3332 - 3339.
9. Fang, C.-H.; Chen, Y.-L.; Yang, C.-H.; Chi, Y.; Yeh, Y.-S.; Li, Elisa Y.; Cheng, Y.-M.; Hsu, C.-J.; Chou, P.-T.; Chen, C.-T. *Chem. Eur. J.* **2007**, *13*, 2686-2694.
10. Lo, S.-C.; Burn, P. L. *Chem. Rev.* **2007**, *107*, 1097-1116.
11. Tour, J. M.; Jones, L.; Pearson, D. L.; Lamba, J. J. S.; Burgin, T. P.; Whitesides, G. M.; Allara, D. L.; Parikh, A. N.; Atre, S. *J. Am. Chem. Soc.* **1995**, *117*, 9529-9534.
12. Schumm, J. S.; Pearson, D. L.; Jones-II, L.; Hara, R.; Tour, J. M. *Nanotechnology* **1996**, *7*, 430-433.
13. Jones, L.; Schumm, J. S.; Tour, J. M. *J. Org. Chem.* **1997**, *62*, 1388-1410.
14. Pearson, D. L.; Tour, J. M. *J. Org. Chem.* **1997**, *62*, 1376-1387.
15. Tour, J. M. *Acc. Chem. Res.* **2000**, *33*, 791-804.
16. Tour, J. M.; Rawlett, A. M.; Kozaki, M.; Yao, Y.; Jagessar, R. C.; Dirk, S. M.; Price, D. W.; Reed, M. A.; Zhou, C.-W.; Chen, J.; Wang, W.; Campbell, I. *Chem. Eur. J.* **2001**, *7*, 5118-5134.

17. Fraysse, S.; Coudret, C.; Launay, J.-P. *J. Am. Chem. Soc.* **2003**, *125*, 5880-5888.

18. Haiss, W.; van Zalinge, H.; Higgins, S. J.; Bethell, D.; Hobenreich, H.; Schiffrin, D. J.; Nichols, R. J. *J. Am. Chem. Soc.* **2003**, *125*, 15294-15295.

19. Kushmerick, J. G.; Naciri, J.; Yang, J. C.; Shashidhar, R. *Nano Lett.* **2003**, *3*, 897-900.

20. Robertson, N.; McGowan, C. A. *Chem. Soc. Rev.* **2003**, *32*, 96-103.

21. Haiss, W.; Nichols, R. J.; Zalinge, H. v.; Higgins, S. J.; Bethell, D.; Schiffrin, D. J. *Phys . Chem. Chem. Phys* **2004**, *6*, 4330-4337.

22. Haiss, W.; van Zalinge, H.; Hobenreich, H.; Bethell, D.; Schiffrin, D. J.; Higgins, S. J.; Nichols, R. J. *Langmuir* **2004**, *20*, 7694-7702.

23. Wang, C.; Batsanov, A. S.; Bryce, M. R.; Sage, I. *Org. Lett.* **2004**, *6*, 2181-2184.

24. Blum, A. S.; Tong Ren; Parish, D. A.; Trammell, S. A.; Moore, M. H.; Kushmerick, J. G.; Xu, G.-L.; Deschamps, J. R.; Pollack, S. K.; Shashidhar, R. *J. Am. Chem. Soc.* **2005**, *127*, 10010-10011.

25. Li, G.; Wang, X.; Wang, F. *Tetrahedron Lett.* **2005**, *46*, 8971-8973.

26. Dong, T.-Y.; Chang, S.-W.; Lin, S.-F.; Lin, M.-C.; Wen, Y.-S.; Lee, L. *Organometallics* **2006**, *25*, 2018-2024.

27. Tam, I. W.; Yan, J.; Breslow, R. *Org. Lett.* **2006**, *8*, 183-185.

28. Wang, C.; Batsanov, A. S.; Bryce, M. R. *Faraday Discuss.* **2006**, *131*, 221-234.

29. Wang, C.; Batsanov, A. S.; Bryce, M. R. *J. Org. Chem.* **2006**, *71*, 108-116.

30. Wang, C.; Palsson, L.-O.; Batsanov, A. S.; Bryce, M. R. *J. Am. Chem. Soc.* **2006**, *128*, 3789-3799.

31. Endou, M.; Ie, Y.; Kaneda, T.; Aso, Y. *J. Org. Chem.* **2007**, *72*, 2659-2661.

32. Leary, E.; Higgins, S. J.; Zalinge, H. v.; Haiss, W.; Nichols, R. J. *Chem. Commun.* **2007**, 3939-3941.

33. Bagrets, A.; Arnold, A.; Evers, F. *J. Am. Chem. Soc.* **2008**, *130*, 9013-9018.

34. Chen, X.; Jeon, Y.-M.; Jang, J.-W.; Qin, L.; Huo, F.; Wei, W.; Mirkin, C. A. *J. Am. Chem. Soc.* **2008**, *130*, 8166-8168.

35. Haiss, W.; Wang, C.; Jitchati, R.; Grace, I.; Martin, S.; Batsanov, A. S.; Higgins, S. J.; Bryce, M. R.; Lambert, C. J.; Jensen, P. S.; Nichols, R. J. *J. Phys.: Condens. Matter* **2008**, *20*, 374119.

36. Hansen, T.; Mujica, V.; Ratner, M. A. *Nano Lett.* **2008**, *8*, 3525–3531.

37. Hsu, L.-Y.; Huang, Q.-R.; Jin, B.-Y. *J. Phys. Chem. C* **2008**, *112*, 10538-10541.

38. Liu, H.; Wang, N.; Zhao, J.; Guo, Y.; Yin, X.; Boey, F. Y. C.; Zhang, H. *ChemPhysChem* **2008**, *9*, 1416-1424.

39. Olivier, C.; Kim, B.; Touchard, D.; Rigaut, S. *Organometallics* **2008**, *27*, 509-518.

40. Wang, C.; Bryce, M. R.; Gigon, J.; Ashwell, G. J.; Grace, I.; Lambert, C. J. *J. Org. Chem.* **2008**, *73*, 4810-4818.

41. Wheeler, W. D.; Dahnovsky, Y. *J. Phys. Chem. C* **2008**, *112*, 13769-13774.

42. Wielopolski, M.; Atienza, C.; Clark, T.; Guldi, D. M.; Martín, N. *Chem. Eur. J.* **2008**, *14*, 6379-6390.

43. Yamada, R.; Kumazawa, H.; Noutoshi, T.; Tanaka, S.; Tada, H. *Nano Lett.* **2008**, *8*, 1237-1240.

44. Lafferentz, L.; Ample, F.; Yu, H.; Hecht, S.; Joachim, C.; Grill, L. *Science* **2009**, *323*, 1193-1197.

45. Nazeeruddin, M. K.; Péchy, P.; Renouard, T.; Zakeeruddin, S. M.; Humphry-Baker, R.; Comte, P.; Liska, P.; Cevey, L.; Costa, E.; Shklover, V.; Spiccia, L.; Deacon, G. B.; Bignozzi, C. A.; Grätzel, M. *J. Am. Chem. Soc.* **2001**, *123*, 1613-1624.

46. Ferrere, S. *Chem. Mater.* **2000**, *12*, 1083-1089.

47. Hagfeldt, A.; Grätzel, M. *Acc. Chem. Res.* **2000**, *33*, 269-277.

48. Grätzel, M. *J. Photochem. Photobiol., C* **2003**, *4*, 145-153.

49. Hara, K.; Sato, T.; Katoh, R.; Furube, A.; Ohga, Y.; Shinpo, A.; Suga, S.; Sayama, K.; Sugihara, H.; Arakawa, H. *J. Phys. Chem. B* **2003**, *107*, 597-606.

50. Grätzel, M. *Chem. Lett.* **2005**, *34*, 8-13.

51. Yum, J.-H.; Chen, P.; Grätzel, M.; Nazeeruddin, M. K. *ChemSusChem* **2008**, *1*, 699-707.

52. Roncali, J.; Leriche, P.; Cravino, A. *Adv. Mater.* **2007**, *19*, 2045-2060.

53. Yamada, H.; Okujima, T.; Ono, N. *Chem. Commun.* **2008**, 2957 - 2974.

54. Usta, H.; Risko, C.; Wang, Z.; Huang, H.; Deliomeroglu, M. K.; Zhukhovitskiy, A.; Facchetti, A.; Marks, T. J. *J. Am. Chem. Soc.* **2009**, *131*, 5586-5608.

55. Facchetti, A. *Mater. Today* **2007**, *10*, 28-37.

56. Murphy, A. R.; Frechet, J. M. J. *Chem. Rev.* **2007**, *107*, 1066-1096.

57. Lundstrom, M. *Science* **2003**, *299*, 210-211.

58. Petty, M. C.; Bryce, M. R.; Bloor, D. *An Introduction to Molecular Electronics*; Oxford University Press: Oxford, 1995.

59. Aviram, A.; Ratner, M. A. *Chem. Phys. Lett.* **1974**, *29*, 277-283.

60. Metzger, R. M.; Chen, B.; Hopfner, U.; Lakshmikantham, M. V.; Vuillaume, D.; Kawai, T.; Wu, X.; Tachibana, H.; Hughes, T. V.; Sakurai, H.; Baldwin, J. W.; Hosch, C.; Cava, M. P.; Brehmer, L.; Ashwell, G. J. *J. Am. Chem. Soc.* **1997**, *119*, 10455-10466.

61. Ho, G.; Heath, J. R.; Kondratenko, M.; Perepichka, D. F.; Arseneault, K.; Pézolet, M.; Bryce, M. R. *Chem. Eur. J.* **2005**, *11*, 2914-2922.

62. Metzger, R. M. *J. Mater. Chem.* **2000**, *10*, 55-62.

63. Baldwin, J. W.; Amaresh, R. R.; Peterson, I. R.; Shumate, W. J.; Cava, M. P.; Amiri, M. A.; Hamilton, R.; Ashwell, G. J.; Metzger, R. M. *J. Phys. Chem. B* **2002**, *106*, 12158-12164.

64. Okazaki, N.; Sambles, J. R.; Jory, M. J.; Ashwell, G. J. *Appl. Phys. Lett.* **2002**, *81*, 2300-2302.

65. Ashwell, G. J.; Kelly, S. H. B. *Synth. Met.* **2003**, *133-134*, 641-643.

66. Kubatkin, S.; Danilov, A.; Hjort, M.; Cornil, J.; Bredas, J.-L.; Stuhr-Hansen, N.; Hedegard, P.; Bjornholm, T. *Nature* **2003**, *425*, 698-701.

67. Tans, S. J.; Verschueren, A. R. M.; Dekker, C. *Nature* **1998**, *393*, 49-52.

68. Joachim, C.; Gimzewski, J. K. *Chem. Phys. Lett.* **1997**, *265*, 353-357.

69. Collier, C. P.; Mattersteig, G.; Wong, E. W.; Luo, Y.; Beverly, K.; Sampaio, J.; Raymo, F. M.; Stoddart, J. F.; Heath, J. R. *Science* **2000**, *289*, 1172-1175.

70. Chen, J.; Reed, M. A.; Rawlett, A. M.; Tour, J. M. *Science* **1999**, *286*, 1550-1552.

71. Ami, S.; Hliwa, M.; Joachim, C. *Chem. Phys. Lett.* **2003**, *367*, 662-668.

72. James, D. K.; Tour, J. M. *Chem. Mater.* **2004**, *16*, 4423-4435.
73. Joachim, C.; Gimzewski, J. K.; Aviram, A. *Nature* **2000**, *408*, 541-548.
74. Nitzan, A.; Ratner, M. A. *Science* **2003**, *300*, 1384-1389.
75. McCreery, R. L. *Chem. Mater.* **2004**, *16*, 4477-4496.
76. Selzer, Y.; Allara, D. L. *Ann. Rev. Phys. Chem.* **2006**, *57*, 593-623.
77. Cui, X. D.; Primak, A.; Zarate, X.; Tomfohr, J.; Sankey, O. F.; Moore, A. L.; Moore, T. A.; Gust, D.; Harris, G.; Lindsay, S. M. *Science* **2001**, *294*, 571-574.
78. Haiss, W.; Wang, C.; Grace, I.; Batsanov, A. S.; Schiffrin, D. J.; Higgins, S. J.; Bryce, M. R.; Lambert, C. J.; Nichols, R. J. *Nature Mater.* **2006**, *5*, 995-1002.
79. Reed, M. A.; Zhou, C.; Muller, C. J.; Burgin, T. P.; Tour, J. M. *Science* **1997**, *278*, 252-254.
80. Gonzalez, M. T.; Wu, S.; Huber, R.; van der Molen, S. J.; Schonenberger, C.; Calame, M. *Nano Lett.* **2006**, *6*, 2238-2242.
81. Liang, W.; Shores, M. P.; Bockrath, M.; Long, J. R.; Park, H. *Nature* **2002**, *417*, 725-729.
82. Heath, J. R.; Ratner, M. A. *Phys. Today* **2003**, *56*, 43-49.
83. Maruccio, G.; Cingolani, R.; Rinaldi, R. *J. Mater. Chem.* **2004**, *14*, 542 - 554.
84. Wassel, R. A.; Gorman, C. B. *Angew. Chem. Int. Ed.* **2004**, *43*, 5120-5123.
85. Benniston, A. C. *Chem. Soc. Rev.* **2004**, *33*, 573-578.
86. Low, P. J. *Dalton Trans.* **2005**, 2821-2824.
87. Goeb, S.; De Nicola, A.; Ziessel, R. *J. Org. Chem.* **2005**, *70*, 1518-1529.
88. Schon, J. H.; Meng, H.; Bao, Z. *Science* **2001**, *294*, 2138-2140.
89. Xu, B.; Tao, N. J. *Science* **2003**, *301*, 1221-1223.
90. Ramachandran, G. K.; Hopson, T. J.; Rawlett, A. M.; Nagahara, L. A.; Primak, A.; Lindsay, S. M. *Science* **2003**, *300*, 1413-1416.
91. Flatt, A. K.; Tour, J. M. *Tetrahedron Lett.* **2003**, *44*, 6699-6702.
92. Flatt, A. K.; Dirk, S. M.; Henderson, J. C.; Shen, D. E.; Su, J.; Reed, M. A.; Tour, J. M. *Tetrahedron* **2003**, *59*, 8555-8570.
93. Purcell, S. T.; Garcia, N.; Binh, V. T.; Jones, L.; Tour, J. M. *J. Am. Chem. Soc.* **1994**, *116*, 11985-11989.
94. Hicks, R. G.; Nodwell, M. B. *J. Am. Chem. Soc.* **2000**, *122*, 6746-6753.

95. Oike, T.; Kurata, T.; Takimiya, K.; Otsubo, T.; Aso, Y.; Zhang, H.; Araki, Y.; Ito, O. *J. Am. Chem. Soc.* **2005**, *127*, 15372-15373.

96. Tour, J. M.; Wu, R. *Macromolecules* **1992**, *25*, 1901-1907.

97. Davis, W. B.; Svec, W. A.; Ratner, M. A.; Wasielewski, M. R. *Nature* **1998**, *396*, 60-63.

98. Sikes, H. D.; Smalley, J. F.; Dudek, S. P.; Cook, A. R.; Newton, M. D.; Chidsey, C. E. D.; Feldberg, S. W. *Science* **2001**, *291*, 1519-1523.

99. Beeby, A.; Findlay, K.; Low, P. J.; Marder, T. B. *J. Am. Chem. Soc.* **2002**, *124*, 8280-8284.

100. James, P. V.; Sudeep, P. K.; Suresh, C. H.; Thomas, K. G. *J. Phys. Chem. A* **2006**, *110*, 4329-4337.

101. Pei, Q.; Yang. *J. Am. Chem. Soc.* **1996**, *118*, 7416-7417.

102. Kreyenschmidt, M.; Klaerner, G.; Fuhrer, T.; Ashenhurst, J.; Karg, S.; Chen, W. D.; Lee, V. Y.; Scott, J. C.; Miller, R. D. *Macromolecules* **1998**, *31*, 1099-1103.

103. Lee, J.-I.; Klaerner, G.; Miller, R. D. *Chem. Mater.* **1999**, *11*, 1083-1088.

104. James, D. K.; Tour, J. M. *Aldrichimica Acta* **2006**, *39*, 47-56.

105. Ley, K. D.; Li, Y.; Johnson, J. V.; Powell, D. H.; Schanze, K. S. *Chem. Commun.* **1999**, 1749-1750.

106. Creager, S.; Yu, C. J.; Bamdad, C.; O'Connor, S.; MacLean, T.; Lam, E.; Chong, Y.; Olsen, G. T.; Luo, J.; Gozin, M.; Kayyem, J. F. *J. Am. Chem. Soc.* **1999**, *121*, 1059-1064.

107. Cai, L.; Yao, Y.; Yang, J.; Price, D. W.; Tour, J. M. *Chem. Mater.* **2002**, *14*, 2905-2909.

108. Shi, Z.-F.; Wang, L.-J.; Wang, H.; Cao, X.-P.; Zhang, H.-L. *Org. Lett.* **2007**, *9*, 595-598.

109. Wei, L.; Padmaja, K.; Youngblood, W. J.; Lysenko, A. B.; Lindsey, J. S.; Bocian, D. F. *J. Org. Chem.* **2004**, *69*, 1461-1469.

110. Dirk, S. M.; Tour, J. M. *Tetrahedron* **2003**, *59*, 287-293.

111. Bong, D.; Tam, I.; Breslow, R. *J. Am. Chem. Soc.* **2004**, *126*, 11796-11797.

112. Cheng, L.; Yang, J.; Yao, Y.; Price, D. W.; Dirk, S. M.; Tour, J. M. *Langmuir* **2004**, *20*, 1335-1341.

113. Stapleton, J. J.; Harder, P.; Daniel, T. A.; Reinard, M. D.; Yao, Y.; Price, D. W.; Tour, J. M.; Allara, D. L. *Langmuir* **2003**, *19*, 8245-8255.

114. West, K.; Wang, C.; Batsanov, A. S.; Bryce, M. R. *J. Org. Chem.* **2006**, *71*, 8541-8544.

115. Ashwell, G. J.; Tyrrell, W. D.; Urasinska, B.; Wang, C.; Bryce, M. R. *Chem. Commun.* **2006**, 1640-1642.

116. Wu, S.; Gonzalez, M. T.; Huber, R.; Grunder, S.; Mayor, M.; Schonenberger, C.; Calame, M. *Nature Nanotechnol.* **2008**, *3*, 569-574.

117. Plater, M. J.; Sinclair, J. P.; Aiken, S.; Gelbrich, T.; Hursthouse, M. B. *Tetrahedron* **2004**, *60*, 6385-6394.

118. Anemian, R.; Mulatier, J.-C.; Andraud, C.; Stephan, O.; Vial, J.-C. *Chem. Commun.* **2002**, 1608-1609.

119. Benniston, A. C.; Li, P.; Sams, C. *Tetrahedron Lett.* **2003**, *44*, 3947-3949.

120. Reck, C. E.; Winter, C. H. *Organometallics* **1997**, *16*, 4493-4496.

121. Tavasli, M.; Bettington, S.; Bryce, M. R.; Attar, H. A. A.; Dias, F. B.; King, S.; Monkman, A. P. *J. Mater. Chem.* **2005**, *15*, 4963 - 4970.

122. Perepichka, I. I.; Perepichka, I. F.; Bryce, M. R.; Pålsson, L.-O. *Chem. Commun.* **2005**, 3397-3399.

123. Yang, C.-H.; Guo, T.-F.; Sun, I. W. *J. Lumin.* **2007**, *124*, 93-98.

124. Shaheen, S. E.; Kippelen, B.; Peyghambarian, N.; Wang, J. F.; Anderson, J. D.; Mash, E. A.; Lee, P. A.; Armstrong, N. R.; Kawabe, Y. *J. Appl. Phys.* **1999**, *85*, 7939-7945.

125. Savvate'ev, V.; Friedl, J. H.; Zou, L.; Shinar, J.; Christensen, K.; Oldham, W.; Rothberg, L. J.; Chen-Esterlit, Z.; Kopelman, R. *Appl. Phys. Lett.* **2000**, *76*, 1501-1503.

126. Kim, D.-H.; Choi, D. H.; Park, J. J.; Lee, S. T.; Kwon, J. H. *Chem. Lett.* **2008**, *37*, 1150-1151.

127. Tang, C. W.; VanSlyke, S. A. *Appl. Phys. Lett.* **1987**, *51*, 913-915.

128. Baldo, M. A.; Lamansky, S.; Burrows, P. E.; Thompson, M. E.; Forrest, S. R. *Appl. Phys. Lett.* **1999**, *75*, 4-6.

129. Cleave, V.; Yahioglu, G.; Barny, P. L.; Friend, R. H.; Tessler, N. *Adv. Mater.* **1999**, *11*, 285-288.

130. Lee, J. K.; Yoo, D. S.; Handy, E. S.; Rubner, M. F. *Appl. Phys. Lett.* **1996**, *69*, 1686-1688.

131. Zhang, Q.; Zhou, Q.; Cheng, Y.; Wang, L.; Ma, D.; Jing, X.; Wang, F. *Adv. Funct. Mater.* **2006**, *16*, 1203-1208.

132. Kido, J.; Hongawa, K.; Okuyama, K.; Nagai, K. *Appl. Phys. Lett.* **1993**, *63*, 2627-2629.

133. Burroughes, J. H.; Bradley, D. D. C.; Brown, A. R.; Marks, R. N.; Mackay, K.; Friend, R. H.; Burn, P. L.; Holmes, A. B. *Nature* **1990**, *347*, 539-541.

134. Janietz, S.; Bradley, D. D. C.; Grell, M.; Giebeler, C.; Inbasekaran, M.; Woo, E. P. *Appl. Phys. Lett.* **1998**, *73*, 2453-2455.

135. Remmers, M.; Neher, D.; Gruner, J.; Friend, R. H.; Gelinck, G. H.; Warman, J. M.; Quattrocchi, C.; dos Santos, D. A.; Bredas, J.-L. *Macromolecules* **1996**, *29*, 7432-7445.

136. Freeman, A.; Fréchet, J.; Koene, S.; Thompson, M. *Macromol. Symp.* **2000**, *154*, 163-170.

137. Adachi, C.; Baldo, M. A.; Forrest, S. R.; Thompson, M. E. *Appl. Phys. Lett.* **2000**, *77*, 904-906.

138. Dixon, I. M.; Collin, J.-P.; Sauvage, J.-P.; Flamigni, L.; Encinas, S.; Barigelletti, F. *Chem. Soc. Rev.* **2000**, *29*, 385-391.

139. Lamansky, S.; Djurovich, P.; Murphy, D.; Abdel-Razzaq, F.; Lee, H. E.; Adachi, C.; Burrows, P. E.; Forrest, S. R.; Thompson, M. E. *J. Am. Chem. Soc.* **2001**, *123*, 4304-4312.

140. Chou, P.-T.; Chi, Y. *Chem. Eur. J.* **2007**, *13*, 380-395.

141. Lowry, M. S.; Bernhard, S. *Chem. Eur. J.* **2006**, *12*, 7970-7977.

142. Williams, J. A. G.; Wilkinson, A. J.; Whittle, V. L. *Dalton Trans.* **2008**, 2081-2099.

143. Slinker, J. D.; Rivnay, J.; Moskowitz, J. S.; Parker, J. B.; Bernhard, S.; Abruna, H. D.; Malliaras, G. G. *J. Mater. Chem.* **2007**, *17*, 2976-2988.

144. Slinker, J.; Bernards, D.; Houston, P. L.; Abruña, H. D.; Bernhardc, S.; Malliaras, G. G. *Chem. Commun.* **2003**, 2392.

145. Yersin, H. *Highly Efficient OLEDs with Phosphorescent Materials*, 1st ed.; Wiley-Vch Verlag Gmbh & Co. Kgaa: Weinheim, 2008.

146. King, K. A.; Spellane, P. J.; Watts, R. J. *J. Am. Chem. Soc.* **1985**, *107*, 1431-1432.

147. Dedeian, K.; Djurovich, P. I.; Garces, F. O.; Carlson, G.; Watts, R. J. *Inorg. Chem.* **1991**, *30*, 1685-1687.

148. Colombo, M. G.; Brunold, T. C.; Riedener, T.; Guedel, H. U.; Fortsch, M.; Buergi, H.-B. *Inorg. Chem.* **1994**, *33*, 545-550.

149. Tamayo, A. B.; Alleyne, B. D.; Djurovich, P. I.; Lamansky, S.; Tsyba, I.; Ho, N. N.; Bau, R.; Thompson, M. E. *J. Am. Chem. Soc.* **2003**, *125*, 7377-7387.

150. Huo, S.; Deaton, J. C.; Rajeswaran, M.; Lenhart, W. C. *Inorg. Chem.* **2006**, *45*, 3155-3157.

151. Ohsawa, Y.; Sprouse, S.; King, K. A.; DeArmond, M. K.; Hanck, K. W.; Watts, R. J. *J. Phys. Chem.* **1987**, *91*, 1047-1054.

152. Lowry, M. S.; Hudson, W. R.; Pascal, R. A.; Bernhard, S. *J. Am. Chem. Soc.* **2004**, *126*, 14129-14135.

153. Zeng, X.; Tavasli, M.; Perepichka, I. F.; Batsanov, A. S.; Bryce, M. R.; Chiang, C.-J.; Rothe, C.; Monkman, A. P. *Chem. Eur. J.* **2008**, *14*, 933-943.

154. Douglas, B.; Mcdaniel, D.; Alexander, J. *Concepts and Models of Inorganic Chemistry*, 3rd ed.; John Wiley & Sons, Inc.: New York, 1994.

155. Huheey, J. E.; Keiter, E. A.; Keiter, R. L. *Inorganic Chemistry: Principles of Structure and Reactivity*, 4 ed.; Haper Collins College Publishers: New York, 1993.

156. Tsuboyama, A.; Iwawaki, H.; Furugori, M.; Mukaide, T.; Kamatani, J.; Igawa, S.; Moriyama, T.; Miura, S.; Takiguchi, T.; Okada, S.; Hoshino, M.; Ueno, K. *J. Am. Chem. Soc.* **2003**, *125*, 12971-12979.

157. Colombo, M. G.; Hauser, A.; Gudel, H. U. *Inorg. Chem.* **1993**, *32*, 3088.

158. Didier, P.; Ortmans, I.; Kirsch-De Mesmaeker, A.; Watts, R. J. *Inorg. Chem.* **1993**, *32*, 5239-5245.

159. Dedeian, K.; Shi, J.; Shepherd, N.; Forsythe, E.; Morton, D. C. *Inorg. Chem.* **2005**, *44*, 4445-4447.

160. You, Y.; Park, S. Y. *J. Am. Chem. Soc.* **2005**, *127*, 12438-12439.

161. Hay, P. J. *J. Phys. Chem. A* **2002**, *106*, 1634-1641.

162. Nazeeruddin, M. K.; Wegh, R. T.; Zhou, Z.; Klein, C.; Wang, Q.; De Angelis, F.; Fantacci, S.; Grätzel, M. *Inorg. Chem.* **2006**, *45*, 9245-9250.

163. De Angelis, F.; Fantacci, S.; Evans, N.; Klein, C.; Zakeeruddin, S. M.; Moser, J. E.; Kalyanasundaram, K.; Bolink, H. J.; Grätzel, M.; Nazeeruddin, M. K. *Inorg. Chem.* **2007**, *46*, 5989-6001.

164. Tamayo, A. B.; Garon, S.; Sajoto, T.; Djurovich, P. I.; Tsyba, I. M.; Bau, R.; Thompson, M. E. *Inorg. Chem.* **2005**, *44*, 8723-8732.

165. Nazeeruddin, M. K.; Humphry-Baker, R.; Berner, D.; Rivier, S.; Zuppiroli, L.; Graetzel, M. *J. Am. Chem. Soc.* **2003**, *125*, 8790-8797.

166. Adamovich, V. I.; Cordero, S. R.; Djurovich, P. I.; Tamayo, A.; Thompson, M. E.; D'Andrade, B. W.; Forrest, S. R. *Org. Electron.* **2003**, *4*, 77-87.

167. Pei, Q.; Yang; Yu, G.; Zhang, C.; Heeger, A. J. *J. Am. Chem. Soc.* **1996**, *118*, 3922-3929.

168. Mitschke, U.; Bauerle, P. *J. Mater. Chem.* **2000**, *10*, 1471-1507.

169. Handy, E. S.; Pal, A. J.; Rubner, M. F. *J. Am. Chem. Soc.* **1999**, *121*, 3525-3528.

170. Slinker, J. D.; Gorodetsky, A. A.; Lowry, M. S.; Wang, J.; Parker, S.; Rohl, R.; Bernhard, S.; Malliaras, G. G. *J. Am. Chem. Soc.* **2004**, *126*, 2763-2767.

171. Altman, R. A.; Buchwald, S. L. *Org. Lett.* **2006**, *8*, 2779-2782.

172. Lowry, M. S.; Goldsmith, J. I.; Slinker, J. D.; Rohl, R.; Pascal, R. A.; Malliaras, G. G.; Bernhard, S. *Chem. Mater.* **2005**, *17*, 5712-5719.

173. Brooks, J.; Babayan, Y.; Lamansky, S.; Djurovich, P. I.; Tsyba, I.; Bau, R.; Thompson, M. E. *Inorg. Chem.* **2002**, *41*, 3055-3066.

174. Finar, I. L.; Rackham., D. M. *J. Chem. Soc. B* **1968**, 211-214.

175. Jitchati, R.; Batsanov, A. S.; Bryce, M. R. *Tetrahedron* **2009**, *65*, 855-861.

176. Cristau, H.-J.; Cellier, Pascal P.; Spindler, J.-F.; Taillefer, M. *Eur. J. Org. Chem.* **2004**, *2004*, 695-709.

177. Sprouse, S.; King, K. A.; Spellane, P. J.; Watts, R. J. *J. Am. Chem. Soc.* **1984**, *106*, 6647-6653.

178. McGee, K. A.; Mann, K. R. *Inorg. Chem.* **2007**, *46*, 7800-7809.

179. Zhao, Q.; Liu, S.; Shi, M.; Li, F.; Jing, H.; Yi, T.; Huang, C. *Organometallics* **2007**, *26*, 5922-5930.

180. Zhao, Q.; Liu, S.; Shi, M.; Wang, C.; Yu, M.; Li, L.; Li, F.; Yi, T.; Huang, C. *Inorg. Chem.* **2006**, *45*, 6152-6160.

181. Su, H.-C.; Fang, F. C.; Hwu, T. Y.; Hsieh, H. H.; Chen, H. F.; Lee, G. H.; Peng, S. M.; Wong, K. T.; Wu, C. C. *Adv. Funct. Mater.* **2007**, *17*, 1019-1027.

182. Su, H. C.; Chen, H. F.; Fang, F. C.; Liu, C. C.; Wu, C. C.; Wong, K. T.; Liu, Y. H.; Peng, S. M. *J. Am. Chem. Soc.* **2008**, *130*, 3413-3419.

183. Dragonetti, C.; Falciola, L.; Mussini, P.; Righetto, S.; Roberto, D.; Ugo, R.; Valore, A.; DeAngelis, F.; Fantacci, S.; Sgamellotti, A.; Ramon, M.; Muccini, M. *Inorg. Chem.* **2007**, *46*, 8533-8547.

184. Goldsmith, J. I.; Hudson, W. R.; Lowry, M. S.; Anderson, T. H.; Bernhard, S. *J. Am. Chem. Soc.* **2005**, *127*, 7502-7510.

185. Muller, C. D.; Falcou, A.; Reckefuss, N.; Rojahn, M.; Wiederhirn, V.; Rudati, P.; Frohne, H.; Nuyken, O.; Becker, H.; Meerholz, K. *Nature* **2003**, *421*, 829-833.

186. Bayerl, M. S.; Braig, T.; Nuyken, O.; Muller, D. C.; Groß, M.; Meerholz, K. *Macromol. Rapid Commun.* **1999**, *20*, 224-228.

187. Rehmann, N.; Ulbricht, C.; Köhnen, A.; Zacharias, P.; Gather, M. C.; Hertel, D.; Holder, E.; Meerholz, K.; Schubert, U. S. *Adv. Mater.* **2008**, *20*, 129-133.

188. Zacharias, P.; Gather, Malte C.; Rojahn, M.; Nuyken, O.; Meerholz, K. *Angew. Chem. Int. Ed.* **2007**, *46*, 4388-4392.

189. Wallikewitz, B. H.; Hertel, D.; Meerholz, K. *Chem. Mater.* **2009**, *21*, 2912–2919.

190. Kim, A.; Powers, J. D.; Toczko, J. F. *J. Org. Chem.* **2006**, *71*, 2170-2172.

191. Katritzky, A. R.; Rees, C. W.; Scriven, E. F. V. *Comprehensive Heterocyclic Chemistry II*, 1st ed.; Pergamon Press Inc, 1996.

192. Craig, P. N. *In Comprehensive Medicinal Chemistry*, Drayton, C. J. ed.; Pergamon Press: New York, 1991; Vol. 8.

193. Ley, S. V.; Thomas, A. W. *Angew. Chem. Int. Ed.* **2003**, *42*, 5400 - 5449.

194. Quan, M. L.; Lam, P. Y. S.; Han, Q.; Pinto, D. J. P.; He, M. Y.; Li, R.; Ellis, C. D.; Clark, C. G.; Teleha, C. A.; Sun, J. H.; Alexander, R. S.; Bai, S.; Luettgen, J. M.; Knabb, R. M.; Wong, P. C.; Wexler, R. R. *J. Med. Chem.* **2005**, *48*, 1729-1744.

195. Maes, B. U. W. *Top. Heterocycl. Chem.* **2006**, *1*, 155-211.

196. Fairlamb, I. *J. Chem. Soc. Rev.* **2007**, *36*, 1036-1045.

197. Stauffer, S. R.; Coletta, C. J.; Tedesco, R.; Nishiguchi, G.; Carlson, K.; Sun, J.; Katzenellenbogen, B. S.; Katzenellenbogen, J. A. *J. Med. Chem.* **2000**, *43*, 4934-4947.

198. Löber, S.; Hüber, H.; Gmeiner, P. *Bioorg. Med. Chem. Lett.* **2006**, *16*, 2955-2959.

199. Wiglenda, T.; Gust, R. *J. Med. Chem.* **2007**, *50*, 1475-1484.

200. Bellina, F.; Cauteruccio, S.; Rossi, R. *Tetrahedron* **2007**, *63*, 4571-4624.

201. Stabler, S. R.; Jahangir. *Synth. Commun.* **1994**, *24*, 123 - 129.

202. Um, I.-H.; Min, S.-W.; Dust, J. M. *J. Org. Chem.* **2007**, *72*, 8797-8803.

203. Klapars, A.; Antilla, J. C.; Huang, X.; Buchwald, S. L. *J. Am. Chem. Soc.* **2001**, *123*, 7727-7729.

204. Antilla, J. C.; Baskin, J. M.; Barder, T. E.; Buchwald, S. L. *J. Org. Chem.* **2004**, *69*, 5578-5587.

205. Cristau, H.-J.; Cellier, P. P.; Spindler, J.-F.; Taillefer, M. *Chem. Eur. J.* **2004**, *10*, 5607-5622.

206. Phillips, D. P.; Hudson, A. R.; Nguyen, B.; Lau, T. L.; McNeill, M. H.; Dalgard, J. E.; Chen, J.-H.; Penuliar, R. J.; Miller, T. A.; Zhi, L. *Tetrahedron Lett.* **2006**, *47*, 7137-7138.

207. Guo, X.; Rao, H.; Fu, H.; Jiang, Y.; Zhaoa, Y. *Adv. Synth. Catal.* **2006**, *348*, 2197-2202.

208. Anderson, K. W.; Tundel, R. E.; Ikawa, T.; Altman, R. A.; Buchwald, S. L. *Angew. Chem. Int. Ed.* **2006**, *45*, 6523-6527.

209. Kiyomori, A.; Marcoux, J.-F.; Buchwald, S. L. *Tetrahedron Lett.* **1999**, *40*, 2657-2660.

210. Zhu, L.; Cheng, L.; Zhang, Y.; Xie, R.; You, J. *J. Org. Chem.* **2007**, *72*, 2737-2743.

211. Ma, H.-C.; Jiang, X.-Z. *J. Org. Chem.* **2007**, *72*, 8943-8946.

212. Huang, Y.-Z.; Gao, J.; Ma, H.; Miao, H.; Xu, J. *Tetrahedron Lett.* **2008**, *49*, 948-951.

213. Verma, A. K.; Singh, J.; Sankar, V. K.; Chaudhary, R.; Chandra, R. *Tetrahedron Lett.* **2007**, *48*, 4207-4210.

214. Cheng, D.; Gan, F.; Qian, W.; Bao, W. *Green Chem.* **2008**, *10*, 171-173.

215. Mao, J.; Guo, J.; Song, H.; Ji, S.-J. *Tetrahedron* **2008**, *64*, 1383-1387.

216. Maheswaran, H.; Krishna, G. G.; Prasanth, K. L.; Srinivas, V.; Chaitanya, G. K.; Bhanuprakash, K. *Tetrahedron* **2008**, *64*, 2471-2479.

217. Zhu, L.; Guo, P.; Li, G.; Lan, J.; Xie, R.; You, J. *J. Org. Chem.* **2007**, *72*, 8535-8538.

218. Bellina, F.; Calandri, C.; Cauterrucio, S.; Rossi, R. *Eur. J. Org. Chem.* **2007**, 2147-2151.

219. Siddle, J. S.; Batsanov, A. S.; Bryce, M. R. *Eur. J. Org. Chem.* **2008**, 2746-2750.

220. Heck, R. F. *Palladium Reagents in Organic Synthesis*, 1st ed.; Academic Press: London, 1985.

221. Stuhr-Hansen, N. *Synth. Commun.* **2003**, *33*, 641-646.

222. Wang, C.; Batsanov, A. S.; Bryce, M. R.; Sage, I. *Synthesis* **2003**, 2089-2095.

223. Barrett, A. G. M.; Cramp, S. M.; Hennessy, A. J.; Procopiou, P. A.; Roberts, R. S. *Org. Lett.* **2001**, *3*, 271-273.

224. Dudek, S. P.; Pouderoijen, M.; Abbel, R.; Schenning, A. P. H. J.; Meijer, E. W. *J. Am. Chem. Soc.* **2005**, *127*, 11763-11768.

225. Hughes, G.; Wang, C.; Batsanov, A. S.; Fern, M.; Frank, S.; Bryce, M. R.; Perepichka, I. F.; Monkman, A. P.; Lyons, B. P. *Org. Biomol. Chem.* **2003**, *1*, 3069-3077.

226. Zhou, C.-Z.; Liu, T.; Xu, J.-M.; Chen, Z.-K. *Macromolecules* **2003**, *36*, 1457-1464.

227. Boer de, B.; Meng, H.; Perepichka, D. F.; Zheng, J.; Frank, M. M.; Chabal, Y. J.; Bao, Z. *Langmuir* **2003**, *19*, 4272-4284.